SAND79-8508
Unlimited Release

UC-62c

Department of Energy Large Solar Central Power Systems Semiannual Review

Prepared by Sandia Laboratories, Albuquerque, New Mexico 87115 and Livermore, California 94550 for the United States Department of Energy under Contract DE-AC04-76DP00789.

Printed May 1979

Sandia Laboratories
energy report

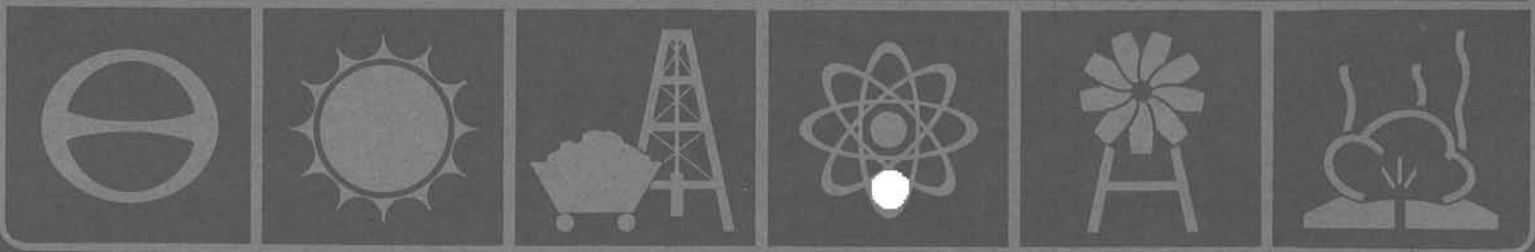

Issued by Sandia Laboratories, operated for the United States Department of Energy by Sandia Corporation.

NOTICE

Printed in the United States of America
Available from
National Technical Information Service
U. S. Department of Commerce
5285 Port Royal Road
Springfield, VA 22161
Price: Printed Copy $11.00; Microfiche $3.00

SAND79-8508
Unlimited Release
Printed May 1979

UC-62c

DEPARTMENT OF ENERGY LARGE SOLAR CENTRAL POWER SYSTEMS SEMIANNUAL REVIEW

Sponsored by

Department of Energy
Division of Solar Technology
Washington, D.C.

ABSTRACT

This report presents the highlights of the Department of Energy Large Solar Central Power Systems Semiannual Review held in Reston, Virginia, on March 21-22, 1979.

CONTENTS

*No paper received.

*No paper supplied.

OVERVIEW OF THE LARGE SOLAR CENTRAL POWER SYSTEMS PROGRAM

G. Braun
Department of Energy

The solar thermal program objective is to reduce the amount of fossil fluids being consumed for electricity production and other uses by aiding the creation of a viable solar power industry. This will be done by establishing the technical and operational readiness of solar thermal high temperature concentrating collector systems (matched to major applications) which can become cost effective with alternate fuels in most of the United States. Given this objective, the elements of the Program have been structured to produce industry involvement in the program. The Solar Thermal Energy Association was created by private industry to advance the interest and concerns of the industrial participants in this program. One of the most important elements of the program, the pilot plant at Barstow, California, has had scheduling problems. However, it is hoped that from these problems will come the experience necessary to conduct future major projects of this type, particularly in terms of scheduling and involving the government in such a way that minimizes the effect of bureaucracy and indecision. In the repowering area, indications are that industry and utilities are poised to join the DOE in moving ahead. DOE's cooperation with the utility industry through the EPRI program appears to be very effective. One example is the recent successful completion of the joint program that produced a 1-MW_t receiver capable of supplying heat to a Brayton cycle. In the case of the heliostat technology, private investment is beginning to appear in this area, which is the real bellweather of future success. In the area of our testing activities, the technical successes include the testing of the 250-kW_t ceramic receiver at Georgia Tech, which is very important--a milestone that indicates that the reality of some of the potential that had been claimed earlier on. In the case of the total energy program we have at Albuquerque at the mid-temperature solar test facility, energy utilization efficiencies in excess of 60 percent. At the Central Receiver Test Facility, I would add that we are now in the process of attempting to establish a regimen of test and evaluation there that reflects the program's intention to provide equipment of the utilities that meets power industry standards.

Budget

In fiscal 1978, the level of funding for the overall Solar Thermal Program reached roughly $100M (Table I) with the first major increment of construction funds for the Barstow pilot plant. From 1978 to 1979, most of the efforts already under way were maintained without many new projects starting.

Additional funds required to complete the Barstow construction represent a good portion of the increase in going from a FY 79 budget of $100M to a requested $121M budget for FY 80 (Table II). The other major increase is in the area of advanced research and development. Here, additional funds would be used to strengthen the storage development effort, and to begin to focus on fuels and chemicals production, related technology, and other high-temperature technology that is not under development in the other programs. Fiscal 1981 should be a period of stabilization without major changes in the levels of effort in solar programs--either up or down.

Major Programs

In FY 77, the overall solar thermal effort was restructured into three program elements: engineering development of central receivers for large-scale applications, engineering development of distributed receivers for small-scale applications, and development of technology to improve or expand the ultimate use of the central and distributed concentrator systems. In 1978 a 1-MW experiment for small community applications was initiated, along with a belated, but hopefully aggressive start in the development of high-temperature parabolic dish technology. Also, the United States, along with nine other countries, initiated the IEA Small Solar Power Project. In 1979, DOE began funding efforts relative to fuels and chemical production of high-temperature solar concentrators, and one of the major efforts this year is to adjust the program to the implications of the National Energy Act and attempt to use this piece of legislation to encourage early implementation of solar technology. In FY 80, the major initiative will be to make the necessary adjustments in the program to reflect that we are now looking to a technology development focus which hopefully provides technology for any foreseeable application of high-temperature concentrators systems. In particular, there's a substantial DOE interest in industrial process heat applications.

In FY 77, the field management roles and responsibilities were clarified, and the decentralization process began. In particular, in 1978 field management responsibilities for the Large Power Program were assigned to the San Francisco Office of DOE and Sandia Livermore. We have now a management plan that defines the responsibilities and authorities of the effective organizations. The biggest problem to date is getting people to accept that their modus operandi

really needs to be different in a decentralized program management configuration. Presently, management responsibility for the advanced technology program is being transferred to SERI. In addition, in 1979 we are at a critical point relative to areas that overlap between programs. In particular, there will be plans documented by the end of this year relative to industrial process heat, thermal storage, and materials development. We do not expect to fund any R&D that is not called for in those plans once they are documented. In FY 80, the major initiative will be to decentralize the management of the small power and distributed receiver programs.

Future Issues

DOE management feels that the solar thermal program, including the Large Power Program, should be oriented toward industrial process heat applications as well as electric applications. There will be a joint program plan for industrial process heat and solar thermal technology which spells out the division of responsibilities between this program and the on-going industrial process heat program. Basically, the division is between technology development, which is the responsibility of the Assistant Secretary for Energy Technology, and commercialization, which is the responsibility of the Assistant Secretary of Conservation and Solar Applications (CNSA). We expect to see a transition, not a hand-off point, where CNSA begins to be involved in taking the technology that is developed into the market. The goal in the central receiver program is to make adjustments relative to process heat without slowing down the efforts already under way. In particular, we must screen varied applications for solar process heat to understand where the best potential exists. In some cases, technologies that may not look attractive for electric power may be essentially indispensible for process heat. Another area of concern, relative to process heat is thermal transport in distributed systems. And also, I believe that although we've been looking at fossil, solar fossil hybrids for electric power, there is, perhaps, a larger incentive and a larger need for hybrid type systems relative to industrial process heat than for electric power.

Another very important issue is repowering. Utility repowering projects appear to be the best possible followup to Barstow, and the utilities seem ready to proceed. Focusing on repowering is appropriate relative to industrial process heat in that the main item is the solar heat source. In terms of repowering, the market is large enough to support the necessary heliostat production levels, and we think that the utility sector provides a good context in which to transfer experience within the industry and from project to project. Another key element in the decision to repower utilities is the National Energy Act, which requires a plethora of exceptions and exemptions of conversion of large boilers that burn oil and gas. The utility boilers are generally larger than industrial boilers, and therefore the Act should be more effective in stimulating retrofits in the utility sector.

TABLE I

BUDGET STATUS
($ in Millions)

	FY 1977	FY 1978	FY 1979
Large Power Systems			
Central Receiver R&D	$21.0	$ 21.8	$ 24.6
Construction*	2.5	41.0	28.0
Small Power Systems			
Distributed Receivers R&D	20.0	28.1	31.0
Advanced Technology	8.1	10.2	13.5
Capital Equipment**	3.0	3.0	3.0
Total -	$54.6	$104.1	$100.1

*10 MW_e Pilot Plant
**Small Power $1.5M, Large Power $1.0M, Advanced Technology $0.5M

TABLE II

SOLAR THERMAL BUDGET PERSPECTIVE
($ in Millions)

	FY 1979	FY 1980
Subsystems and Components ($22M)		
Parabolic Trough	$ 7.0	$ --
Parabolic Dish	5.0	--
Heliostat/Receiver	9.0	--
Hemispherical Bowl	1.0	--
Systems ($54M)		
Central Receiver ($38M)		
Baseline (Barstow)	30.0	+ 8.5
Retrofit	3.0	+ 2.0
High Temperature	5.0	--
Parabolic Trough	8.5	--
Parabolic Dish	7.5	--
Advanced Technology	14.0	+ 9.0
Management/Studies/Misc.	10.0	+ 1.5
	$100.0	$121.0

TECHNICAL OVERVIEW
LARGE SOLAR CENTRAL POWER SYSTEMS PROGRAM

A. C. Skinrood
Sandia Laboratories, Livermore

Program

The elements of the Large Power Systems Program are as follows:

- Major Projects
  - •CRFT
  - •Barstow
- Large System Applications
  - •Storage Coupled
  - •Repowering
  - •Hybrid
  - •EPRI/DOE Cooperative Projects
  - •Line Focus
- Component Development
  - •Heliostats
  - •Receivers
  - •Storage

Two projects have been approved as shown in Figure 1. Construction of the Central Receiver Test Facility (CRTF) has been completed, and the facility is now fully operational. The facility has 222 thirty-seven square meter heliostats which can produce a beam of concentrated solar radiation on a target test area. Experiments can be mounted on the top of a 61-meter high tower or in bays in the tower at various heights. Testing of the first prototype receiver developed

	Capacity	Select Conceptual Design	Start Detailed Design	Operation
Approved				
CRTF	5 MW_t	1/75	2/76	10/78
Barstow, California	10 MW_e (50 MW_t)	8/77	9/78	9/81
Proposed				
DOE/EPRI Hybrid	2 MW_e	10/80	4/81	3/84
Repowering		9/80	12/80	12/84

Figure 1. Approved and Proposed Projects

by Boeing under Electric Power Research Institute (EPRI) funding is nearly complete. A receiver developed by McDonnell Douglas under DOE funding has been installed and testing has started. The second project is a pilot plant with an electrical output of 10 MW that will be constructe · Barstow, California. The plant will have a water/steam receiver and use 1700 he_ostats, each with an area of 40-45 m^2. Initial operation is scheduled for late 1981. The plant will be operated by the Southern California Edison Company as a part of their grid network. Two other projects have been proposed: a DOE/EPRI hybrid plant and repowering of an existing electrical plant or industrial process. Neither the funding nor the schedule is firm on these two projects.

Storage-Coupled Power Plants

Conceptual designs of sodium receiver systems have been completed by the Energy Systems Groups and General Electric, and a molten salt system has been designed by Martin Marietta. Boeing completed a study for a Brayton cycle system using air as the heat transport fluid. The Martin Marietta and General Electric designs (Figure 2) have been selected to receiver additional funding. Each will design, fabricate, and test a 3- to 5-MW_t receiver experiment at the CRTF. Completion of this work will be in early 1981.

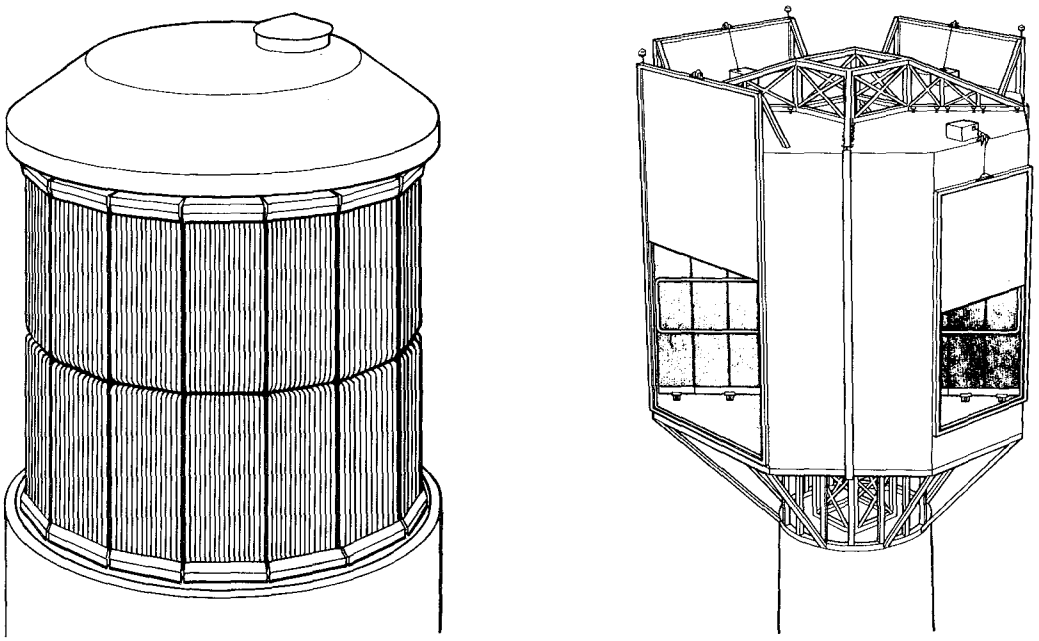

General Electric

Martin Marietta

Figure 2. Sodium or Salt Receivers

Repowering

Repowering is the addition of a solar capability to an existing electrical generation plant or an industrial process (Figure 3). The final report on a feasibility study by Public Service Company of New Mexico was issued in November, 1979. The Solar Energy Research Institute is continuing an analysis of the potential of repowering and will issue a report at the completion of their study in July, 1979. An RFP for conceptual designs for solar repowering/ industrial retrofit was issued on March 16, 1979. Under this procurement, site-specific designs will be developed which have the potential for construction and operation by 1985.

Hybrid

Hybrid plants combine a solar energy source with a non-solar source to produce electricity or operate an industrial process. Conceptual designs are being done based on a molten salt receiver (Martin Marietta) sodium receiver (ESG) and an air/heat pipe receiver (Bechtel). Completion of these studies will be in October, 1979. The Bureau of Reclamation, with partial DOE funding, is examining the feasibility of incorporating solar central power plants into their grid network. The study is 12 months in duration and started in February 1979.

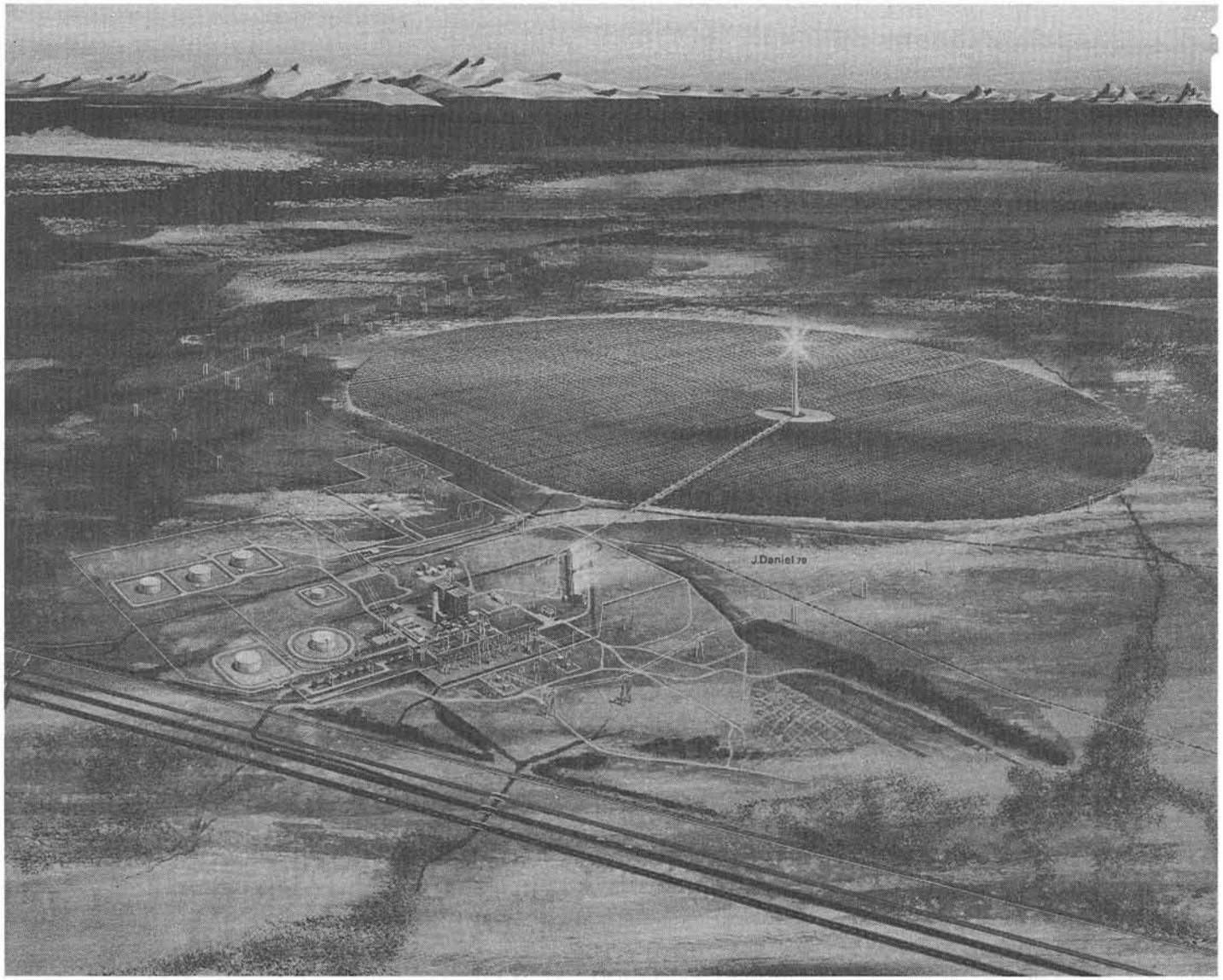

Figure 3. Solar Repowered Generating Plant

Line Focus

Twelve-month feasibility study contracts were awarded for systems using parabolic troughs (BDM), fixed mirror solar concentrators (General Atomic), and tower mounted receivers (SRI). These studies will be completed in September, 1979.

DOE/EPRI Cooperative Projects

The Department of Energy is working closely with the Electric Power Research Institute to develop new technology and disseminate information to potential users. Included are:

- Testing of the EPRI/Boeing Brayton cycle receiver at the CRTF
- Testing of the EPRI/Black and Veatch Brayton cycle receiver at the CRTF
- Co-funding of the Public Service Company of New Mexico repowering study
- Developing a source data book on central solar technology.

Source Data Document

Sandia Laboratories is preparing a document which will allow prospective users to assess the feasibility of using large solar power systems technology. Information on economics, siting, operation, maintenance, and construction will be provided. Inputs have been received from three utilities as to what information is desired. Publication of the document is scheduled for August, 1979.

Heliostat Performance Calculation Code

Sandia Laboratories has issued a user's guide for a new computer code to calculate heliostat performance. MIRVAL is a Monte Carlo program which simulates the heliostat and a portion of the receiver of a central receiver power plant. Models for three types of receiver and four types of heliostats are included in the code. The performance of fields containing up to 30,000 heliostats can be calculated. Details are contained in the report A User's Guide for MIRVAL--A Computer Code for Comparing Designs of Heliostat-Receiver Optics for Central Receiver Solar Power Plants, SAND77-8280, P. L. Leary, J. D. Hankins, February, 1979.

Heliostats

Contracts are being negotiated by Sandia Laboratories for the design, fabrication, and testing of second-generation heliostats. Contracts are also being negotiated for components and equipment that will contribute to third-generation designs. A variety of special studies are under way including:

- Inverted Stowage Study - McDonnell Douglas
- Field Reflectometer Development - Beckman
- One-Piece Plastic Dome Development - Boeing
- Plastic Film Development and Aging Studies - General Electric
- Mirror Deterioration Studies - Sandia Laboratories
- Heliostat Component Development - McDonnell Douglas
- Drive System Development - Solaramics
- Westinghouse Heliostat Testing - Sandia Laboratories
- Mirror Silvering Specifications - Battelle
- Solarization/Weathering of Glass - Sandia Laboratories

Receivers

Several new designs were developed as a part of both the advanced central receiver system and hybrid contracts. In addition, Sandia has awarded contracts to Babcock and Wilcos, Combustion Engineering, and Martin Marietta for the design of improved water/steam receivers. The steam conditions being studied are the current values of 510°C and 10.2 MPa, and the improved values of 538°C and 16.6 MPa. These studies will be complete in November, 1979.

An intensive program is being conducted to obtain experimental data in receiver performance. The 1-MW_t EPRI/Boeing testing at the CRTF is nearly complete. The 5-MW_t McDonnell Douglas panel has been installed at the CRTF (Figure 4), and testing is starting. A radiant test of a five-tube water/steam receiver panel (Figure 5) is being set up by Sandia Laboratories. The panel will be heavily instrumented in order to obtain a better understanding of once-through boiling phenomena. The schedule of testing is as follows:

October, 1978 - March, 1979	EPRI/Boeing Receiver Test
March, 1979 - July, 1979	McDonnell Douglas Panel Tests
April, 1979 - August, 1979	5-Tube Panel Tests

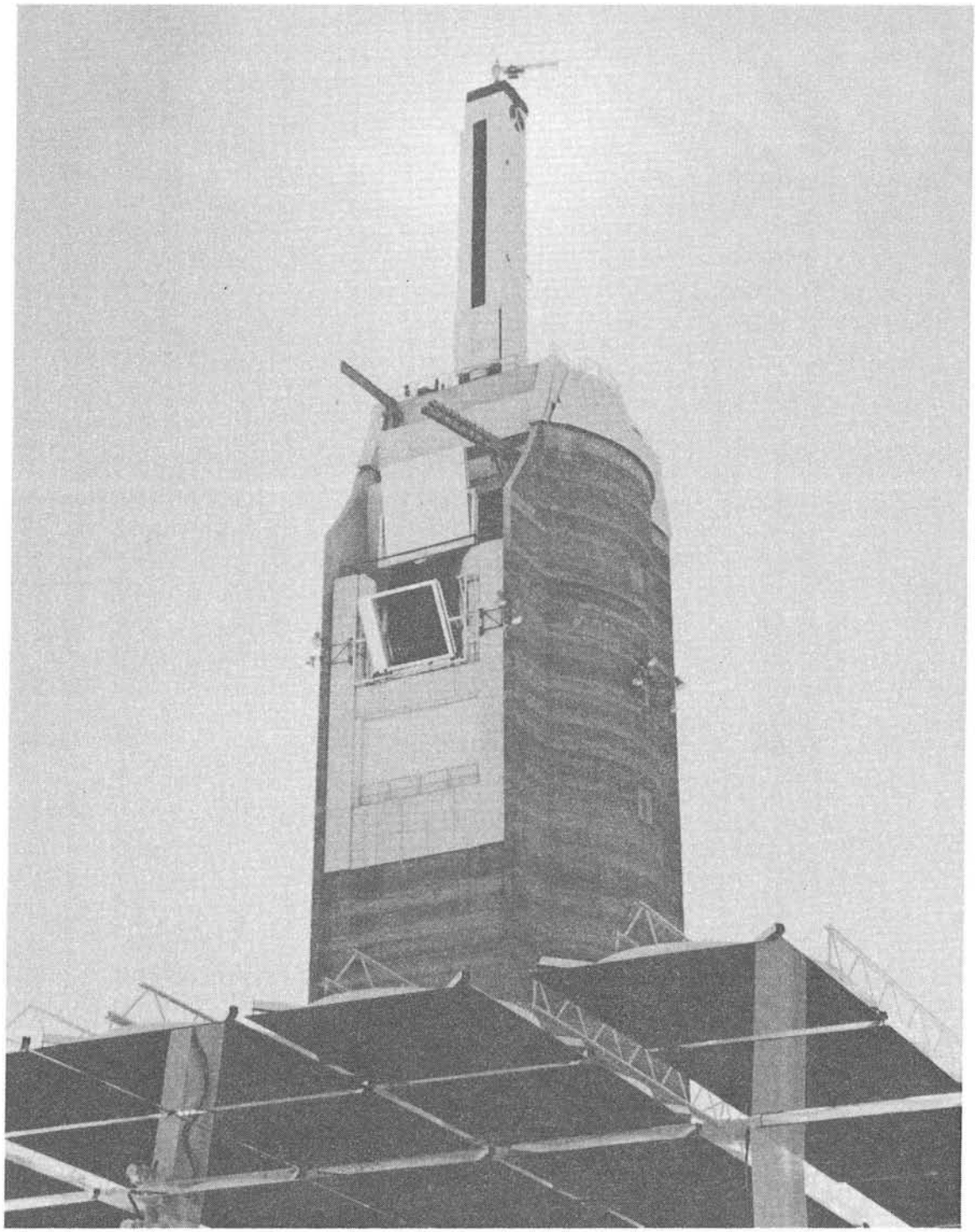

Figure 4. McDonnell Douglas 5-MW_t Panel

July, 1979 - October, 1979	EPRI/Black & Veatch Receiver Tests
June, 1980 - January, 1981	Martin Marietta and General Electric Receiver Tests

The following special receiver studies are being done:

Convective Losses	University of Illinois
Two-Phase Flow	University of Minnesota
Design Standards for Receivers	Foster Wheeler
Materials Testing	Argonne Laboratories
Tower Cost Study	Stearns-Roger

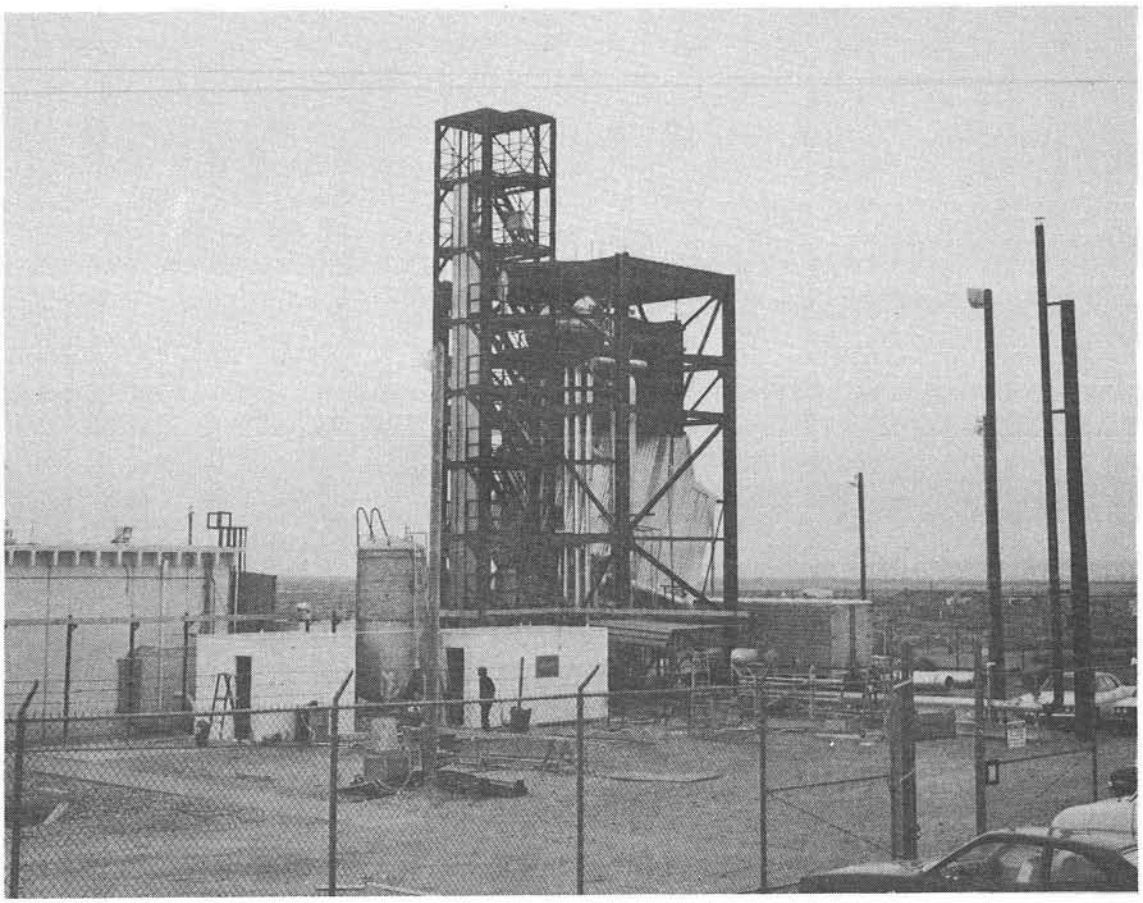

Figure 5. Five-Tube Water/Steam Receiver Panel Radiant Test

Thermal Energy Storage

The DOE Division of Energy Storage has primary responsibility for the development of new energy storage methods. Some storage development has been done as part of the Advanced Central Receiver System development contracts. In addition, an oil sidestream processor is being developed by Martin Marietta for possible use in the Barstow plant. Martin Marietta is developing internal insulation for tanks to store molten salt.

Summary

The schedule for the Program is shown in Figure 6. The Barstow pilot plant will provide large-scale design, construction, and operational data. The development of improved receivers and heliostats is being done on a time scale which will allow the resulting receivers to be incorporated in a repowering project scheduled to be constructed starting in FY 81.

Rapid technical progress is being made on the large central power concept. Projected energy costs for this concept are tending to be lowered as a result of improved performance and better, more manufacturable designs. The economic competitiveness of the large solar power concept depends, to a large degree, on the economic assumptions which are made. However, the relative position of solar options as compared to possible options is improving.

Rapid technical progress is being made on the large central power concept. Projected energy costs for this concept are tending to be lowered as a result of improved performance and better, more manufacturable desings. The economic competitiveness of large solar power concepts is improving rapidly.

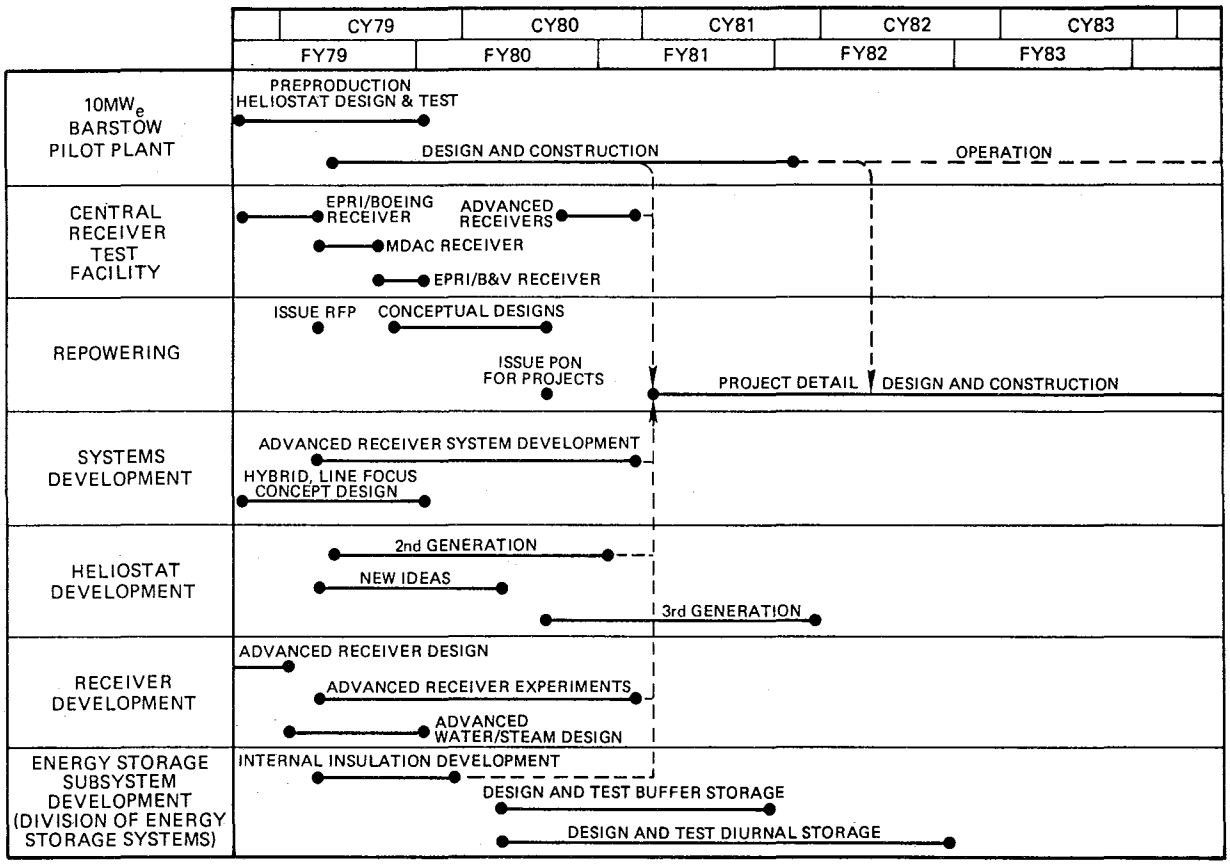

Figure 6. Large Power Systems Program Schedule

10 MW_e SOLAR THERMAL CENTRAL RECEIVER PILOT PLANT

R. N. Schweinberg
Department of Energy

J. N. Reeves
Southern California Edison Company

Background

The 10-MW_e Solar Thermal Central Receiver Pilot Plant is a large-scale experiment designed to provide data that will move solar powered electrical generation plants closer to technical and commercial feasibility. The necessary technology is either in hand or has been demonstrated in experiments and test facilities, but has not previously been integrated into a full system for operation in a utility context.

DOE Headquarters' responsibility for the project has been assigned to the Division of Central Solar Technology within the Office of Solar, Geothermal, Electric, and Storage Programs. A Solar Ten Megawatt Project Office (STMPO) has been established by the San Francisco Operations Office (SAN) with responsibility for the day-to-day planning, direction, execution, and control of the project within the approved envelope of technical objectives, cost estimates, and schedule milestones. The overall project costs, shown in Figure 2, are divided between DOE and the Associates. DOE is funding the solar facilities portion of the plant, and the Associates are funding the turbine-generator facilities. The Associates, comprised of Southern California Edison Company, the Los Angeles Department of Water and Power, and the California Energy Commission, are participating in the engineering management and construction of the project within the STMPO, in accordance with a cooperative agreement between DOE and the Associates. Figure 1 shows an artist's conception of the plant, which will be built on Southern California Edison property east of Barstow at Daggett, California.

The project schedule, Figure 3, shows that all the Major DOE design contractors (Martin Marietta of Denver, Colorado, and McDonnell Douglas Astronautics of Huntington Beach, California) started in September, 1978, on a thirteen-month competitive collector subsystem design phase, including preproduction hardware fabrication. One of these contractors will be selected in October, 1979, to fabricate the 1600 to 1800 heliostats for the plant. The third contract is for the design integration of the solar facilities with the turbine generator facilities and for the design of the remaining solar facilities, i.e., receiver, thermal storage, master control, and plant support. McDonnell Douglas of Huntington Beach initiated work

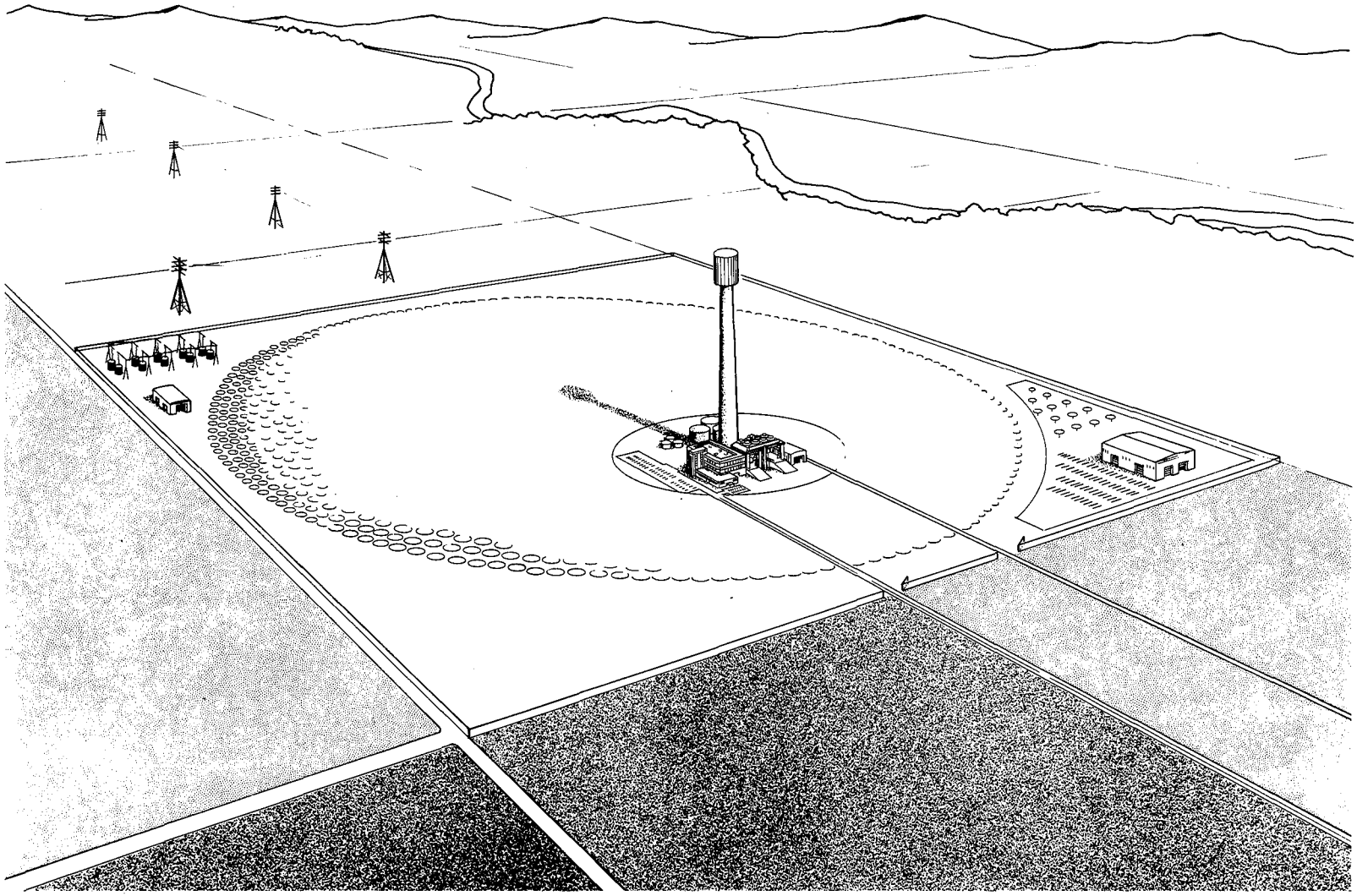

Figure 1. 10 Megawatt Solar-Electric Pilot Plant

Total Project	$123M
DOE	$108M
Associates	$ 15M

Figure 2

Design and Construction	
DOE Selects Site	January 1977
DOE Selects Plant Concepts	August 1977
Doe Selects Solar Designers	August 1978
Start Construction	June 1979
Doe Selects Collector Fabricator	October 1979
Complete Construction	March 1981
Initiate Plant Operation	September 1981
Initial Testing Period	
Five Years	

Figure 3. Project Schedule

as the Solar Facilities Design Integration (SFDI) in December, 1978. In addition to design, the SFDI will supply limited hardware items, e.g., control hardware, the receiver steam generator, and components with long lead times.

Collector Subsystem

The key features of each contractor's heliostats are shown in Figures 4 through 7. Starting in July, 1979, the preproduction hardware will be subject to a three-month evaluation and test program that consists of: (a) overall heliostat and control system evaluation at the Central Receiver Test Facility (CRTF) in Albuquerque, N.M., (b) structural drive assembly testing, (c) environmental drive assembly testing, and (d) optical characteristic and environmental testing of the mirror panels. Based upon the results of the preproduction unit performance and the contractor's production proposal, DOE will select one contractor in October, 1979, to fabricate, install, and check out the heliostats for the pilot plant.

Heliostat Glass

A contract for approximately one million square feet of low iron ($\approx$0.05%) float glass of one-eighth inch thickness has been awarded by DOE to the Ford Motor Company of Detroit, Michigan. Samples of this glass will be tested for flatness and solar energy transmittance (a minimum of 88 percent transmittance is required). This glass will be delivered to the selected heliostat contractor for mirroring and fabrication into finished heliostat panels.

Cloud Measurements

A need had been identified for high resolution measurements of insolation variations which might be expected at the pilot plant. These data are necessary to determine the thermal stresses in the receiver and control system transient requirements.

Insolation variations due to clouds have been continuously measured at the Barstow/Daggett plant site since the first of August, 1978. The actual insolation is monitored at 16-second intervals at 4 points along the perimeter of a representative size field. This monitoring was initiated by STMPO because no relevant insolation data of sufficient resolution is available from any other source. The experiment site is the evaporation pond area of the Southern California Edison Coolwater Generating Station, approximately 1/2 mile from the actual pilot plant site. The measurement equipment used are Lambda and Eppley pyranometers and an Eppley pyreheliometer mounted on a sun tracker. The data are automatically digitized and recorded for later computer-aided analysis at the Aerospace Corporation. Figure 8 shows the location of the insolation measuring devices (stations 1 through 4) and how they have been deployed. These stations are

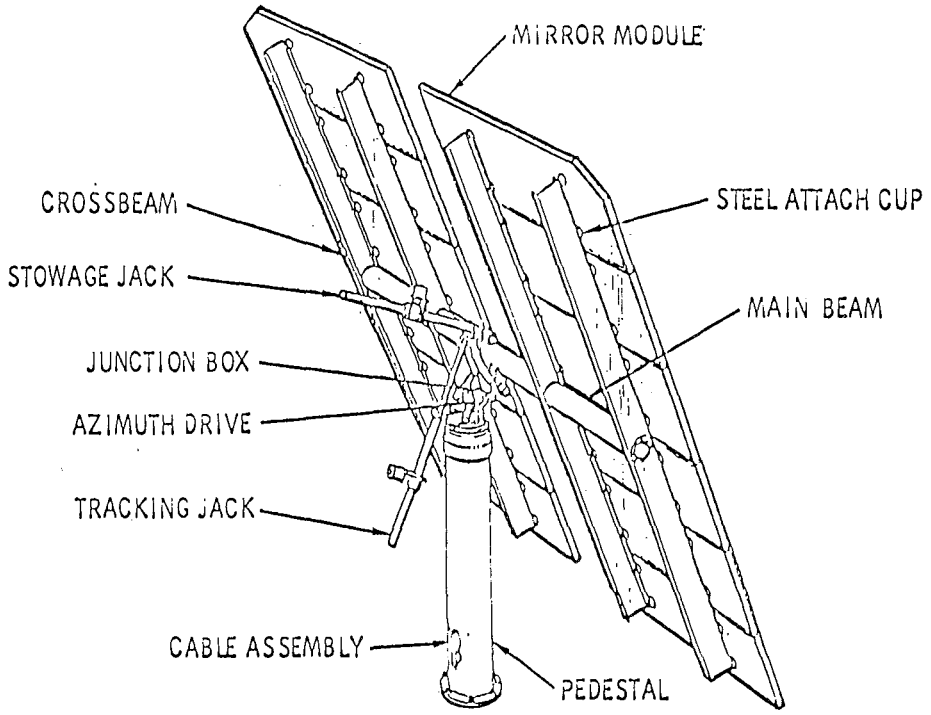

Figure 4. Heliostat Assembly

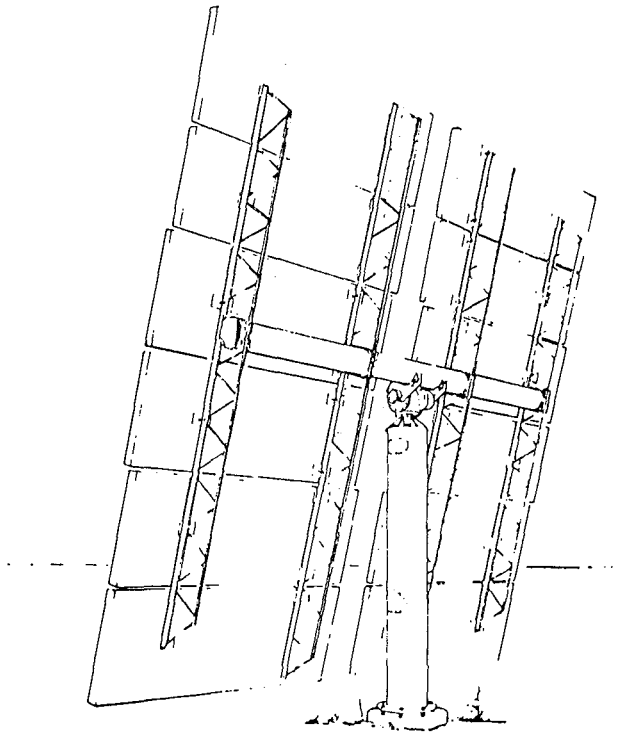

Figure 5. 10 MW_e Solar Pilot Plant - Heliostat

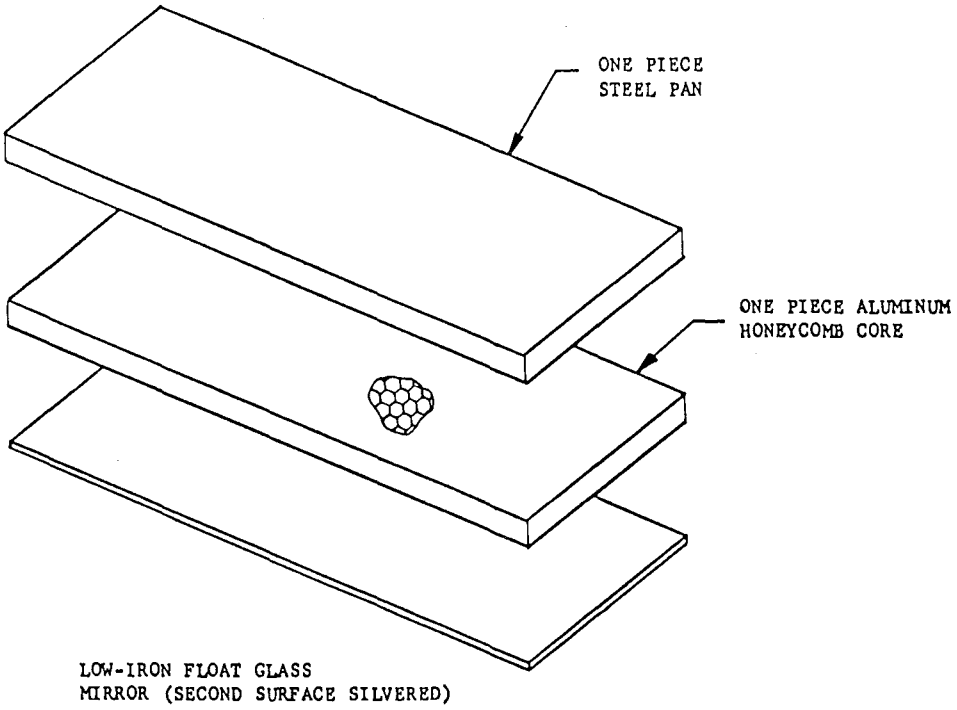

Figure 6. Exploded View of H neycomb-Core Mirror Assembly

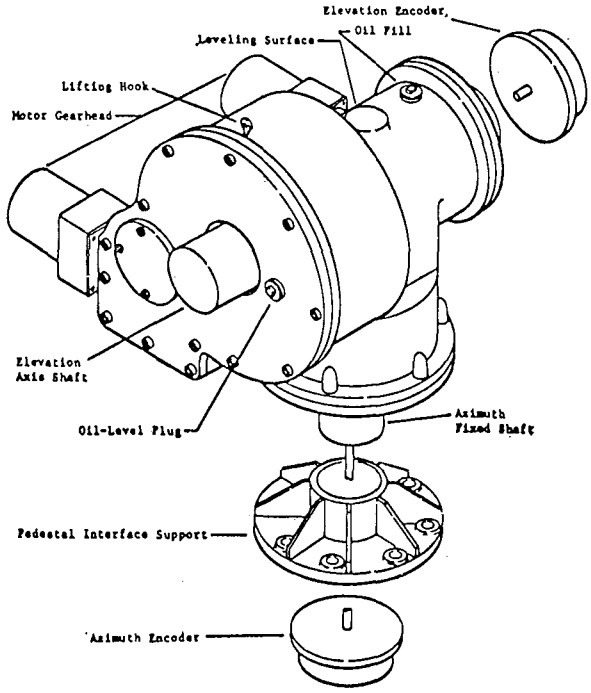

Figure 7. Heliostat Combined Azimuth and Elevation Drive

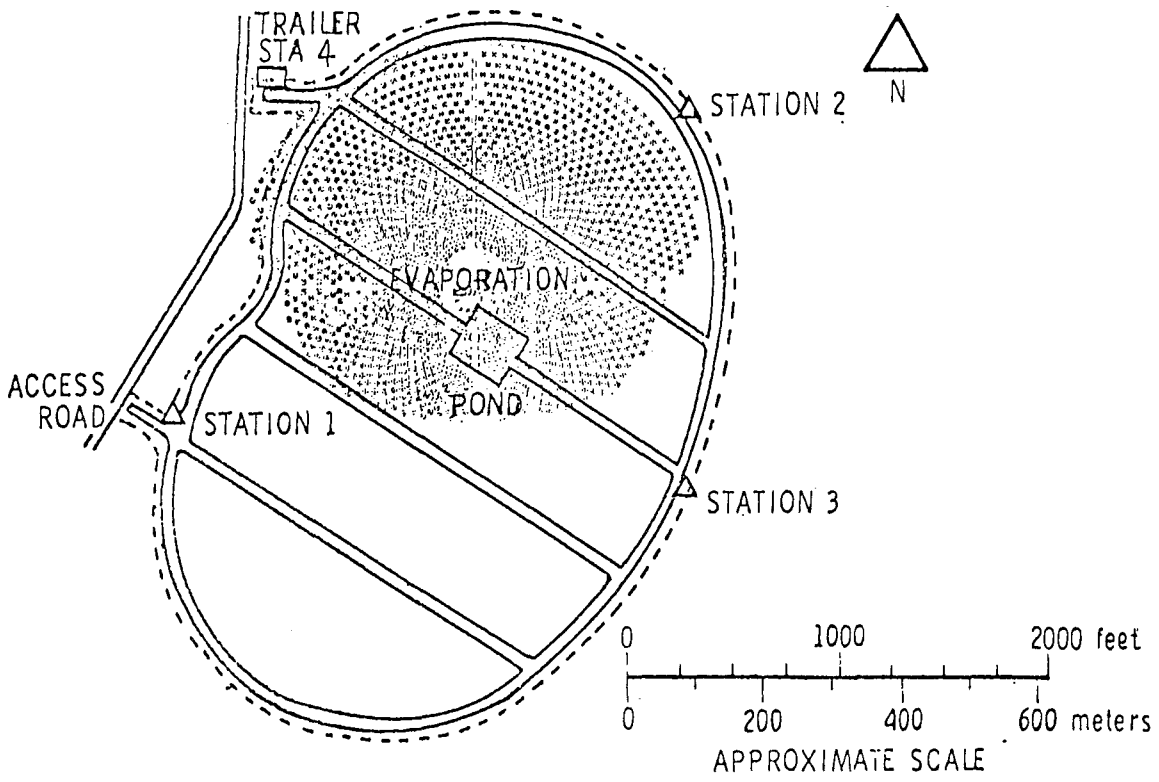

Figure 8. Daggett Insolation Variation Experiment Site

arranged to encompass an area approximately equivalent to that of the collector field for the pilot plant. The initial data analysis results are discussed in detail in an Aerospace report covering the first three months of experiment operations (Report No. ATR-79 (7747)-2).

Shown in Figure 9 is a summary of the data from the first month of experiment operation. The presence of a horizontal line indicates the insolation measurement experiment was operating. The heavy sections on the lines (e.g., much of August 21) indicate clouds were present that caused the insolation records to deviate from those expected for a clear day. (Either there was no direct insolation or the insolation was varying.) The cloud periods amounted to 8 percent of the daylight hours when the experiment was operational. Similar plots have been prepared for September and October and these indicate that 15 percent of the daylight hours were affected by clouds.

A quantitative measure of insolation variation will be required for the plant control system design. Since the expected variation was unknown at the beginning of the experiment, the initial review concentrated on a detailed analysis of four periods in August. The direct insolation recorded at station 4 during each of these four periods is shown in Figure 10. Note the temporal insolation variations can be very different. The insolation variations apparent from the analysis are illustrated graphically in Figure 11. This figure is a plot of the insolation observed at each of the four stations in the experiment as a function of time. It

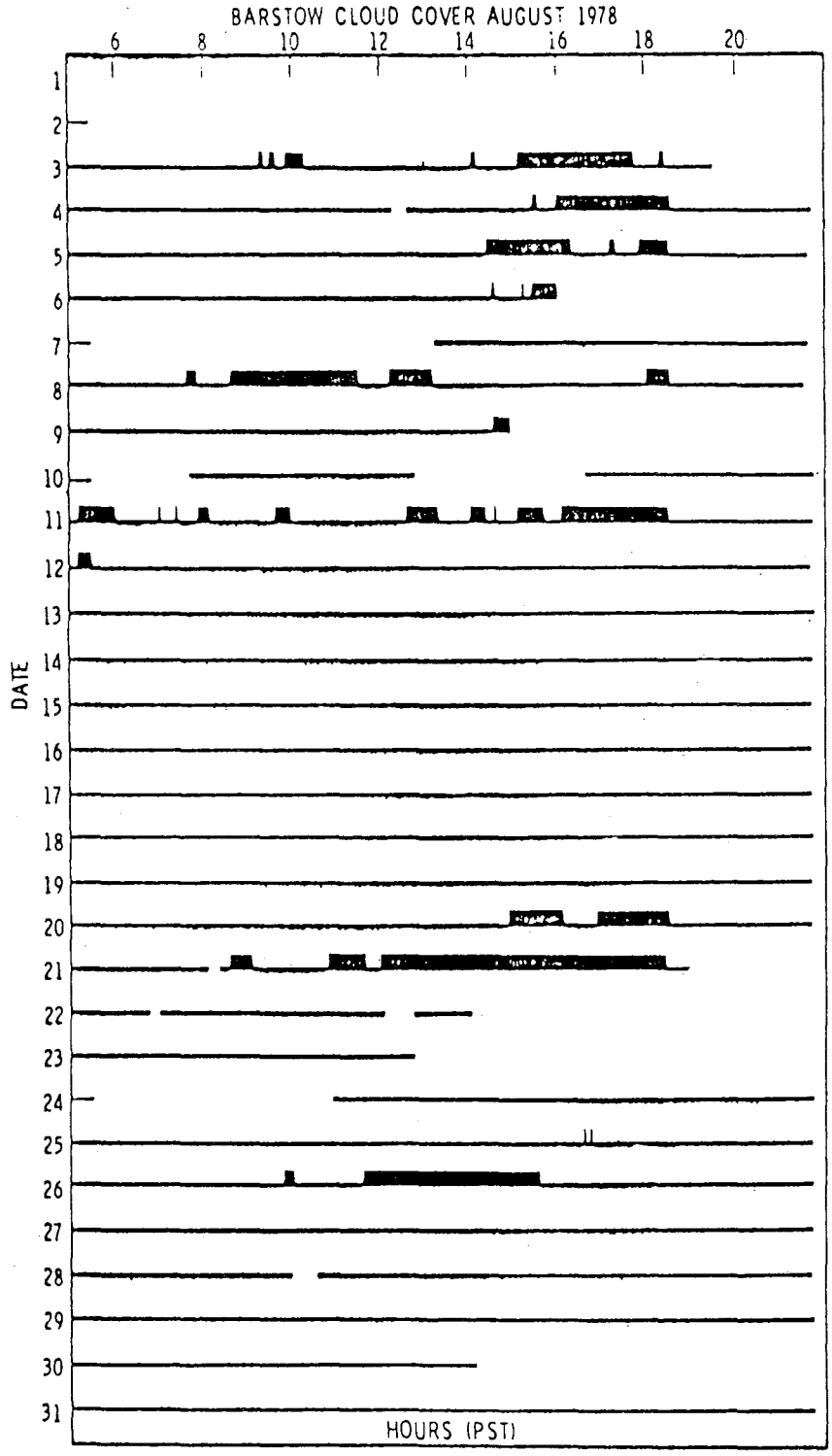

Figure 9. Insolation Variation Experiment
(Data Summary August)

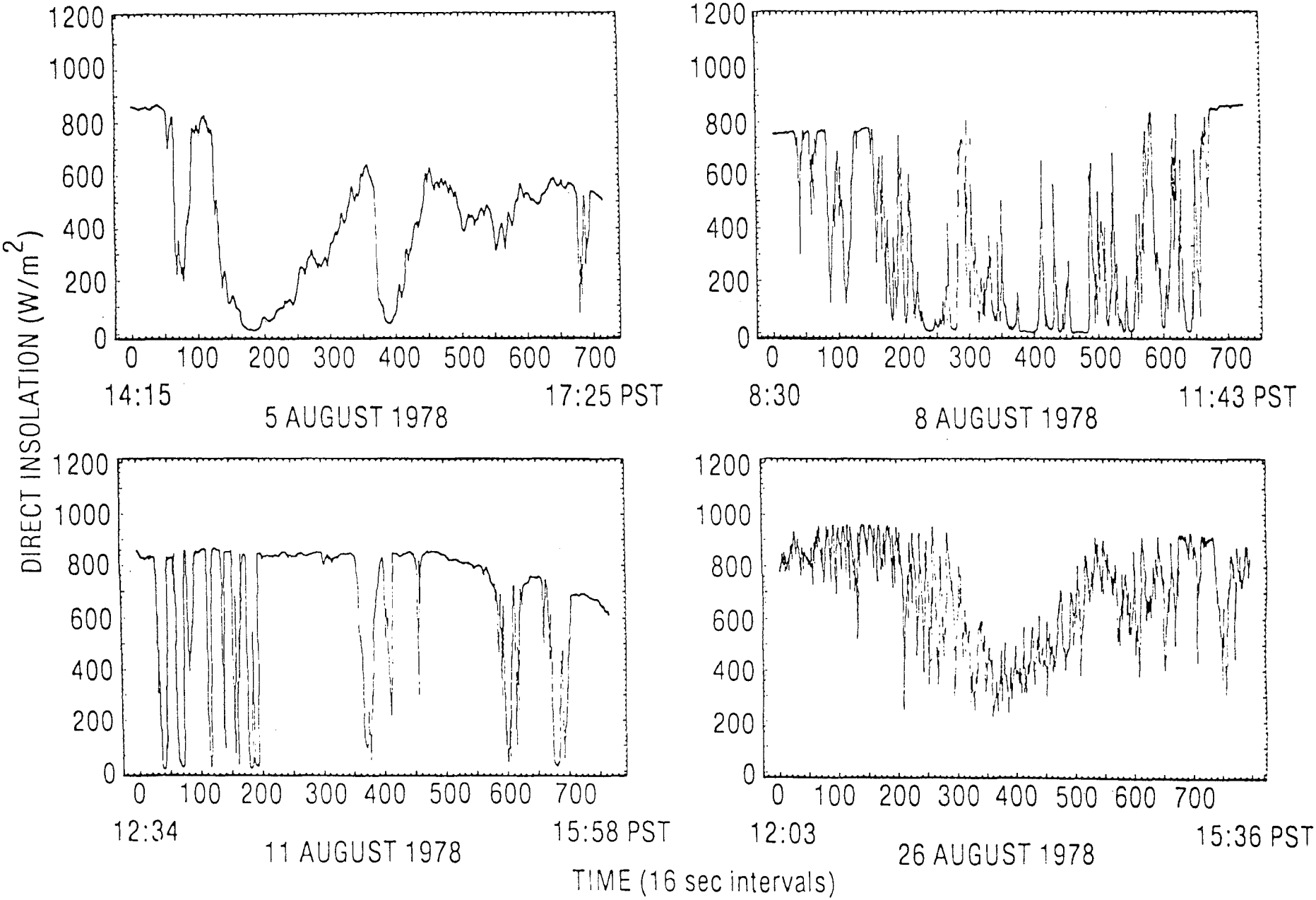

Figure 10. Direct Insolation (Daggett, California)

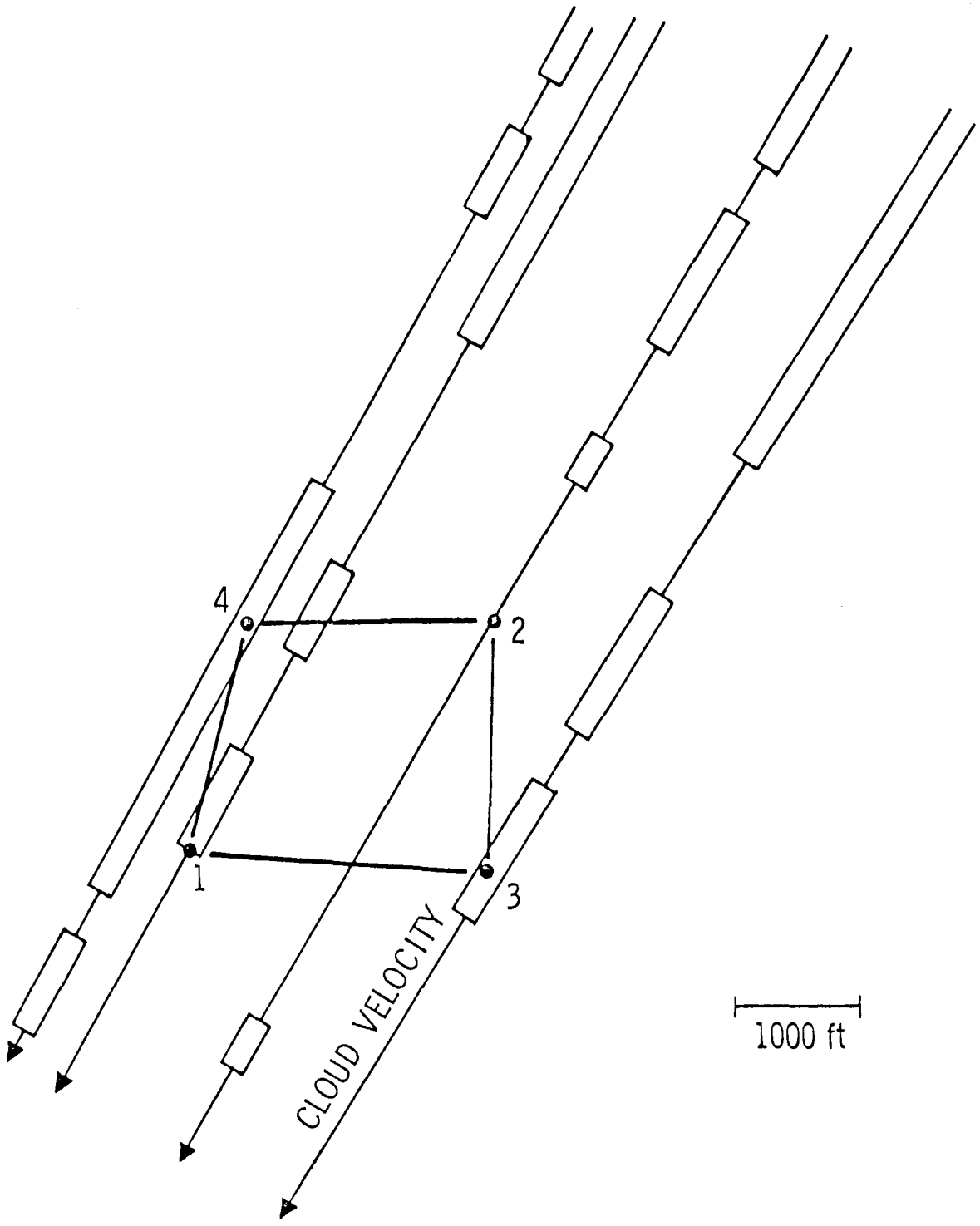

Figure 11. Cloud Shadows Passing Experiment
(August 8, 1978, Speed 9 m/s)

is presented in terms of a timed snapshot of the cloud shadows over and about to pass over the experiment, together with the effective cloud velocity vector derived from the data. The important point illustrated by this figure and supported by the analysis is that cloud shadows can be, and often are, smaller than the size of the collector field, and the various portions of the collector field are not affected simultaneously. Thus the semi-infinite cloud which has been used in initial pilot plant transient analysis studies is not representative and actually may lead to incorrect assumptions. The conclusions derived from the experiment to date can be summarized as follows:

- Clouds could be present up to 15 percent of the time during the fall months.
- Shadow dimensions smaller than the collector field will be present.
- Rates of insolation change greater than 30 $W/m^2/s$ have been measured.
- Spacial averaging over the collector field reduces the rate of insolation change on a receiver panel but increases overall outage time.
- Active cloud monitoring activities must be performed by the plant operators.

The data during the fall months indicate a much higher frequency of variations of solar insolation than were previously expected. These variations indicate that the velocities are sometimes greater than the 30 mph previously expected, and therefore the thermal transients on the receiver may be very significant. The data does indicate, however, that insolation averaging over the entire field acts to mitigate the problem somewhat. Control strategies for unloading the south field in the event of shadows in the north field may have to be implemented in the master control subsystem software. The measurements analyzed thus far also indicate that there will likely be a need for weather observations by the plant operator throughout the day in order to determine which of the various plant's operating modes should be used for changing cloud coverage conditions.

Construction Packages

DOE is encouraging small business participation in the pilot plant construction activities by setting aside all construction packages estimated at two million dollars or less for small business bidding. There are eleven DOE prime construction packages currently planned, and their costs are estimated at 30 million dollars. Of these eleven packages, eight are set aside for small business; their total estimated costs are 40 percent of the overall construction costs, or 12 million dollars.

Townsend and Bottum, Inc., of Ann Arbor, Michigan, has been selected as the Construction Manager and will manage all the DOE prime construction contractors at the Daggett site.

Accomplishments and Planned Activities

The accomplishments since the last meeting and the activities planned for the near future are shown in Figures 12 and 13, respectively.

• Collector Design Work Initiated With Martin Marietta and McDonnell Douglas	Sept 78
• Collector Production Glass Ordered From Ford Motor Company	Dec 78
• SFDI Design Work Initiated by McDonnell Douglas	Dec 78
• Turbine-Generator Facility Design Initiated by Southern California Edison	Dec 78
• Visitor Center Design Completed	Jan 79
• FAA Approval Obtained for Receiver Tower	Jan 79
• Small/Minority Business Briefings in Los Angeles, San Bernardino, and Barstow	Feb/Mar 79
• First Project Technology Transfer Meeting	Mar 79

Figure 12. Recent Accomplishments

• Start Construction - Visitors Information Center	June 79
• Award Contract for Turbine-Generator	July 79
• Initiate Heliostat Evaluation and Test Program	July 79
• Complete Heliostat Evaluation and Test Program	Sept 79
• Select Collector Production Contractor	Oct 79
• Start Plant Construction	Oct 79

Figure 13. Key Activities Next Six Months

Turbine-Generator Specification and Procurement

The turbine-generator specification has been completed, but final approval is pending because of reviews being conducted by McDonnell Douglas Astronautics Company (MDAC). As the SFDI, MDAC is reviewing the steam cycle heat balance and considering alternate configurations which could change the design parameters for the turbine-generator. It is estimated that this work will be completed by March 30, 1979. Allowing for revisions of the specification, if necessary, approval and bid issuance is planned for April 15. Proposal receipt, evaluation, and negotiation activities will cover the next 3-1/2 months, leading to a contract award for the turbine-generator on August 1, 1979.

There are several unique aspects of the turbine-generator requirements, such as the fact that a 10-MW_e net unit is unusual for electrical utility applications. In addition, the specification must reflect a level of uncertainty in the procurement parameters because the heat balances and process-cycle definitions are the responsibility of the aerospace-oriented SFDI, who is inexperienced in utility practices, procedures, and methods. The specification must allow for negotiated revisions and compensate for those uncertainties.

The turbine-generator requires a dual admission configuration (Figure 14). Two steam throttles using receiver steam and thermal storage steam are required. There will be a governor system for dual steam inputs suitable for throttle valve ratio control between steam sources. Even though it is a small unit, there are to be four steam extraction ports for feedwater heating. The electrical rating that the turbine-generator must currently meet is as follows (note that thiese figures are in gross MW_e):

12.5 MW_e gross - using receiver steam

8.0 MW_e gross - using thermal storage steam

2.5 MW_e gross - minimum output

Seven steady-state operating modes with transitions impose restrictions on unit design, particularly for startup/shutdown scenarios with varied transitions between steam sources. The machine must have a fair tolerance to temperature, pressure, and flow variations to operate from the:

(a) receiver only;
(b) thermal storage only;
(c) receiver and thermal storage;
(d) receiver, while charging thermal storage;
(e) thermal storage, while the receiver is charging thermal storage; and
(f) receiver and thermal storage, while also charging thermal storage.

The final mode calls for the receiver charging thermal storage without the turbine-generator operating. There is potential variance in main (RS) steam conditions due to the once-through boiler response to solar transients (e.g., clouds).

Dual Steam Throttle Ports:

- Primary, utilizing Receiver Steam ± 1465 psia, 950°F
- Secondary, or Admission Utilizing Thermal Storage Steam @ 400 psia, 525°F

Governor System(s) for Dual Steam Inputs Suitable for Throttle Valve Ratio Control Between Steam Sources

Four Extraction Ports for Feedwater Heating

- L. P.
- Deaerator
- Two H.P.

Electrical Rating:

- 12.5 MW_e Gross When Using Receiver Steam
- 8.0 MW_e Gross When Using Thermal Storage Steam
- 2.5 MW_e Minimum Output

Application Life: - 5 Years

Operational Constraints

- Daily Start-up and Shutdown
- Transitions Between Steam Sources

} Thermal Cycling Limitations?

- Once Through Boiler Implications, e.g., Limited Boiler Turndown and Resultant Water Ingestion Potential
- Back Pressure 2.5 in Hg Nominal

Figure 14. Turbine Generator Design Criteria

Technology Transfer Program

The technology transfer program was developed to promote public and institutional knowledge and acceptance of solar energy systems. Among the programs being developed to disseminate solar thermal technology are two committees--the Project Advisory Committee and the Project Review Committee. These committees will provide for design and operating reviews with potential users, such as utilities, related-equipment manufacturers, and architect-engineer firms. The Project Advisory Committee, listed in Figure 15, will initially meet semi-annually, and then quarterly during construction and operational testing. Members will be

able to input continuing program appraisals. Each year one of these meetings will be designated the Annual Technology Review Meeting and will have a combined attendance of the Project Advisory Committee and the Project Review Committee. This annual meeting will provide members with a full project examination including a site tour as appropriate, and a comprehensive project report will be published.

The First Annual Technology Review Meeting was held in Los Angeles on March 15, 1979. The 60 attendees represented the project participants (SCE, LADWP, CEC, and DOE) and their contractors (McDonnell Douglas Astronautics Co., Martin Marietta Corp., and Townsend and Bottum), along with representatives of approximately 30 organizations. Of this group of 30 potential users of solar thermal technology, half are already members of either the Project Advisory Committee or the Project Review Committee, and the remainder of the group attended to aid in formulating their decision regarding joining.

A. Project Advisory Committee

1. Tucson Gas and Electric Company
2. Colorado-Ute Electric Association, Inc.
3. Nevada Power Company
4. Bonneville Power Administration
5. Johnson Controls, Inc.
6. Bechtel Power Corporation

B. Project Review Committee

1. Sacramento Municipal Utility District
2. Pacific Gas and Electric Company
3. Public Service Company of Colorado
4. Hawaiian Electric Company, Inc.
5. The Washington Water Power Company
6. City of Tacoma, Department of Public Utilities
7. Bureau of Reclamation, Lower Colorado Regional Office
8. Public Service Company of New Mexico
9. Stone and Webster Engineering Corporation

Figure 15. Technology Review Committees

Through the establishment of these two committees we hope to accelerate the dissemination of the technology advances, and to give the participants completely current information, along with "hands-on" experience for their own applications.

Presentations will cover the progress of all phases of the project--including design, construction, startup, operation and maintenance, and testing of the pilot plant. These presentations will be enhanced by providing site tours for graphic demonstrations. In addition, the participating organizations will have the opportunity to select from a listing of project documents, which will be made available to them as they are developed (Figure 16).

Department of Energy	Associates
Design	**Design**
Overall Plant Design Description	Turbine-Generator Specification (all related equipment specifications)
System Specification	Site Related Data
Subsystem Specifications	**Operation**
Safety Analysis	Operations Manuals
Solar Insolation	Power Generation Test Data
Plant Simulation Data	**Cost**
Testing	Cost/Schedule Information (design, operation, and maintenance)
Test Plan	**Licensing**
Test Specifications	Environmental Impact Report
Operating Procedures	Licensing and Permit Applications
Cost	**Miscellaneous**
Cost Breakdown Structure	California Energy Commission Activities
Recurring and Non-Recurring Costs	Public Information Literature (brochures, films, fact sheets, educational materials)
FERC Code of Accounts Format	
Schedule	
Overall Project Schedule	
Subsystem Schedules	

Figure 16. Project Document Listing

Licensing/Regulatory Activities

The permit acquisition for the solar pilot plant is basically Edison's responsibility. DOE's construction manager, Townsend and Bottum, will be obtaining those construction permits required for activities under their supervision. The permit requirements are simplified for this pilot plant because it will be less than 50 MW. It does not require the California Energy Commission's site certification nor the California Public Utility Commission's Certificate of Convenience and Necessity. Because there will be no combustion in the solar pilot plant, and therefore no emission of air contaminants, the project has made the assumption that authorization to construct is not required from either the Air Quality Management District or from the Environmental Protection Agency.

Approvals obtained to date include the Federal Aviation Administration's (FAA) air navigation and heliport determinations. An application for airspace approval for the receiver tower was submitted because of the tower height (352 feet above ground) and its close proximity (3 nautical miles) to the Barstow-Daggett Airport. A study conducted by the FAA determined that the tower would not be a hazard to air navigation provided it was marked and lighted appropriately. The establishment of a heliport for private use also received approval for use during visual flight rules conditions only. San Bernardino County approved the zoning change and site plan. Additional permit requirements to be obtained from the county include grading and building permits, and fire protection review. Certain construction activities will require permits from the California Occupational Safety and Health Administration (Cal OSHA) and the pressure vessels permit will need to be obtained from the State Department of Industrial Relations, Division of Industrial Safety.

500 kW_e CENTRAL RECEIVER SYSTEM (CRS) OF THE IEA SMALL SOLAR POWER SYSTEMS PROJECT (SSPS)

Wilfried Grasse
International Energy Agency (IEA)

Introduction

The SSPS Project consists of a central receiver system (CRS) plant and a distributed collector system (DCS) plant with similar outputs that are constructed adjacent to each other in the Province of Almeria, Spain. The main objective of the project is to demonstrate, within about two years, the technical feasibility of operating a solar power plant in an interconnected grid as well as in the stand-alone mode. Therefore, both plants are demonstration pilot plants rather than test facilities.

The project was activated by the International Energy Agency (IEA), Paris, and is performed by the DFVLR, acting as Operating Agent on behalf of ten IEA member countries: Austria, Belgium, Germany, Greece, Spain, USA, Sweden, Switzerland, and--during Stage 1 of the project--Italy and United Kingdom. The United States contribution to SSPS was 22% in the design phase and is planned to be again about 22% in the hardware phase. Supervision authority is exclusively with the SSPS executive committee, in which each member country has one vote.

CRS - Design

Early in October 1978 the CRS-Consortium, headed by the German company Interatom, presented the final design. This design is characterized by:

- A heliostat field of 160 Martin-Marietta third-generation heliostats that use curved mirror facets in five different focal lengths and deliver 4.2 MW through the aperture (equinox noon).
- A cavity-type sodium receiver with an aperture of 3 x 3 m. The tube bundle is arranged as a vertical half cylinder, and the outlet temperature of the sodium is 530°C

- A one-loop heat transfer system with a hot and a cold sodium storage tank and a steam generator. According to the basic SSPS requirement, all components of the sodium loop are proven technology.

- A power conversion subsystem very similar to that of a conventional steam power plant. The proposed prime mover is a condensating steam turbine (100 bar, 500°C) with three bleeding points.

- A control system similar to conventional power plants, with an operator in the control loop.

During the design phase, a detailed performance and cost analysis was presented. The projected cost of the design as described above turned out to be greater than the financial contributions participating countries are able to make. Therefore, cost reduction possibilities have been investigated both by the operating agent and the contractor (see Figure 1). As a result:

- The design point was changed to equinox noon with 920 W/m^2 insolation, which resulted in a field of 200 heliostats, delivering now 2.7 MW_{th} energy input into the cavity instead of 4.2 MW_{th}

- Energy storage capability was reduced from 2 MWh to 1 MWh

- Design lifetime is now 10 years instead of 30 years

- A less sophisticated prime mover will be selected and proposed.

Status of CRS Stage 2

According to current planning (see Figure 2), the hardware phase (stage 2) of SSPS Project will start on June 1, 1979. Manufacturing, erection, and acceptance will be accomplished within 24 months. Accordingly, the CRS plant could be put into operation in the summer of 1981, together with the distributed collector system.

Due to various reasons, some problem areas still have to be solved before a signature of all participating countries can be assured.

Heliostat Field

Contrary to all other subsystems in the CRS, a final recommendation for the heliostat supplier has not been made yet. In principle, four suppliers would be able to match SSPS schedule: Martin-Marietta, McDonnell Douglas, SENER (Spain), and MBB (Germany). To make maximum use of the stage 1 heliostat design, DFVLR prefers to have an American supplier, and therefore has invited the two companies to submit their proposals. So far, no positive answer has been received.

SPECIFICATION	STAGE 1 FINAL DESIGN	STAGE 2 DESIGN
POWER OUTPUT	500 KW_E AT 700 W/M^2 V_{NOM} : + 10 %/- 5 % Hz : + 5 %/- 3 %	500 KW_E AT EQUINOX NOON ($920\ W/M^2$) ——
POWER DELIVERY	UTILITY GRID SUBSTITUTE LOAD	——
ENERGY STORAGE	EQUIVALENT TO 2 MWH AVAILABLE UP TO 24 H AFTER FULLY CHARGED, TO BE LOADED UNDER FULL, PARTIAL, ZERO EL. OUTPUT	EQUIVALENT TO 1 MWH —— ——
OPERATIONAL MODES	INSOLATION ONLY INSOLATION AND STORAGE STORAGE ONLY	——
OPERABILITY - INSOLATION $[W/M^2]$ - WIND [KM/H] - EARTHQUAKE - HAIL [MM]	FULL: 1100 / 18 / 0,03 M/S^2 REDUCED (50 %): - / 50 / 0,3 M/S^2 SURVIVAL: - / 144 / 0,6 M/S^2 / 19 AT 20 M/S	——
AVAILABILITY	95 % AT 700 W/M^2 OR MORE	(OPEN)
LIFETIME	30 YEARS	10 YEARS
LAND USE FACTOR	LESS THAN 20 %	——
COOLING	EVAPORATIVE WATER COOLING MAX. 1.5 LITER OVER 15 HOURS	——
SAFETY PRECAUTIONS	EMERGENCY POWER DEFOCUSSING DEVICES INDEPENDENT SAFETY INSTRUMENTATION ALARM AND PROTECTION SYSTEMS	——
SERVICE INTERVALS	EQUIV. TO STATIONARY INDUSTRIAL EQUIPMENT	——

Figure 1. Central Receiver System (CRS) Changes After Stage 1 Design

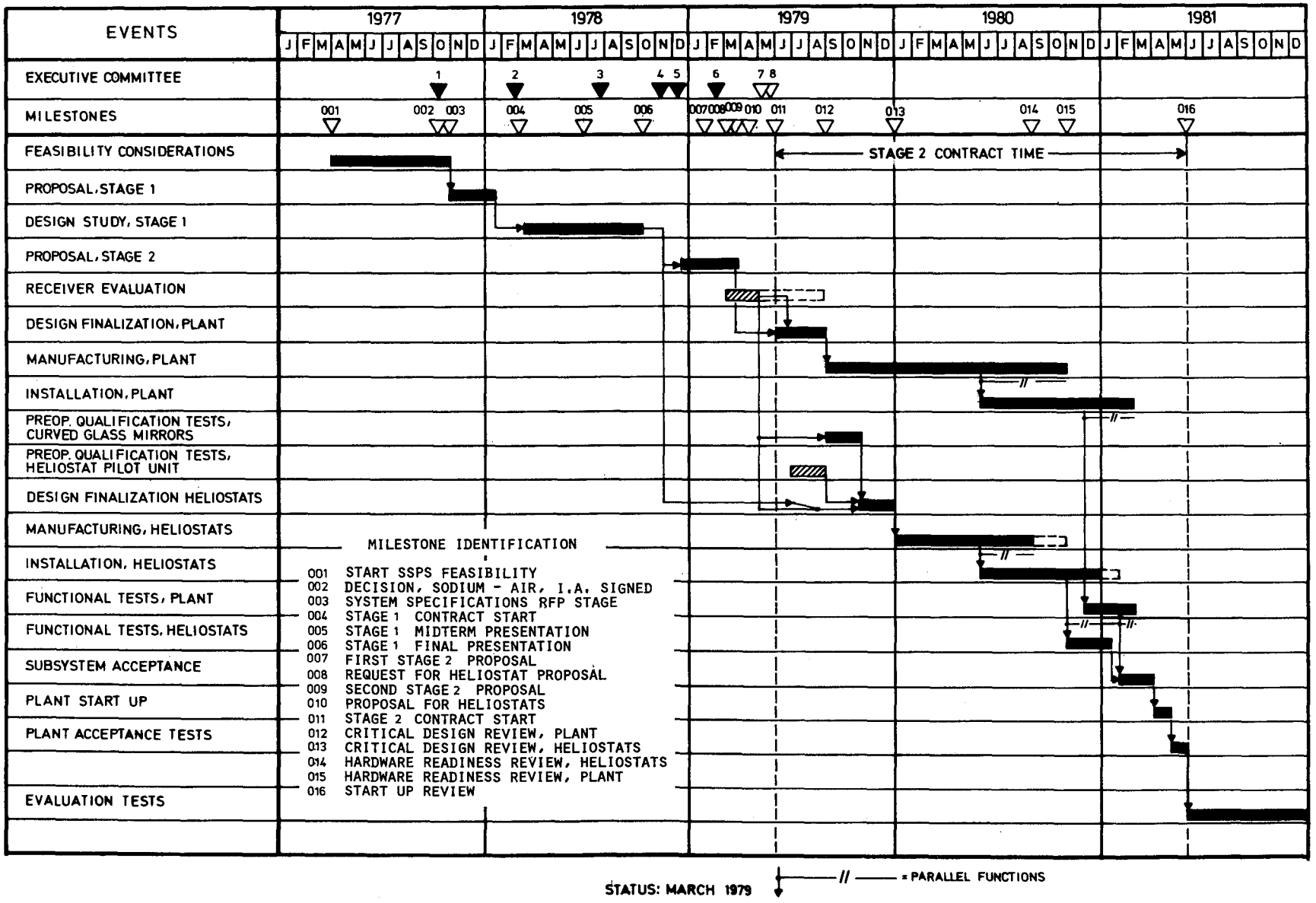

Figure 2. Time Schedule for CRS-Project

Sodium Receiver

Because the receiver performance and lifetime have to be guaranteed by the stage 2 contractor, the proposed operation assumptions are rather conservative: peak heat-flux 0.63 MW/m^2; average heat flux: 0.16 MW/m^2. Very recently, DOE expressed its wish to examine this design in view of a possible increase of that receiver's potential for providing data necessary for designing sodium receivers to be used on larger systems. A working group was established to investigate such possibilities. This investigation indicated that it is probable that after the guaranteed term, a 50 percent higher heat flux (up to 1 MW/m^2) could well be applied. This flux could be used in a test program applicable to high-power, high-flux systems. It is the task of this working group to provide relevant inputs for the design finalization early in stage 2.

Prime Mover

In relation to the total system costs, the proposed turbine seems to be too elaborate and very expensive. As an alternative, a steam-driven piston motor was proposed by the contractor. Efficiencies are comparable with those of the turbine (net efficiency of the power conversion system: 24,3 for a four piston motor, 25,5 for a five piston motor, and 24,8 for the turbine). Provided that no major disadvantages are found, a considerable price reduction for the PCS seems to be obtainable.

Summary

Stage 2 of the CRS should begin on June 1, 1979, even if the heliostat field cannot be procured until later this year. Therefore, DFVLR, acting as operating agent for the SSPS Project, will include this recommendation in its final stage 2 report to be submitted by April 24, 1979.

OPERATION OF THE CENTRAL RECEIVER TEST FACILITY

B. W. Marshall
Sandia Laboratories, Albuquerque

Activities During Past Six Months

Elevating Module

Repair of the 100-ton tower elevating module was completed on December 22, 1978. The module was damaged on September 20 when a contractor's hoist system, installed in the tower to erect the MDAC receiver panel on the module, failed during load tests. This failure allowed approximately 44,000 pounds of test weights to drop about 30 feet onto the module roof. The top one-half of the module had to be almost entirely rebuilt. Demolition started on October 9 and rebuilding started on November 6. Test weights were placed on the reconstructed module and lifted to the tower top on December 15-17. This load testing completed the rebuilding and qualified the module for use with the MDAC receiver panel. Re-installation of computer and instrumentation equipment, none of which was damaged in the incident, was completed in mid-January.

Heliostat Operation

Operation of the facility to perform the EPRI/Boeing tests has provided additional data on heliostat operation and maintenance. During these tests, over 12,000 heliostat-hours of operation were accumulated and the total now exceeds 55,000. In the same period, on the average less than 10 percent of the heliostats were inoperable, with maintenance concentrated on the heliostats used in these tests. Figure 1 is a summary of these data along with the cumulative repair totals for the heliostats.

During the past six months (September-February), 85 heliostat units were repaired, whereas in the prior six months 137 were repaired. The heliostat control electronic (HCE) units are now the major cause of heliostat failure, with moisture in the HCE box and component failure the primary problem areas. Repair of drive units has decreased significantly. Moisture accumulation in the drives is now seldom encountered, with encoder misadjustment now the primary cause of drive failure. In addition, numerous intermittent problems are encountered when the heliostat field is operated at low ambient temperatures (e.g., -16°C). Overall, the corrective actions taken to date in the repair and maintenance program appear to be successful in that no significant failures of components which were replaced

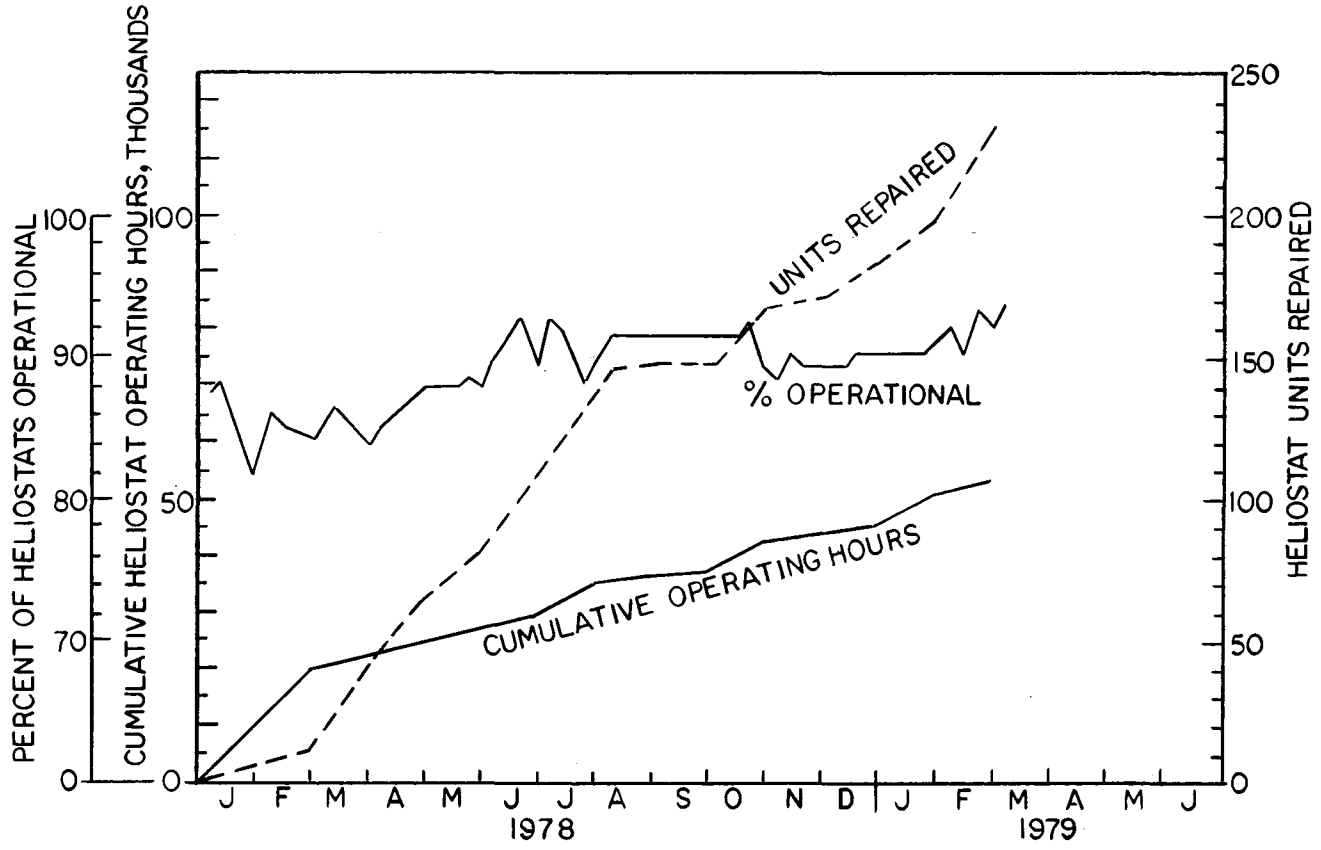

Figure 1. Heliostat Operational History

during earlier repairs have been observed. However, in some cases, other components in the same unit have been replaced in repeated repair operations.

Two portable anemometer stations were installed in the heliostat field. The instruments record wind speeds and direction at 15-minute intervals and are presently positioned directly north of the tower. One is located about 4 m above the ground (just below the stowed heliostat surface) and the other about 5 m above the ground (just above the stowed heliostat surface). In December, wind speeds of 96 mph at the 61-m level and 60 mph at the 10-m level were measured by anemometers on the metro tower. The heliostats were in stow position and no damage or effect on subsequent heliostat field operation was seen.

Reflectivity Measurements

Weekly reflectivity measurements on mirror samples mounted throughout the heliostat field were continued. Figure 2 presents the resulting data together with general notations of precipitation and weather. These data are obtained by taking the samples to a Sandia optics laboratory and measuring the reflectivity at carefully repeated locations. The reflectivity is measured at a single wavelength (0.5 m), and the solar average reflectivity is calculated using an empirical relationship which has been confirmed by measured data.

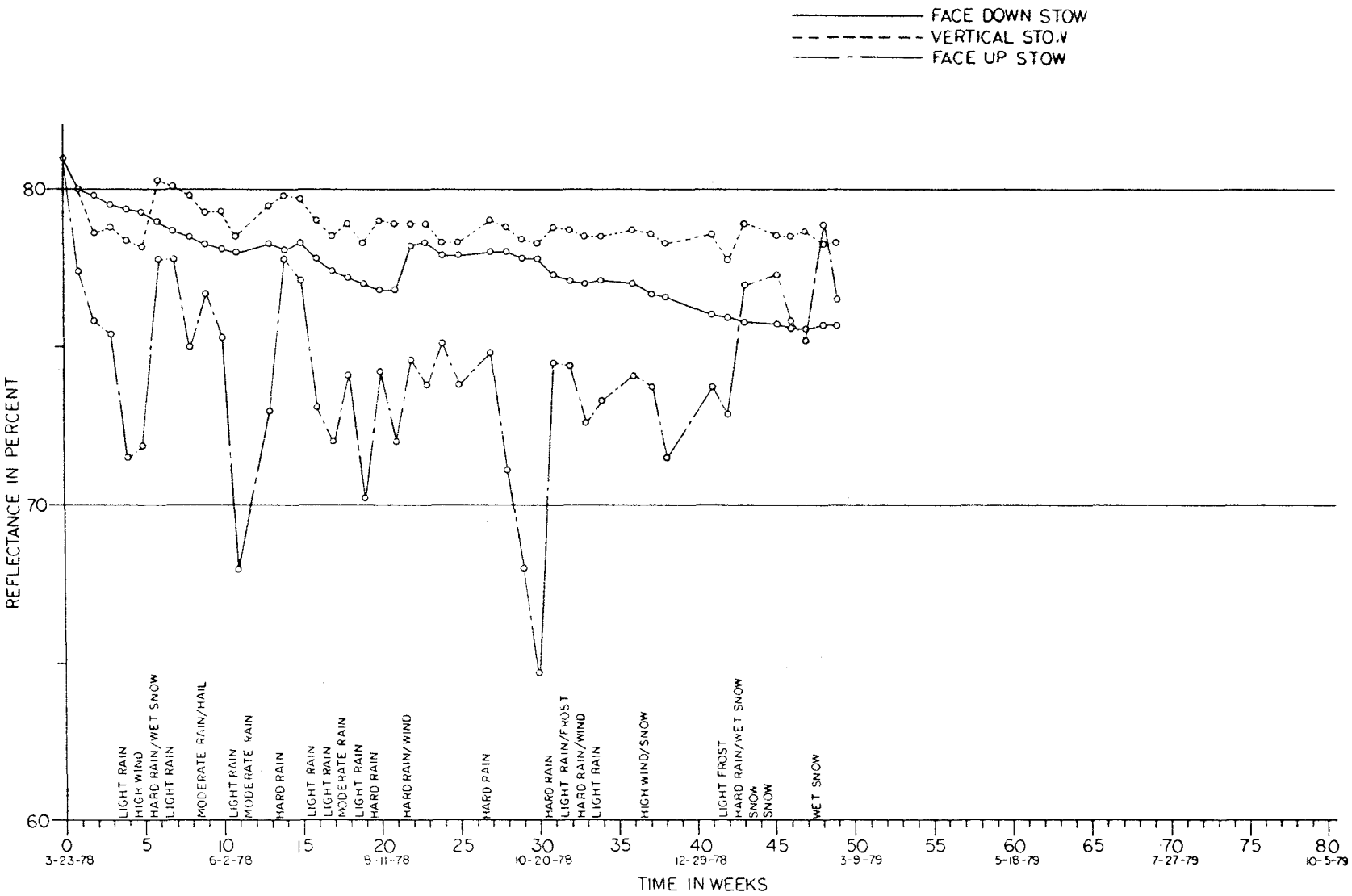

Figure 2. Reflectance Versus Time for Different Storage Orientations in CRTF Heliostat Field

Recently, in-field reflectivity measurements on actual heliostat surfaces were initiated using a Sandia-designed portable reflectometer. Only limited measurements have been made but the initial data generally agree with the 75 to 79 percent values resulting from laboratory measurements made on the samples. Modifications to improve the field use of the instrument are under way, and correlation with laboratory measurements will continue.

Two heliostats were positioned with their mirror surfaces upward about 15 degrees from horizontal during a recent rain. The rain lasted about 6 to 8 hours and produced 17 mm of precipitation. Figure 3 shows one of the "washed" heliostats and an adjacent "unwashed" heliostat which remained face-down during the rain. Visually, the rain was highly effective in removing dust and spots from the surface, and reflectivity measurements made the following day confirmed this observation. Figure 4 presents measured data for the stowed, unwashed heliostat and the rain-washed heliostat. The higher mean reflectivity and lower standard deviation of the data for the washed mirror illustrate the effects of naturally washing the mirrors. The mean reflectivity of the washed mirror returned to within 1 percent of the original, laboratory clean value. Based on these results, all of the field, except the north two rows which were retained for control purposes, was turned up in a more recent rain.

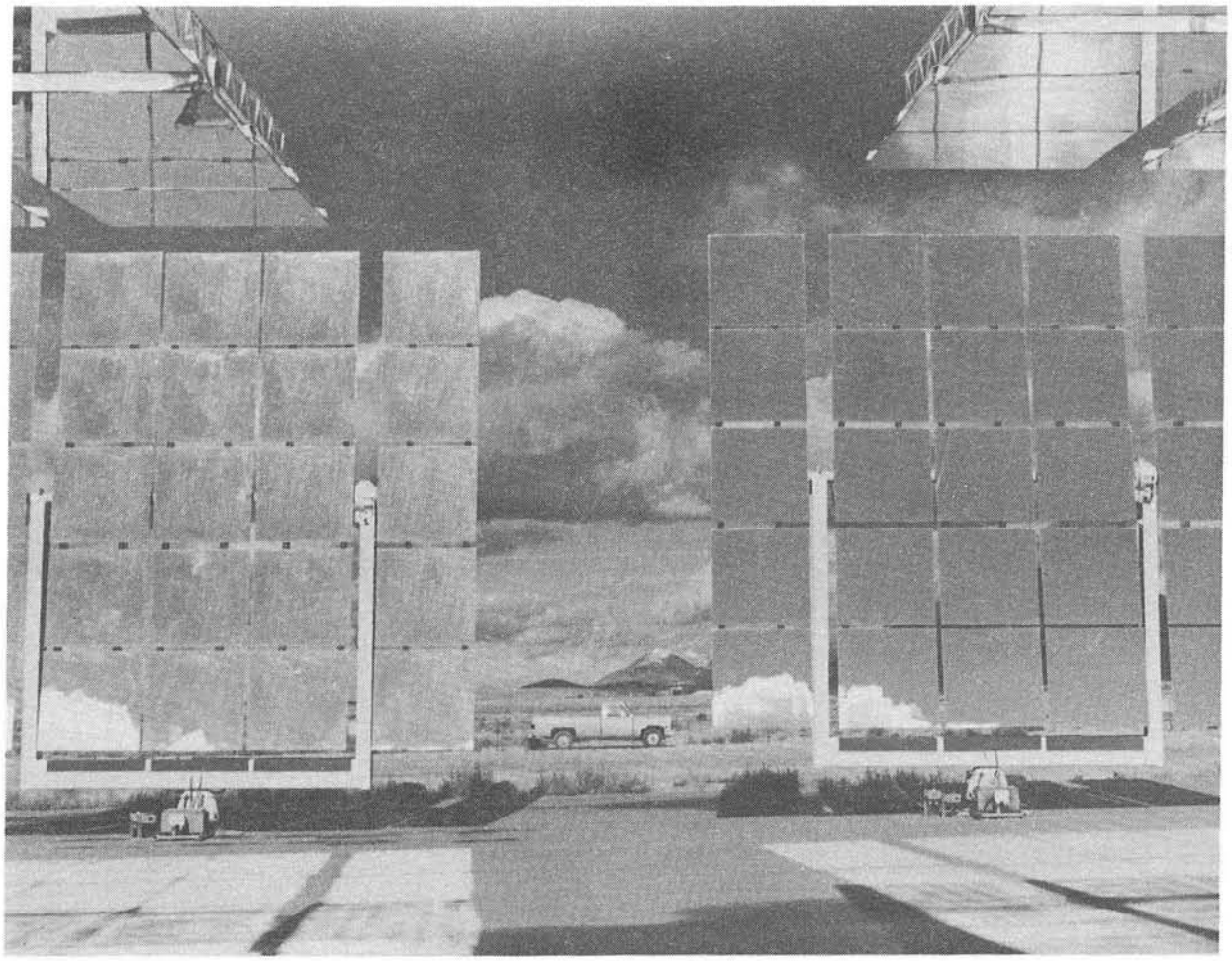

Figure 3. Rain-Washed Heliostats (Unwashed heliostat on left for comparison)

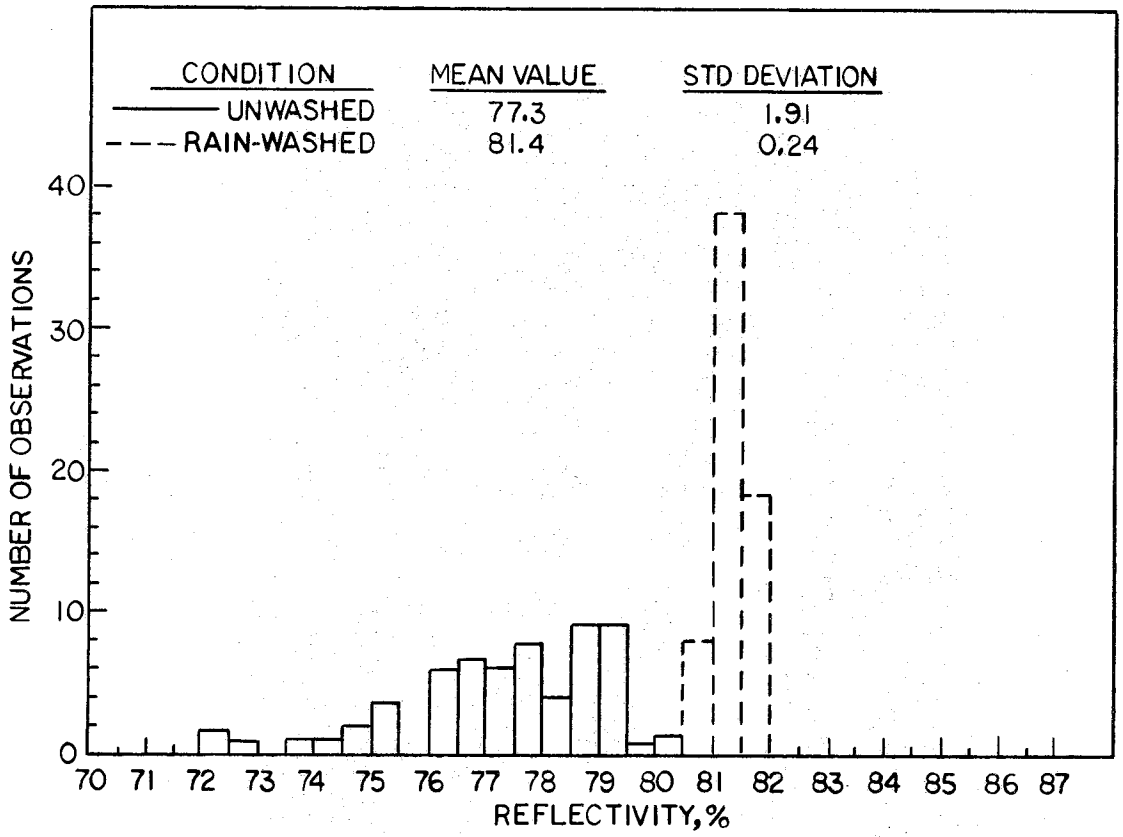

Figure 4. Reflectivity Data for Unwashed and Rain-Washed Heliostats

Tests on EPRI/Boeing Receiver

A reduced test matrix for this air-cooled, 1-MWt bench model receiver was completed on January 31. Initial solar checkout of the receiver occurred on October 27, and testing continued throughout the period as operational considerations permitted. Figure 5 illustrates the portion of the heliostat field used in the initial solar testing, and Figure 6 summarizes the operational experience. Holidays, weather, and facility/experiment equipment problems combined to limit test operations in the first two months to 12 days, during which 6 tests were completed and 3 others were partially completed. During January, 15 days of solar operations were conducted with 18 separate test conditions completed and 2 others partially completed. During the course of the program, the input power was varied from about 20 kW (single heliostat) to near 1000 kW, with as many as 81 heliostats used at any one time.

Data which illustrate a complete day of testing are shown in Figure 7. Heliostats were initially brought onto the receiver at 7:42 a.m. and all were removed at 4:05 p.m. Throughout the day heliostats were brought onto and removed from the receiver as requested by the experimenter.

The real time aperture flux (RTAF) system, mounted about 2 feet in front of the receiver aperture, was used throughout the tests to measure the flux and power conditions. In addition, during the initial checkout tests, a water-cooled

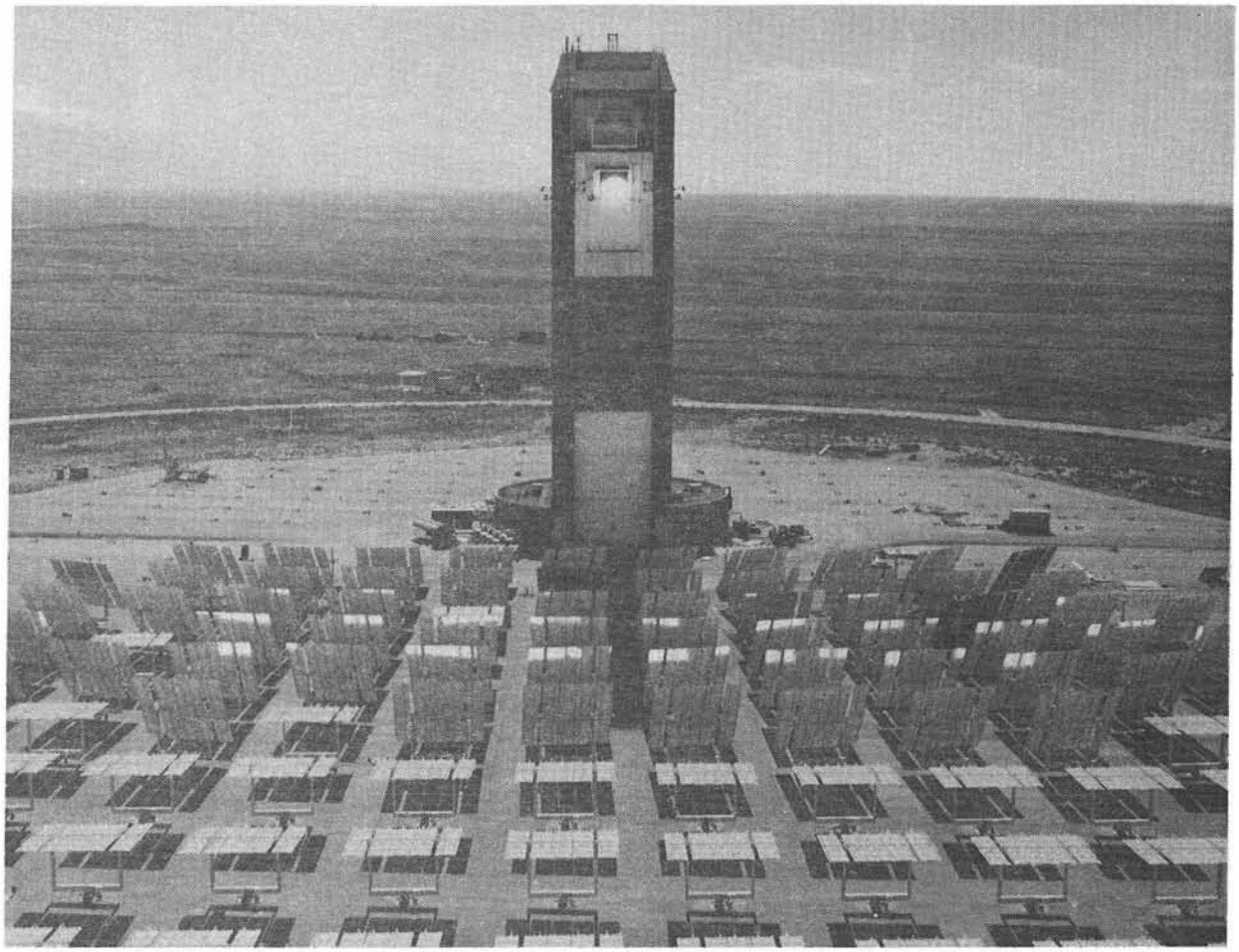

Figure 5. Tests on EPRI/Boeing Receiver

- Started MCS/Receiver Checkout - October 23
- Initial Solar Checkout Tests - October 27
- Summary of Testing - October 27-January 31

  (97 Calendar Days)

  - 28 Days of Solar Operations
  - 28 Days System Ready But Weather Cloudy
  - 25 Days for Other Activities (Module Repair, Holidays, etc.)
  - 8 Days of No Tests Due to CRTF Equipment
  - 8 Days of No Tests Due to Experiment
- 15 Days of Solar Operations in January
  - 20 Test Conditions

Figure 6. Summary of EPRI/Boeing Test Operations at CRTF

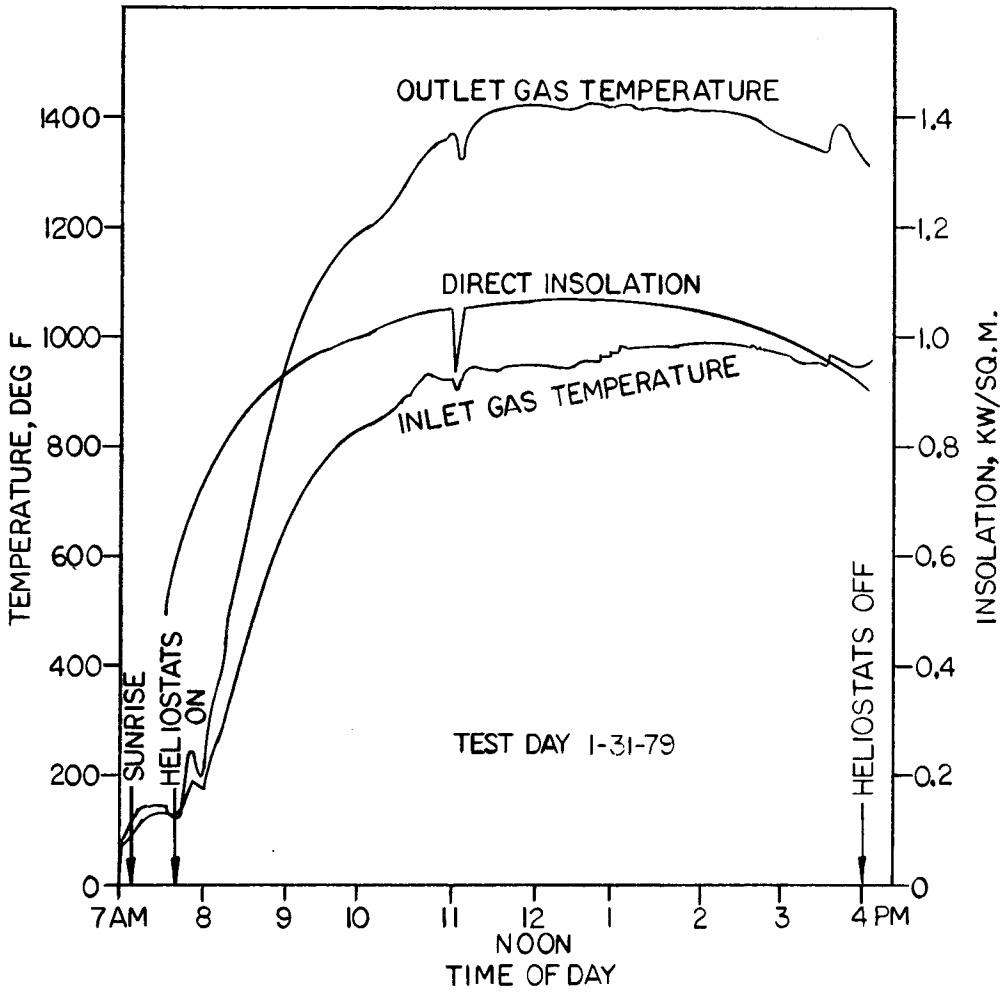

Figure 7. Typical Data for EPRI/Boeing Receiver Tests

cross, instrumented with 12 flux gages, was placed in the receiver aperture. This "aperture flux detector" was used to measure the flux directly into the receiver to confirm an anlaytically derived "transfer function." This transfer function was then used throughout the tests to provide real time estimates of power into the receiver. Figure 8 presents a comparison of the input power derived from the cross data with that calculated using the transfer function and the RTAF data for four different test conditions.

The computer program HELIOS is used in posttest interpretations of the RTAF measurements. RTAF and HELIOS data can be presented in a variety of displays including 3-, 2-, and 1-dimensional contours taken at any desired location. Figure 9 is a comparison of the measured and calculated flux density distribution taken at the geometric center point of the RTAF field. The peak flux density agreement is within 4 percent, and the integrated power agrees to within 5 percent. Analyses and calculations of input power conditions continue for this test program.

Case No.	Power Determined from Cross Integration (kW)	Power Calculated Using Transfer Function (kW)	Difference (%)
1	240	223	-7.08
2	244.6	248	1.39
3	365	382	4.66
4	392.5	366	-6.75

Figure 8. Comparison of Measured and Calculated Input Power Into EPRI/Boeing Receiver Aperture

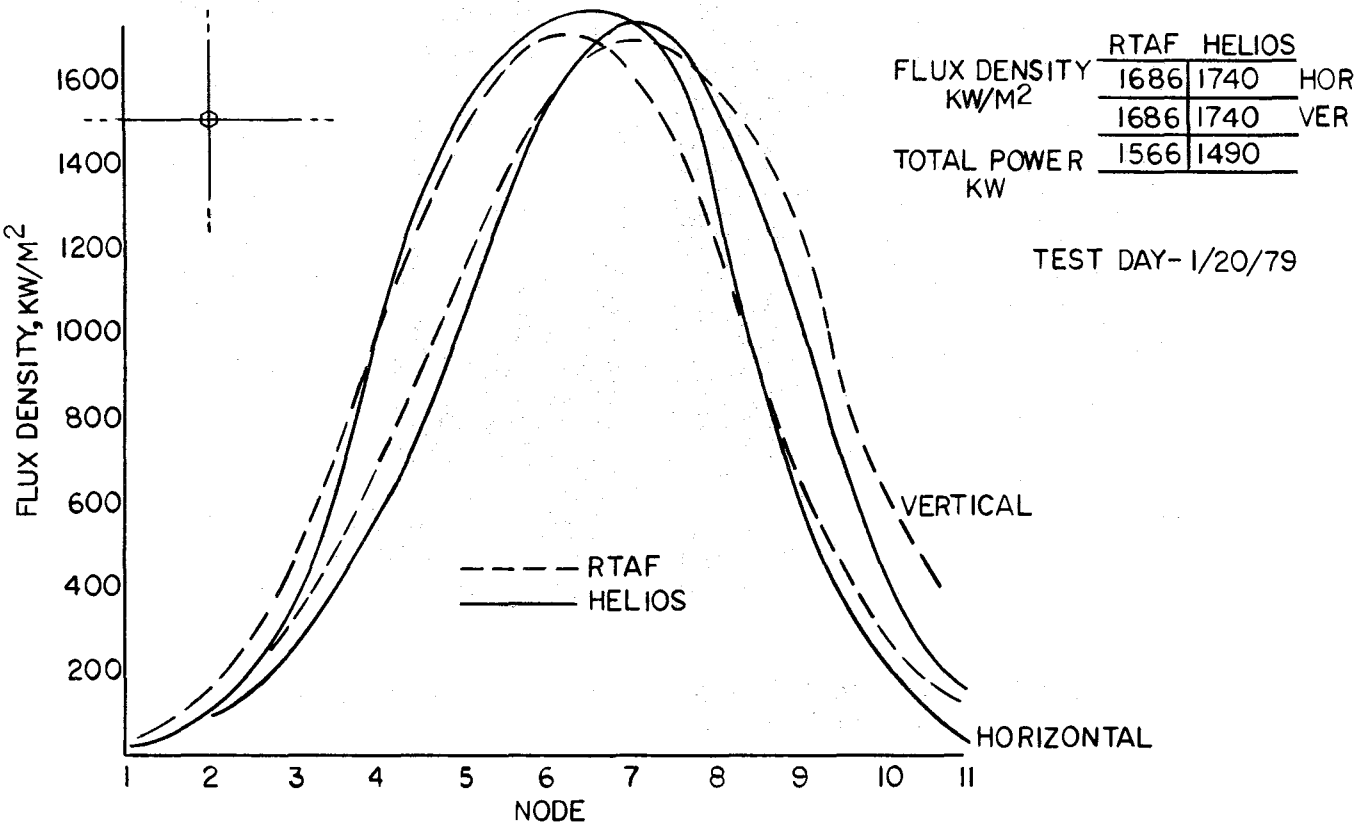

Figure 9. Comparison of RTAF Data and Helios Calculations for EPRI/Boeing Receiver Tests

Tests on DOE/McDonnell Douglas Receiver

The McDonnell Douglas/Rocketdyne receiver panel was erected on the elevating module on January 9. Three cranes, two attached to the top and one to the bottom as shown in Figure 10, were positioned in the ground level door to make the lift. All installations and interconnections that could be made at this location were completed, and the receiver was elevated to the top of the tower on January 25-26. The receiver is shown in its final test location in Figure 11. Final interconnections for cooling, electrical power, and control and data cables were made at the tower top.

The initial solar checkout test on the panel was conducted on February 23. Single heliostats, groups of 10, and a group of 20 were independently targeted onto the uncooled receiver. Surface temperatures up to 650°F were measured. These tests were to confirm the ten different target zones required for heliostat pointing, to measure the heat capacity of the dry panel, and to identify any instrumentation problems.

The second test on this receiver will be the first opportunity to combine MCS control of all elements of the facility heat rejection system (HRS) with control of the receiver through the controller. Pressurization of the panel with water at 400°F inlet temperatures has been accomplished. The test procedure was rehearsed without solar input to ensure that the test operations are satisfactory; the solar test will be continued in the near future.

Prototype Heliostat Evaluation

During the past six months, a beam characterization system (BCS) to measure the quality of beams reflected from heliostats has been under development. The BCS will be used first to evaluate a prototype heliostat developed by Westinghouse and the pilot plant prototypes developed by Martin Marietta and McDonnell Douglas. All BCS hardware has been received. Software to analyze and display the data is essentially complete. A schematic of the BCS system is shown in Figure 12, and the location of the heliostats relative to the tower-mounted target is shown in Figure 13. Figure 14 is a summary of the data which will be obtained using BCS. To check out the BCS prior to its use with the first prototype heliostats, single heliostats in the CRTF field were focused onto the facility alignment target at the 160-ft level and the image recorded. Figures 15 and 16 illustrate two types of data which can be obtained with the system.

A 30 x 30-ft target will be located at the 120-ft level of the tower with installation to begin in May. The six foundations indicated in Figure 13 are identical with those in the facility heliostat field. The 10-MW_e pilot plant prototype heliostats are designed to mate to these foundations, whereas the Westinghouse prototype has been located on a special concrete pad adjacent to the foundations. Other foundation types required for future advanced prototypes will be designed and located in this area.

Figure 10. Erection of McDonnell Douglas/Rocketdyne Receiver Panel

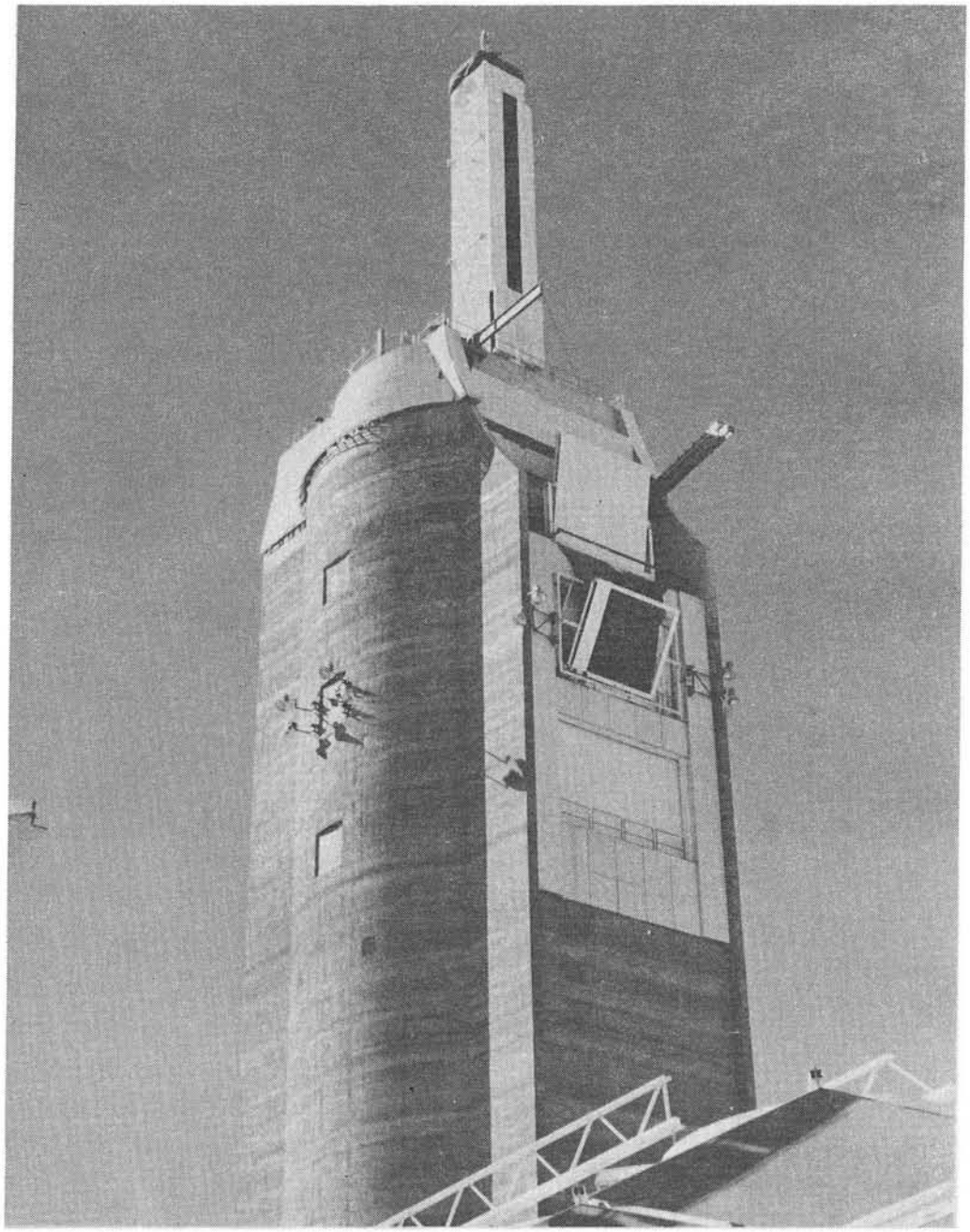

Figure 11. McDonnell Douglas/Rocketdyne Receiver Panel in Test Location

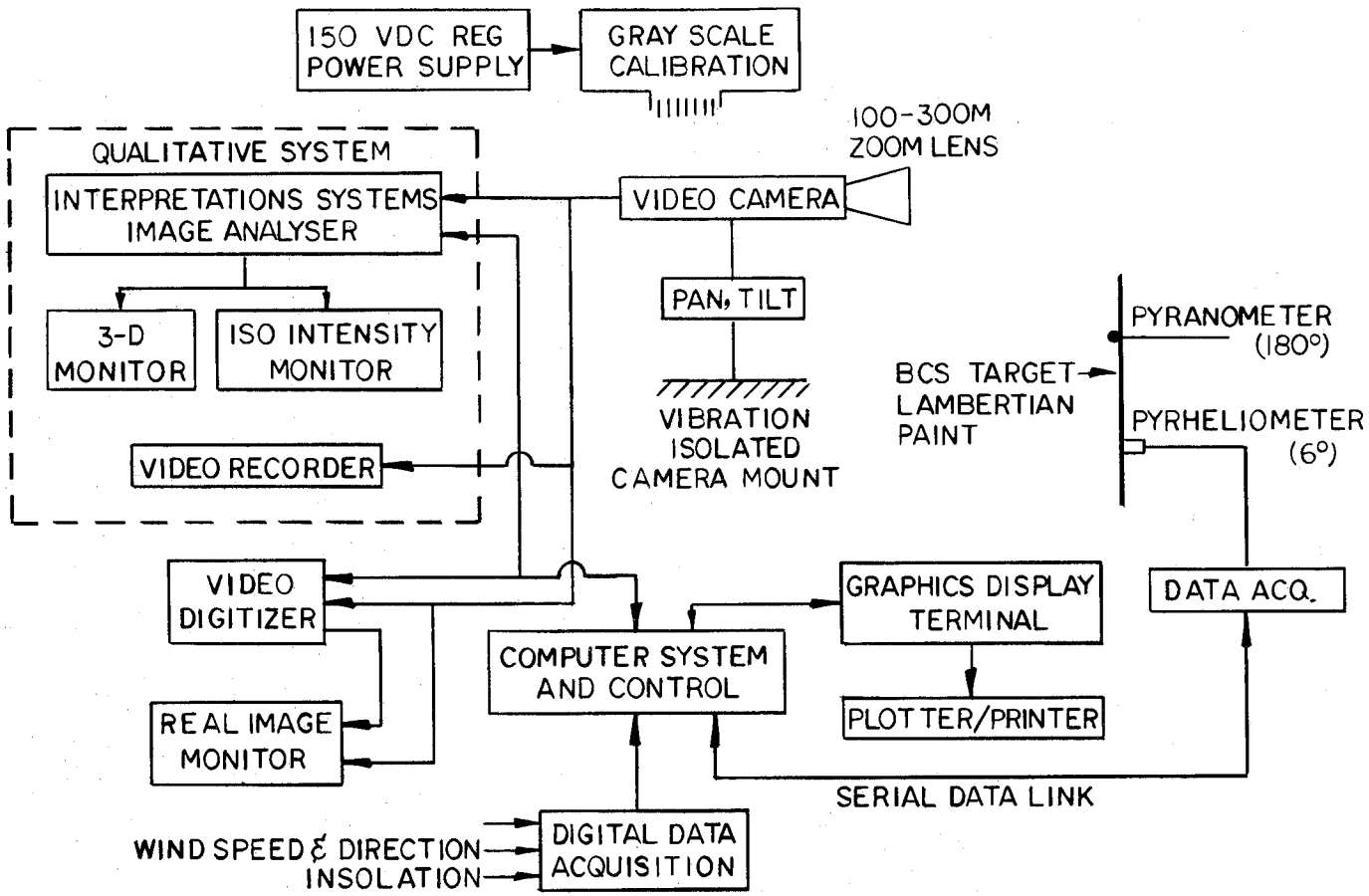

Figure 12. Schematic of Beam Characterization System

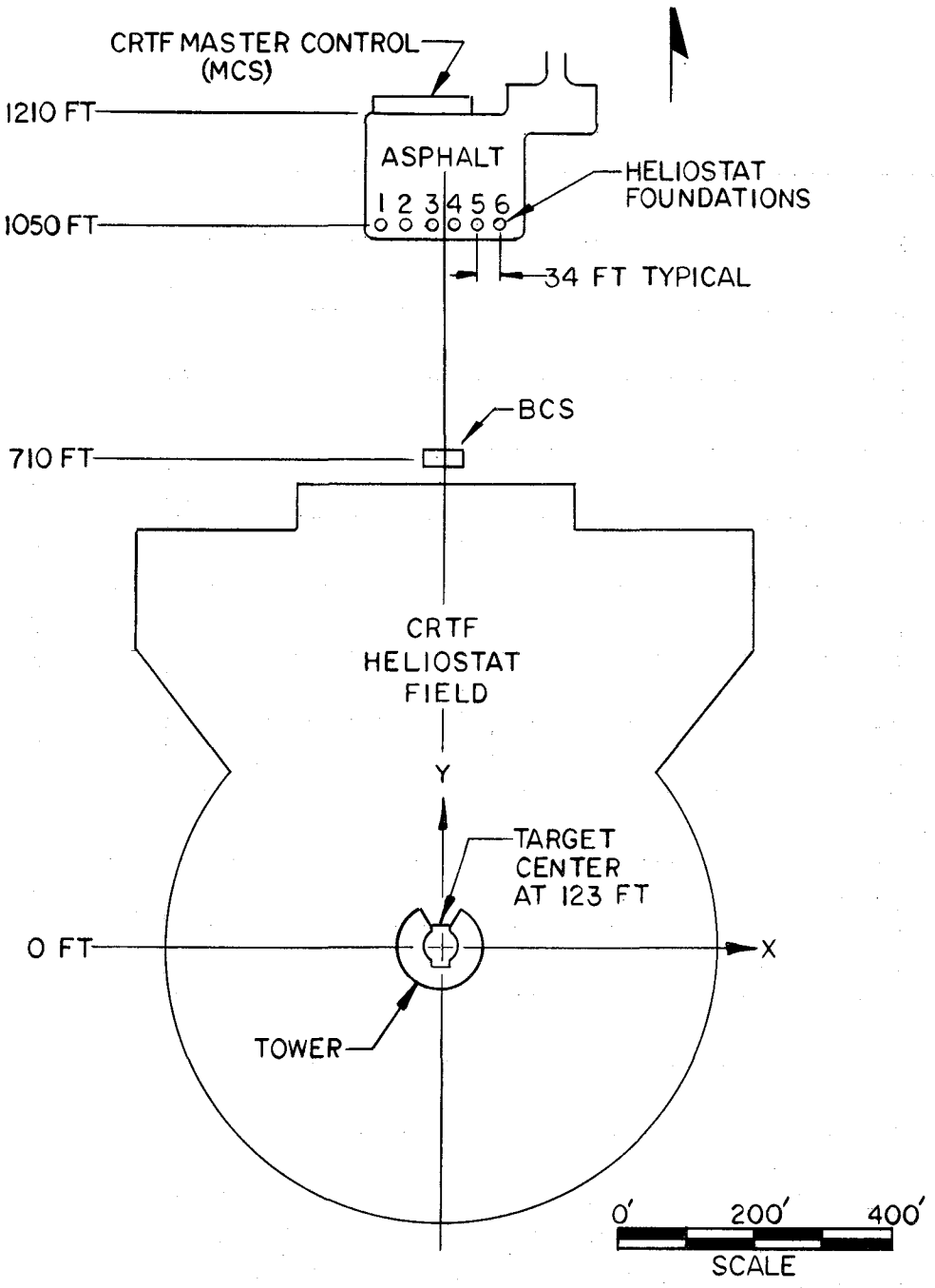

Figure 13. Facility Layout for Heliostat Evaluation

Basic Output

- 256 x 256 Matrix of Heat Flux (W/cm^2)

Computer Reducted Outputs

- Flux Level Plots (W/cm^2)

  1-Dimensional Slices
  2-Dimensional Iso-Flux Contours
  3-Dimensional Profile

- Beam Centroid Location (Relative to Aim Point)
- Total Beam Power
- Percent of Total Power Versus Radius from Beam Centroid

Test Legend Outputs

- Test Definition (Heliostat, Date, Time, etc.)
- Insolation Level During Test
- Wind Speed and Direction

Other Data Taken During Test

- Sunshape (LBL Circumsolar Telescope)
- General Meteorological Data

Qualitative Assessment of Field Alignment Tool

Figure 14. Beam Characterization System (BCS) Outputs

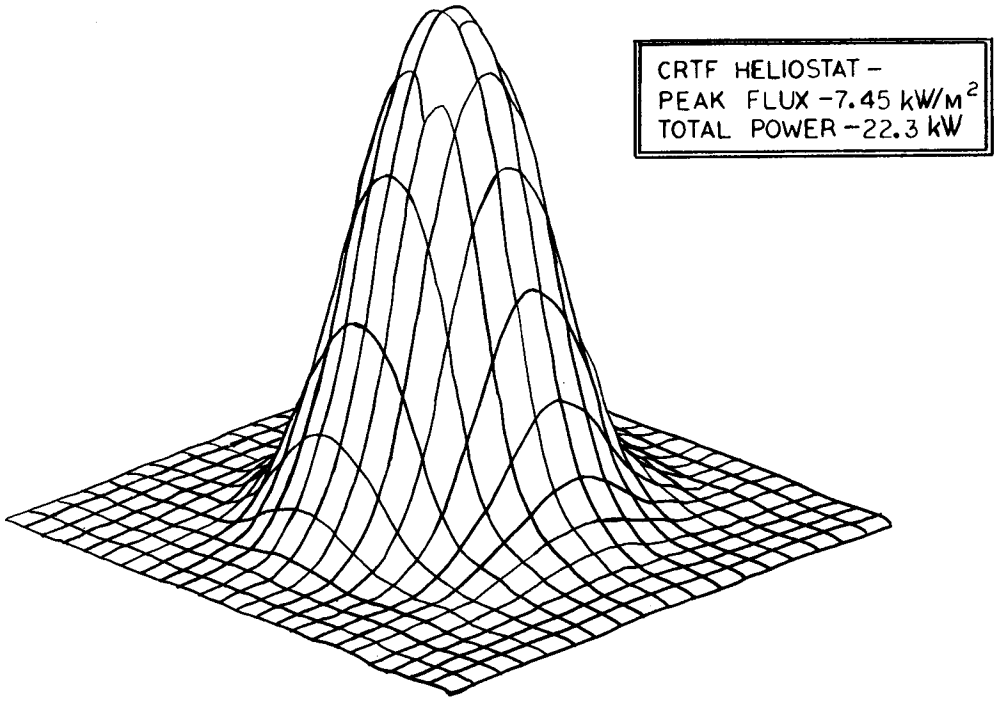

Figure 15. Typical BCS 3-Dimensional Output

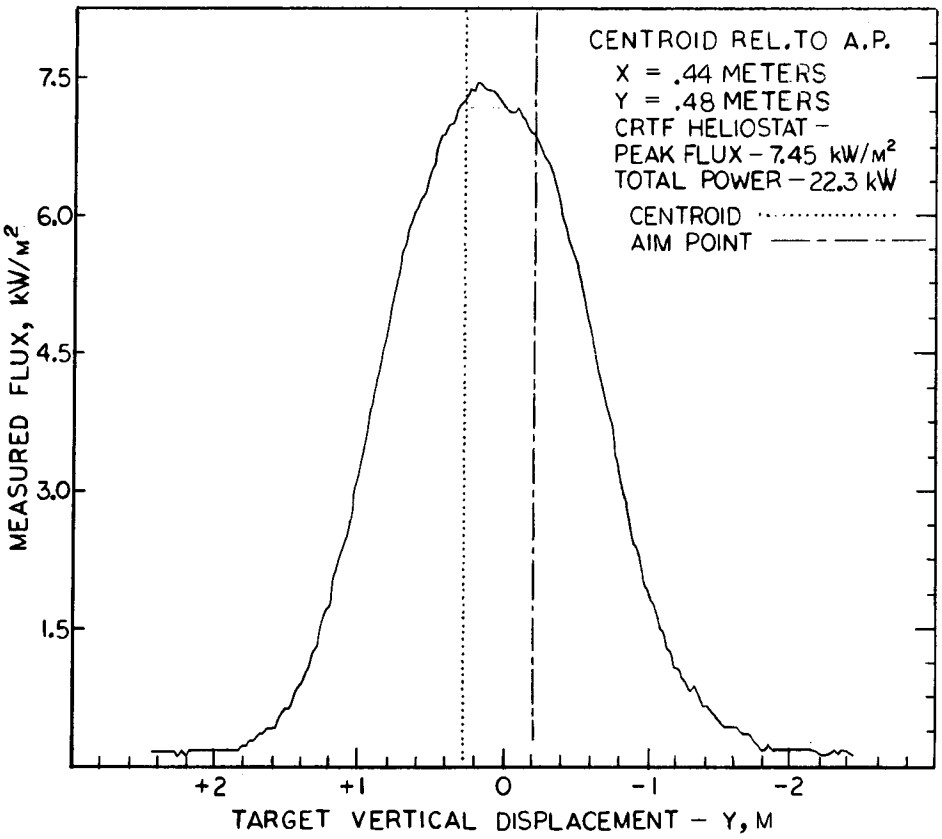

Figure 16. Typical BCS 3-Dimensional Output

Planned Activities

During the next six months, both receiver testing and prototype heliostat evaluation will be performed. Figure 17 presents a milestone schedule for FY 79, and Figure 18 presents the projected test schedule for FY 79 and FY 80.

The primary emphasis in receiver testing during the next 6 months will be to complete the McDonnell Douglas panel tests. A total of 35 tests is scheduled. After 28 tests are completed, a secondary concentrator system will be attached to the receiver. This concentrator is necessary to attain the flux levels (up to 400 kW/m^2) required for the final seven tests. The present schedule calls for completion of the McDonnell Douglas tests by July.

The EPRI/Black & Veatch receiver is presently expected at the CRTF in June. At that time, the EPRI/Boeing receiver will be removed from the 140-ft level and the Black & Veatch receiver placed in its position. Checkout and initial tests of that system will begin following completion of the McDonnell Douglas tests.

Activities related to tests of two photovoltaic arrays will be continued. The first is a 1-kW_e silicon array and testing is expected soon. Flux densities up to 200 kW/m^2 are required with test durations of a few minutes. The second photovoltaic panel is made up of gallium arsenide cells and requires flux densities up to 1500 kW/m^2. The array will be cooled using the tower cooling system and a closed loop temperature control system. Testing is expected in late FY 79 or early FY 80.

Requests have been received from two non-DOE agencies to use the facility for tests which are not solar technology related. The test applications were coordinated with the Solar Thermal Test Facilities - User's Association and forwarded to DOE/Division of Solar Technology for consideration. The test programs are relatively short but are shown as dashed lines over a long period due to the uncertainty of the schedule. If approved, the tests will be performed on a non-interference basis with solar related tests.

Testing of advanced central receivers is not scheduled until FY 80 but preliminary planning will begin in FY 79. Flux density levels up to 1800 kW/m^2 have been indicated and secondary concentrators will be required. Analyses and preliminary design studies will be conducted in FY 79.

In the next six months, evaluations of the Westinghouse prototype and the pilot plant prototypes from Martin Marietta and McDonnell Douglas are scheduled. The Westinghouse prototype is presently being installed and will be evaluated first. The pilot plant prototypes are expected in June with evaluation to be performed from July through September. Preliminary planning and coordination will continue to prepare for advanced prototypes now projected for evaluation in mid-FY 80.

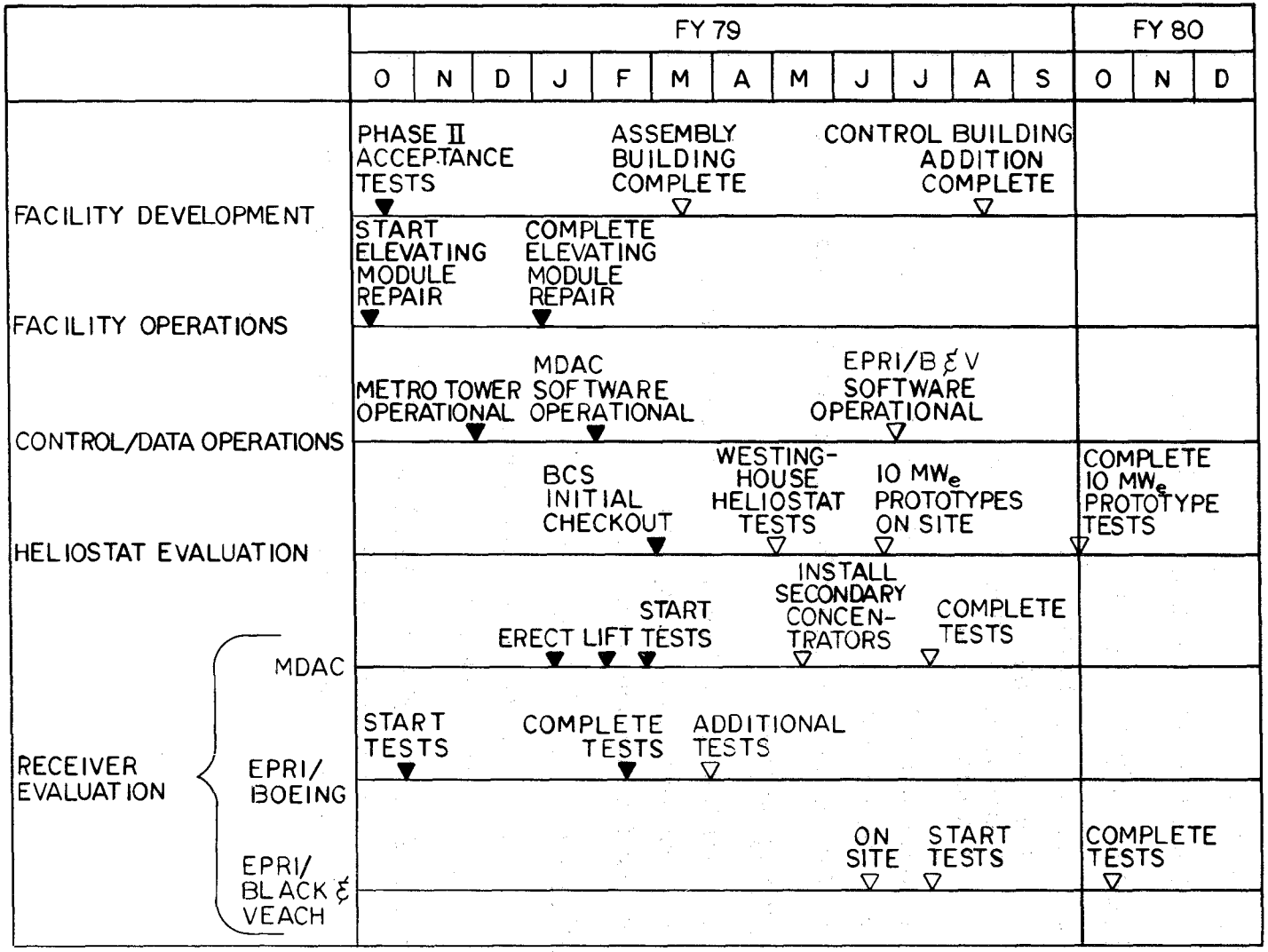

Figure 17. Central Receiver Test Facility Milestone Schedule

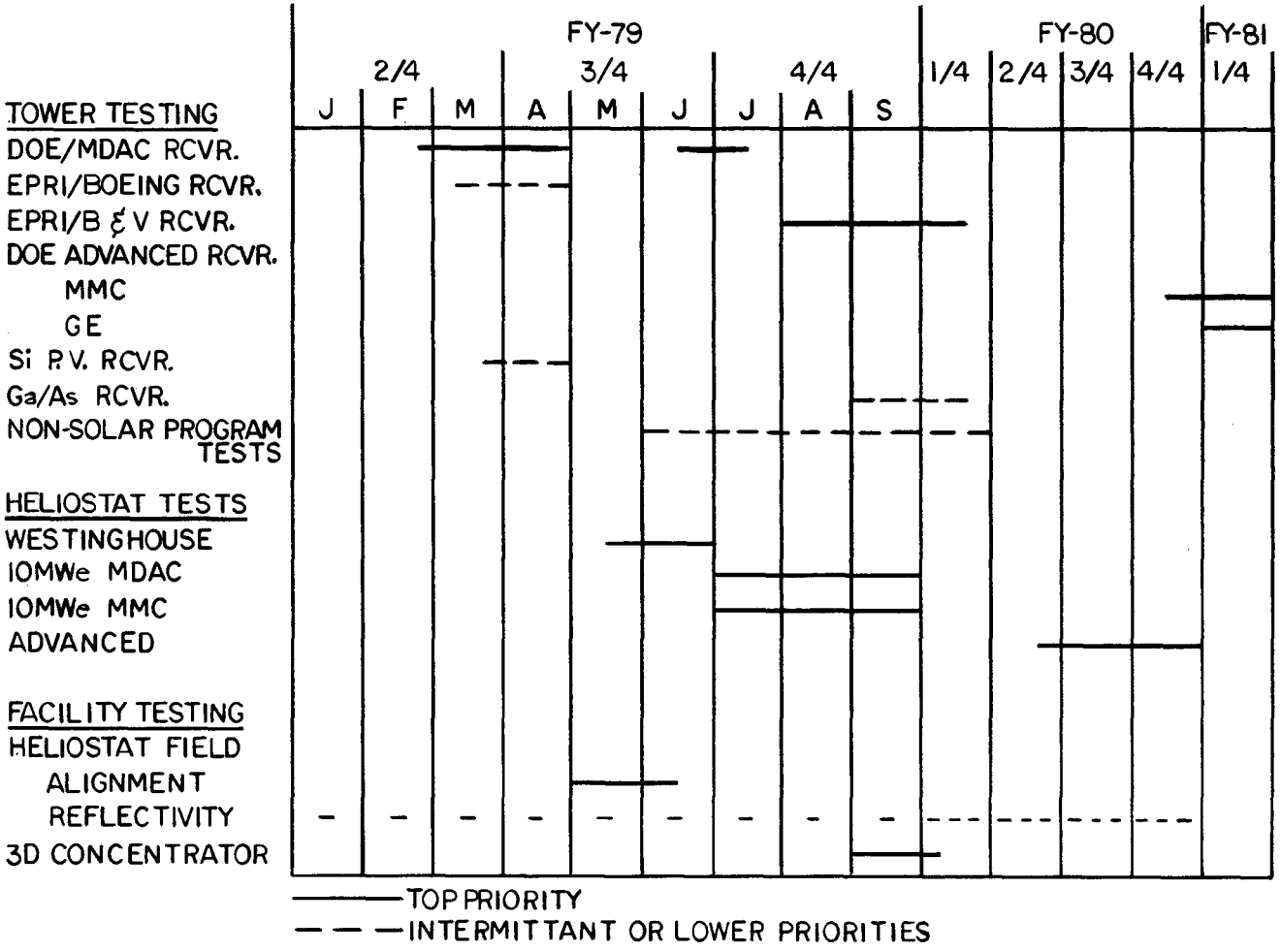

Figure 18. CRTF Testing Schedule (3/79)

THE DOE REPOWERING PROGRAM

S. D. Elliott, Jr.
San Francisco Operations Office

The objective of solar repowering/industrial retrofit is to demonstrate that solar energy is an option for industry in meeting the objectives of the Power Plant and Industrial Fuel Use Act of 1978. This Act, one of the five bills comprising the National Energy Act, restricts use of oil or natural gas in new electric utility facilities or in new industrial boilers with a fuel heat input rate of 100 million Btu's per hour or greater, unless exemption is granted by DOE. Similarly, the Act encourages, and in some cases requires, existing oil and natural gas facilities to convert to coal or an alternate fuel.

It is felt that hands-on experience by the energy consumer with solar thermal equipment is a prerequisite for establishing a market potential for solar thermal energy components and systems. DOE sponsorship of large-scale applications of this technology in conjunction with commercial operations is a timely and cost effective way to demonstrate solar thermal hardware. The plan for accomplishing this demonstration is to establish two construction projects, one for electric power generation and one for industrial process heat, based on information obtained from conceptual design studies initiated in 1979 (Table I). These studies will include both system definition and economic assessment for specific application concepts. Up to ten user-developer teams will be funded to provide these data as a result of a solicitation for Solar Repowering/Industrial Retrofit Systems (DE-RP03-79SF10506), issued in March 1979. This procurement emphasizes user identification of the site and existing facilities and user selection of the solar central receiver technology deemed most appropriate for the application proposed. Concurrently, major acquisition planning has been initiated which, if approved by the Executive Branch and Congress, is expected to lead to further solicitations in future years. Through this nonphased procurement approach DOE intends to accomplish the following:

- Data gathering for the preparation and programmatic defense of the major project acquisitions
- Advancement toward realization of specific repowering/retrofit applications, and
- Broad placement of funds (within practical limits) with utility/industrial users to stimulate their interest in and understanding of solar thermal projects.

TABLE I

HIGHLIGHTS: RFP DE-ACO3-79SF10506 SOLAR REPOWERING/ INDUSTRIAL RETROFIT SYSTEMS

(Conceptual Design - Economic Analysis)

Release Date:	March 16, 1979
Pre-posal Conference:	March 28, 1979
Proposals Due:	May 21, 1979
Anticipated Award Date:	August, 1979
Performance Period:	Nine Months (to May, 1980)
Level of Effort:	8,000 - 10,000 Person-Hours
Number of Awards:	Up to Ten
Categories:	a. Electric Power Generation b. Industrial Process Heat
Specific Sites/Applications	
Maximum User Latitude in Technology Selection	
Not a Phased Procurement; Open Competition for Follow-On	

Doe efforts for solar repowering/industrial retrofit will be structured from the following studies and analyses:

- The Public Service of New Mexico Technical and Economic Assessment of Solar Hybrid Repowering
- MITRE studies of Solar Thermal Repowering
- SERI Repowering Strategy Analysis
- Westinghouse Analysis of a Real Texas Utility (an extension of the Westinghouse analysis provided to PNM)
- The Solar Repowering/Industrial Retrofit Systems contract efforts (activities following from DE-RP03-79SF10506)

The schedule given in Figure 1 indicates the time phasing of these efforts.

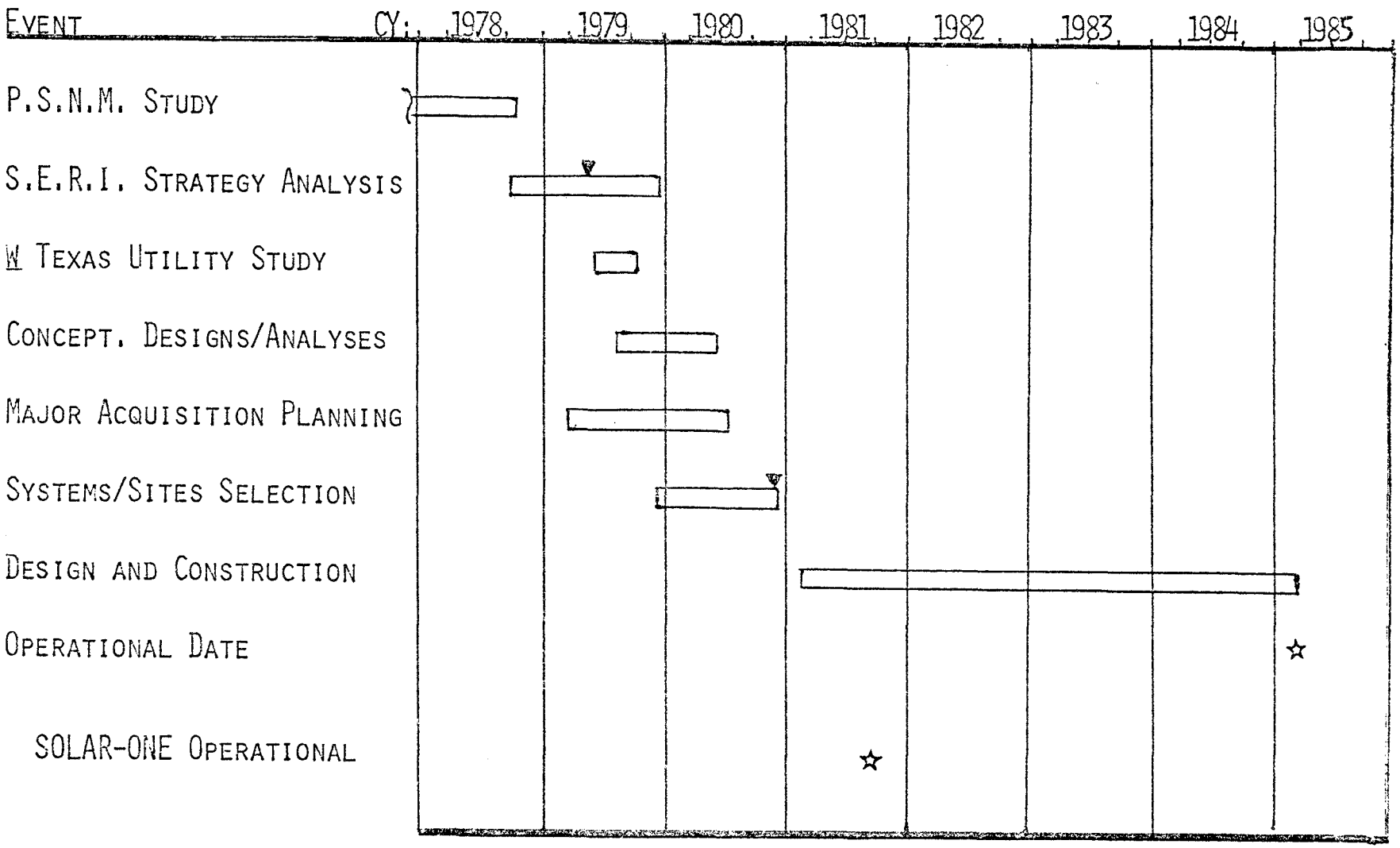

Figure 1. Solar Repowering/Industrial Retrofit Program Schedule

SOLAR REPOWERING OF UTILITY ELECTRIC PLANTS

Prem N. Mathur
The Aerospace Corporation

This paper summarizes the results of repowering studies. Various options for repowering are identified and example calculations of the economics of a repowering plant in a utility system are presented.

Aerospace Contract Objectives

The Aerospace Corporation is providing system engineering studies and technical and management support to DOE/SAN on Contract No. EY-76-C03-1101 under the overall cognizance of Mr. R. Hughey, Director of Division of Solar Energy, and the general direction of Mr. L. Prince and Dr. S. D. Elliott, Program Managers, DOE/SAN.

These studies investigate and evaluate potential solar central power system options and provide data which support planning and technical monitoring of industry contracts. "Repowering" is one element of this effort.

Repowering Options

Figure 1 presents a matrix of possible solar and non-solar repowering options for utility steam electric plants. The matrix represents combinations of the solar and non-solar repowering technology, the type of steam plants to be repowered, and the type and manner in which the retrofit heat is incorporated into the plant cycle. The ACR technology can offer improved operational characteristics and may expand the size of the solar repowering market. Selection of a particular option will depend on economics and other factors, including the preference of technology by the user. General comments related to various repowering options are noted in the last column.

RETROFIT TECHNOLOGY OPTIONS	TYPE OF STEAM PLANT	TYPE OF HEAT INPUT	REMARKS
CURRENT TECHNOLOGY SOLAR STEAM	NON-REHEAT	• SOLAR BOILER • SOLAR FWH	• STORAGE, IF NEEDED, IS NOT COMPATIBLE WITH EXISTING TURBINES • SOLAR FWH PROVIDES LOW SOLAR FRACTION. APPLICABLE TO REHEAT PLANTS ALSO
ADVANCED TECHNOLOGY SOLAR STEAM (a) BOILER + REHEAT RECEIVER (b) BOILER AND NEW FOSSIL REHEATER	REHEAT	SOLAR BOILER, SOLAR OR FOSSIL REHEAT	• REQUIRES DEVELOPMENT OF RECEIVER WITH HIGHER STEAM CONDITIONS • OPTION (a) REQUIRES DEVELOPMENT OF RECEIVER WITH REHEAT PANELS • STORAGE IS NOT COMPATIBLE WITH EXISTING HIGH TEMPERATURE TURBINES
ACR TECHNOLOGY (a) LIQUID SODIUM (b) MOLTEN SALT (c) BRAYTON	REHEAT OR NON-REHEAT	SOLAR HEAT FOR BOILER AND REHEAT	• ACR DESIGNS CAN BUFFER AGAINST INSOLATION TRANSIENTS • STORAGE IS COMPATIBLE WITH TURBINES • SALT SYSTEM NEEDS REDESIGN FROM 950°F TO 1,000°F STEAM
CONVENTIONAL TECHNOLOGY (a) COAL BOILER (b) BRAYTON TOPPING (c) NEW EPGS AND/OR BOILER	REHEAT OR NON-REHEAT	FOSSIL STEAM	• ENVIRONMENTAL AND INSTITUTIONAL PROBLEMS • OPTIONS APPEAR ECONOMICALLY UNATTRACTIVE

Figure 1. Repowering Options - Utility Plants

Characteristics of Candidate Plants

Figure 2 presents basic characteristics of candidate repowering steam plants and their representative repowered configurations. The typical candidate units are non-reheat and reheat steam turbines with power generating capacity in the overall range of 10-1000 MW_e. The throttle steam conditions are as shown in the figure. A review of market survey data indicates that a large majority of candidate steam reheat plants use 1000°F/1000°F and 1500-2400 psi steam conditions which are compatible with the ACR solar technology.

Utility System Analysis

More than 60 percent of the solar repowering market identified in the surveys are in the Texas-Oklahoma region. Figure 3 presents estimates of a cost/benefit ratio for a repowered plant integrated into a synthetic utility system with insolation, load demand characteristics, and the generation mix representative of that region. The generation or fuel mix shown represents operating capacities in percent of a total installed capacity of 8000 MW_e. Other important input assumptions of the analysis are also listed.

The calcuations are made for the cost/benefit ratio for various collector field sizes and associated receiver and tower designs to determine the optimum retrofit configuration as shown. The cost/benefit ratio is calculated by dividing the present worth of solar retrofit lifetime costs by the benefits derived by it. The lifetime cost includes cost of solar retrofit and O&M costs for solar equipment based on current solar steam receiver technology. The benefit is the present worth of savings to the utility in the costs of conventional generation as a result of solar repowering. These savings include costs of oil and coal fuel and O&M saved plus a 20-year capacity credit assessed independently of the cost of solar retrofit.

Solar Versus Fossil Repowering

Figure 4 compares the economics of solar repowering with one conventional repowering option that might be available to a utility. A spectrum of existing candidate non-reheat plants, represented by varying boiler and EPGS efficiencies, are assumed to be retrofitted. The solar retrofit option is the baseline case reported in the previous figure for the collector area of 5.0 m^2/kW_e. The conventional retrofit involves replacement of boiler and EPGS equipment of the candidate plants by new high efficiency equipment with characteristics shown in Figure 4. For this case, the results indicate that the specified conventional retrofit is more cost effective than solar only for plants with very low efficiencies.

NONREHEAT PLANTS

- 200 MW_e CAPACITY
- T_2: 700-950°F
- P_2: 1200-1800 psi

REHEAT PLANTS

- 50-1000 MW_e CAPACITY
- $T_2 = T_4$: 1000-1050°F
- P_2: 1500-2400 psi

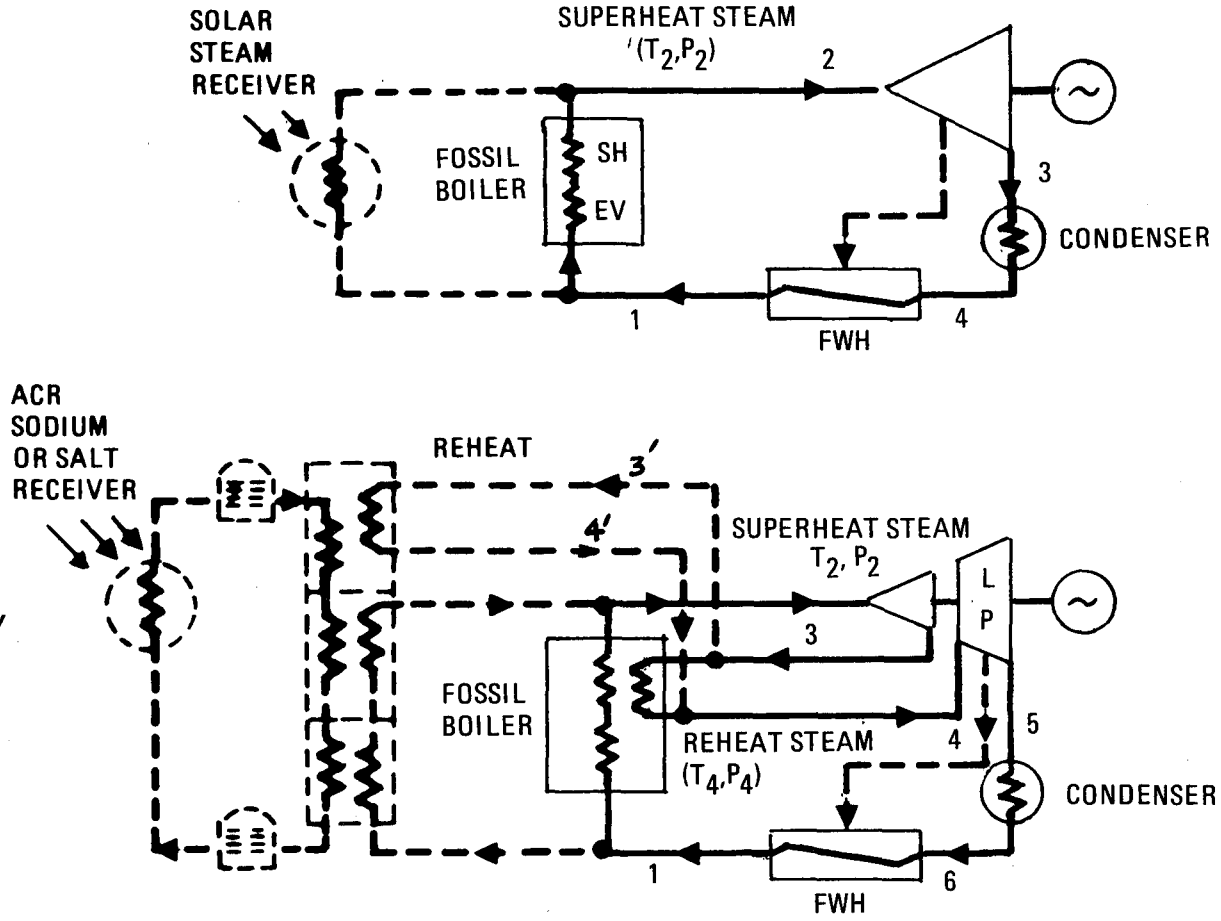

Figure 2. Characteristics of Candidate Plants

KEY ASSUMPTIONS

- INITIAL OPERATION - 1985
- REPRESENTATIVE TEXAS UTILITY
- GENERATION MIX (operating capacity) AS SHOWN
- PLANT AVAILABILITY EPRI-TA GUIDE
- 5% SOLAR PENETRATION
- 50 MW_e FOSSIL PLANT AND SOLAR CAPACITY
- NON-REHEAT STEAM PLANT
- 30 YEAR LIFE
- SCHEDULED RETIREMENT 1995
- FUEL COSTS (1985)/ESCALATION RATES
  - No. 2 OIL - 5.5 $/MBtu/12%
  - No. 6 OIL - 5.0 $/MBtu/12%
  - COAL - 1.0 $/MBtu/12%
- COST OF CAPITAL = 11%
- CAPITAL RECOVERY FACTOR = 11.5%
- FIXED CHARGE RATE = 18%
- COLLECTOR COST = $70/$m^2$
- O&M = 2% OF CAPITAL COST, 8% ESCALATION RATE

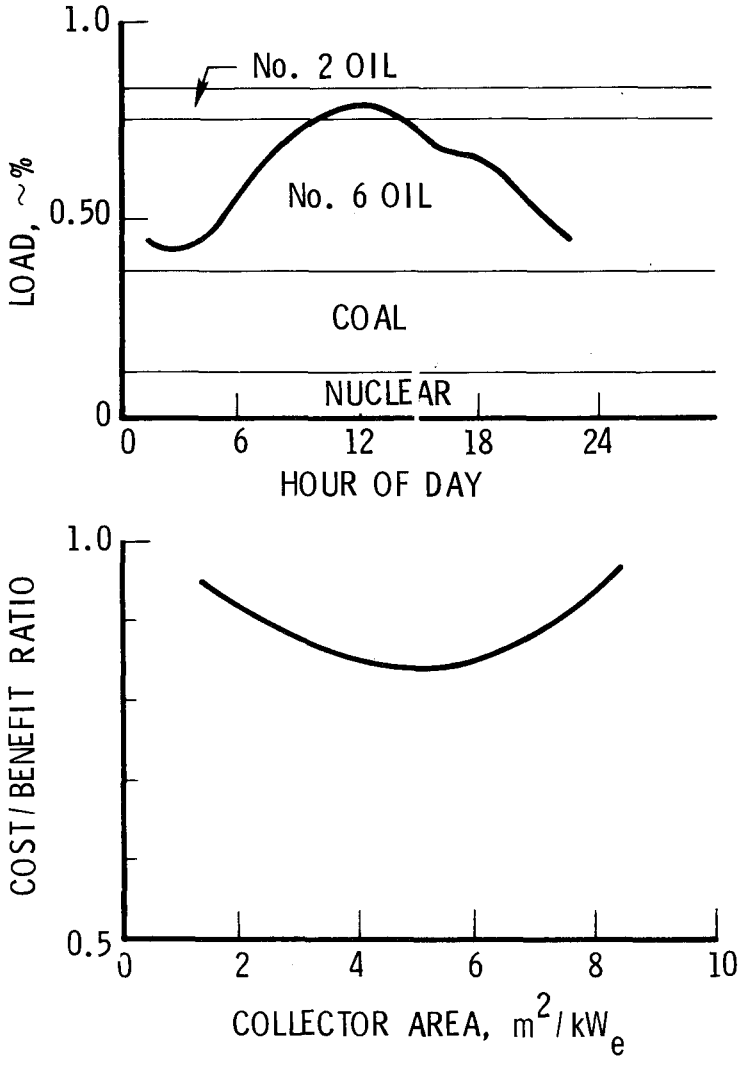

Figure 3. Utility System Analysis

- SOLAR REPOWERING OPTION
  - CURRENT TECHNOLOGY SOLAR
    - 50 MW_e CAPACITY
    - NO STORAGE
  - EXISTING BOILER AND EPGS
- FOSSIL REPOWERING OPTION
  - INSTALL NEW EPGS
    - CYCLE EFFICIENCY = 0.38
    - CAPITAL COST = 150 \$/kW_e
  - INSTALL NEW BOILER
    - PEAK EFFICIENCY = 0.87
    - CAPITAL COST = 110 \$/kW_e
- EXISTING FOSSIL PLANTS
  - PLANT TYPE
    - 50 MW_e CAPACITY
    - OIL FIRED, NON-REHEAT CYCLE
  - PLANT PERFORMANCE (varied)
    - CYCLE EFFICIENCY, η_{0c}
    - BOILER EFFICIENCY, η_{0b}
    - PLANT EFFICIENCY, $\eta_{0p} = \eta_{0c}\ \eta_{0b}$

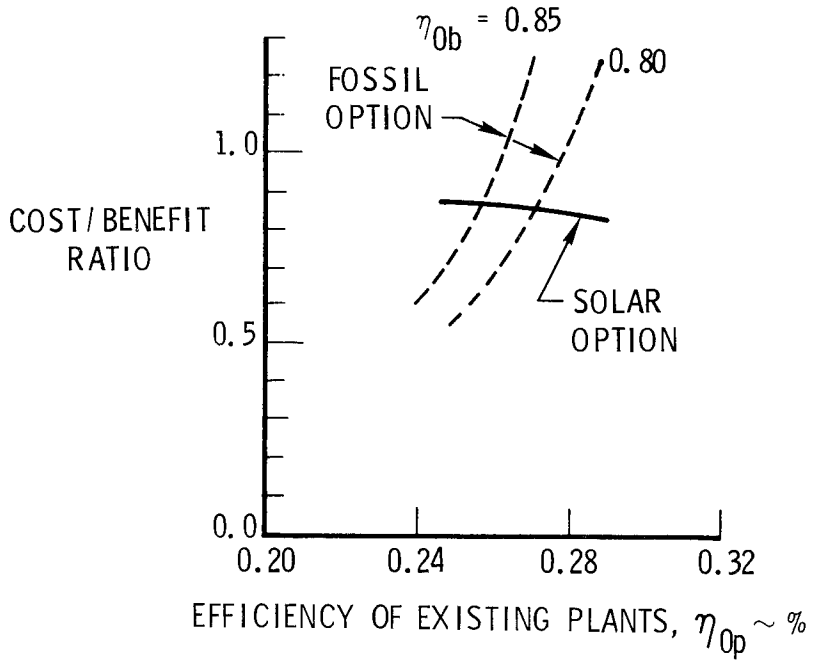

Figure 4. Solar Repowering Versus Fossil Repowering

Summary

In repowering, solar technology is incorporated in a redundant mode with a steam plant which is already operating in a utility grid. By proper design and development, the reliability of a solar repowered plant can be made to be comparable to that of a conventional fossil plant. Based upon various studies to data, solar repowering appears to offer an economic advantage over other solar applications for near term commercialization.

The market for solar repowering based upon a survey of utilities by PSNM and MITRE is summarized in Figure 5. These data indicate that reheat steam plants also represent an important portion of the repowering market. Analysis of repowering opportunities indicates that a successful demonstration should be accomplished by the mid-1980s to encourage commercialization of central power technology within the utility industry.

Several repowering options have been identified. Selection of a specific repowering option will depend upon its economics relative to other options as well as upon other important non-economic factors including the user's preference for a given technology. Estimates of a cost/benefit ratio for solar repowering for the region investigated indicate solar repowering has the potential to be economically attractive for utility applications.

It should be noted that similar concepts and considerations apply to process heat applications. The economics of solar retrofit for a process heat plant is expected to be more favorable because of direct displacement of expensive oil, as opposed to a utility in which solar energy displaces both oil and coal.

Repowering Study Plans

Plans for the next six months for the system engineering studies on repowering are outlined in Figure 6.

- OFFERS POTENTIAL FOR
  - LOW RISK COMMERCIALIZATION OF SOLAR TECHNOLOGY
  - LOWER COST THAN OTHER SOLAR OPTIONS
- SOLAR CAPACITY MARKET POTENTIAL
  - 2,000 MW_e WITH NON-REHEAT STEAM PLANTS
  - 8,000 MW_e WITH REHEAT STEAM PLANTS
- REPOWERING OPPORTUNITY
  - 1985 - 2,000 NON-REHEAT PLANTS
  - 1990 - 2,010$^+$ REHEAT PLANTS
- REPOWERING OPTIONS
  - CURRENT TECHNOLOGY SOLAR STEAM
  - ACR AND ADVANCED SOLAR STEAM
  - NON-SOLAR ALTERNATIVES
- REPOWERING ASSESSMENT FACTORS
  - RETROFIT COST, VALUE, COST/BENEFIT RATIO, AND SAVINGS IN FUEL
  - ECONOMICS OF COMPETING REPOWERING OPTIONS
  - ENVIRONMENTAL AND INSTITUTIONAL FACTORS

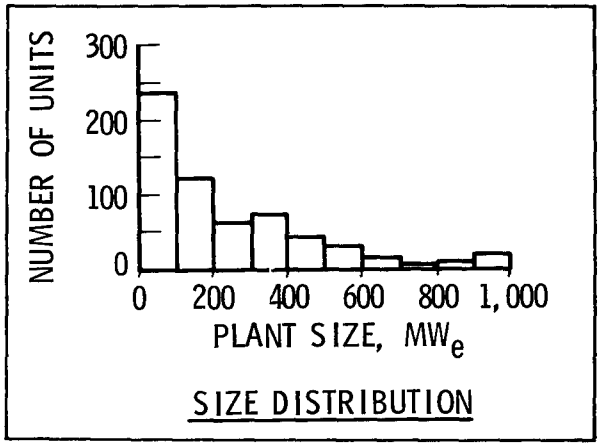

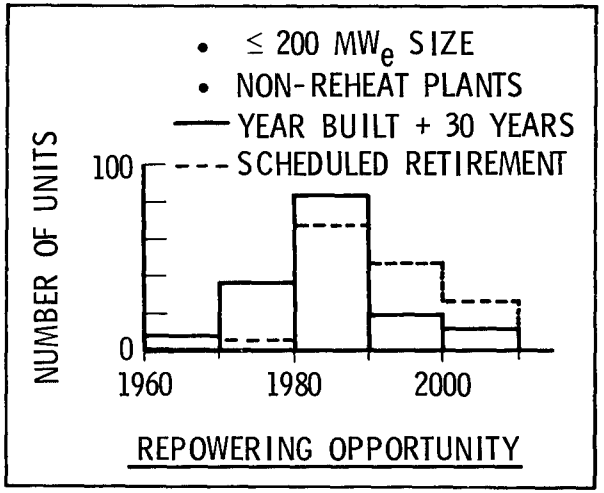

Figure 5. Summary

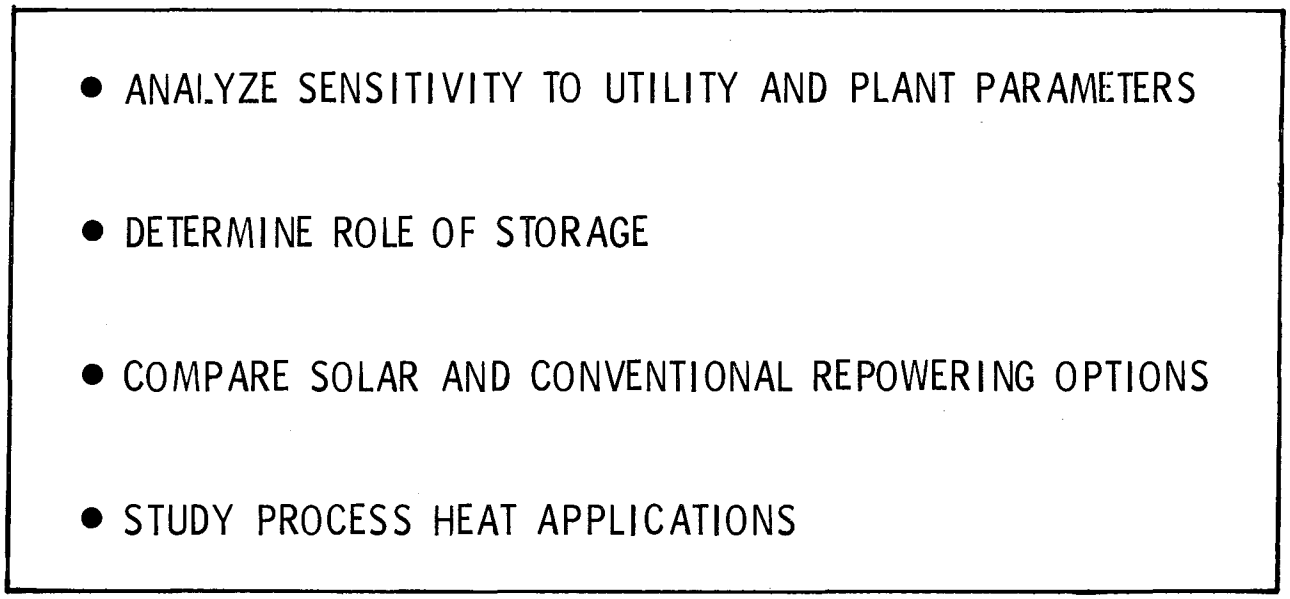

Figure 6. Repowering Study Plans

TRADE-OFFS IN CENTRAL RECEIVER SYSTEMS

T. A. Dellin
Sandia Laboratories, Livermore

Introduction

Sandia is conducting basic research into the design trade-offs in central receiver systems. A design change affects both performance and costs. The performance, as a function design variables, can be calculated using existing techniques. However, the component costs, as a function of design variables, are not as well known. Recognizing this, the approach taken in the present studies has been to quantify the "break-even cost" associated with a change in the performance of a component. The break-even cost is defined as the new capital cost required for a component whose performance is changed so that the cost of energy will be the same as in a system using the original cost and performance of the component. If the actual cost is less than the break-even cost, the design change is desirable and vice-versa. Ultimately, these results will be tempered by considerations of technical risk and utility acceptibility.

Break-even costs provide a quantification of the leverage on energy cost produced by system design parameters and put the design of central receiver systems into a useful perspective. The results of these studies have been and will be used in the selection and evaluation of technical contracts. In addition, they can help identify industries to participate in the central receiver program by providing specific cost performance goals for subcomponents, compoents, and complete systems.

Preliminary results will be considered from two separate trade-off studies. The first, which was initiated as part of the Phase I evaluation of the Advanced Systems Contracts, concerns the peak flux capability of external receivers. The second study, by Miriam J. Fish and T. A. Dellin, has just been started and is a detailed design trade-off study detailed at the International Solar Energy Congress, Atlanta, Ga., May 28-June 1, 1979.[1] (A third study, involving Sandia Albuquerque and Livermore, on the design of small power central systems is also beginning, but will not be discussed.)

Methodology of Trade-Off Studies

The same general approach is used in all of the trade-off studies. The sequence is:

1. Select a baseline technology, including performance and costs, for each subsystem in a central receiver plant.

2. Find the cost of energy in a system that is optimized using the baseline components with the DELSOL computer program.[2]

3. Consider a design change in one of the components. Determine its effect on the performance specification for that component.

4. Using the original cost of the new component, find the cost of energy in a system that is optimized with the new performance specification.

5. From the costs of energy in (2) and (4), determine a new cost for the redesigned component that would produce the same cost of energy in the redesigned system as in the baseline system.

The procedure is generally repeated for a range of performance values for the redesigned component.

The break-even costs are sensitive to many variables including the power level, the costs of other components, and the baseline technologies selected. It will, therefore, be necessary to investigate the sensitivity of the break-even costs to these variables. The result will be a range of break-even costs instead of a single value. Initial results indicate that the break-even costs are not very sensitive to the power level over the range of 50-400 MW_e. The effect of the other variables is being determined.

Flux Constraint on Receivers

To achieve a 30-year lifetime, the peak flux on the receiver must not exceed a maximum flux limit. The one-sided irradiation of receiver tubes leads to a nonuniform temperature distribution around the tube that is accompanied by strains which will cause fatigue failure after many daily cycles. Increasing the flux level increases the strains and reduces the lifetime. However, increasing the thermal conductivity of the cooling media flowing through the tubes decreases the temperature gradients and strains around the tube and increases the lifetime. Therefore, for a fixed lifetime, the higher the conductivity of the cooling media the higher the flux limit. The thermal conductivity of candidate cooling media, and hence the peak flux capabilities of their receivers, are ranked as follows:

$$\text{Na} < \text{Salt} \geq \text{Water} > \text{Air}$$

Representative values of the flux limit are 1.8 MW_t/m^2 for Na and 0.7 MW_t/m^2 for salt.

The study of the flux constrains on receivers has been divided into two parts. First, the maximum peak fluxes that occur in optimum central receiver systems will be calculated as a function of power level. An optimum system is defined as one that produces the minimum energy cost at a given power level. There will be no need to pursue technologies with flux capabilities in excess of these maximum values as they will not reduce the cost of energy. Second, the break-even costs for receivers with flux limits below these maximum values will be described.

The base case will correspond to an advanced design based on a Na technology. The heliostat is described in Table I. The present study will only consider external, cylindrical receivers. Cavity receivers, which will be included at a later date, may offer some advantages in low flux capability systems because of relatively smaller receiver losses.

TABLE I

BASE CASE HELIOSTAT

Size:	7.4 x 7.4 m
Mirror Area:	49 m^2
Errors (Standard Deviation):	
Azimuth angle	0.75 mrad
Elevation angle	0.75 mrad
Surface	1.00 mrad
Reflectivity (Time Average):	0.89
Canting:	12 cant panels, single cant for the whole field equal to the maximum slant range

In the absence of flux limitations, a "single aiming strategy" can be used in which all heliostats are aimed at the center of the receiver as shown in Figure 1a. The optimum receiver is sized to intercept most of the image of the farthest heliostat, which is usually much bigger than the image of an inner heliostat. It is possible, therefore, to consider a "smart aiming strategy" in which the images of the inner heliostats are spread out over the receiver by aiming alternate heliostats at different points on the receiver as shown in Figure 1b. The spillage is essentially the same, but the flux is more uniform and the peak flux is reduced with smart aiming. With flux limitations, smart aiming must be used.

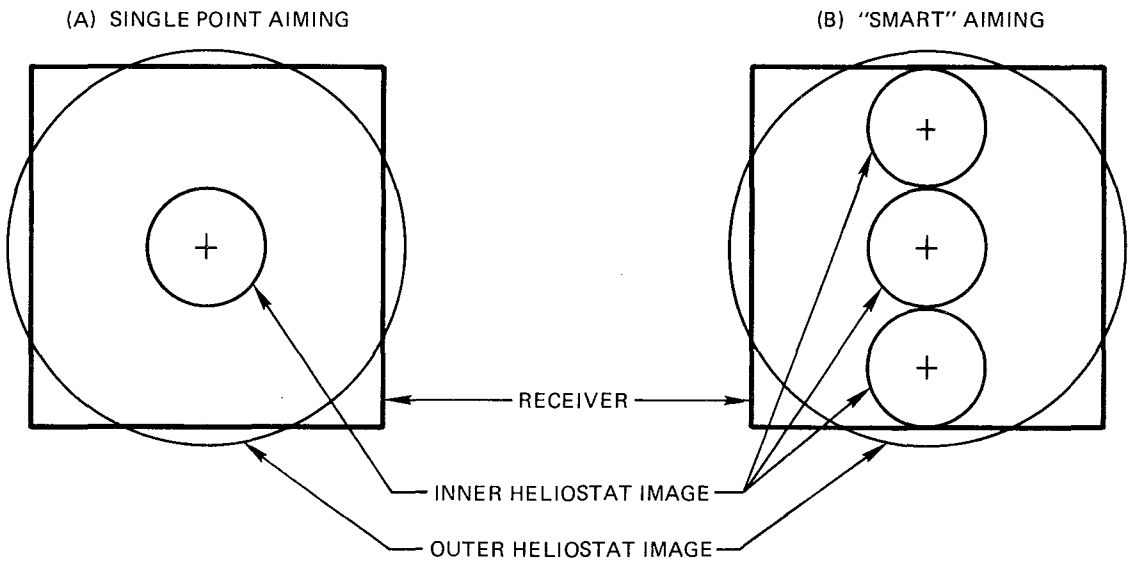

Figure 1. "Smart" Aiming Reduces the Peak Flux Without Increasing Spillage

The optimum peak flux as a function of the design point power level using a smart aiming strategy is shown in Figure 2. The optimum fluxes occur in the systems that produce the minimum energy cost at each power level. The flux increases at small power levels due to the finite heliostat size and then levels off at high power levels. The maximum flux is 2.2 MW_t/m^2 at 100 MW_e. The optimum peak flux increases if (1) the radiation and convection losses increase, (2) the receiver cost increases, or (3) a single aim point is used. For example, with a single aim point the maximum flux would be 2.6 MW_t/m^2 at 400 MW_e.

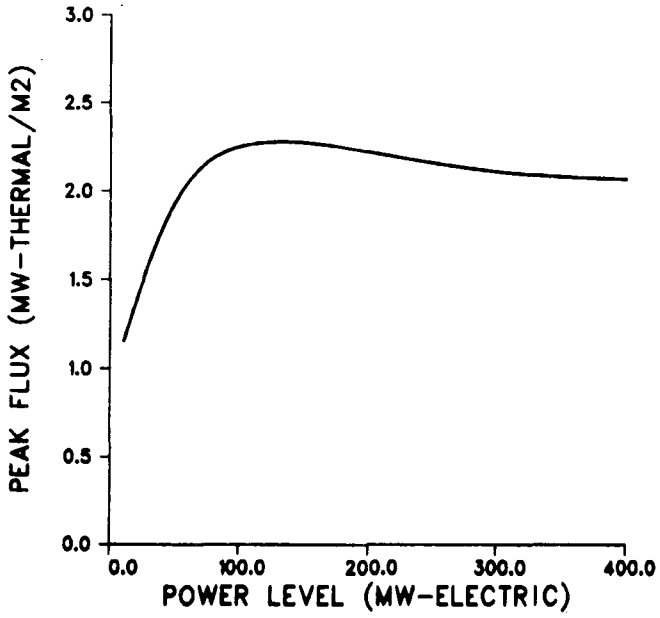

Figure 2. Optimum Peak Receiver Flux Versus Plant Power Level

If the receiver flux limit exceeds the optimum flux given in Figure 2, then the energy cost and break-even cost will be the same as a receiver whose flux limit equals the optimum flux. If the flux limit is below the value in Figure 2, the system has to be redesigned. A larger receiver will be required to spread the power over a larger area in order to lower the flux to the flux limit. The receiver area as a function of the flux limit is shown in Figure 3a for a 100-MW_e system. The area scales as

$$\text{Receiver Area} \quad \frac{\text{Optimum Flux}}{\text{Flux Limit}}$$

The increased receiver area required when the flux limit is less than the optimum flux affects both the performance and cost. The performance as a function of the flux limit is shown in Figure 3b. Starting at a flux limit equal to the optimum flux (2.2 MW_t/m^2 at 200 MW_e), the efficiency is first constant and then decreases rapidly as the flux limit decreases. The increasing radiation and convection losses are initially balanced by decreasing cosine and spillage losses but then the readiation and convection dominate at small flux limits. For a fixed cost model, the cost increases as the flux limit decreases, as shown in Figure 4, for 10 and 300 MW_e using sodium-cooled technology. Observe that, starting at the optimum flux, the cost increases slowly at first because all that is required is to purchase a larger receiver. The cost increases more rapidly at the lower flux levels because, in addition to a larger receiver, more heliostats are required to compensate for the decreasing efficiency shown in Figure 3b.

The break-even cost as a function of the flux limit is shown in Figure 5 for 100- and 300-MW_e systems. Since the flux limit changes because of changes in the receiver cooling fluids, the break-even costs include every subsystem that is affected by the fluid: receiver, piping, pumps, storage, and heat exchanges. The shape of the break-even durves is similar at both power levels. For fluxes greater than 0.8 MW_t/m^2, the break-even cost is essentially constant. Below 0.8 MW_t/m^2 it drops rapidly because of the decreasing efficiency.

To illustrate the use of these break-even curves, assume that a sodium-cooled system has a receiver flux limit of 1.7 MW_t/m^2 and a salt-cooled system has a limit of 0.7 MW_t/m^2. From Figure 5, it is seen that the break-even cost is essentially the same for both systems at 100 MW_e, whereas at 300 MW_e the salt system break-even cost is 10 percent less than the sodium. The actual costs are comparable because while salt systems require a larger and more expensive receiver it also has lower storage costs. Therefore, even though there is a large flux difference between sodium and salt receivers, the energy costs are comparable.

Heliostats

The heliostat field is the most expensive subcomponent of a central receiver system, typically accounting for one-half of the total capital cost. A detailed study has been initiated of the break-even costs of heliostats as a function of the following design variables:

Tracking errors
Surface errors
Size
Shape
Reflectivity
Canting and/or focusing strategy

The baseline heliostat is the same as for the flux study.

RECEIVER SIZE INCREASES

- AREA $\alpha \frac{\text{OPTIMUM FLUX}}{\text{FLUX LIMIT}}$

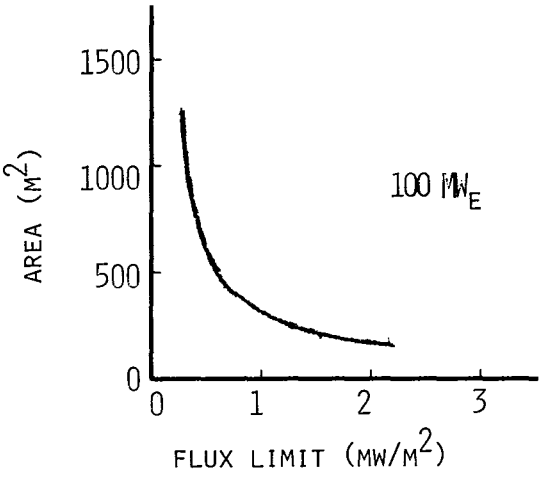

EFFICIENCY CHANGES

- RECEIVER LOSSES INCREASE
  α AREA
- SLIGHT DECREASE IN
  SPILLAGE + COSINE LOSSES

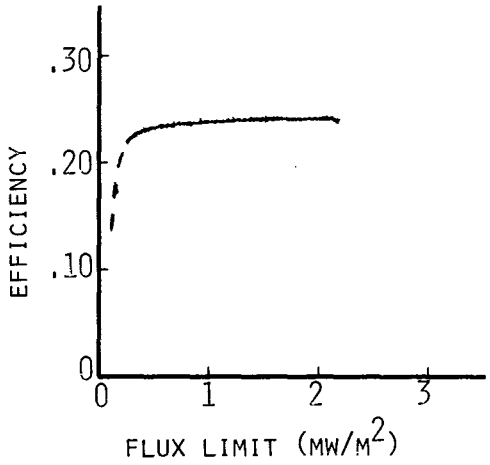

COST CHARGES

- LARGER RECEIVERS MORE EXPENSIVE
- COST OF STORAGE, PIPES, PUMPS + MEDIA CHANGE

Figure 3. A Receiver Flux Limit < Optimum Flux

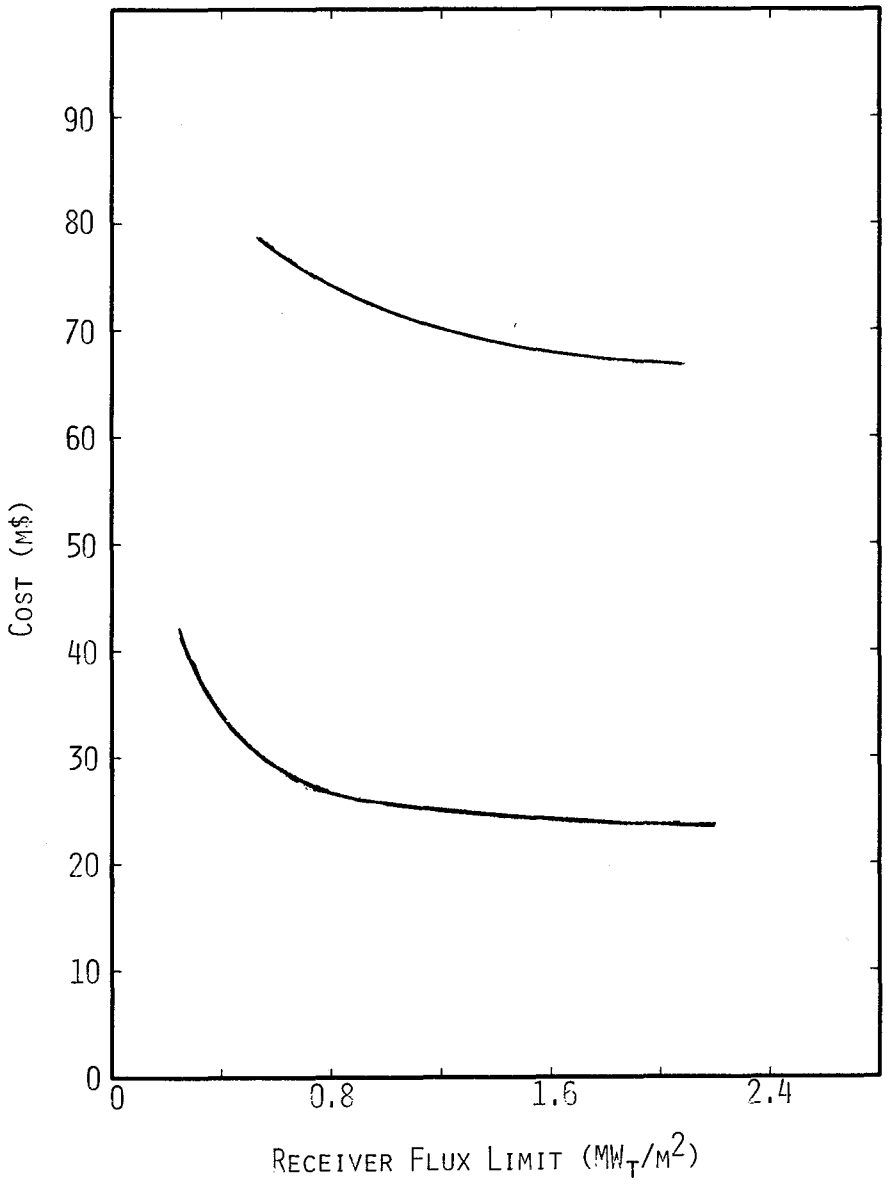

Figure 4. Cost of a Sodium-Cooled System Versus Receiver Flux Limit

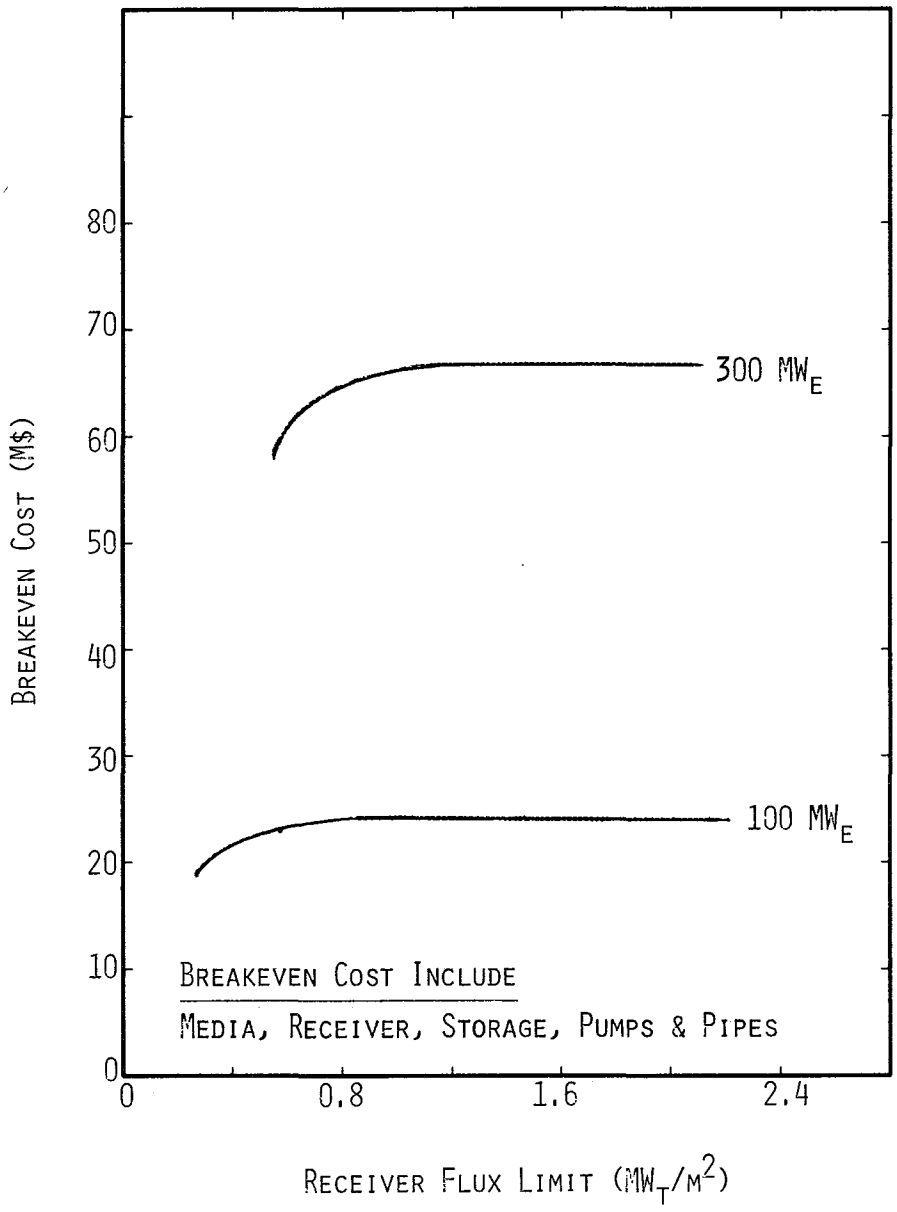

Figure 5. Break-Even Cost Versus Flux Limit

The break-even cost for heliostats as a function of the elevation angle tracking error is shown in Figure 6. The baseline cost is $\$65/m^2$ at an error of 0.75 mrad (one standard deviation). As the error increases, the break-even cost decreases and vice versa. The break-even costs for heliostat subcomponents can also be determined. For example, assume that the elevation error is changed because a new tracking motor is used in the baseline design. The dashed line in Figure 6 shows the cost of the heliostat without the elevation drive motor. The difference between the solid and dashed lines is the break-even cost for the elevation drive. The break-even cost for the drive decreases with increasing error. Observe that for errors greater than 3.5 mrad, the break-even cost for the drive is negative. A negative break-even cost means that even if the drive were free, the energy cost would be greater than the baseline case. Therefore, the design engineer need only consider drives with errors less than 3.5 mrad. Similar results have been found for azimuth and surface errors.

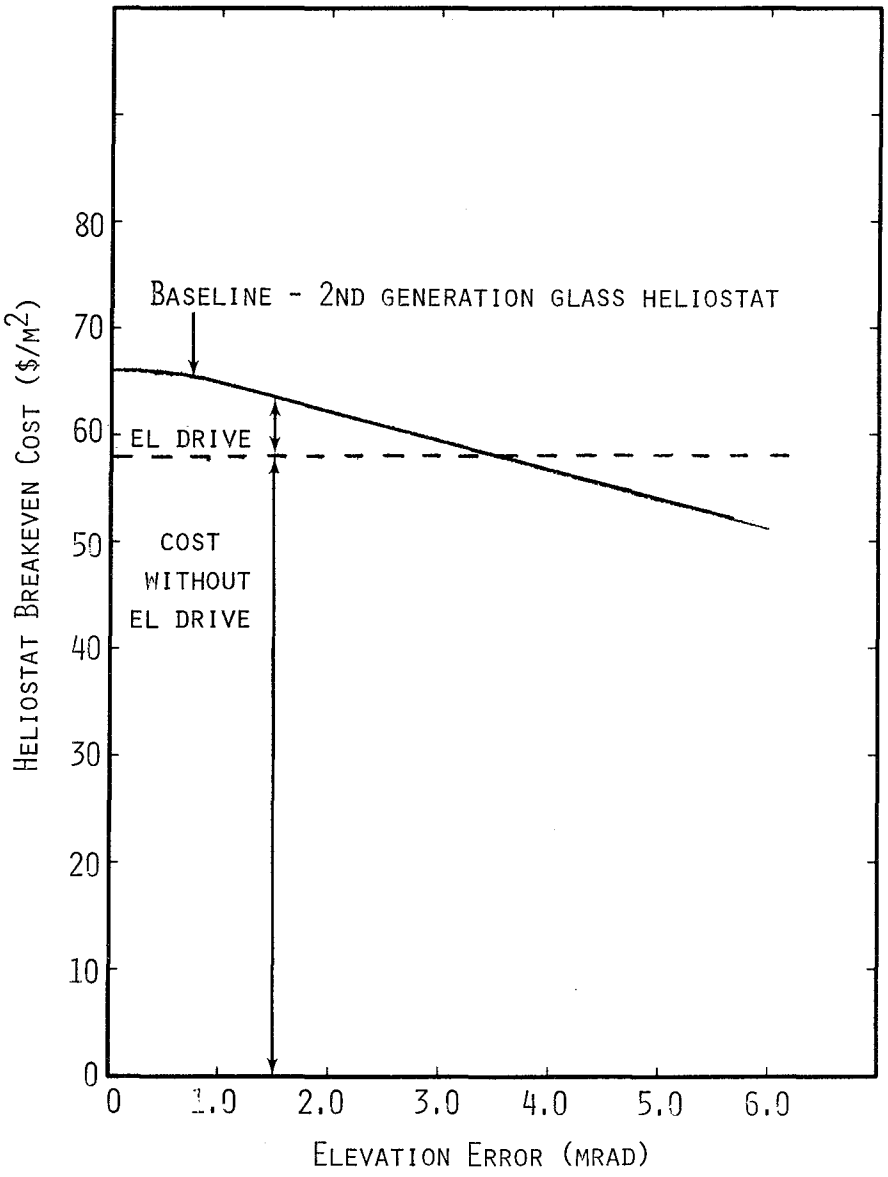

Figure 6. Breakeven Cost Versus Elevation Error

References

1. Miriam J. Fish and Theodore A. Dellin, The Cost/Performance of Large Central Power Systems as a Function of Heliostat Design Parameters, to be presented and published at the 1979 meeting of ISES, Atlanta, GA, May 28-June 1, 1979.

2. Theodore A. Dellin and Miriam J. Fish, DELSOL: A Computer Code for Calculating the Optical Performance, Field Layout, and Optimal System Design for Solar Central Receiver Plants, to be published.

SOLAR CENTRAL RECEIVER HYBRID POWER SYSTEM CONCEPTUAL DESIGN - MOLTEN SALT RECEIVER

C. N. Bolton
Martin Marietta Corporation

Martin Marietta is engaged in a study of solar central receiver hybrid power systems under a contract from DOE/SAN. The objective of this study is to develop a hybrid power system design that: produces minimum cost electrical power; minimizes the capital investment and operating cost; permits capacity displacement; and obtains utility acceptance for market penetration. By meeting the first three of these objectives, it is believed that the fourth, utility acceptance, will become a reality. The Martin Marietta concept, which combines a central receiver design, that uses high-temperature salt as the primary heat transfer fluid and thermal storage media with a fossil fired nonsolar energy source, is capable of meeting these objectives.

Table I shows the team members and their primary areas of responsibility. Martin Marietta provides the program management, the overall system design, and optimization of the solar and nonsolar subsystems and the collector and receiver subsystems. The nonsolar subsystem includes the nonsolar energy source and the nonsolar support facilities. The nonsolar energy source will consist of either a fossil fired steam boiler, which provides rated steam directly to the turbine, or a fossil fired salt heater, which can provide high temperature salt to a steam generator for direct conversion to rated steam or to thermal storage for later conversion to steam.

As shown in Figure 1, the contract period of performance is from October 1978 through September 1979. During Task 1, the requirements definition document was reviewed and comments and recommendations were provided to DOE/SAN. In the event that additional comments or recommendations are warranted as a result of further study, these will also be provided for consideration. Task 2 consisted of a market analysis to evaluate the potential market of solar hybrid power plants. Twenty-two utilities were selected within nine regions of the country. Both written and verbal correspondence were used to assess solar hybrid power plants with respect to the utilities' future requirements and plans. The parametric analysis of Task 3 evaluated a wide range of subsystem configuration and sizes. These analyses included both subsystems from the stand-alone alternative central receiver power system, using high temperature salt, and fossil fuel nonsolar subsystems. Task 4, selection of the preferred commercial system configuration, is using the parametric analysis developed in Task 3 to select configuration of subsystem for the commercial plant design. Task 5 will consist of a conceptual design of the selected commercial plant configuration and the related cost and performance.

TABLE I

TEAM MEMBERS AND RESPONSIBILITIES

ORGANIZATION	RESPONSIBILITY
Martin Marietta	Program Management, System Design and Optimization, Interface Definition, Heliostat Field and Receiver
Badger Energy, Inc.	Conceptual Design, Analysis and Optimization of the High Temperature Salt Subsystems
Gibbs & Hill, Inc.	Conceptual Design, Analysis and Optimization of the EPGS, Tower, and Nonsolar Support Facilities
Foster Wheeler Development Corp.	Conceptual Design, Analysis and Optimization of the Nonsolar Energy Source
Arizona Public Service	Provide Utility Engineering review of System Design, Utilization and Economics and Develop the Market Analysis

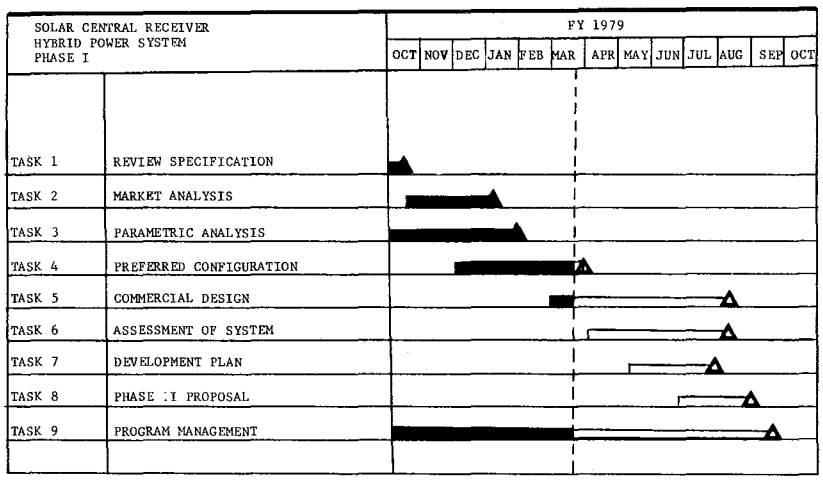

Figure 1. Program Schedule

Task 6 will assess the selected configuration for future potential improvements or limitation to widespread implementation of the hybrid power plants. During Task 7, a plan will be developed that identifies the stages of development required to assess the viability of the proposed hybrid concept. Task 8 will provide a plan and proposal for Phase II of the hybrid program. Task 9 is the ongoing program planning and management aspects of the program. Under this task the program plan was developed early in the program.

The market analysis (Figure 2) shows that the projected additional plant capacity to be added between 1978 and 1995 for each of nine regions totals 690,100 MW_e. Selected utilities in each of these regions were contacted to determine their future requirements, plans, and ideas. Utilities within the regions were selected based on their capacity and growth rate and the amount of insolation within the region. Of the 97 utilities identified, 22 were selected to form a representative matrix for the market analysis. For each region, the dashed line in Figure 2 shows the capacity represented by these selected utilities. As indicated, the selected utilities give a fair representation of each region except for New England. The selected utilities represented in the New England region form only a small amount of capacity; however, this representation is not a significant concern considering the insolation of the region. The large amount of capacity represented in the East South Central region is dominated by the TVA.

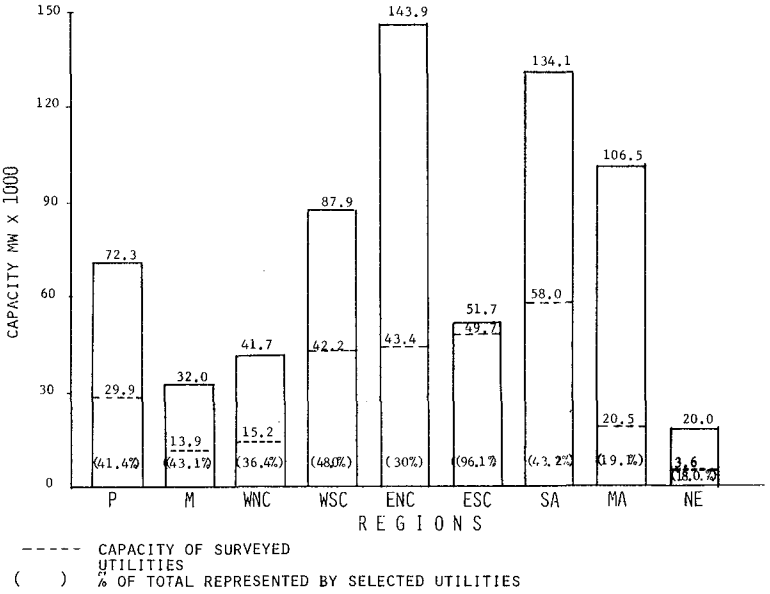

Figure 2. Projected Market Additions by Regions Between 1978 and 1995 (Includes all plant types)

Based on the market analysis, several factors emerged which require consideration in a hybrid solar power system design. With respect to fuel there are, as one would expect, conflicting requirements based on the various parts of the country. In the northeast, oil and gas are generally not available, whereas in the southwest there is a near term excess. In addition, coal is generally not permitted in California. The fossil fuel projected to increase the most is coal.

The general conclusion is that both the coal and the oil option should be held open in hybrid plants. From a dispatch strategy standpoint, the nonsolar part of the plant will be in competition with the total mix, and in general oil will be dispatched last. There is a desire to consider nonsolar subsystem ratings that are smaller than the plant ratings and to consider maintaining nonsolar subsystems in a hot standby or minimum load condition. In general, a large percentage of the utilities were interested in solar hybrid plants and also desire more related information. Also of interest was that time of day pricing has had no significant impact on load curves to date but most utilities are still assessing this factor.

The hybrid power plant design concept is based on a steam cycle with a parallel configuration of the solar and nonsolar subsystems. The steam cycle is a high efficiency reheat cycle using regenerative feedwater heating. The solar portion of the plant uses a surrounding field of heliostats which reflect energy onto a receiver located on top of a tower. A high-temperature salt is used as the heat transport fluid in the receiver, the heat transport fluid to transfer the heat to the storage subsystem and/or the steam generator, and as the thermal storage fluid. The steam generator is a series of heat exchangers that heats feedwater from the steam cycle with the hot salt to generate superheated steam and also reheats steam from the high-pressure stage of the turbine. Two fossil fuel nonsolar subsystems are being considered for the parallel configuration with the solar subsystems. The functional schematic, Figure 3, shows the concept using a fossil fuel boiler which generates superheated steam and furnishes this, in parallel with the salt heat exchanger steam generator, to the turbine. The functional schematic, Figure 4, shows the concept using a fossil fuel salt heater that heats salt and furnishes this, in parallel with the salt heated in the receiver, to either the storage subsystem or to the salt heat exchanger steam generator for the generation of superheated steam.

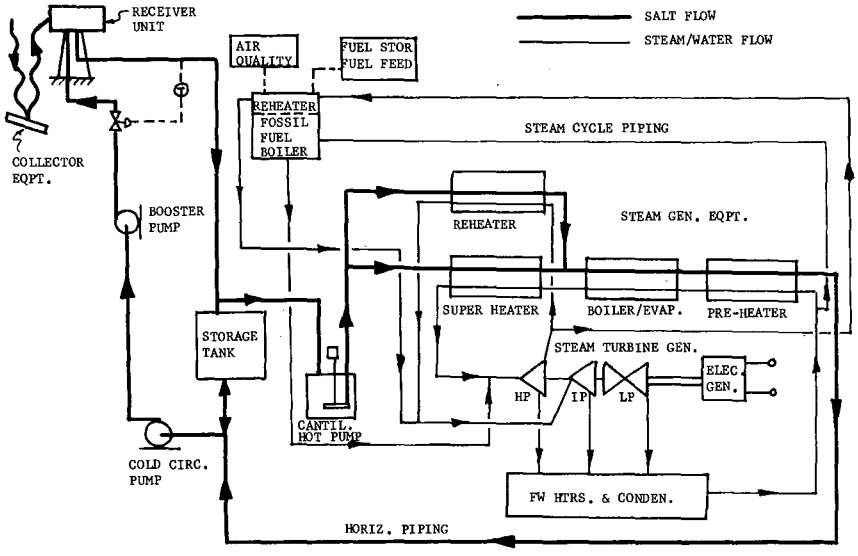

Figure 3. SCR Hybrid Power System - Steam Boiler Option

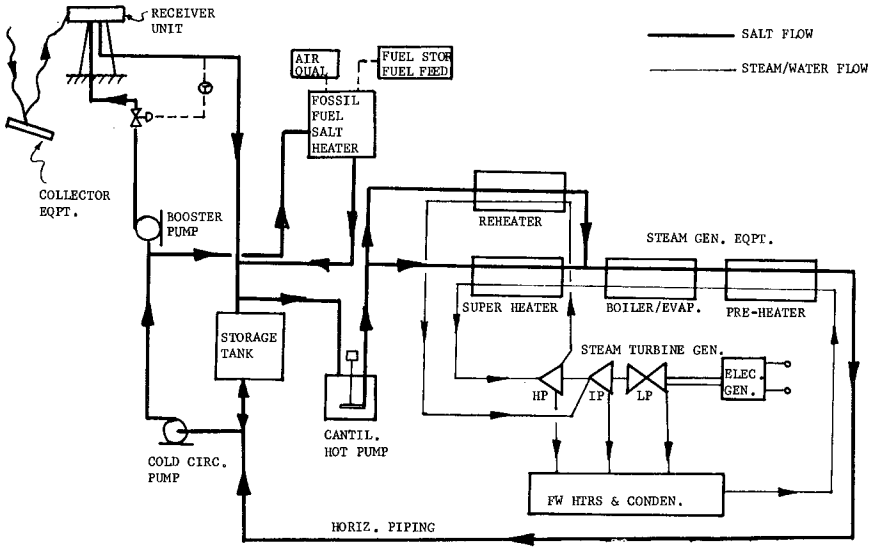

Figure 4. SCR Hybrid Power System - Salt Heater Option

For either of these configurations, the system can be operated from solar alone, solar plus storage, storage alone, fossil-fired alone, fossil-fired plus storage, or fossil-fired plus solar. For either configuration the salt temperatures and steam conditions are the same, whether operating from solar or nonsolar subsystems. The salt temperature at the outlet of the receiver or the fossil fired salt temperature at the outlet of the receiver or the fossil fired salt heater is 565°C (1050°F); the salt enters these units at 288°C (550°F). The main steam conditions to the turbine are 510°C (950°F), 16.5 MPa (2400 psig) with 510°C (950°F), from the fossil fired boiler, the salt heat exchanger steam generator or both. The optimum size of these systems is expected to be in excess of 100 MW_e and will be established during the selection of the preferred system configuration.

The selection of a fossil fuel boiler or a fossil fired salt heater for the nonsolar subsystem is one of the key considerations for selection of the preferred commercial system configuration. The existing boiler technology is compatible with the requirements of a hybrid power system and was used as a basis of comparison for the fossil fired salt heater. In addition, a comparison was made to existing technology used for heaters in the process industry. The design of a heater for application in the utility has many similarities to a boiler designed for utility application. The design constraints change depending on the fuel (coal, oil, gas) but have a similar effect for a particular fuel. These similarities include the overall size of the unit, which results from requirements of combustion volume, volumetric heat release rates, gas temperatures and velocities, and thermal duties. Since th heat transfer characteristics are dominated by the gas side rather than the fluid side (for a salt heater, steam boiler, etc.) the heat exchange surface areas will be similar. There are different requirements for the flow circuitry for the two types of units including the operating pressures and materials of construction. These factors tend to offset one another with respect to cost, but slightly favor the boiler. The higher cost materials associated with the heater are not fully offset by the reduction in material quantity due to the lower pressure requirements, when coupled with manufacturing constraints. In addition,

the maintenance and life requirements for utility applications will be the same. Operationally, the system incorporating the fossil fired heater has more system flexibility than the one with the fossil fired boiler, since it heats salt which can either generate steam or be stored, and it does not require a steam blending system.

The heaters normally used in the process industry have several significant differences when compared with heaters used in utility applications. These differences include life, number of cycles, unit sizes, type of fuel used, startup times, and the hardware scope of supply. The average life requirement for process heaters is 10 years as compared to 30 years for utility applications. The number of cycles required for process heaters is normally one or less per year where baseload and cyclic utility applications typically require 25 and 225 respectively. The unit sizes (or thermal duty) of process heaters average an order of magnitude smaller than typical utility applications. Process heaters are not presently manufactured that use coal. The startup time for process heaters are generally much slower than required in the utility industry. One must also be careful in comparing cost of process heater to a fossil fired heater for utility application since the scope of hardware supplied with a process heater is normally less than that quoted for comparable utility applications. In addition, care must be taken when comparing unit efficiencies since the process industry traditionally calculates efficiency based on the lower heating value of the fuel, rather than higher heating value, and thus indicates a higher efficiency for the same conditions.

Studies have been performed to assess collector-receiver modularity for central receiver power plants, as shown in Figure 5. The curves show the cost of the collector-receiver module in terms of dollars per MW-HRth of annual energy produced versus the collector-receiver module peak output. As shown, single module configurations are most cost effective for smaller power levels. As the total plant power requirement is increased, it becomes more cost effective to use several smaller modules even when considering the associated piping cost. Figure 5 does not necessarily represent the optimum cost figure but shows an example of using multiple 200 MW_{th} modules.

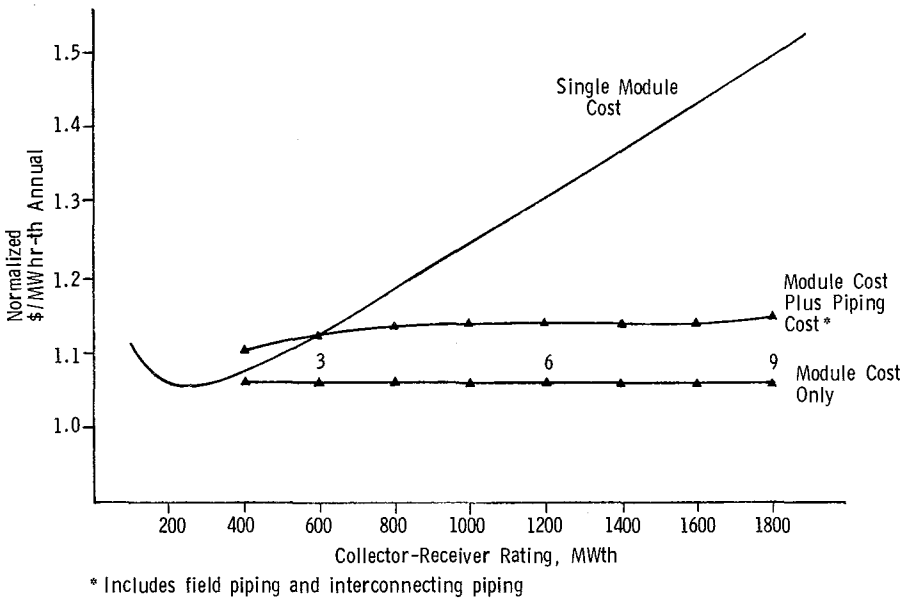

Figure 5. Example of Modularity Parametric Analysis for 200 MW_{th} Module Size

Figure 6 shows the levelized busbar energy cost, as a function of capacity plant factor, for hybrid plants that use coal and oil. As can be seen, the cost of fuel has a significant influence on the plant configuration depending on the desired plant capacity factor. The capital cost of the nonsolar portion of the plant, the capital cost of the solar storage, and the cost of fuel taken together form the basis of selection of the preferred system configuration. An important consideration in the selection is the extremely cost effective storage that is provided when using high-temperature salt as the storage media. This is emphasized in Figure 7, which compares the cost of storage to fuel cost as a function of additional plant capacity factor. The storage cost includes the storage media, containment, and the associated heliostat fields, receivers, and piping. The cost of fuel doe not include any capital related cost.

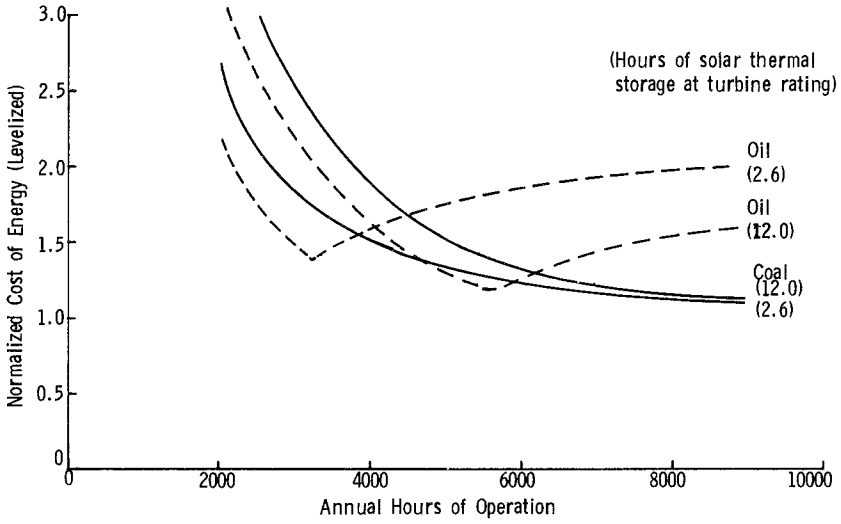

Figure 6. Hybrid Power System Costs of Energy

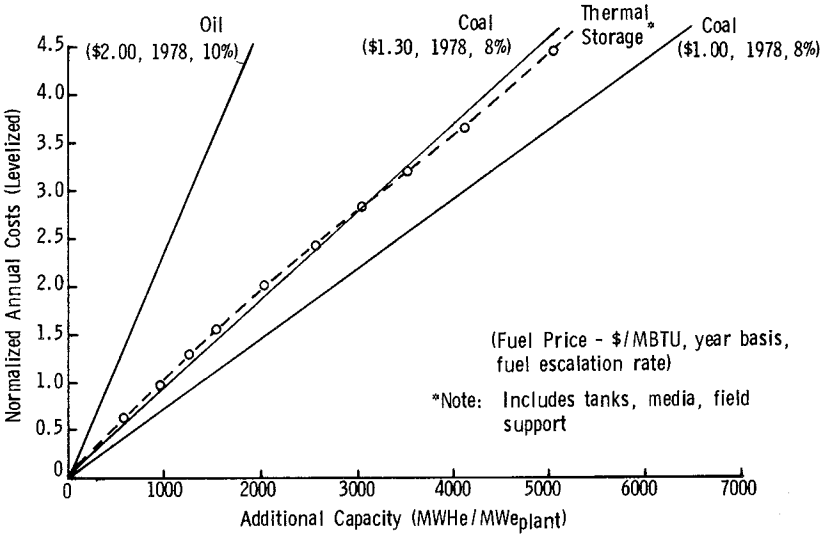

Figure 7. Fuel Cost Comparison With Thermal Storage (Barstow Insolation)

In summary, it has been shown that molten salt hybrid plants are competitive with conventional plants at baseload and/or intermediate capacity factors, for designs using the various types of fossil fuel. The incorporation of cost effective molten salt storage permits increased amounts of storage and reduced amounts of fossil fuel consumption and related decreases in the cost of energy. These factors are independent of the type of nonsolar subsystem utilized, fossil fuel boiler, or fossil-fired salt heater.

SOLAR CENTRAL RECEIVER HYBRID POWER SYSTEM SODIUM-COOLED CONCEPT

Energy Systems Group, Rockwell International
Babcock & Wilcox
McDonnell-Douglas
Salt River Project
SRI International
Stearns-Roger
The University of Houston

The Hybrid Concept

One concept that appears to have a high probability for producing large-scale electrical power (300 to 500 MW_e) on an economically competitive basis is the advanced, sodium-cooled central receiver. One attractive application of this concept is the hybrid system in which the sodium-cooled central receiver is combined with a fossil-fired unit to create a power plant with full capacity credit. In short, the rated output of the plant can be maintained at all times regardless of the availability of solar energy.

There are several ways in which the solar and fossil-fired parts of the plant can be combined, but the most cost effective configuration (i.e., the method that appears at this time to result in the lowest cost of power produced by the plant) is to place the fossil unit on the sodium side of the plant in parallel with the receiver in the manner depicted in Figure 1. This figure, which outlines the major functions of the hybrid concept, shows a typical operating condition in which most (90%) of the power (260 MW_t) required to drive the turbine is supplied by the solar receiver. The power from the fossil-fired unit is turned down to the lowest point it can operate and still be available for rapid load pickup in case of the loss of solar insolation.

In terms of plant operation constraints, only enough thermal energy is generally stored in buffer or storage tanks in a hybrid system as is required to cover any mismatch in the ramp rates of the solar and fossil parts of the plant. This process allows the plant to be switched from predominantly solar to predominantly fossil operation and back again without changing the plant output. However, in terms of economics, it may be desired to have a considerable amount of thermal energy stored, the amount being highly dependent on the cost of the fossil fuel relative to storage, on the cost of storage as a function of the size and amount of

storage, and on various other economic assumptions. In Figure 1, the storage is designated as a "temperature buffer," in order to convey the idea that the quantity of thermal energy stored may vary from as little as 10 or 15 minutes (buffering) to as much as 12 to 13 hours.

Also depicted in Figure 1 is a sodium-to-steam steam generator where the heat energy derived from the receiver and/or the fossil heater is transferred to the working fluid (steam) which drives a conventional steam turbine. From the steam turbine, sodium is allowed to flow into a cold (288°C) temperature buffer tank which is approximately the same size as the hot (593°C) buffer tank. From the cold buffer tank, sodium is then pumped up to the top of the tower and/or the fossil-fired heater.

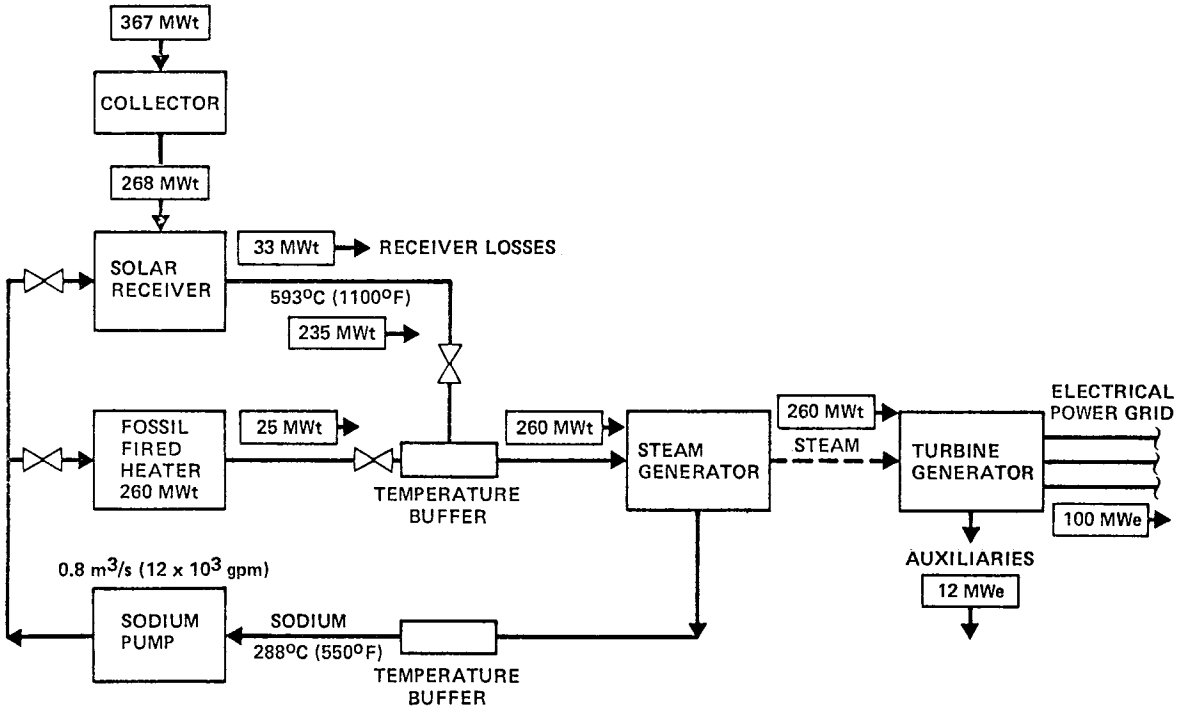

Figure 1. Solar Central Receiver Hybrid Power System

Hybrid Cycle Description

The principle of operation is shown in Figure 2. In this concept, sodium at 550°F is pumped through a riser up to the top of a tower and through a receiver whose midplane is approximately 120 meters above ground level. The riser is about 51 cm in diameter and is constructed of carbon steel. The receiver is composed of 24 panels oriented to form a cylinder about 10 m in diameter and 12 m high. The outer surface of each panel is the absorber surface (coated with Pyromark) and is exposed to the environment, thus forming an external-type receiver. Each panel in the receiver has a control valve that regulates the flow of sodium so that the outlet temperature from each panel is 593°C. After passing

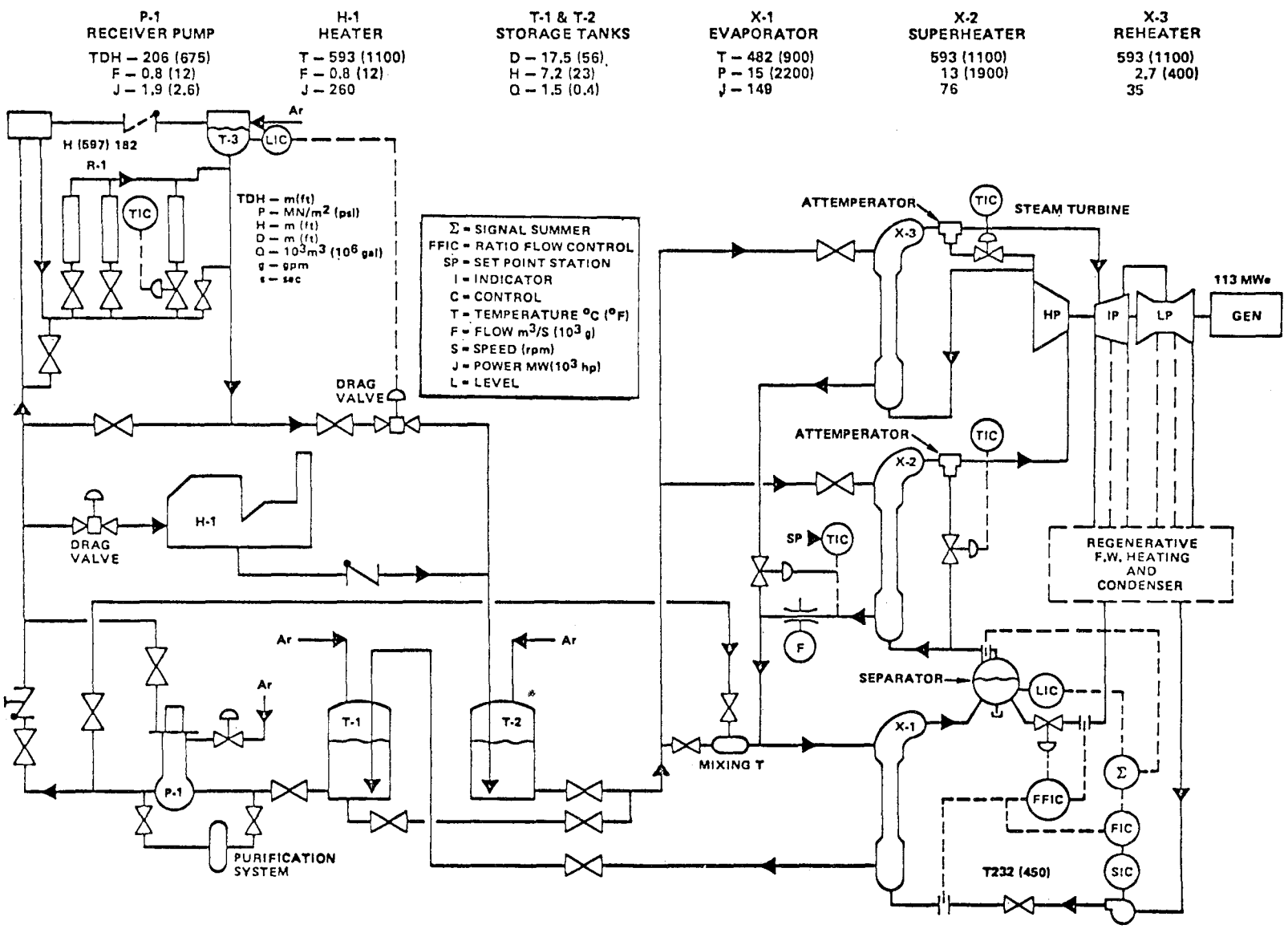

Figure 2. Solar (100 MW_e) Central Receiver Hybrid Power System

through the receiver panels, the sodium flows into a manifold which leads to a 51-cm diameter downcomer constructed of Type 304 stainless steel. Just before the sodium enters the buffer tank T-2, it passes through a drag or pressure reducing valve, which dissipates the static head and allows tank T-2 to operate at atmospheric pressure. Tank T-2 is constructed of Type 304 stainless steel. From tank T-2, the sodium flows through a series of sodium-to-steam steam generators. The first two units, the reheater and superheater, are constructed of stainless steel and operate in parallel. The flow from these two units is recombined and goes to an evaporator unit that is constructed of 2-1/4 Cr-1 Mo. From the evaporator, the sodium flows to tank T-1, which is constructed of carbon steel, and then is pumped up to the top of the tower by pump P-1. Operating in parallel with the receiver is a coal-fired heater which can heat the sodium from 288°C to 593°C. The output of the receiver and heater are identical, and the power from each can be split so as to minimize the consumption of fossil energy while allowing an uninterrupted production of steam from the steam generator.

The steam side of the plant consists of a steam plant, turbine/generator, regenerative feedwater, and condensing units. The steam temperature produced by the steam generator is 538°C, although higher temperatures could readily be achieved. Typical steam pressures available are 1800 to 2400 psi.

An artist's rendering of a 100-MW_e, sodium-cooled, hybrid plant is shown in Figure 3, and a preliminary plant layout is depicted in Figure 4. The major plant parameters are shown in Table I, which delineates the initial values that were assumed for the plant at the beginning of the program and the values that represent the current reference concept. The field receiver power ratio (FRPR) listed in the table is the ratio of the power that can be delivered to the receiver by the mirror field (assuming that the receiver can absorb any power level) to the power absorbed by the sodium in the receiver operating at its design limit. For this particular concept, the FRPR was found to optimize at a value of 1.05. Based on this value, the number of heliostats for the optimum 100-MW_e plant is 7760.

Advantages

Liquid sodium offers numerous operational, cost, and near-term marketing advantages for the hybrid. Most of these advantages have been enumerated in previous publications pertaining to the sodium-cooled, stand-alone, solar plant. For example, because liquid sodium is such a good heat transport fluid, heat fluxes in the receiver can be high (up to 1.7 MW/m^2 in current designs). These high heat fluxes permit the receiver to be small, thus reducing losses and allowing external, low-cost, light-weight receivers to be used. Similarly, the sodium heater can potentially be made smaller than a conventional power plant steam boiler that produces the same power to the turbine. Also, reheat is very cost effective in the sodium concepts.

Since large sodium components (such as 33,000-gpm pumps, 100-MW_t steam generators, 35-MW_t heaters) have been built and operated, the uncertainties in component availability and performance are greatly minimized and the cost estimates of these components, as they apply to solar applications, can be estimated with reasonable confidence. Also, as a result of more than 25 years of operating experience and studies on sodium systems, there are no materials compatibility

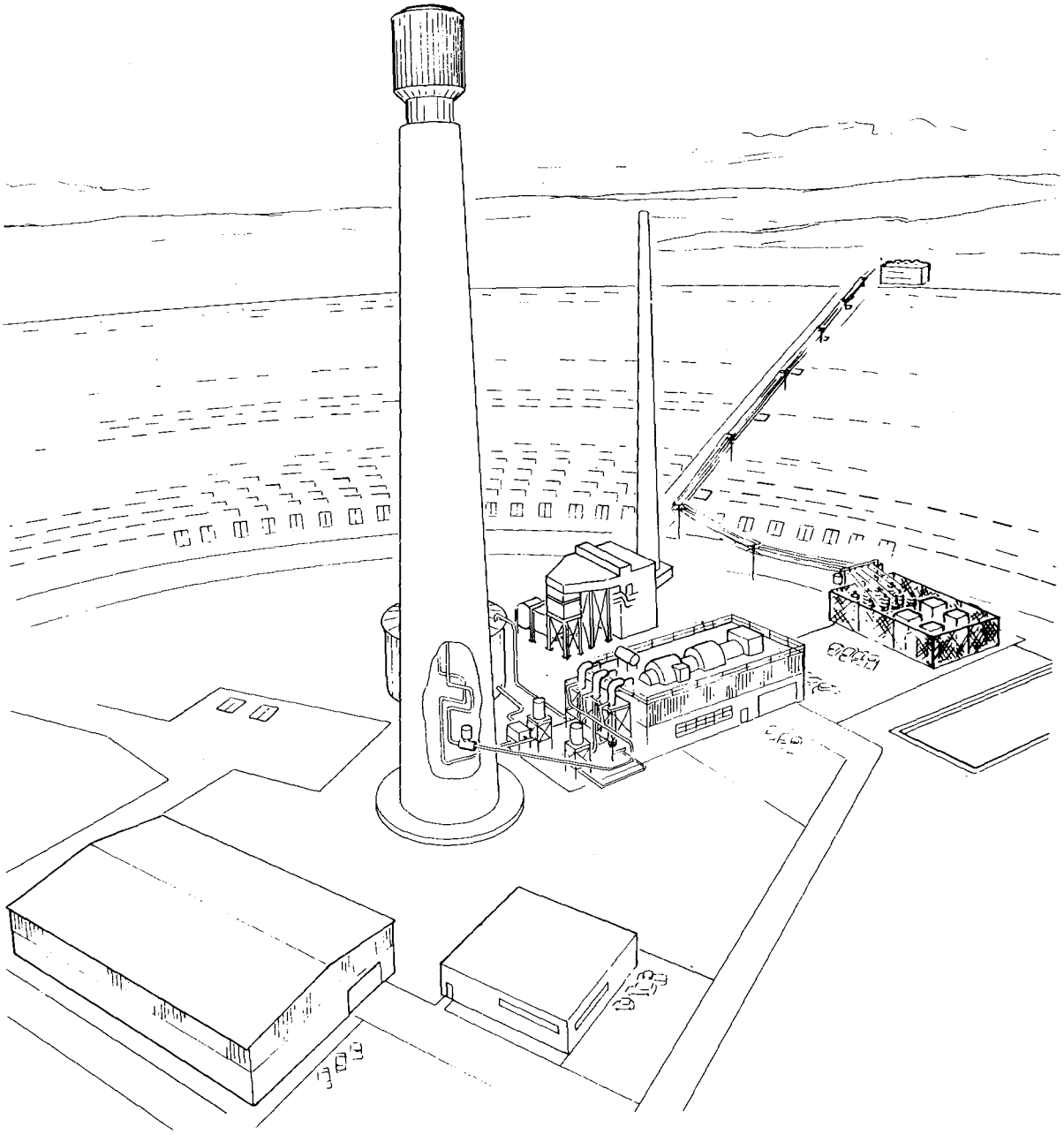

Figure 3. Solar Central Receiver Hybrid Power System

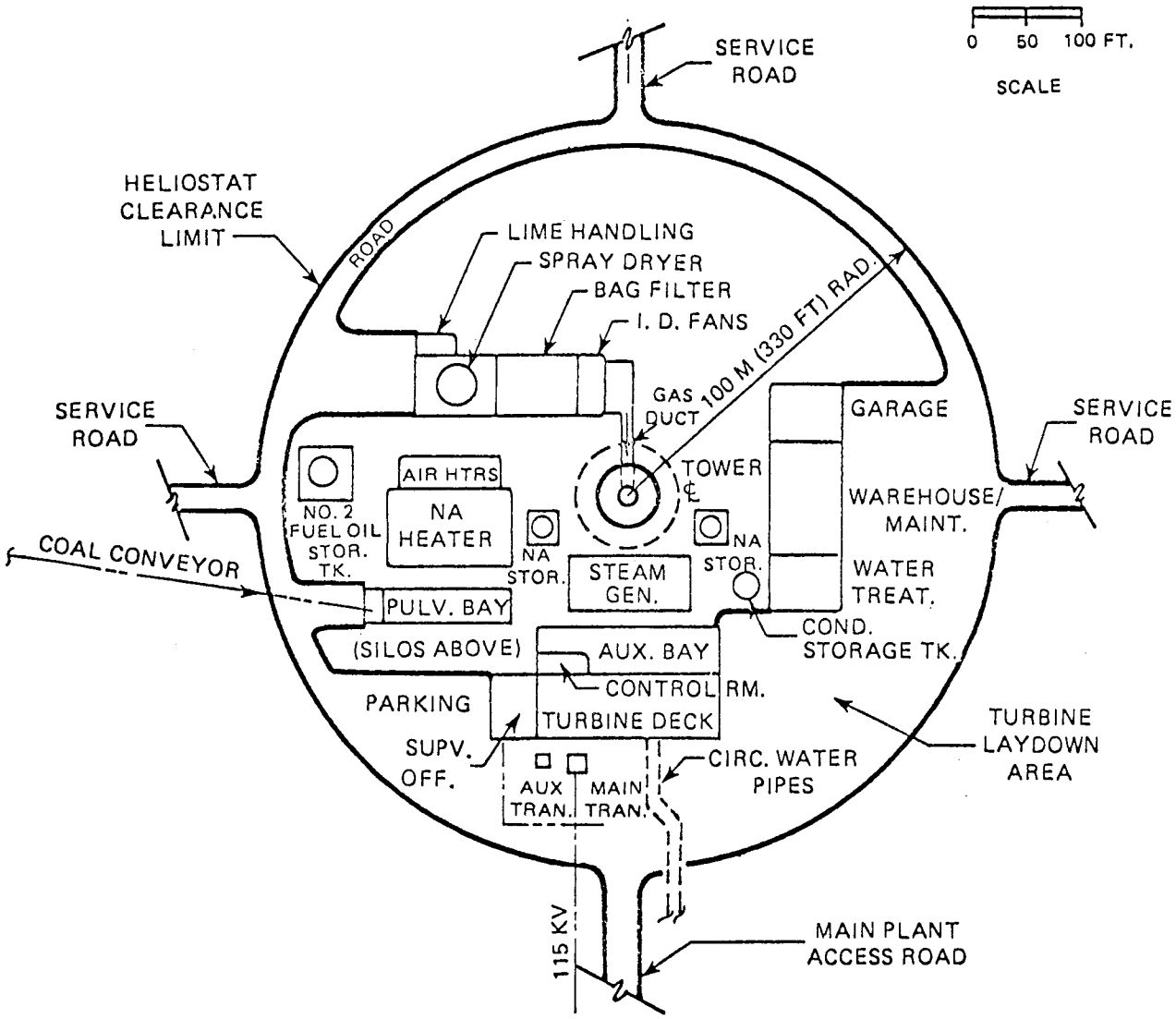

Figure 4. Plant Layout (Preliminary)

TABLE I

HYBRID CURRENT PLANT SUMMARY

SYSTEM	PARAMETER	UNITS	INITIAL VALUE	CURRENT VALUE
ELECTRIC	NET POWER	MWe	OIL-FIRED 100	COAL-FIRED 100
	GROSS CYCLE EFFICIENCY	%	43.1	43.5
RECEIVER	SOLAR MULTIPLE SM		0.9	0.8
	THERMAL POWER	MWt	(90%) 234	(80%) 208
	MIDPOINT ELEVATION	m (FT)	135 (443)	120 (394)
	HEIGHT AND DIAMETER	m (FT)	12.3 x 12.3 (40.4 x 40.4)	10.4 x 10.4 (34.1 x 34.1)
	FIELD TO POWER RATIO	-	1.00	1.05
	SODIUM FLOW RATE	KG/HR (LB/HR)	2.19×10^6 (4.82×10^6)	1.94×10^6 (4.29×10^6)
	SODIUM TEMPERATURES	^oC (^oF)	288/593 (550/1100)	288/593 (550/1100)
HEATER	THERMAL POWER	MWt	(10%) 26	(20%) 52
	SODIUM FLOW RATE	KG/HR (LB/HR)	0.24×10^6 (0.54×10^6)	0.49×10^6 (1.07×10^6)
	SODIUM TEMPERATURES	^oC (^oF)	288/593 (550/1100)	288/593 (550/1100)
EPG	TURBINE IN PRESS.	MN/M^2 (PSIA)	12.5 (1815)	17.5 (1815)
	SUPERHEATER TEMP.	^oC (^oF)	538 (1000)	538 (1000)
	REHEATER TEMP.	^oC (^oF)	538 (1000)	538 (1000)
COLLECTOR	MIRROR AREA	KM^2 (FT^2)	0.41 (4.5×10^6)	0.37 (4.0×10^6)
	NO. OF HELIOSTATS			
	FRPR 1.0		8464	7390
	1.05		—	7760

problems with applying sodium technology to solar hybrid concepts. Finally, because of the high-temperature capability of sodium, modern, high-efficiency steam conditions can readily be achieved.

The current hybrid configuration has several advantages over other potential configurations. For example, a parallel arrangement for the heat/receiver can be shown to minimize thermal cycling, and therefore improve component lifetime. By placing the heater on the sodium side of the plant as opposed, for example, to building a new fossil-fired steam boiler to feed the turbine in parallel with the sodium-to-steam steam generator, one can achieve a much simpler system to operate and can avoid long piping runs when reheat is employed. From a utility viewpoint, the sodium-cooled, hybrid concept has the advantage that full capacity credit can be assigned to the plant, and the solar side of the plant is totally decoupled from the steam side of the plant.

Trade-Off Studies

Numerous trade-off studies have been conducted in order to arrive at the above described reference design, and several more are scheduled to be carried out before Phase I of the project is completed. One of the more important studies has been the selection of the fossil fuel for the reference plant. Although the use of oil results in a plant with considerably lower capital cost and substantially lower operating and maintenance costs, the cost of coal appears to be a deciding factor. For the economic model that formed the basis of the coal versus oil selection study, the cost of oil was taken to be $2.00/MBtu, whereas the cost of coal was assumed to be $1.00/MBtu. For equal escalation rates for both fuels and certain capital cost assumptions, it was found that the levelized busbar energy cost over a plant life of 30 years, starting in the year 1990, was lower for coal than for oil for capacity factors greater than about 35 to 40 percent. This trend is shown in Figure 5, which gives the busbar energy cost for a coal and an oil-fired hybrid plant as a function of capacity factor for a fuel escalation of 8 percent per year. For all fuel escalations from 6 through 15 percent, the same conclusions could be drawn: the busbar energy cost from a coal-fired, solar hybrid plant was less than that of an oil-fired plant, although the crossover point rose to higher values for the capacity factor as the escalation rate decreased.

In addition to the busbar energy cost factor, there are several other considerations that tend to favor coal as a fuel. Among these considerations are the availability of oil, the abundance of coal, the fact that a coal-burning heater can be readily converted to an oil-burning heater, and the fact that the burning of coal is less likely to have restriction placed on it as a result of political constraints.

Acknowledgments

The Energy Systems Group of Rockwell International is the prime contractor on the hybrid, central receiver program. Other members of the study team are (1) Babcock and Wilcox, which is responsible for the design of the sodium heater

and the estimate for its cost and performance; (2) McDonnell Douglas Corporation, which, in association with the University of Houston, provides design data, cost estimates, and performance values for the collector subsystem; (3) the Salt River Project, which is an Arizona utility and provides design reviews, operational guidelines, and utility acceptance criteria; (4) SRI International, which is conducting the market analysis; and (5) Stearns-Roger, which is responsible for the electric power generation subsystem, tower design and cost, and the plant layout.

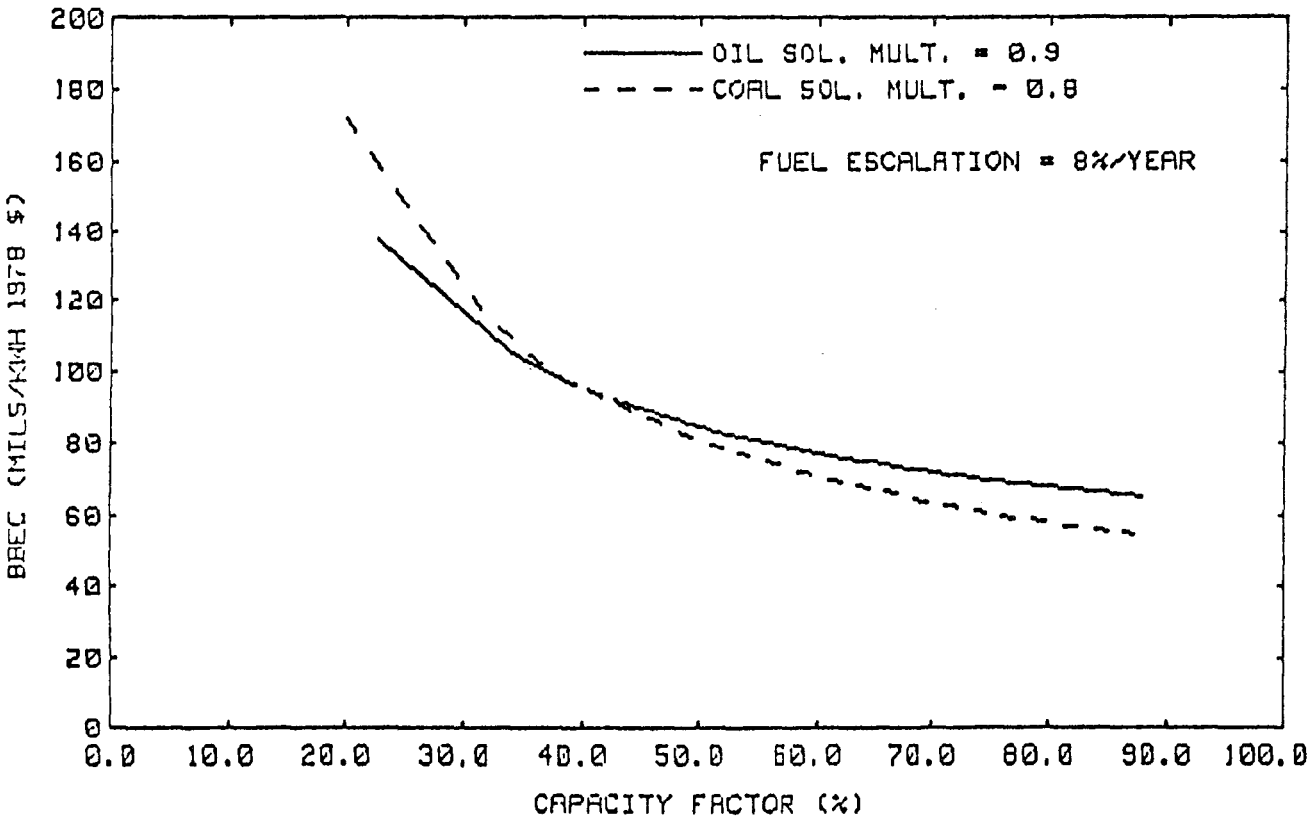

Figure 5. Oil and Coal Hybrid Busbar Energy Costs
(First Plant - Fixed O&M)

COMBINED CYCLE SOLAR CENTRAL RECEIVER HYBRID POWER SYSTEM

J. H. Westsik
Bechtel National, Inc.

Introduction

A potentially economical method to conserve the rapidly diminishing fossil fuel supply, particularly oil and natural gas, is to use solar hybrid power plants. Such installations would be operated with a combination of solar energy and conventional fossil fuel. New or repowered hybrid plants can deliver reliable, uninterrupted electric power to the utility grid regardless of the availability of solar energy. This could overcome one of the major utility objections to stand-alone solar power plants, which are dependent on the availability of sunshine or on extensive storage provisions.

Solar hybrid power plants with conventional steam Rankine or gas turbine cycles have been proposed. The Bechtel team chose the combined cycle hybrid power system for its studies. This system offers significant advantages that include the following:

- The efficiency of state-of-the-art combined cycle plants is excellent.
- Efficient combined cycle equipment is commercially available and an increasing number of combined cycle plants are being ordered by utilities for peaking and intermediate load service.
- As the high-temperature receiver and gas turbine technology progresses, significant performance improvements are attainable.
- The system is suitable for use with a variety of liquid and gaseous fuels.
- The fossil fuel system can respond rapidly to solar energy fluctuations without need for buffer storage.
- Results of previous studies indicated that combined cycle power plants are potentially the most economical hybrid option.

The objectives of the Phase I study are to:

- Develop and assess the concept of a combined cycle central receiver power system for commercialization in the 1985-1990 time frame.
- Prepare development plans to achieve technical readiness and competitive status by the desired commercialization data.

To simplify the comparative evaluation of the competing hybrid systems, a nominal power rating of 100 MW_e was specified for the study by DOE.

During the initial phase of the study, two basically similar combined cycle hybrid power systems were considered. The near term, "strawman," system has a heat pipe receiver with receiver outlet temperatures in the range of 816°C (1500°F) and a gas turbine inlet temperature of 1093°C (2000°F). These gas turbine inlet conditions are considered to be within current commercial technology. The advanced system, "advanced strawman," has a receiver outlet temperature of 1093°C (2000°F), which requires a ceramic receiver. The nominal gas turbine inlet temperature is set at 1316°C (2400°F) which will be feasible for power-station type gas turbines as a result of current development efforts. The proposed technical approach calls for parametric analyses and market potential studies on both of these system options, leading to the selection of one of these for continuation into conceptual design/cost evaluations and for subsequent assessment of the concept.

The project is in its sixth month and is within a few weeks of the planned schedule, which is shown in Figure 1.

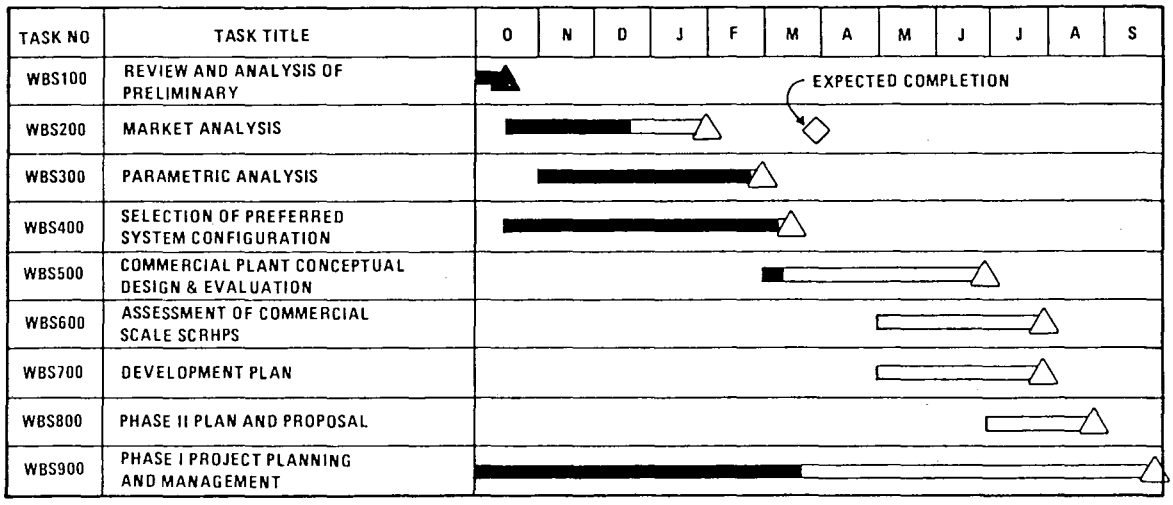

Figure 1. Project Schedule

Plant Description

Figure 2 is an artist's conception of the combined cycle hybrid plant. The collector field occupies an elliptical land area with approximate overall dimensions of 1040 x 1300 meter s (3400 x 4300 ft). The receiver tower is located south of the field geometric center. The tower height to the receiver center line is 175 m (574 ft) for the strawman and 19 m (643 ft) for the advanced strawman concept. The receiver is of the cavity type and is divided into four quadrants. A circular area at the foot of the receiver tower is occupied by the combined cycle energy conversion equipment, the switchyard, the central control building, maintenance and warehouse facilities, and administration building and access roads. The cooling towers are outside the perimeter of the collector field.

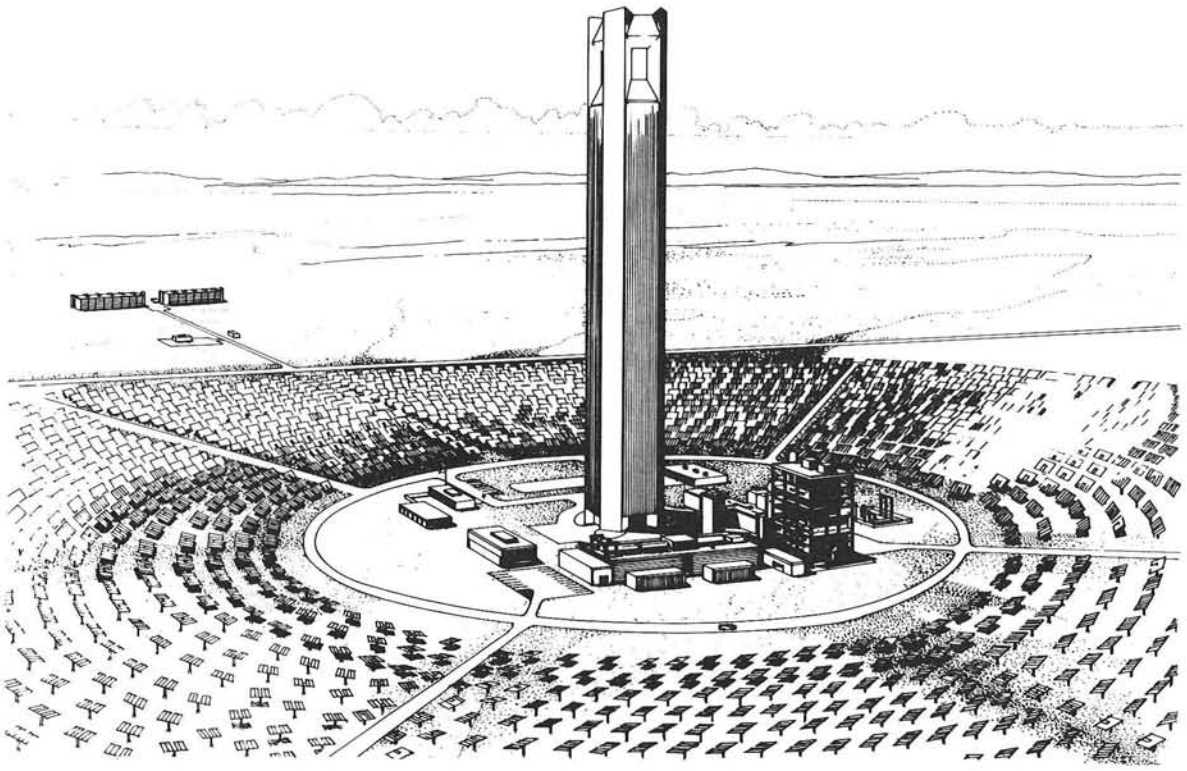

Figure 2. Artist's Conception of the Combined Cycle Hybrid Plant

Salient features of the combined cycle hybrid configuration are shown in the system schematic in Figure 3. The major system characteristics, as well as performance data, are tabulated in Table I. Note that the solar receiver operates in series with the combustor in the hybrid mode (i.e., when solar energy is available). In this mode the function of the combustor is to raise the air temperature from the receiver outlet level to the gas turbine inlet conditions. Since the full air flow is passed through the receiver, the outlet

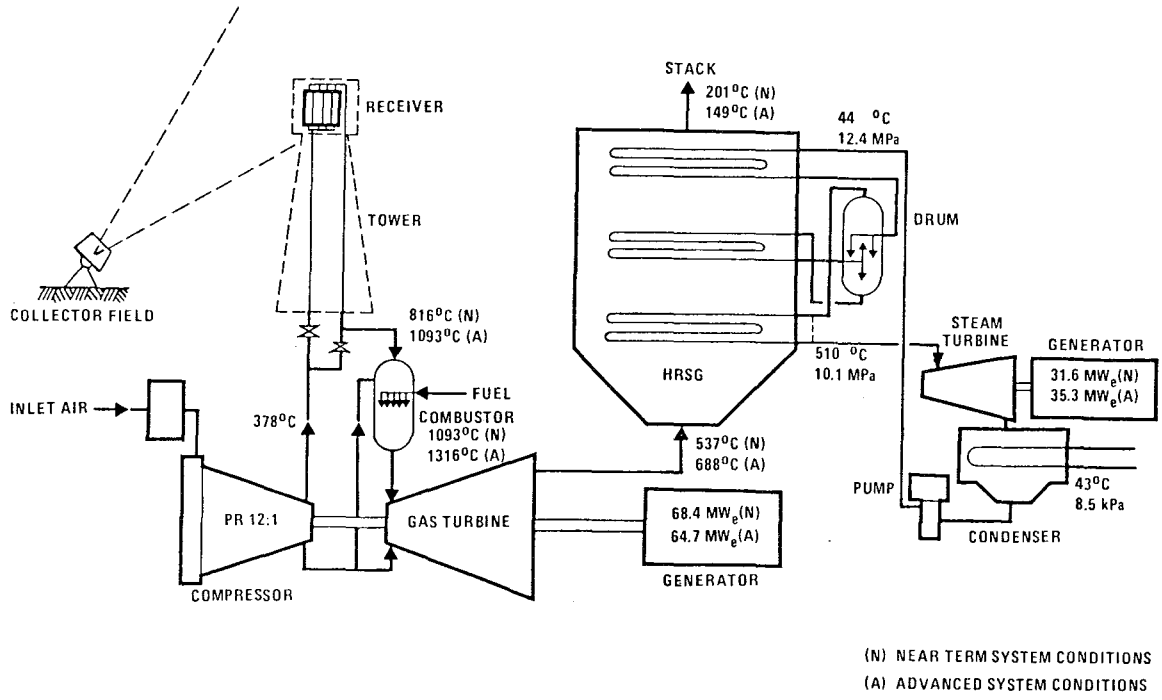

Figure 3. System Schematic

TABLE I
SYSTEM PERFORMANCE

	STRAWMAN	ADVANCED STRAWMAN
NUMBER OF HELIOSTATS	5,496	7,071
HELIOSTAT REFLECTIVE AREA (m^2)	38.6	38.6
COLLECTOR FIELD SHAPE	ELLIPTICAL, SOUTH OFFSET	
SITE AREA ($10^{-6} m^2$)	1.35	1.6
RECEIVER APERTURE ELEVATION (m)	175	196
RECEIVER TYPE	HEAT PIPE	CERAMIC TUBE
RECEIVER CONFIGURATION	SEGMENTED/CAVITY TYPE	SEGMENTED/CAVITY TYPE
SOLAR FRACTION (%)		
– DESIGN POINT	56.3	71.9
– ANNUAL AVERAGE DAYTIME	31.2	40.8
RECEIVER OUTLET/TURBINE INLET TEMPERATURE (°C)	816/1093	1093/1316
POWER CYCLE	AIR COMBINED CYCLE, UNFIRED HEAT RECOVERY STEAM GENERATOR	
ENERGY CONVERSION EFFICIENCY (%) (THERMAL TO ELECTRIC; NET)	43.5	47.7
REFERENCE FUEL	No.2 FUEL OIL	No. 2 FUEL OIL
ENERGY STORAGE	NONE	NONE

temperature is continuously varying over the diurnal cycle. The receiver is bypassed when solar energy is not available. This approach eliminates the parasitic head losses in the receiver and the piping and results in lower fuel demand during nonsolar operation. The energy recoverable in the steam bottoming cycle of the near-term concept is limited by the pinch point temperature difference at the economizer. The lower performance of this cycle is due, in part, to the resulting greater stack losses, evidenced by the high discharge air temperature. This deficiency may be alleviated with a dual steam pressure cycle, and the energy conversion efficiency may be raised from the tabulated 43.5 percent to 45.3 percent. In plants with power rating higher than 100 MW_e where reheat steam turbines are available, efficiencies of 45.8 percent may be attained by the use of the reheat feature.

The advanced strawman conditions offer a major improvement in solar fraction and in cycle efficiency. At the design point, the advanced system can provide a solar fraction of 0.719 compared with 0.563 of the nominal near-term system. (In this system configuration, the solar fraction is dictated by the ratio of the receiver temperature rise to the total temperature rise in the air stream up to the gas turbine inlet.) At the same time, the energy conversion efficiency of the advanced combined cycle is 47.7 percent against 43.5 percent of the strawman system. The pinch point temperature difference is not limiting the energy recovery in the advanced cycle.

The combined cycle solar hybrid system does not require buffer energy storage since the combustor of the gas turbine cycle can respond fast enough to compensate for fluctuations in solar input to permit steady power delivery.

A marginal value analysis was conducted to determine if long-term storage would be economically advantageous for the combined cycle hybrid power systems. The results show no positive economic values below fuel escalation rates of 12 percent even with 100 percent efficient storage systems. With a more realistic storage system efficiency of 60 percent, the marginal value of storage remains negative below 14 percent fuel escalation. These results lead to the conclusion that energy storage cannot be economically justified in this combined cycle hybrid power system. Nevertheless, technically viable storage concepts have been advanced for high-temperature energy storage in recent DOE-funded studies and could be coupled to the combined cycle hybrid plants if they became economical in the future.

The collector field performance is indicated in Figure 4. This stair-step graph reflects the performance of a 6500 heliostat field delivering 156.4 MW_t of the incident 238.4 MW_t to the receiver surface. The energies collected for the actual strawman and advanced strawman systems are 134.6 and 173.2 MW_t respectively. The geometric efficiency of the collector field is about 66 percent. The north-facing cavity receives 34 percent of the delivered solar energy; each of the remaining three cavities receives 22 percent of the total energy. A comparison of solar subsystems costs indicated that it is more economical to use 49 m^2 (527 ft^2) heliostats than the earlier adapted 38.6 m^2 (415 ft^2) units.

The ceramic receiver of the advanced strawman is made of banks of SiC U-tubes placed against the inside walls of the cavities. The heat pipe receivers of the strawman design consist of rectangular ducts serving as air passages. The heat pipes serve to evenly distribute the incident solar energy through the air stream and function as structural members as well. Approximately 790 heat

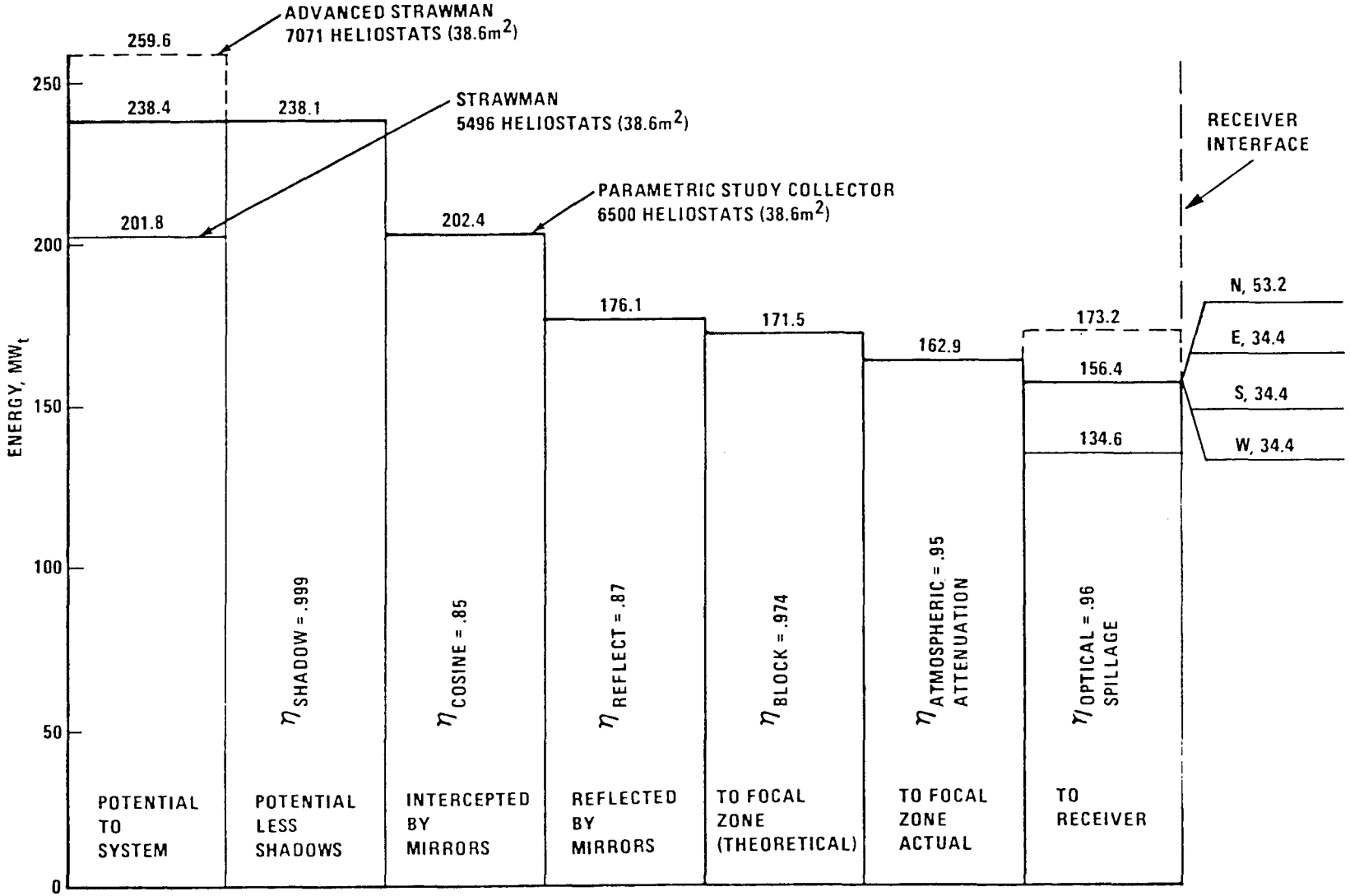

Figure 4. Energy Balance Stair Step, Collector Field

pipes are used in each panel. The north-facing cavity has 11 such panels; each of the remaining cavities has 9 panels. Figure 5 shows the maximum incident solar flux along the length of the north receiver panels. The highest flux represents approximately 10 kW_t per heat pipe, which is less than 60 percent of the peak flux tested with these pipes in the laboratory.

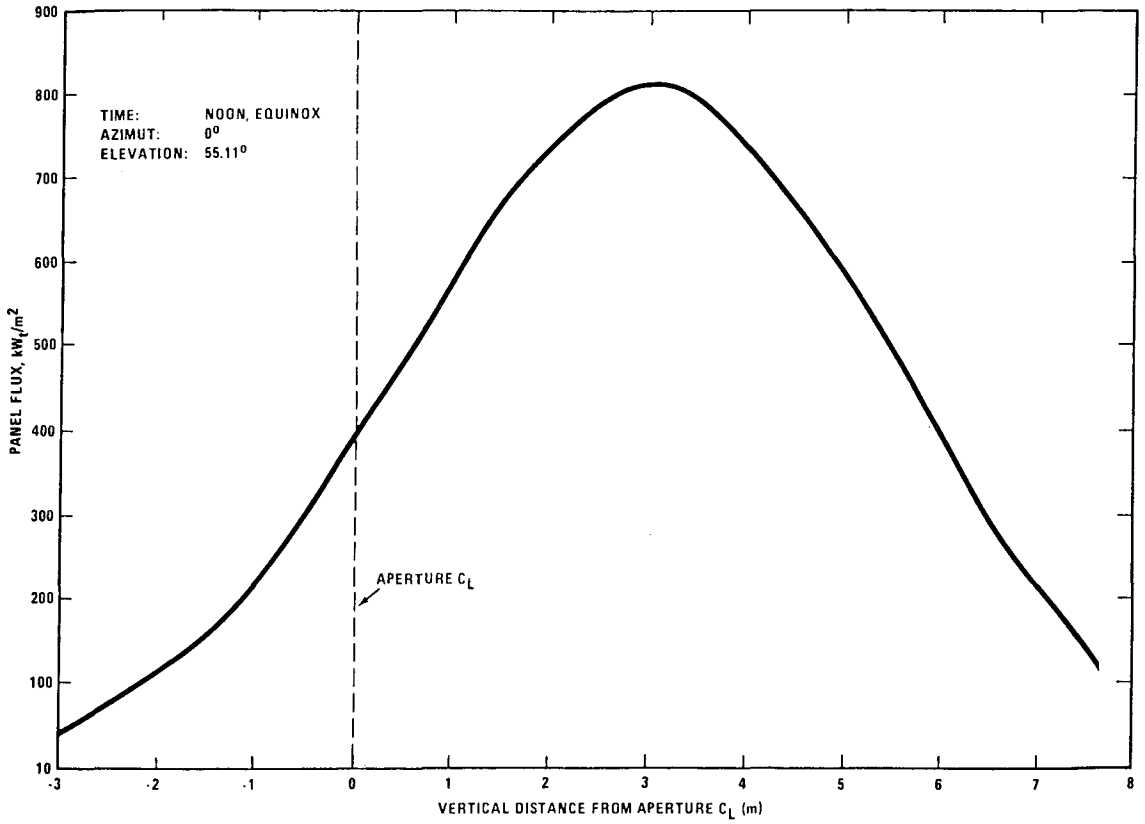

Figure 5. Cavity Flux, North Receiver

Significant Findings

- The use of heliostats with 49 m^2 (527 ft^2) reflective area improves the system cost due to significant savings in tower and land costs. The expected lower cost per square meter of the larger heliostats will represent additional savings.

- Gas turbines have sufficiently fast response times to obviate the need for buffer energy storage normally required by other solar power systems for compensation during short-term loss of solar energy input. On the basis of a special study conducted to determine the value of long-term energy storage, it was concluded that energy storage could not be economically justified

except when the escalation rate of the fossil fuel is above 14 percent per year during the expected life of the combined cycle hybrid plant. Nevertheless, if long-term storage would become a necessity for institutional reasons, it could be coupled to the combined cycle hybrid system.

- A number of high nickel alloys were examined to identify the most suitable type for the heat pipe receiver. Considerations included: costs, high-temperature strength, fabricability, raw material availability, and the effects on receiver weight. Inconel 617 appears to be the best all around choice.

- Two major technical issues have been identified in the studies thus far:

  1. High-Temperature Receiver Technology

     The technology of high-temperature receivers is lagging behind those designed to meet the requirements of steam Rankine power systems. Neither the ceramic tube nor the heat pipe receivers have reached the prototype development level. Assembly of SiC tubes into a receiver test article was just recently initiated. Although alkali metal heat pipe performances were measured in laboratory tests, additional information is needed to verify their performance under cyclic operating conditons. Data on failure modes and the potential safety aspects of failures are also required. Finally, the interaction between the heat pipes and receiver panels must also be evaluated.

  2. The major issue with the gas turbines is the adaptability of the combustor to operation with air inlet temperatures ranging from 378°C (712°F) to 816°C (1500°F). It was found that the NO_x emission is aggrevated at higher air inlet temperatures. However, specially designed combustor configurations or so-called "catalytic combustors" can be used to alleviate this problem. These combustors are currently under development in the gas turbine industry.

CONCEPTUAL DESIGN OF ADVANCED CENTRAL RECEIVER POWER SYSTEMS

J. A. Elsner
B. D. Pomeroy
General Electric Company

General Electric's conceptual design is based upon a liquid-metal cooled receiver and a high efficiency reheat steam cycle which receives its thermal input from sodium heated in the receiver. Liquid sodium was selected as the receiver coolant and heat transfer medium because of its very favorable high-temperature heat transfer characteristics. Compared to water and gas coolants, the high heat transfer coefficients of liquid sodium permit higher solar fluxes at the receiver surface. Consequently, the size of the receiver may be reduced, which will decrease receiver thermal losses and capital cost. The use of liquid sodium as the heat transfer medium also permits a more efficient reheat steam cycle because the steam generators are located at the base of the tower.

As indicated in the program schedule shown in Figure 1, a parametric analysis identified the preferred commercial plant configuration. The selected concept was then analyzed to provide estimates of the plant performance, land requirements, and equipment requirements. (This work was completed late last summer and was reported at the last semiannual review.) The commercial plant assessment and cost estimate were completed in mid-November. The safety analysis, the environmental analysis, and the development plan including pilot plant and SRE descriptions were completed in early December.

The General Electric plant configuration is shown schematically in Figure 2. The receiver is cylindrical with a 195 m tower surrounded by a 5.6 km^2 field containing 20,415 enclosed heliostats. Sodium is heated to 1100°F in the receiver, with the flow regulated in each of the 24 absorber panels by 24 electromagnetic (EM) pumps. The pump at the tower base is centrifugal. The steam cycle has 2400 psi/1000°F throttle conditions with reheat to 1000°F. The cost of the solar steam supply in this case justifies additional expenditures for feedwater heating above the reheat point and a large annulus exhaust on the low pressure turbine, both of which boost the gross cycle efficiency to over 44 percent.

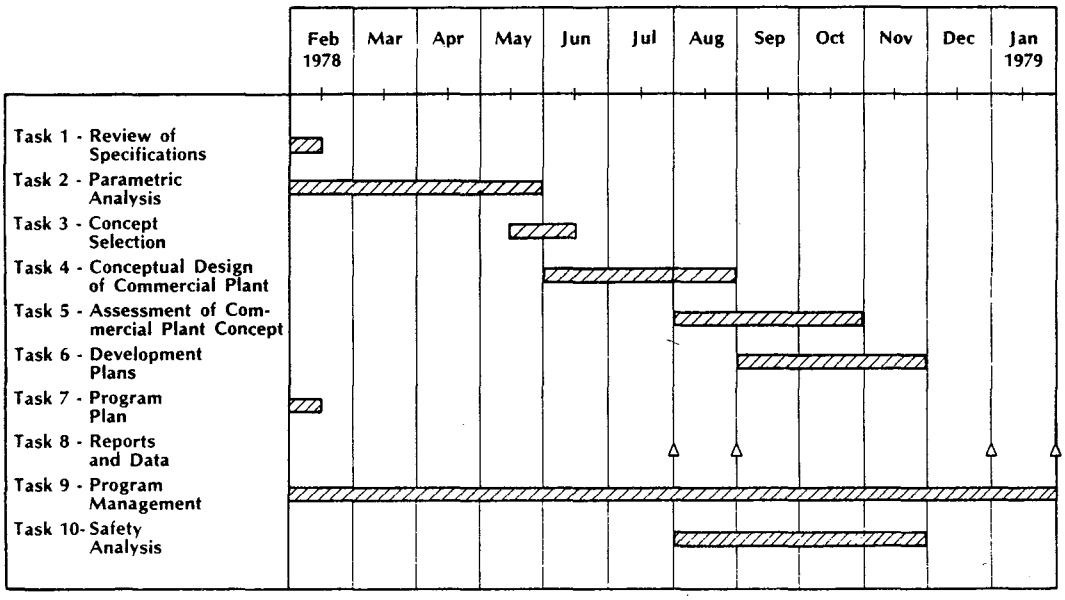

Figure 1. Conceptual Design of Advanced Central Receiver Power Systems Program Schedule

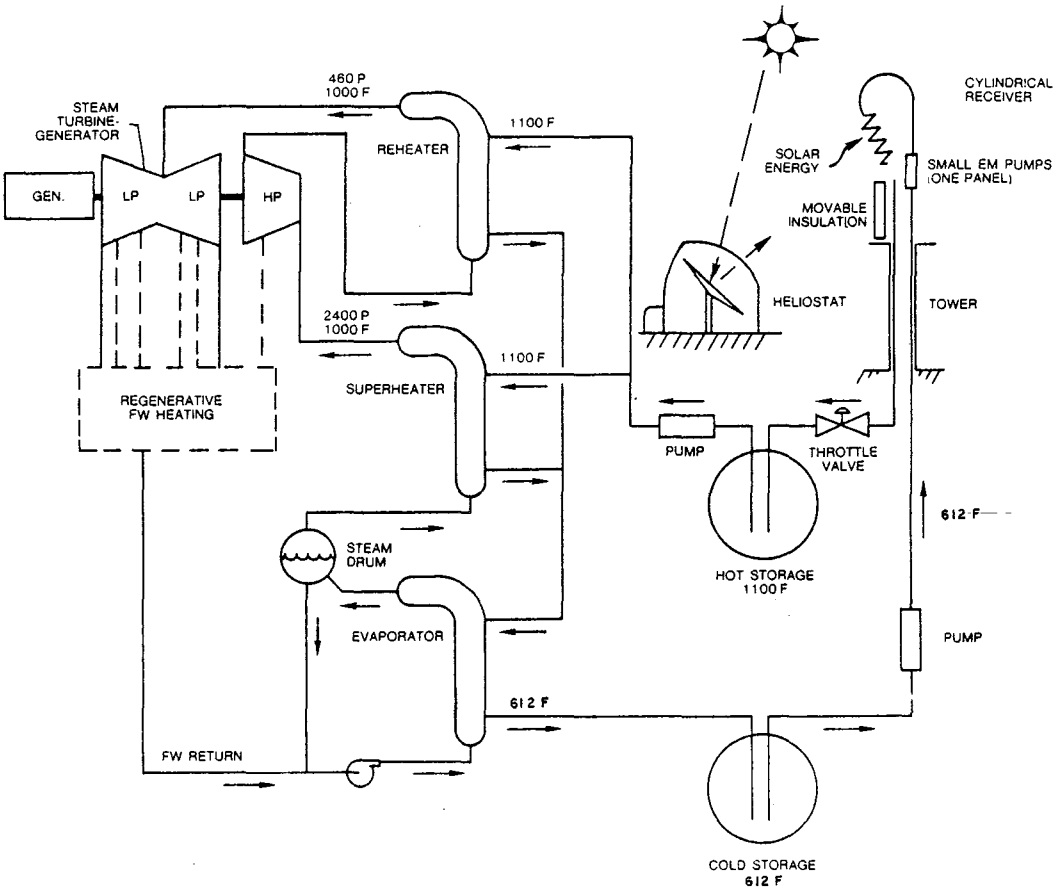

Figure 2. Advanced Central Receiver Power System Commercial Plant Configuration

Figure 3 shows an energy balance for this system at the design point. The receiver captures 89 percent of the solar power incident upon it (414 MW). Thermal power at the tower base is converted to electricity at a net efficiency of 40 percent (after deducting parasitic loads). Thus the overall conversion efficiency from power incident on the receiver to electricity at the busbar is 36 percent. Net electrical output at the design point is 99.6 MW; the parasitic power requirement is 11.8 MW.

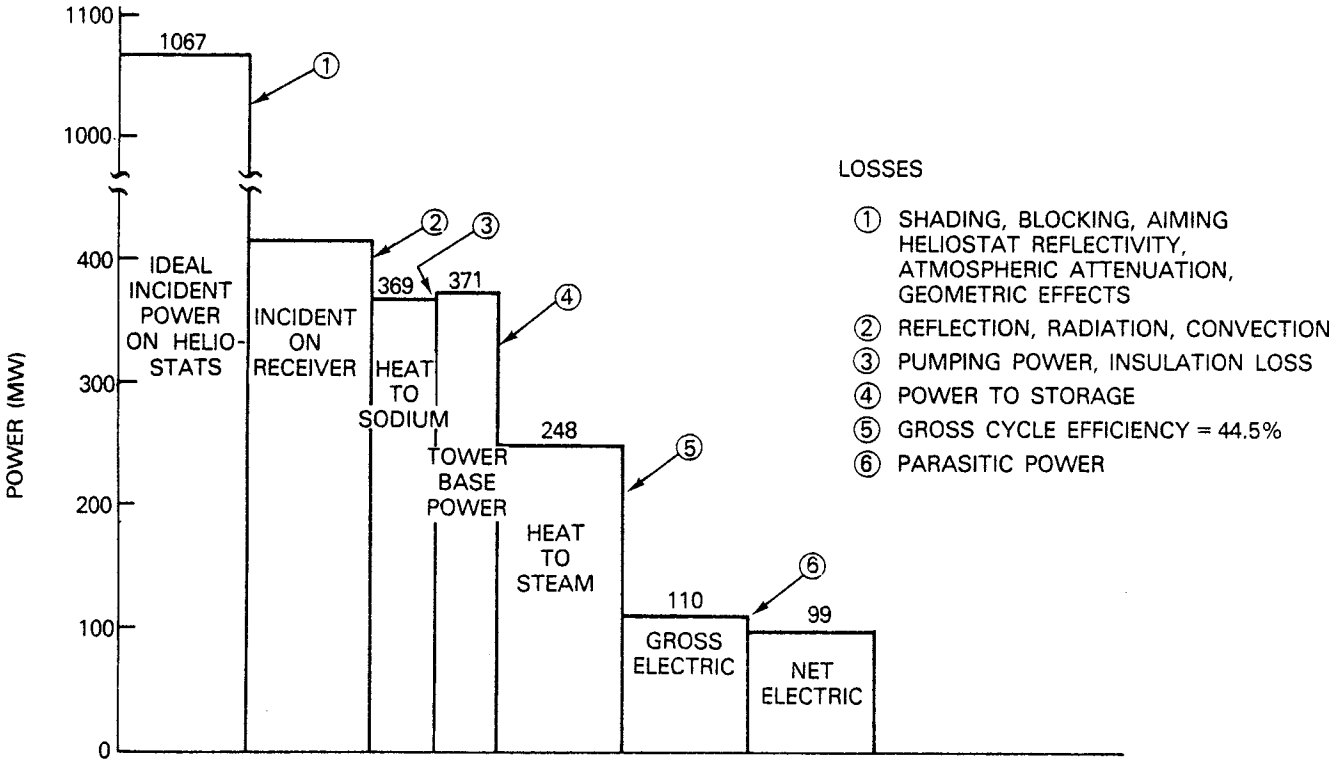

Figure 3. System Power Flow at Design Point (Noon, Summer Solstice)

The capital cost for the first commercial version of this concept is shown in Table I to be 2105M$. This cost includes land charges and all of the direct equipment, field material, and labor costs. Appropriate allowances for plant design, architect/engineer (A/E) fees and a contingency have been added through the distributables account, based on the assumption that an A/E would perform the plant design and startup, but would subcontract the actual construction work. The cost as quoted does not include owner's administrative costs, interest, and escalation during construction or the cost of obtaining permits and licenses.

Table I also lists a cost estimate of $163.7M for the Nth commercial power plant. The heliostat cost shows a significant decrease in this case due to the anticipated effects of experience and a high mass production level. The plant contingency allowance has been decreased by a factor of three because experience in building the same plant configuration will reduce the frequency of field change orders. The cost of liquid metal components also decreases slightly due to reduced vendor design requirements in the later production units.

TABLE I

"GROUND UP" CAPITAL COST ESTIMATE SUMMARY FOR FIRST AND Nth ACR COMMERCIAL POWER PLANTS
(In millions of 1978 dollars)

	First Commercial Power Plant	Nth Commercial Power Plant
Site, Structures, and Miscellaneous Equipment	10.7	10.7
Turbine Plant Equipment	20.1	20.1
Electric Plant Equipment	6.7	6.7
Collector Equipment	45.8	22.3
Receiver Equipment	36.2	31.7
Thermal Storage Equipment	19.2	19.2
Subtotal	138.7	110.7
Distributables	71.8	53.0
Total	210.5	163.7

While performing the plant design analysis and cost estimate, several improvements were identified which could not be implemented due to scheduling constraints; these improvements are listed in Table II.

TABLE II

POTENTIAL IMPROVEMENTS TO COMMERCIAL PLANT CONCEPTUAL DESIGN

2400 psi/1050°F/1050°F Steam Turbine Inlet Conditions
Improved Receiver Coatings
Improved Absorber Surface Geometry
Storage Vessel Support Design

First, the performance and costs quoted above are based upon a steam cycle having 1000°F peak steam temperature. After this selection was made, it was discovered that increasing the peak temperature to 1050°F could potentially reduce the total plant $/kW by 1 percent. Second, by changing the absorber coating from Pyromark to an etched metallic surface it might be possible to increase solar absorptivity to 98 percent and reduce infrared emmisivity to 10 percent. However, the life of this surface is unknown; experimental work is required to evaluate its durability.

Third, absorber performance could also be improved by designing the surface with numerous mini-cavities on a scale smaller than the convective boundary layer thickness. In this way, the effective solar absorptivity could be increased without increasing the convection losses. Since 10 percent of the solar energy is lost by reflection and infrared radiation in the present concept, small improvements in either absorptivity or emissivity could yield large benefits with respect to plant performance and cost. Lastly, the hot storage vessels are supported on "316" stainless steel legs which operate at the temperature of the tanks. By placing insulating pads between the tanks and the supports it may be possible to construct the legs out of carbon steel and realize a savings of about 1 percent on the total plant cost.

Table III describes the major considerations involved in selecting the pilot plant configuration and size. The field/receiver configuration was chosen to provide at least 0.5 MW/m^2 peak flux on the receiver. This minimum level of flux was required to demonstrate reasonably high receiver efficiency and provide believable scaling to the commercial flux of 1.8 MW/m^2. Based on rough scaling estimates of the various options, a 60 m tower with focused (canted) glass heliostats (north field) was selected and detailed field design calculations were performed. The flat receiver was chosen to be 10 m square to provide reasonable scaling of convection losses. Only one hour of storage capacity was chosen instead of three since the scaling of this storage concept is not an issue. One hour provides enough capability to demonstrate startup, run, and shutdown of the turbine from storage alone.

TABLE III

PILOT PLANT SELECTION

Collector/Receiver	
Objective:	Provide at Least 0.5 MW/m^2 Flux
Options:	Shrink Heliostats and Tower
	Remove Heliostats with Same Tower Combinations
	Use Small Field of Focusing Heliostats
Selection:	Focused Glass Heliostats with 28 MW Input to Sodium
Storage	
Objective:	Provide Demonstation of All Storage Operation Modes
Options:	Minimum Size Allows Turbine Startup, Synchronization, and Shutdown (about one-half hour)
Selection:	One Hour Capacity
Steam Turbine/Steam Generators	
Objective:	Provide Realistic Turbine/Steam Generator Interaction Including Reheat
Options:	Limited in Small Sizes
Selection:	1450 P/950 F/950 F - 10 MW (Electric), 28 MW (Steam)

The scale of the pilot plant was determined by the availability of reheat steam turbines. A reheat cycle was selected because the pilot plant should be able to successfully demonstrate the control interactions which will occur in the commercial facility. A further consideration is that sodium reheat loops have not been demonstrated on a large scale in the United States. The smallest reheat turbine found in an initial survey requires 28 MW of heat to steam at full load and produces 10 MW at the generator terminals. The size of this turbine sets the size of storage and the receiver subsystem (solar multiple = 1.0).

Figure 4 shows a schematic of the pilot plant. The turbine is a two-shaft marine drive unit geared to run a generator at 3600 rpm. The evaporator and superheater run at full commercial plant pressure (2600 psi) to maintain thermal stress scaling in the evaporator. High pressure steam is then throttled to 1450 psi to match the high-pressure turbine design condition. The reheater scaling from the commercial plant is not quite as good as the evaporator and superheater scaling because the reheat steam pressure is lower than in the commercial plant; however, this difference is not critical with respect to thermal stresses. The storage tanks are spherical, field fabricated structures as in the commercial concept. The receiver has ten absorber panels, each 1 m wide by 10 m long, with ten EM pumps for flow control. The collector field contains 917 heliostats and produces 28 MW of absorbed power at equinox noon with a peak flux of 1.5 MW/m^2 for a four-point aiming strategy.

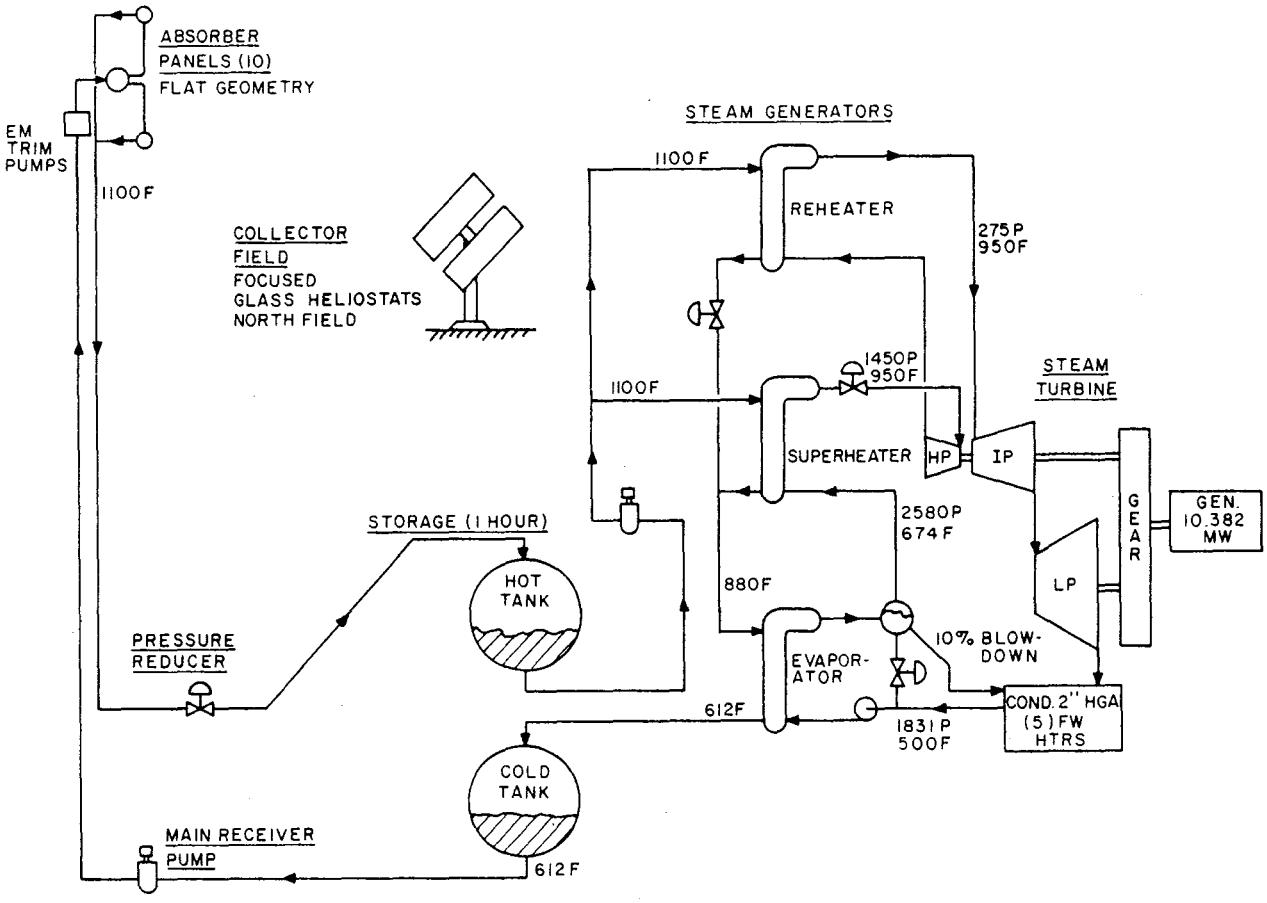

Figure 4. Pilot Plant Schematic Diagram

Table IV shows a performance comparison of the pilot and commercial concepts at their respective design points (equinox noon for the pilot, summer solstice noon for the commercial). The pilot plant shows somewhat poorer electrical conversion efficiencies than the commercial plant because the smaller pilot turbine is less efficient. However, the overall conversion from solar at the heliostats to electricity is better for the pilot plant. The difference is attributed to the fact that the pilot plant uses glass heliostats, whereas the commercial concept has enclosed heliostats which reduce flux to the receiver because of transmission losses through the heliostat enclosures.

TABLE IV

PILOT PLANT OUTPUT SUMMARY
(Design Plant)

	Pilot	Commercial
Power Incident on Receiver	32.23	414.14 MW
Power at Tower Base	28.00	371.32 MW
Power to Steam	27.83	247.89 MW
Net Electric Power	9.31	98.63 MW
$\frac{\text{Electricity}}{\text{Steam}}$	33.5	39.8%
$\frac{\text{Electricity}}{\text{Solar Incident - Receiver}}$	28.9	35.7%
$\frac{\text{Electricity}}{\text{Solar Incident - Heliostat}}$	21.8	13.9%
Solar Multiple	1.0	1.5

The pilot plant cost estimate is summarized in Table V; the commercial plant cost is also shown for comparison. The overall cost of the pilot facility ($4777/kW) is larger than for the commercial facility ($2015/kW) for three reasons. First, the turbine and electric plant equipment cost more on a unit basis for the smallest pilot facility; secondly, the liquid metal equipment costs are for prototype components rather than production units; and lastly, the contingency allowance on plant construction funds is much larger for the pilot plant.

A number of subsystem research experiments have been proposed to support the design of this pilot plant; these are listed in Table VI. SRE 1 involves the design and construction of a single pilot scale absorber panel to be tested at the Central Receiver Test Facility in Albuquerque, N.M. This test would verify the manufacturing techniques, sodium flow control logic, and heat transfer predictive techniques developed thus far. SRE 2 includes six materials experiments aimed

at providing background and design data for the absorber panels and steam generators. SRE 3 includes two experiments. The first would screen a number of alternative absorber coatings and surface geometries, while the second would address the uncertainties in current convection loss prediction techniques. SRE 4 would develop a thermal scanning technique for remotely sensing overheated absorber tubes.

TABLE V

PILOT PLANT CAPITAL COST COMPARISON

Cost Category	Commercial Plant Concept	Reference Pilot Plant
4100 Site, Structures, and Miscellaneous Equipment	10,714,750	4,576,788
4200 Turbine Plant Equipment	20,070,400	5,585,400
4300 Electric Plant Equipment	6,759,000	4,030,000
4400 Collector Equipment	45,828,746	4,493,300
4500 Receiver Equipment	36,174,418	9,988,090
4600 Thermal Storage Equipment	19,178,700	1,161,300
Subtotals	138,726,014	29,834,878
4800 Distributables	71,790,190	17,930,415
Grand Total (MS)	201.5	47.77

TABLE VI

SUBSYSTEM RESEARCH EXPERIMENTS

SRE 1 - Absorber Panel Test	SRE 2E - SB Tube/Sheet Weld Development
SRE 2 - Materials SRE's	SRE 2F - SG Tube/Tube Sheet Double/ Barrier
SRE 2B - Panel Inspection and Evaluation	SRE 3A - Panel Absorptivity Improvement
SRE 2C - Stress Corrosion and Fatigue	SRE 3B - Panel Convective Loss Improvement
SRE 2D - Fatigue Crack Growth and Fracture Toughness	SRE 4 - Panel Overtemperature Detection

A schedule has been prepared for the research experiments and pilot plant activities which show how these lead up to the commercial plant construction (Figure 5). Phase II, which includes the SRE's and a preliminary design of the pilot plant, would begin now and extend to the beginning of 1981. Phase III starts in late 1981 with a detailed design of the pilot plant and continues through the construction and startup of this facility. The commercial plant preliminary design is also completed in this time span. Finally, in Phase IV the commercial plant detailed design and construction is initiated.

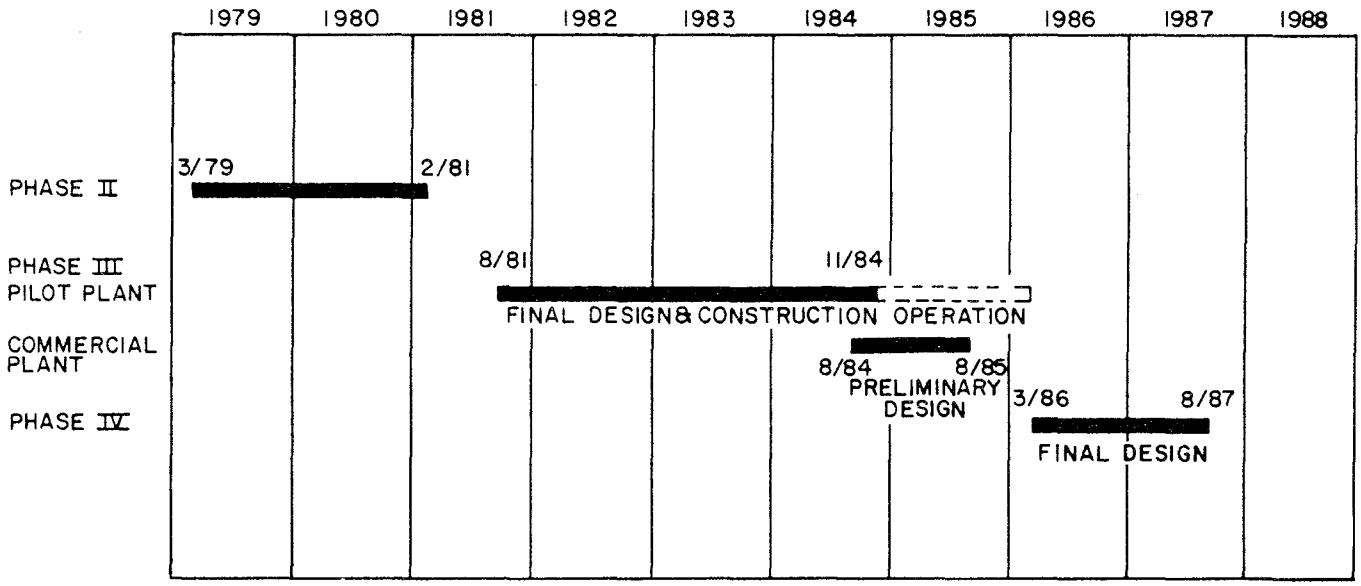

Figure 5. Proposed Advanced Central Receiver Development Plan

HIGH-TEMPERATURE LINE-FOCUS SOLAR THERMAL CENTRAL POWER SYSTEM

Arthur Slemmons
SRI International

The conceptual design of the high-temperature, line-focus (HTLF) solar thermal central power system described herein is being studied under a prime contract to SRI International (SRI), Menlo Park, California. Subcontractors to SRI include Bechtel Corporation, San Francisco, California; Foster Wheeler Development Corporation, Livingston, New Jersey; and Acurex/Aerotherm, Sunnyvale, California. Pacific Gas & Electric Company of San Francisco is consultant to the design team. The objectives of the study are to analyze the HTLF solar thermal central power system, perform parametric analyses on the various subsystems, optimize both the subsystems and the system, provide a conceptual design of the optimized system, minimize bus bar energy cost (BBEC), and determine the commercial market for HTLF solar power plants.

The accomplishments during the previous six months include the completion of the optical system analysis program, completion of the receiver thermal analysis program, completion of the BBEC optimization program, and initiation of the parametric analyses. The plans for the next six months include completion of the parametric analyses, selection of the optimum commercial plant size, completion of the conceptual design of commercial plant, estimation of its cost and performance, completion of the cryogenic tunnel test of the receiver, assessment of the market for commercial HTLF systems, and planning the development of the HTLF solar central power system.

The system chosen by SRI and its subcontractors is the HTLF central receiver system (see Figure 1), thought to have good potential for the commercialization of central solar power plants. It is analogous to the line-focus, parabolic cylinder "trough" collector/receiver, but is much larger in size. (Similarly, the point-focus, central-power "power tower" concept is analogous to the point-focus, paraboloid "dish" collector/receiver, but much larger.) The HTLF system retains the simplicity of the single-axis parabolic cylinder collector and requires less piping than does a distributed system, enabling a reduction in heat loss, cost, and absorber-fluid pressure drop. The cavity receivers of the HTLF system also significantly reduce the reflection and radiation losses usually associated with the exposed tube receiver of the smaller line-focus system. The cavity provides for a higher stagnation temperature and results in higher collection and system efficiencies. A schematic drawing of the system is shown in Figure 2.

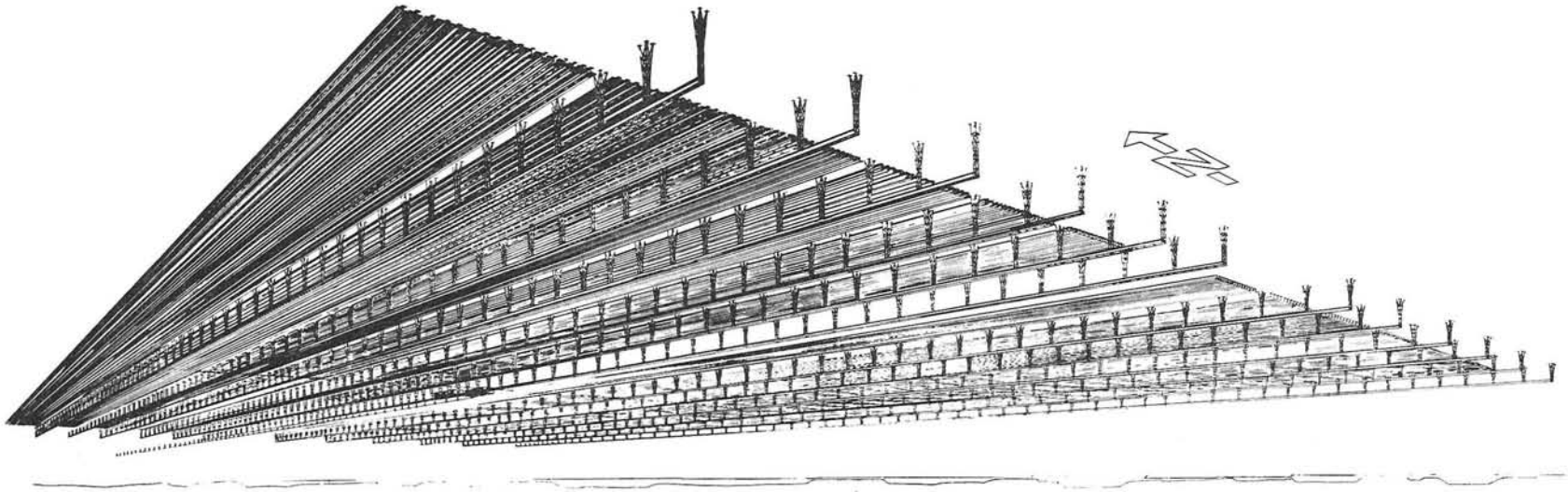

Figure 1. 100-MW_e High-Temperature, Line-Focus, Central-Receiver Solar Power System

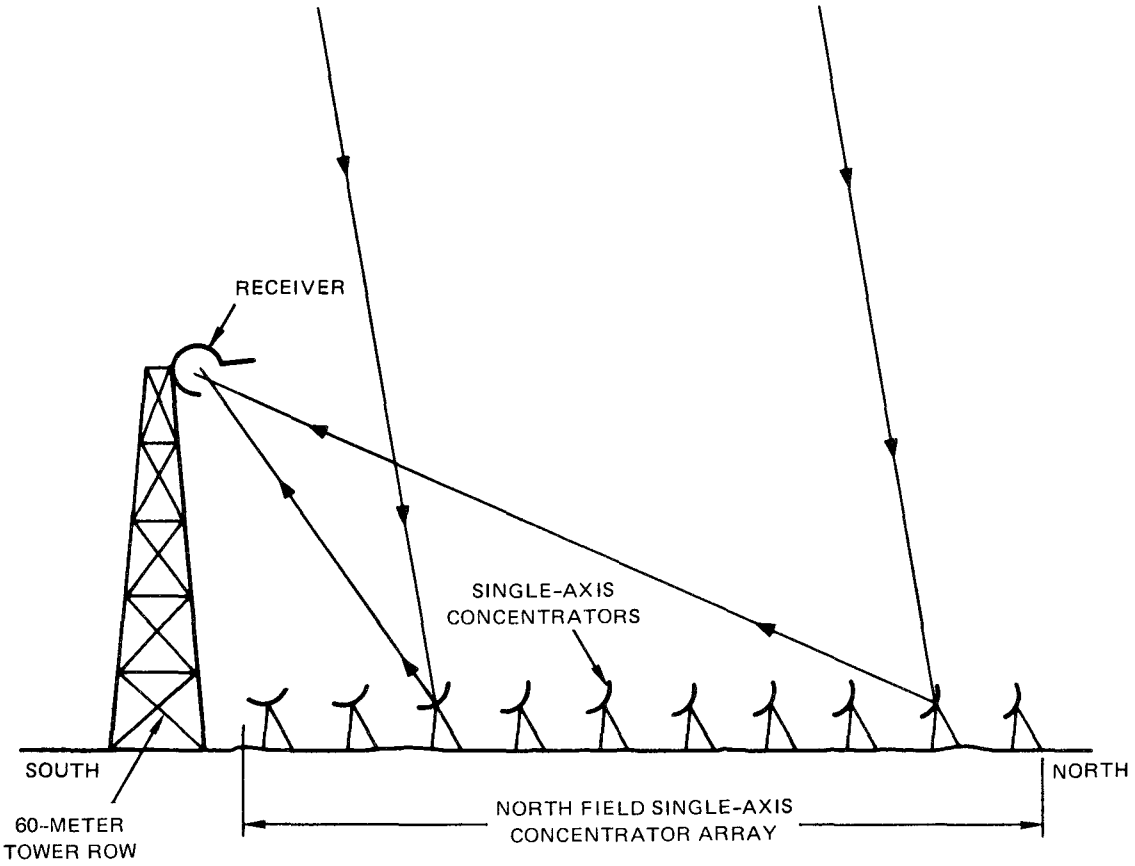

Figure 2. High-Temperature, Line-Focus, Central Receiver System

The sun's rays are reflected from second-surface mirror panels mounted on the concentrator frame (see Figure 3). The single-axis concentrators are each about 3 m wide and 36 m long. Each concentrator is made up of two 18-m long modules and is driven by a single stepping motor connected to a zero backlash, worm-gear reducer. Each concentrator is capable of rotating ±180 degrees for stowing, with the reflective surfaces facing downward during the night and during inclement weather. The concentrators are controlled by a central computer through field controllers and local heliostat controllers. All the heliostats move in synchronism. Each is focused to reduce the sun's image from the 3-m width of the concentrator to the 1.2-m (4-ft) receiver aperture width.

The HTLF receiver is a horizontal cylindrical cavity 1.8 m (6 ft) in diameter with a 1.2-m (4-ft) aperture. The aperture faces downward to the north at an angle of about 40 degrees to the horizontal (see Figure 4). The top edge of the aperture has a door, the reflective inside surface of which acts as a secondary concentrator. At night, it closes to conserve heat. The inside of the cavity is lined with horizontal heat-exchanger tubes backed by fiber insulation. The heat absorber tubes are arranged to take advantage of once-through, multipass, counter-flow heating of molten draw-salt by locating the incoming tubes near the aperture, with the final pass in the center where the flux density is the greatest. Each section between towers will have an independent modular heat absorber with manifolds that feed the final pass to common downcomers. The hot salt is delivered through insulated downcomers and an insulated common horizontal pipe both directly

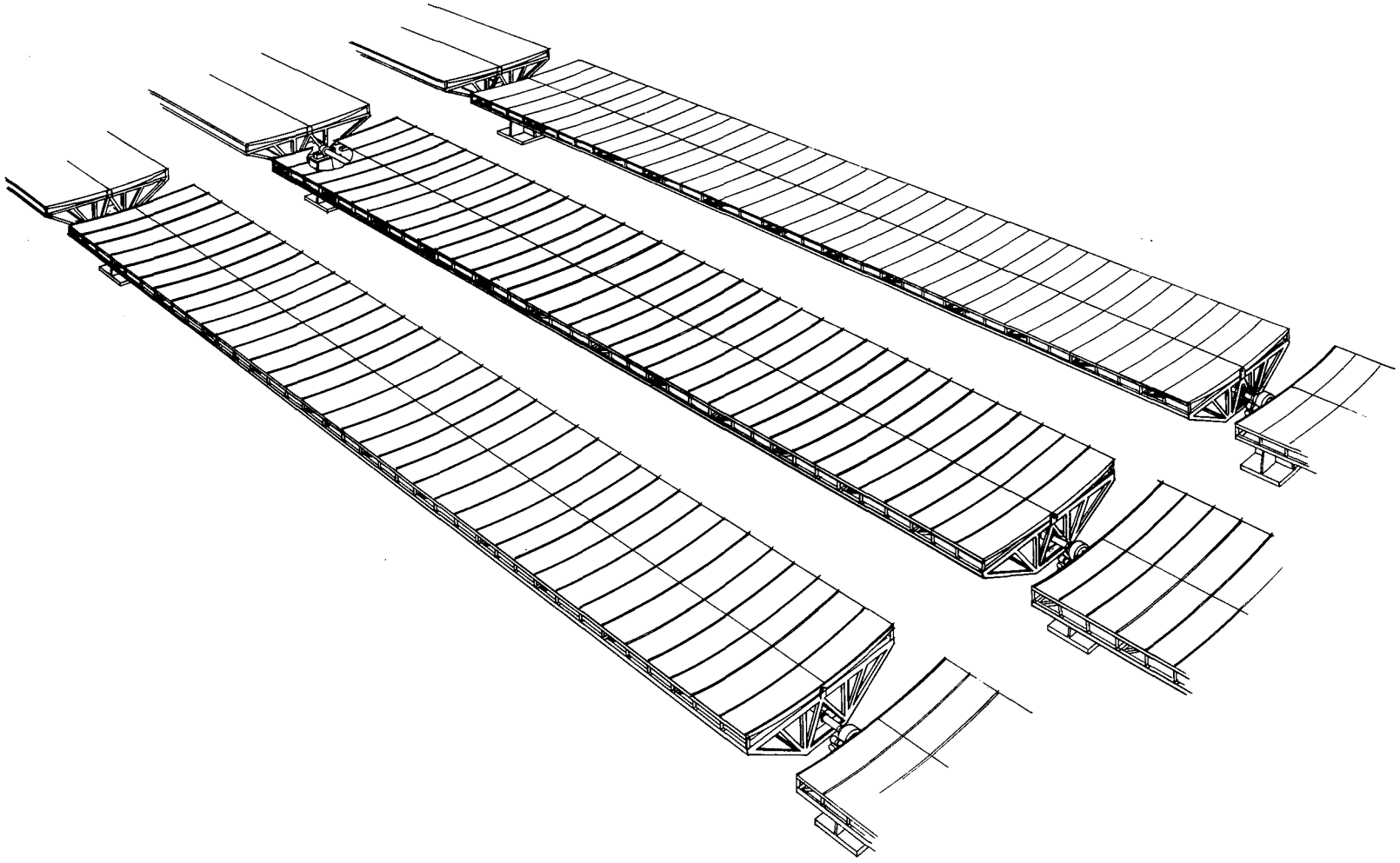

Figure 3. Artist's Sketch of Concentrators

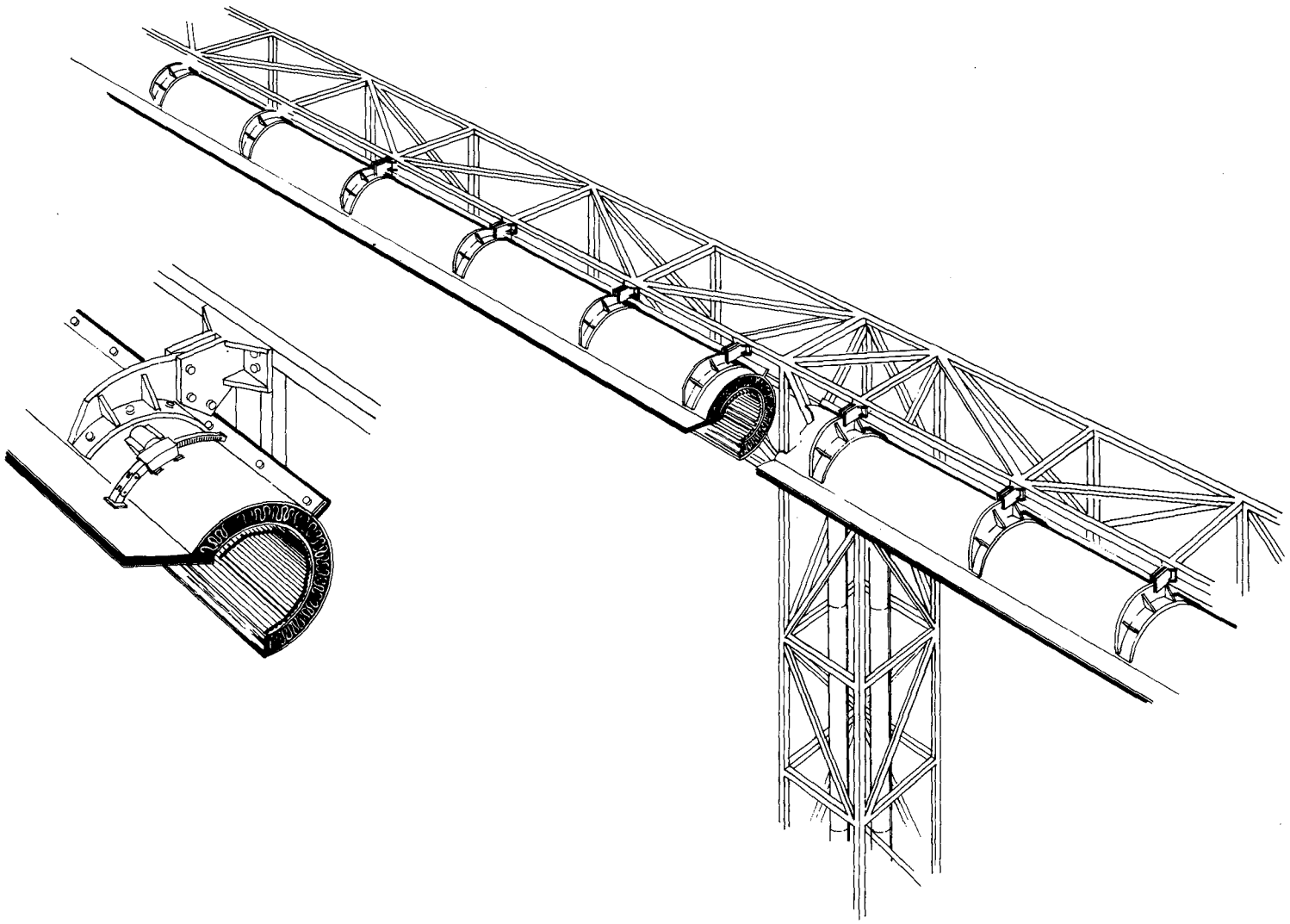

Figure 4. High-Temperature, Line-Focus, Central Receiver

to storage tanks and to the heat exchanger that generates steam for the turbine/generator. The most cost-effective power-conversion system to be used will be determined by the system analysis. At the present time, a 510°C (950°F) and 9.6 MPa (1400 psia) reheat steam cycle appears to be the most promising candidate for the 100-MW_e system.

The function of the energy-storage subsystem (ESS) is to buffer the electric-power-generation subsystem (EPGS) from the results of excessive variations in insolation, and to extend the plant's generating capabilities into periods of low or no insolation. The EPGS uses commercial steam turbine technology.

The high-temperature, line-focus receiver system should have an inherently high reliability for two main reasons: reliability of the proposed subsystems and redundancy. The redundancy inherent in the heliostat and heat-absorber subsystems also enhances this reliability. A few extra solar flux absorber modules in the receiver can provide for continued operation during repair should one module malfunction. The heliostats with their controls are in parallel. One favorable characteristic of the HTLF system is that the use of modular receiver heat absorber units permits partial shutdown and accompanying quick replacement of facility components during the continuing operation of the rest of the system. The cavity receiver concept has two 30-m heat-absorber modules in each 60-m section between towers. Because these absorber modules have separate controls and feed pumps, the remaining absorbers can still deliver energy to the turbine or storage in the event that one absorber module malfunctions.

The SRI team members are performing parametric cost/performance studies for the various subsystems. The technique being used by SRI to make the system parametric analyses is shown in Figure 5. Starting with the capacity of producing 100 MW_e net at 2:00 p.m. on winter solstice, the program calculates the energy directed into the cavity receiver by the heliostat field per unit length of the system. All optical losses are taken into consideration. The amount of energy per unit length of the system absorbed by the molten salt is calculated. Conduction, wind, reflection, and radiation losses are considered. The losses in the heat transport subsystem and heat storage subsystem are then calculated on a per-unit-length basis for the system. For a given EPGS efficiency at the steam inlet temperature chosen, the length L of the system to produce 100 MW_e net is calculated. Then the computer calculates on an hourly basis the energy collected and transformed into net kilowatt hours for winter solstice, summer solstice, and equinox. A yearly kWh total is calculated. Using the cost parameters of the various subsystems estimated on a cost-per-unit-length, where applicable, and using known fixed and operating costs, the yearly average BBEC is calculated. The sensitivity of BBEC to variations of the various subsystem parameters are studied and optimized on the basis of yearly BBEC.

Figure 6 shows the cost parameters for the storage system for two types of tanks and two tank locations. Placing the storage tanks in the heliostat field is clearly cost-effective for solar multiples higher than 1.0. The thermocline storage principle also appears to be more cost-effective than the use of two tanks.

Figure 7 shows the reduction in BBEC with increasing capacity factors. The utilization of the IPGS, computer, controls, and balance of plant for greater portions of the day gives a lower BBEC. Figure 8 shows the variation of the cavity receiver optical efficiency for various salt outlet temperatures, with and without selective surfaces. Although convection and wind losses will reduce the value of efficiencies shown, these losses will be less than for an external receiver. A

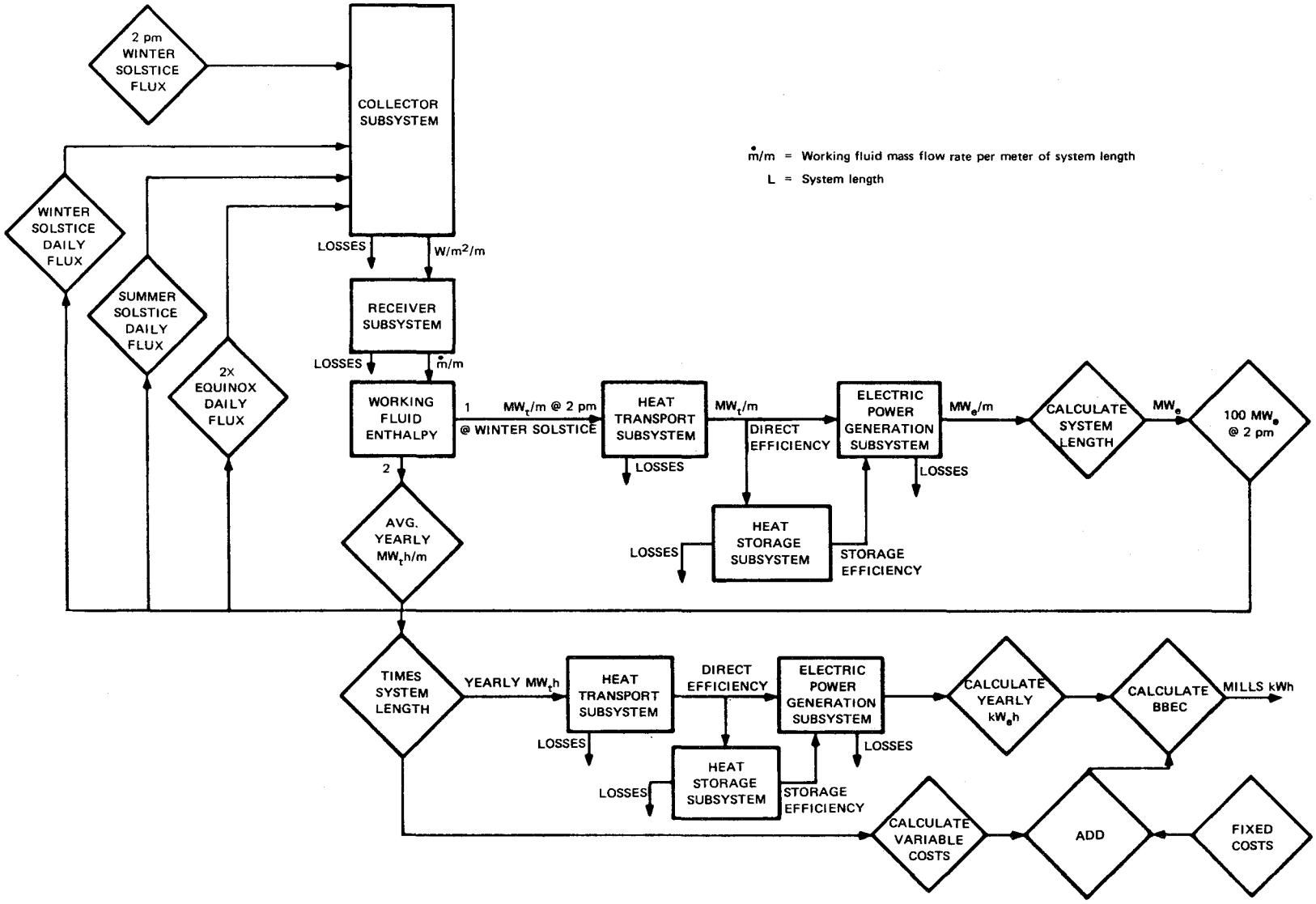

Figure 5. Flow Chart for Calculating Bus Bar Energy Cost

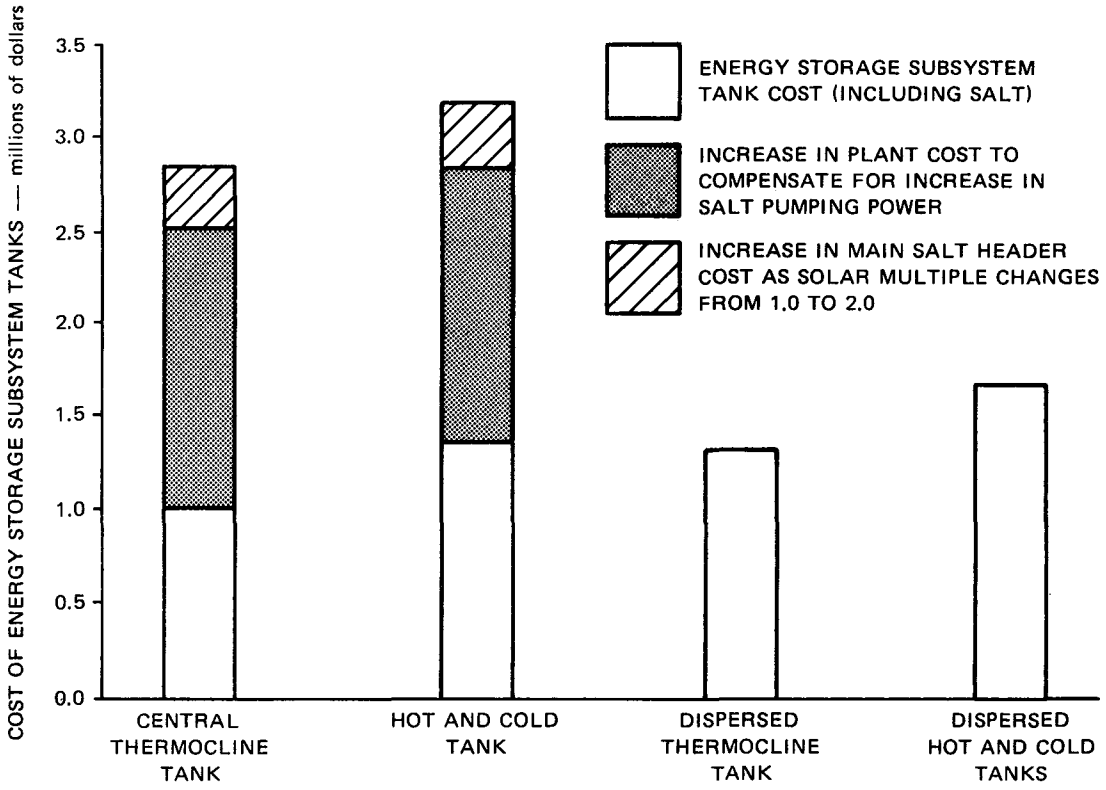

Figure 6. Selection of Type and Location of the Energy Storage Subsystem Baseline Plant Design

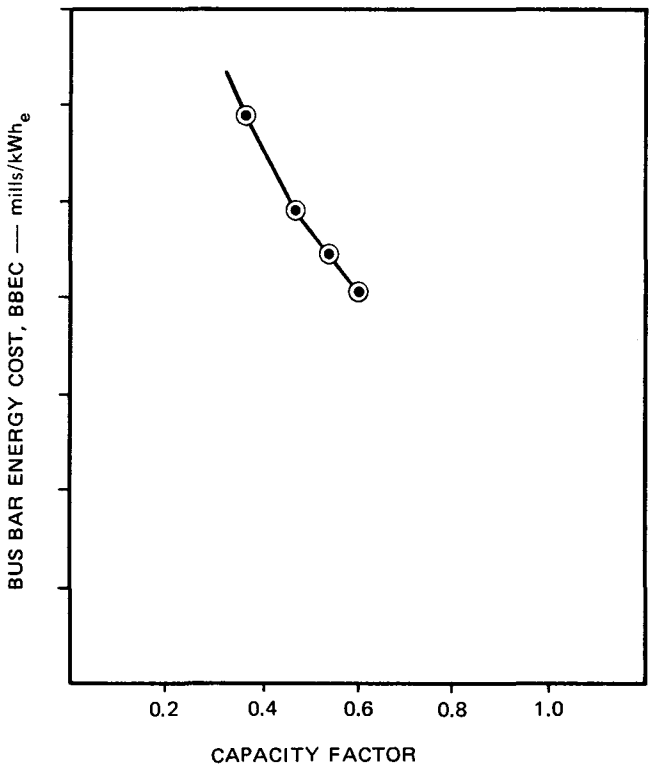

Figure 7. BBEC as a Function of Capacity Factor for HTLF Solar Central Power System

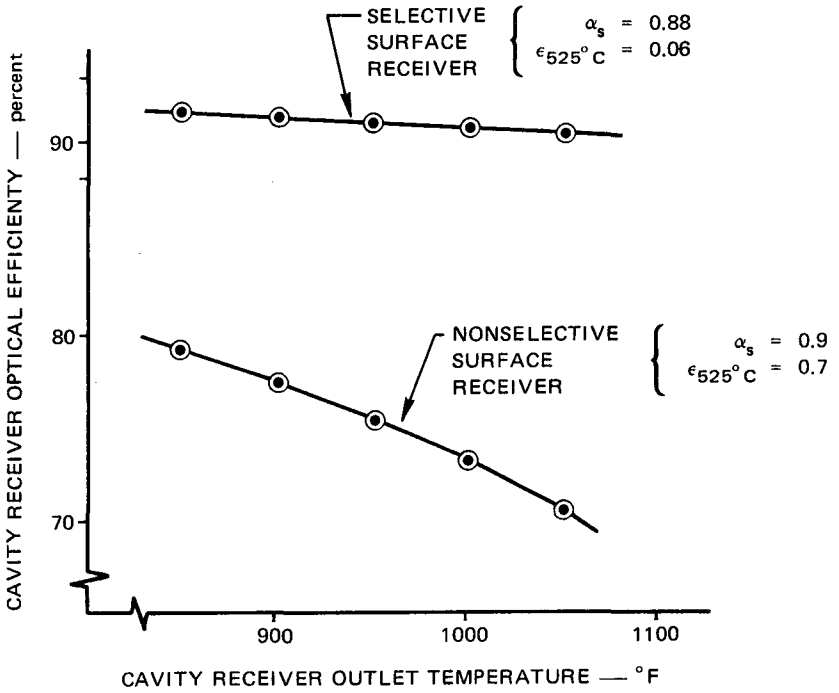

Figure 8. Optical Efficiency of HTLF Solar Central Power System Receiver as a Function of Outlet Temperature - Inlet Temperature = 500°C

cryogenic wind tunnel test is planned to better determine wind losses. The cavity effect of reducing reflection and radiation losses accounts for about five of these percentage efficiency points. Figure 9 shows how these practical receiver efficiencies are achieved at relatively low solar concentrations. At high concentrations, the receiver efficiency is relatively insensitive to the emissivity of the receiver surface. As the concentration decreases, however, the receiver efficiency becomes more sensitive to the emissivity of the receiver surface. As the emissivity approaches zero, the receiver efficiency approaches the value of the solar absorptance $_S$ for all solar concentration ratios. SRI has chosen to use a conservative value of $\alpha_{525°} = 0.06$ for the trade-off studies, although passivated selective surfaces have been shown to retain an emissivity ($\epsilon 500°$) of 0.045 for the 500°C blackbody spectrum, after 1000 hours at 500°C. Heretofore, only point focus systems will benefit greatly from the development of these selective surfaces.

The parametric analysis is continuing. Several optimization approaches have already shown high potential for reducing the cost of electricity from solar thermal central power plants of the high-temperature line-focus type.

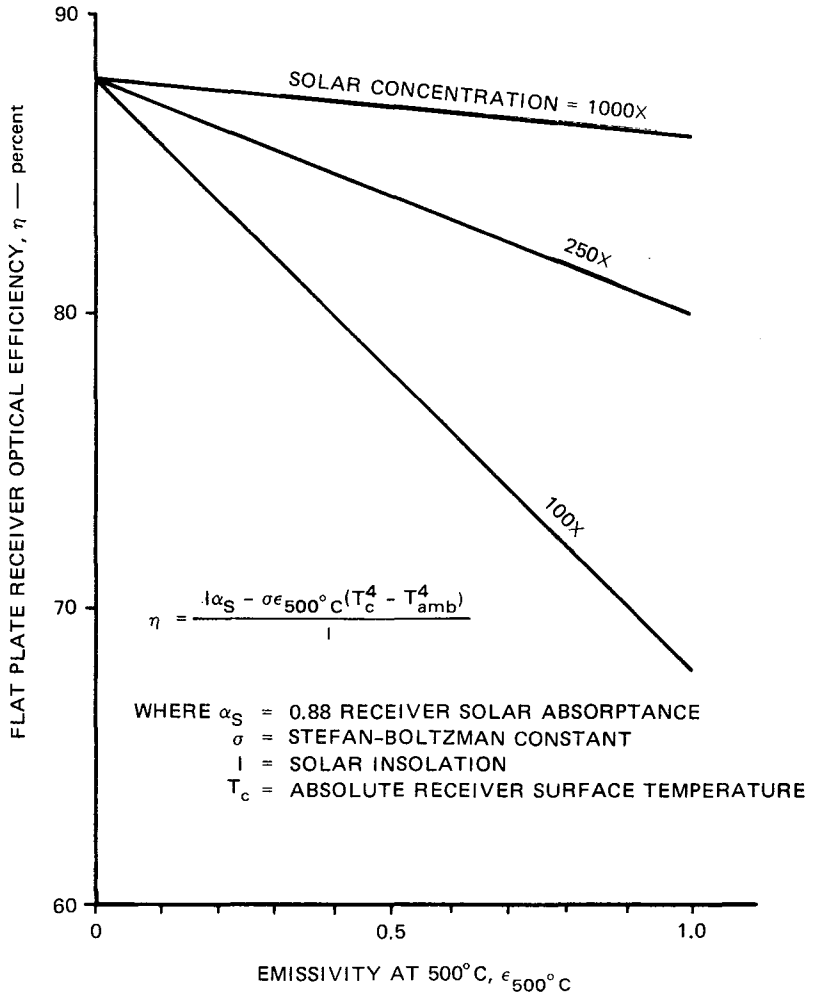

Figure 9. Solar Receiver Efficiency

CONCEPTUAL DESIGN OF A LINE-FOCUS SOLAR CENTRAL POWER SYSTEM

J. R. Schuster and J. M. Neill
General Atomic Company

Introduction and Summary

This paper describes conceptual studies made thus far for the U.S. Department of Energy on a 100-MW_e power plant using line-focus solar collectors. The work has been performed by General Atomic Company (GA), Bechtel National, Inc., Southwestern Public Service Company, and Energy Systems Group of Rockwell International.

The line-focus collector employed in the study is GA's fixed mirror solar concentrator (FMSC)[1,2,3] which comprises a series of fixed longitudinal mirror facets oriented on a reference cylinder in such a way that the light reflected from them produces a line focus. As the sun moves, the line focus moves around the reference cylinder and is tracked by a moveable linear heat receiver. Figure 1 illustrates a 2800 ft^2 demonstration array of FMSCs constructed by GA for Sandia Laboratories in Albuquerque, N.M.

Figure 2 presents a simplified block diagram of the solar power plant being studied by GA. The plant is designed to produce 100 MW_e directly from insolation on 10 a.m., December 21, to have a storage capacity capable of providing 420 MW_e hours of power generation, and to use a modern steam reheat power conversion cycle.

Heat Transport Fluid Selection

In order to provide a technical basis for selecting the heat transport and storage fluid, system point designs were prepared for three fluids: Therminol 88, draw salt (a 50% molar mixture of potassium nitrate and sodium nitrate), and sodium. Other fluids considered but not analyzed are:

1. Therminol 66 - operating temperature limit too low.
2. Silicone oil - too expensive at $2/lb. Silicone oil would have been added to the study if Therminol 88 had appeared promising.

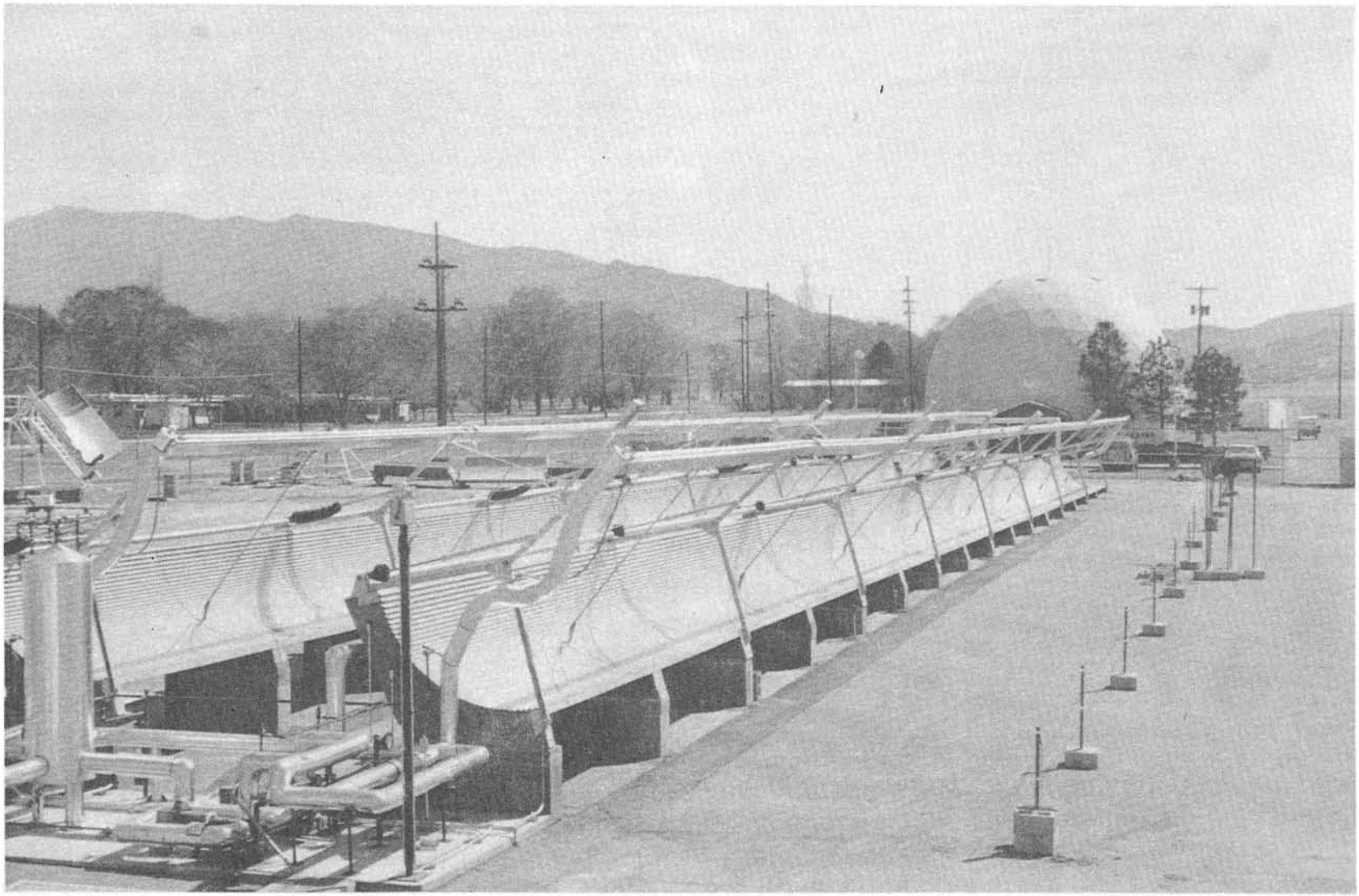

Figure 1. 2800 ft^2 FMSC Subsystem at Sandia Albuquerque

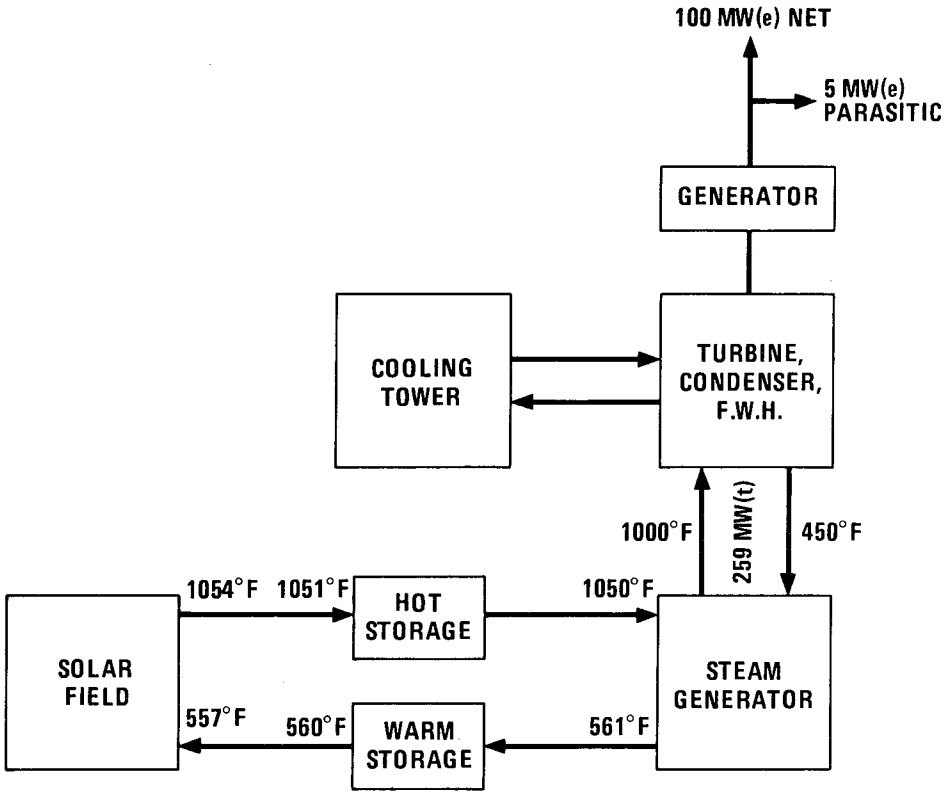

Figure 2. Simplified System Diagram

3. Water or steam - shown in past studies to have severe design and cost penalties because of high fluid pressure.
4. NaK - more expensive than pure sodium with poorer heat transport properties and greater hazard if exposed to air when hot.

Preliminary calculations indicated that for each fluid system the heat collection efficiency was not very sensitive to changes in fluid outlet temperature. This observation is confirmed by measurements of receiver thermal loss made at Sandia on the demonstration FMSC system. Figure 3 presents the loss as reported in Reference 4. The FMSC had the lowest thermal losses of the heat receivers tested. As a consequence, the system parameters for the three point designs were chosen based on limitations in the fluid properties (e.g., decomposition, charring), and on the need to stay at a reasonable temperature increment above the melting point or pour point of the fluid. Collector and power conversion efficiency calculations (based on a single reheat) yielded the values given in Table I. Storage was based on rock-filled thermoclines for Therminol 88 and draw salt and on a multiple tank system for sodium. The data presented in Table I shows that:

1. There is more variation in the power conversion efficiency than in the solar collector efficiency.
2. The Therminol 88 system has the largest collector field and largest piping. Draw salt has the smallest piping.

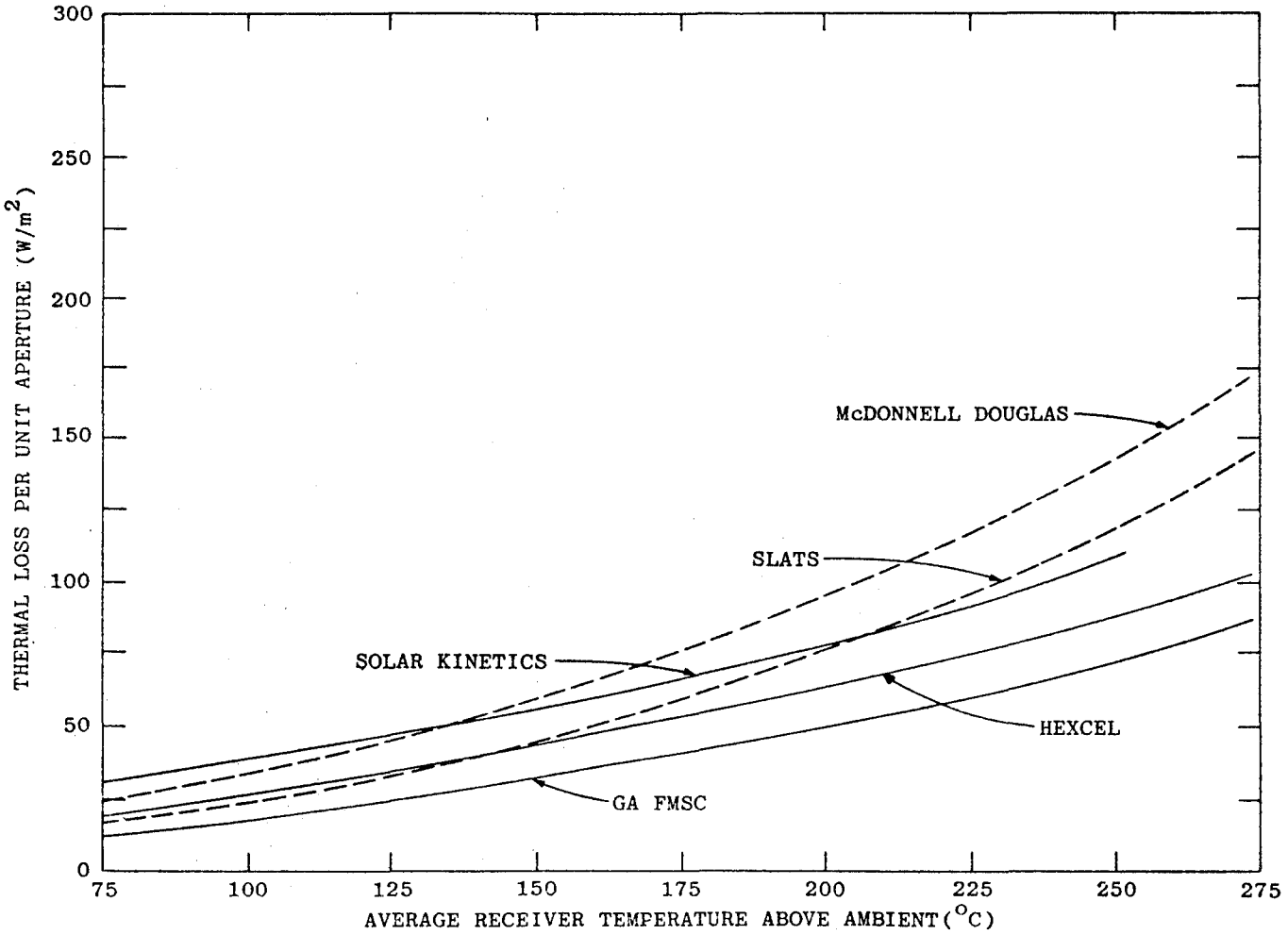

Figure 3. Comparison of Thermal Loss Per Unit Area Collector Aperture

TABLE I

POINT SYSTEM DESIGN TECHNICAL DATA
(100 MW[e] Plant with 420 MW[e] Hours Storage)

Item	Therminol 88	Draw Salt	Sodium
Receiver Fluid Inlet/Outlet Temperature (°F)	550/740	550/1050	550/1100
Receiver Fluid Average Temperature (°F)	645	800	825
Fluid Melting or Pour Point (°F)	293	430	208
Fluid Density ρ at T_{AV} (lb/ft^3)	53.6	110	53.0
Fluid Specific Heat C_P at T_{AV} (Btu/lb°F)	0.572	0.373	0.303
ρC_P (Btu/ft^3 °F)	30.7	41.0	16.1
Collector Row Length (ft)	600	900	800
FMSC (Collector) Efficiency (%)	54.6	52.1	51.8
Maximum Steam Temperature (°F)	720	1003	1052
Collector Mirror Surface Area (10^6 ft^2)	9.76	8.92	8.93
Net Power Conversion Efficiency (%)	33.5	39.2	39.8
Heat Collection Rate (MW[t])	310.2	262.1	260.3
Piping Thermal Losses (MW[t])	9.80	6.39	8.35
Pumping Power at 10 A.M. Dec. 21 (MW[e])	0.642	0.227	0.387
Pumping Power at 12 P.M. Mar. 21 (MW[e])	1.927	0.655	0.969
Piping, Diameter/Length (in./ft.)	30/5420	16/5056	20/5982
	20/9920	10/9200	14/6560
	10/65040	8/40448	12/1640
			10/44656
Number of Storage Tanks	13	6	3
Storage Tank, Diameter/Height (ft.)	48.8/40	42.2/35	86.2/40
Steam Generator Area (ft^2)	36399	40627	26367

3. The lower pumping power and heat loss of the draw salt system relative to the sodium system evens out the latter's advantage in power conversion efficiency so that the net collector areas are about the same.
4. The storage fluid volume required is the lowest for draw salt.
5. The thermal losses in the piping field are significant (2-3%) and, therefore, steps should be taken to reduce overnight losses.

Cost estimates for the three point designs were then prepared using available cost data. Cost differences relative to the draw salt case are presented in Table II. Of the three systems, draw salt has the lowest cost with sodium being $17.8 million more costly and Therminol 88 $19.6 million more costly.

Draw salt was selected as the transport fluid based on the following factors:

a. Capital cost
b. Operational cost
c. Cost uncertainties
d. Development requirements
e. Design flexibility
f. Design credibility and marketability
g. Reliability/availability

Significant factors which lead to the choice of draw salt, in addition to lowest capital cost, were:

1. Draw salt had the lowest cost thermal storage and lowest sensitivity to change in storage requrements (some electric grids may need 5 to 6 hours of storage in order to translate the peak solar power generation to the peak demand; see Figure 4 for example). Sodium is particularly sensitive.
2. Therminol 88 has a relatively high degradation rate, a relatively high projected cost*, and unlike Therminol 66, requires a trace heating system.
3. A distributed piping system is vulnerable to damage and leakage. Therefore, a heat transfer fluid which does not seriously interact with air or the environment is preferred. While hot draw salt is a powerful oxidant, the absence of carbonaceous material around potential release points will minimize leakage consequences.
4. Molten salt heat transfer fluids have found increasing favor so the technology base for applying this fluid should rapidly increase. Draw salt has been selected as the heat transfer fluid for a point focus central receiver design (Reference 5). It is also a favored fluid for thermal storage applications. Finally, Hitec, which is very similar to draw salt, is being employed by GA for a solar test rig expected to be operational in April, 1979.

*Therminol 88 is mixed terphenyl and is quoted as 65¢/lb in 24,000 lb lots. Reference case utilized 25¢/lb. Degradation rate of Therminol 88 at 740°F may be in excess of 5% per week while reference case considered only 1% per week.

TABLE II

PLANT COST INCREASES RELATIVE
TO DRAW SALT SYSTEM ($mm)

Account No.	Description	Therminol 88	Draw Salt	Sodium
4100	Site /Structures/Misc. Equip.	+0.1	0.	0.
4200	Turbine Plant Equipment	+1.1	0.	0.
4300	Electric Plant Equipment	0.	0.	0.
4400	Collector/Concentrator Equip.	+6.2	0.	0.
4500	Receiver Equipment	+3.6	0.	0.
4600	Thermal Storage Equipment	+3.1	0.	+8.7
4700	Heat Transport Equipment (Includes Steam Generator)	+2.2	0.	+6.1
4800	Distributables/Indirects	+3.3	0.	+3.0
	TOTALS	+19.6	0.	+17.8

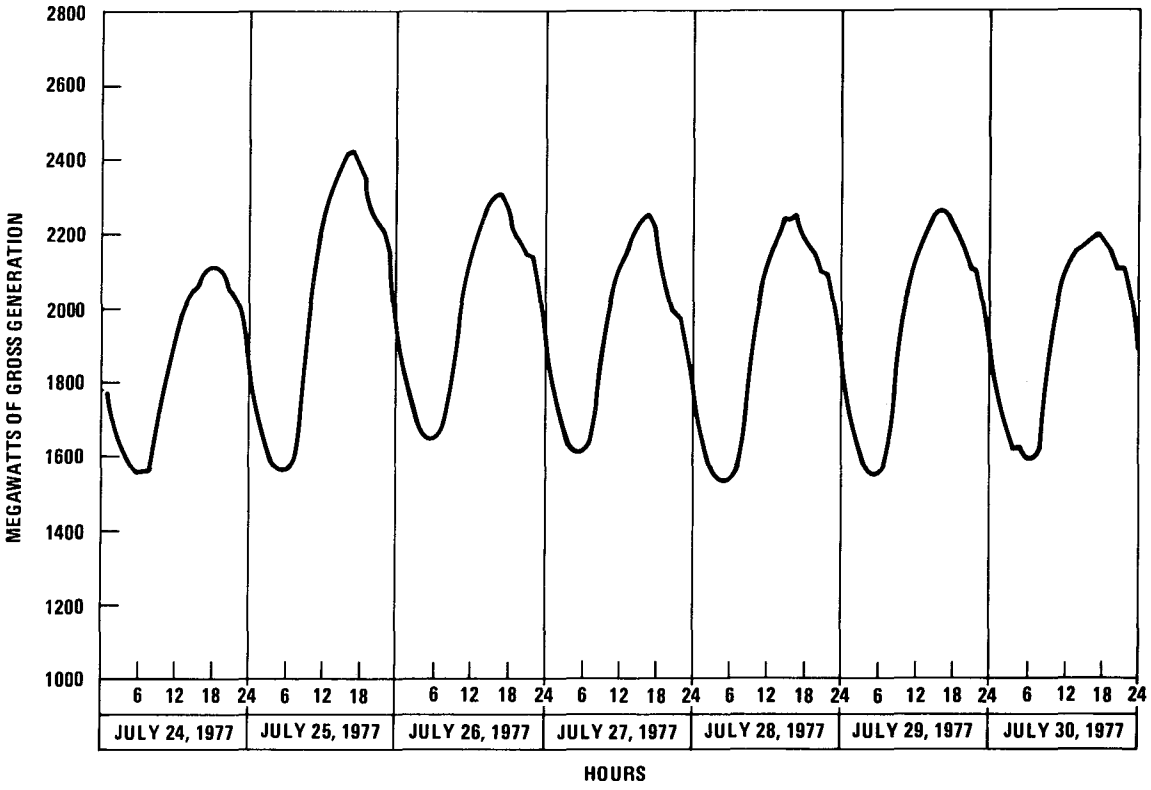

Figure 4. Southwestern Public Service Company Daily Load Flow for July 24, 1977 through July 30, 1977

Heat Receiver

An analysis of the cost of the FMSC array at Sandia Laboratories identified the heat receiver assembly (HRA) and its support structure and drive as high cost items. In addition, the desirability of various mechanical improvements in the design were identified.

The configuration in Figure 5 illustrates one approach to improving the HRA. The receiver is much longer (36 ft) than the 25-ft-long units at Sandia Laboratories. The structural support function is no longer performed by the receiver shell but is achieved by a separate, low-cost, trussing system of tubing. This approach permits a smaller, lighter receiver. The secondary concentrator and receiver shell are simple rolled or pressed sections instead of aluminum extrusions, which achieve significant cost and weight reductions. The coolant duct, previously rectangular, is now round with a detachable nickel clad copper conducting plate. The copper plant provides a replaceable light absorbing surface with a solar selective absorber coating. The coolant duct is made of carbon steel for portions where the temperature will be below 800°F, and of Incoloy 800 above 800°F.

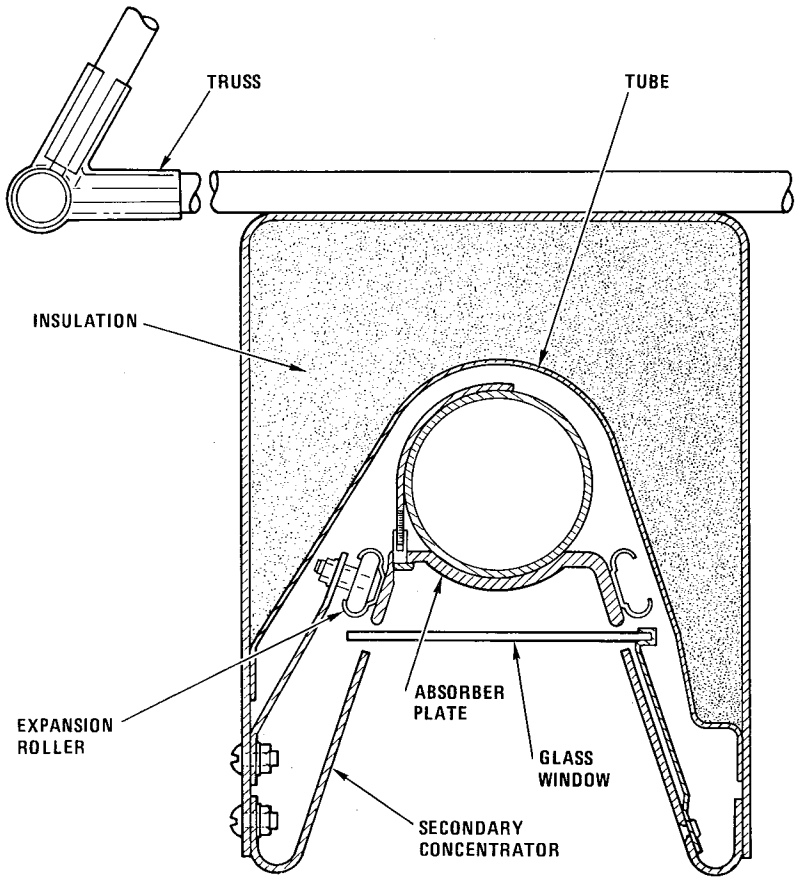

Figure 5. Improved Heat Receiver

The insulation is canned in order to eliminate formation of dust. The cover glass is mounted with clips so that the edges of the glass remain hot, thus preventing the glass from cracking. The glass can be removed and replaced without disassembling the HRA. Expansion rollers are provided. The sections of coolant duct are welded since draw salt is known to weep readily through tube fittings. Since welding can destroy selective coating properties, a further advantage is obtained with the detachable copper absorber plate.

Primary Concentrator

An analysis has been conducted of the sensitivity of the system performance to the magnitude of the slope error of the fixed mirror facets. The analysis concludes that 10 milliradians will give acceptable performance. This tolerance is considered well within the capabilities of a cast concrete system. Effort has, therefore, been directed toward a low-cost means for fabricating cast concrete FMSC panels. The method considered uses a master steel male mold to produce reinforced concrete female molds. These are in turn fiberglass coated, finished, and placed together so that a 200-ft long panel section can be made using a screed. This section is prestressed and steam cured so that a fast (two-day) mold turnaround can be achieved. The panels are then cut into the appropriate lengths. The proposed concentrator fabrication approach is considered state-of-the-art and offers a low installed cost.

Other concentrator fabrication approaches were investigated including the use of rectangular steel tubing for the panel and a fiberglass-reinforced, foamed plastic panel. Both offered the potential for higher mirror facet accuracy than the concrete system. However, the optical analysis has shown that greater accuracy is not necessary. The foamed plastic panel may have a cost advantage over the concrete system but has more technical uncertainties, such as expansion compatibility with mirror glass and resistance to environmental conditions (e.g., ultraviolet light). For these reasons, concrete remains as the base panel fabrication method.

Electrical Power Generation Subsystem

Power conversion cycle heat balances were determined based on a single reheat steam turbine with the reheater and superheater heated in parallel by the draw salt and the draw salt then heating the economizer/boiler. For these calculations the pinch point of the economizer outlet was kept fixed at 20°F. The common approach temperature for the reheater and superheater was taken as 100°F, although subsequently a reduction to 50°F was found advantageous. The heat balances were calculated with the following parameters systematically varied:

- Throttle pressure
- Heat transport fluid inlet temperature (to steam generator)
- Feedwater temperature

A plot of the gross turbine heat rate as a function of fluid and feedwater temperatures is shown in Figure 6. From these data, a reference data set was selected corresponding to 2400-psig throttle pressure, and 950°F superheat and reheat temperature. The resulting gross turbine heat rate of 8192 Btu/kW(e) hr corresponds to a gross electric efficiency of 41.65 percent. This value can be

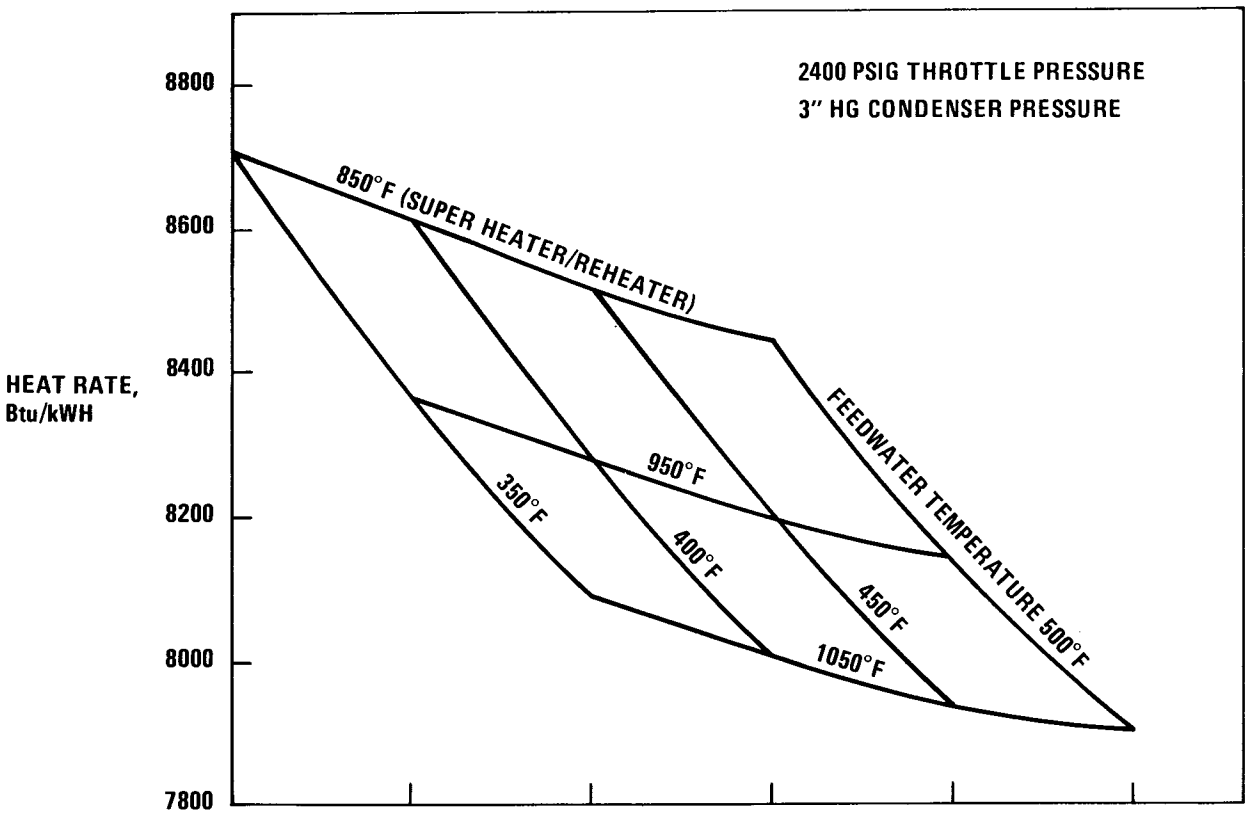

Figure 6. Gross Turbine Heat Rate

improved upon as the approach and pinch point temperature differences are reduced, the condensor back pressure is reduced, and the plant is scaled up; these studies are in progress. It is to be noted that the plant may be scaled down to 75 MW_e before a reheat steam turbine becomes commercially unavailable.

One concern has been that the 2400-psig turbine, constructed with thick casings, would be susceptible to thermal stress cracking. Preliminary investigations indicate that this will not be a problem.

Table III provides details of the steam generator design based on the reference performance data set. Of significance are the material choices of Incoloy 800 for reheater and superheater, SS-347 for the boiler, and carbon steel for the economizer. A drum-type boiler is used with salt on the tube side. This is the best economic choice and also favors turn-down capability.

Thermal Storage Subsystem

The thermal storage alternatives considered have included:

Rock (taconite)-filled draw salt thermocline

Pure draw salt thermocline

Separate hot and warm tanks

Figure 7 illustrates thermal storage costs for the three alternatives.

Table III

BASELINE STEAM GENERATOR DESIGN DATA

- 105 MW(e) Gross Alternator Output
- 450°F Feedwater
- 2400 Psig Throttle Pressure
- 950°F Superheat/Reheat

	Reheater	Boiler	Superheater	Reheater
Duty Btu/hr	229,200,000	231,300,000	251,400,000	148,000,000
ΔT_m °F	55.42	64.36	123.1	177.5
Area ft^2	16200	11600	10200	6100
U Btu/hr ft^2 °F	256	301	200	137
Salt Flow	Tube	Tube	Shell	Shell
	CS	347 SS	Incoloy 800	Incoloy 800
Water/Salt Flow	Shell	Shell	Tube	Tube
	CS		Incoloy 800	Incoloy 800

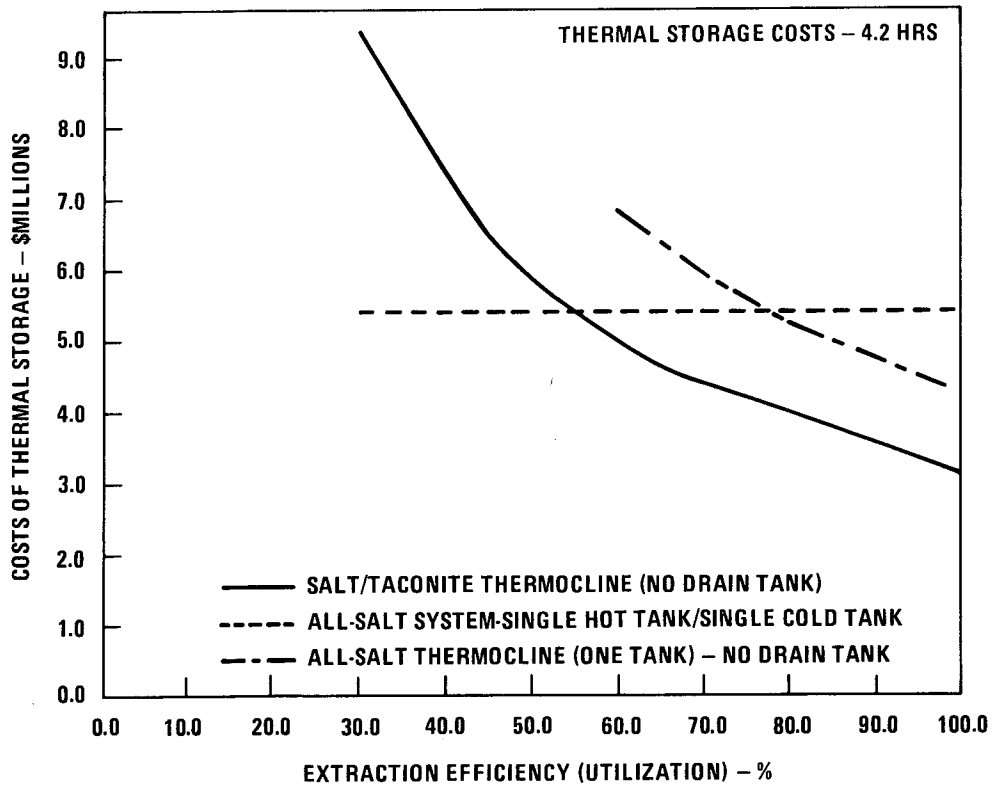

Figure 7. Costs of Alternate Thermal Storage Systems

Equilibrium charge and discharge cycles have been determined for the taconite-salt thermocline. Bed utilizations of up to 60 percent appear achievable but give marginal economic incentive over separate hot and warm tank systems. The disadvantages of the taconite-draw salt thermocline include:

a. Difficulty of starting up with cold rocks.
b. Difficulty of repairing a tank containing hot rocks.
c. Unknown long-term chemical interaction between rocks (taconite) and hot draw salt.

The pure salt thermocline has been studied only from an economic viewpoint. As Figure 7 shows, an extraction efficiency of nearly 80 percent is needed to better the cost of a separate tank system. The pure salt thermocline requires careful design of inlet and outlet manifold systems in order to prevent degradation of the thermal interface. The pure salt thermocline also requires a flow reversal system. Finally, the performance of a pure salt thermocline is unknown since related experimental work has been limited to small systems. It is to be noted that Figure 7 does not include the cost of a drain tank for the thermoclines and does not include the penalty associated with the thermocline that arises due to the reduction in power conversion efficiency caused by the reduction in hot fluid temperature near the end of the discharge cycle. This is particularly apparent with a rock-filled thermocline.

The cost of the thermal storage system is only about 3 percent of the total plant cost for the given storage requirements of 420 MW_e hours. In view of the reservations associated with both types of thermoclines, a thermal storage system of separate hot and warm tanks has been adopted for this plant design.

Heat Transport Subsystem

Study of the heat transport subsystem has included investigation of piping layouts, pipe sizes and material choices, trace heating and line purging requirements, and determination of system pumping power. The investigations were based on a collector row length of 900 ft, a length selected so as to minimize optical end losses yet not so long as to impede vehicle access or impose requirements on local topology. It has become clear that the collector length must be short enough that during startup the molten salt can traverse the empty coolant duct (it is drained at shutdown) without either cooling to a point where it could no longer be gravity drained or without allowing over-heating the receiver surface, which could impair the solar selective absorber coating.

General observations on the heat transport system are that the hot piping is made of expensive Incoloy 800, but since it maintains its strength properties well at 1050°F, it is possible to use Schedule 10 piping. The warm side piping uses Schedule 40 carbon steel piping. Optimal insulation thicknesses are 4-1/2 inches for hot side piping and 2-1/2 inches for the warm side. It clearly pays to keep the hot side piping to a minimum and this has ruled against butterfly-type piping layouts. It is better to use the heat receiver itself to transport heat from the warm supply to the hot collection point.

The piping layout shown in Figure 8 should lead to low cost. Cost analysis of this system is in progress as well as an investigation of the operational questions of distributed thermal storage. It is to be noted that this approach is ill suited to thermocline storage.

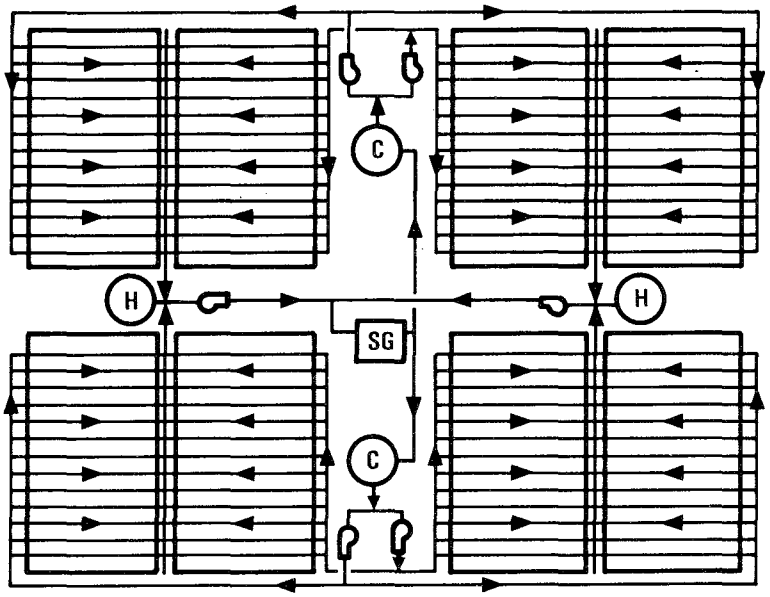

1. MINIMUM NEED FOR THROTTLING TO BALANCE FLOWS
2. MINIMUM NUMBER OF HOT MANIFOLDS
3. LINES BETWEEN TANKS AND STEAM GENERATOR SIZED ON SOLAR MULTIPLIER OF 1
4. SEPARATE PUMPS FOR INNER AND OUTER SUPPLY MANIFOLDS
5. LAYOUT BASED ON SEPARATE HOT AND COLD TANKS
6. NOT AS AMENABLE TO THERMOCLINES OR (N-1) MULTIPLE STORAGE TANKS
7. UTILIZES HOT SALT PUMPS

Figure 8. Tentative Layout of Heat Transport Subsystem

Overall System

The plant design is based on a minimum of 400 MW_e/hr of generation for each clear day of the year using Barstow insolation. For the FMSC, which has a fixed aperture, the design day sizing the collector field is December 21 for the period 10 a.m. to 2 p.m.

The overall system analysis and design effort has concentrated on the following areas:

a. Improved calculation of the optical train.
b. Modification of the receiver design code to handle alternate duct configurations.
c. Modelling of the entire plant for cost-performance optimization.
d. Dynamic analysis of the collector field in order to determine design requirements imposed on components.

The exercise of preparing cost algorithms for the cost optimization code has already indicated where system improvements can be achieved. Figure 9 illustrates

some representative data from this code showing the impact of variations in heat receiver fluid outlet temperature on collector efficiency, plant cost, and collector area. These data were based on a fluid inlet temperature of 550°F. While the receiver efficiency declines with increasing temperature, the power conversion efficiency increase more than offsets it so that the collector area required declines throughout the range. However, the receiver cost increases with outlet temperature so that the total plant cost changes quite modestly above 1000°F and appears to reach a minimum at about 1150°F. It turns out that outlet temperature is set more by practical limits pertaining to fluid decomposition rate, uncertainty over long-term corrosion effects from the draw salt, and selective absorber coating temperature limit. The current upper limit for draw salt operation has been selected to be 1050°F; however, Figure 9 shows that the incentive for further increase in temperature is small, indeed, backing off to 1000°F would not have a large economic impact.

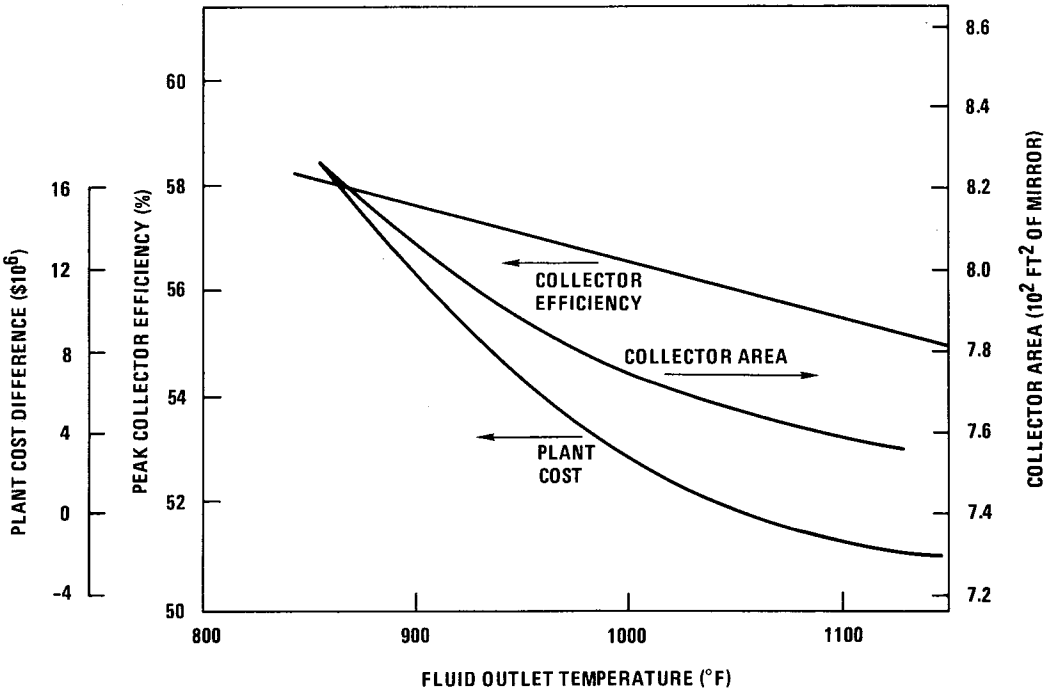

Figure 9. Variation of FMSC Peak Efficiency, Collector Area and Plant Cost (Relative to Plant Cost at 1050°F) With Fluid Outlet Temperature (Constant Inlet of 550°F)

REFERENCES

1. Russell, J. L., E. P. DePlomb, and R. K. Bansel, "Principles of the Fixed Mirror Solar Concentrator," General Atomic Report No. GA-A12902 (Rev.), May 21, 1974.

2. Eggers, G. H., et al., "Solar Collector Field Subsystem Program on the Fixed Mirror Solar Concentrator," Sandia Contract 02-7671D, General Atomic Report No. GA-A14209 (Rev.), December 31, 1976.

3. Schuster, J. R., J. L. Russell, and G. H. Eggers, "Design, Construction, and Testing of a Fixed Mirror Solar Concentrator Field," 13th Intersociety Energy Conversion Engineering Conference Proceedings, August 20-25, 1978, San Diego, California.

4. V. E. Dudley and R. M. Workhaven, "Summary Report: Concentrating Solar Collector Test Results, Collector Module Test Facility," SAND78-0815, May 1978.

5. "Conceptual Design of Advanced Central Receiver Power System, Phase I," Martin Marietta, Badger, Black and Veatch, and Arizona Public Service Co., Report to DOE under Contract EG-77-C-03-1724, September 1978.

CONCEPTUAL DESIGN AND ANALYSIS OF A 100-MW_e LINE FOCUS SOLAR CENTRAL POWER PLANT "LFPP"

M. G. Semmens
A. Fong
The BDM Corporation

Introduction

The BDM Corporation and its subcontractors, Stearns-Roger, Solar Kinetics, Inc., and the Public Service Company of New Mexico, are performing a conceptual design and analysis of a nominal 100-MW_e solar central power plant to assess the applicability of line focus technology for central power plants when operating at temperatures in excess of 700°F (370°C). The three specific objectives of the program are to:

1. Develop the optimum line focus solar central power plant system conceptual design.

2. Identify the most attractive utility/commercial line focus application and assess the overall market potential.

3. Compare the line focus solar central power plant with the first-generation point focus central receiver technology on the basis of cost effectiveness.

Approach

BDM's approach to the conceptual design of the line focus power plant (LFPP) was to establish a high confidence, low risk design with the use of current state-of-the-art technology, and then to identify areas where advanced materials and/or technology could enhance the overall performance of the LFPP. A program involving ten separate tasks was implemented; the general flow and interaction of each of these tasks is shown in Figure 1. The minimum performance requirements were defined early in the program and documented as guidelines to be used by all contractors throughout the subsequent analyses. The objective of identifying and designing the optimal LFPP is being carried out in Task 2 and Task 3. Parametric analysis (Task 2) involves the examination of each major subsystem within the line focus plant in an effort to identify the

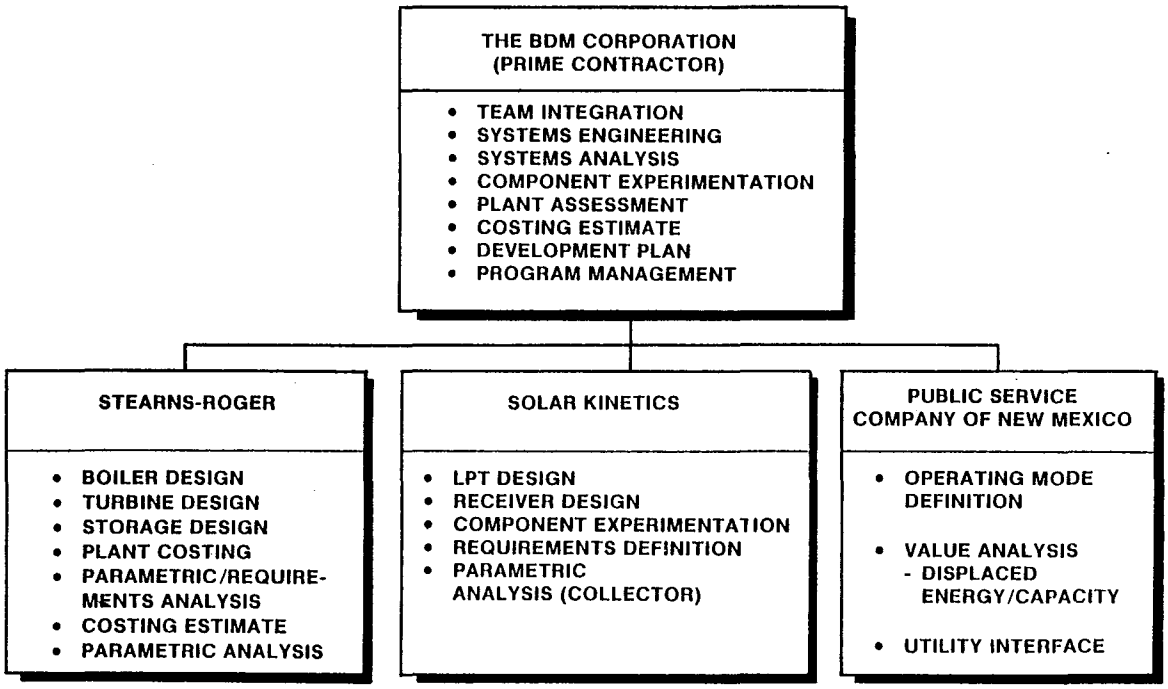

The BDM/LFPP Design Team

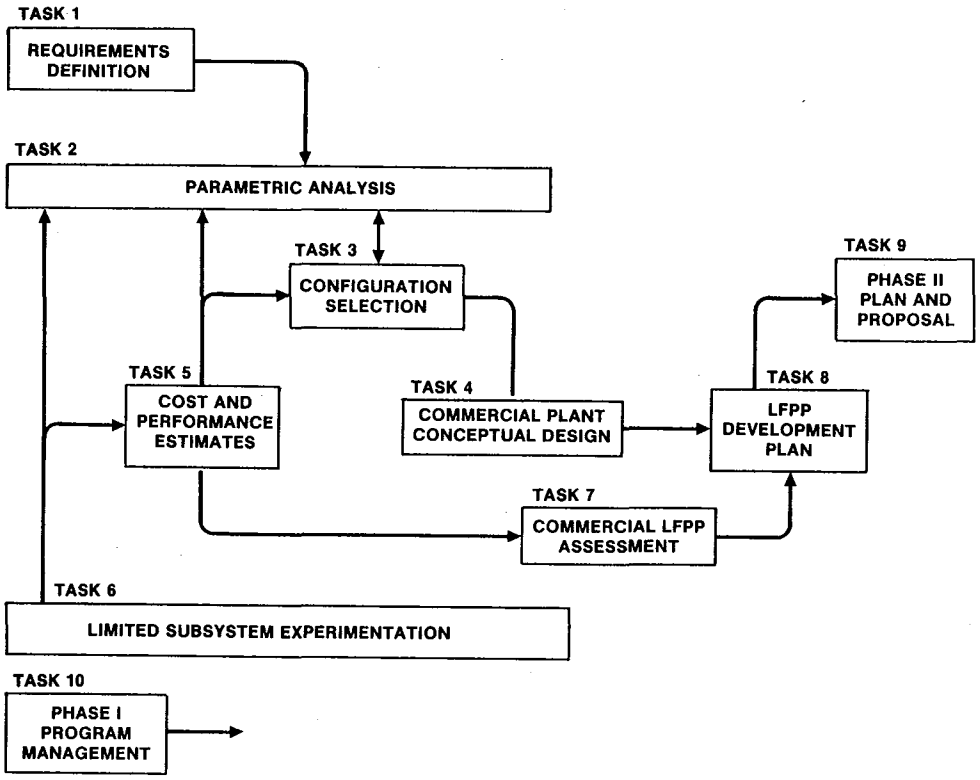

Figure 1. Program Overview

most attractive subsystem design and configuration. The final configuration selected will be the result of extensive system level analysis. This analysis will identify the throttle temperature and pressure, as well as the subsystem and plant size which produce the minimum levelized bus bar energy costs. Preliminary analyses have been performed in this area, and very attractive bus bar energy costs have been identified. These analyses have been supported by detailed cost analyses being conducted as part of Task 5, as well as by the commercial LFPP assessment (Task 7) which has identified the intermediate power plant segment to be the most appropriate utility market for the line focus power plant technology. The engineering documentation for the selected LFPP is being carried out as part of Task 4. All collector design tools used during the system level design and analysis are being validated as part of Task 6, where through limited collector experimentation, new receiver tube materials and geometries are being evaluated for the line focus collectors.

The first phase of the program is nearing the halfway point and emphasis to date has been on the identification of the optimal line focus power plant. In the subsequent half of the program, BDM will define the LFPP development plan which will delineate the requirements for advancing the line focus technology to the commercial scale.

Subsystem Analyses

The major portion of the parametric analysis has been directed at the seven major LFPP subsystems defined in Figure 2. In examining the collector subsystem, BDM, in conjunction with Solar Kinetics, Inc., has performed extensive trade-offs involving the structural material, reflective material, and linear parabolic trough size that have led to substantial improvements in collector performance and major cost reductions. In fact, the single most significant step in developing an economically attractive line focus power plant technology was in enhancing the performance and substantially reducing the costs of the linear parabolic trough.

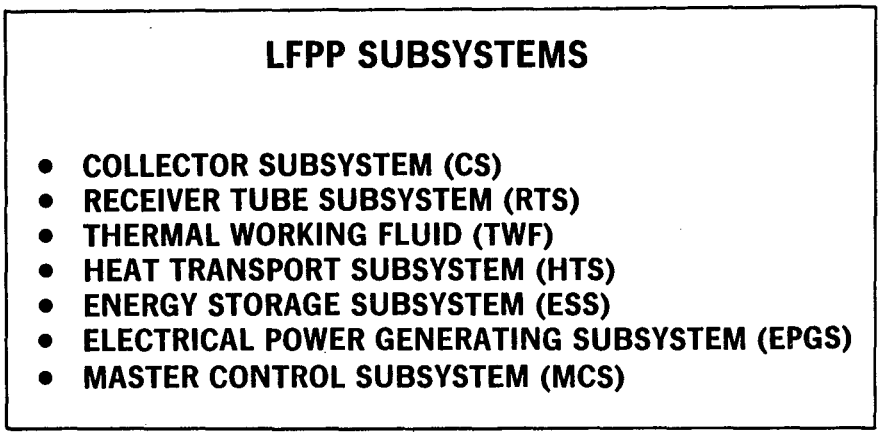

Figure 2. Major Power Plant Subsystems

The linear parabolic trough (LPT) initially proposed for the line focus power plant was a Solar Kinetics, Inc. T-700. The SKI T-700 is currently fabricated from aluminum and uses a monocoque construction technique for the reflective mirror. The T-700 also uses hydraulic tracking and FEK-244 as reflective material. BDM, in conjunction with SKI, performed trade-offs in three areas. The first was in the structural material. Solar Kinetics, Inc. determined that the same collector design could be fabricated from steel at a much lower cost in large-scale production. With the assistance of Sandia Laboratories in Albuquerque, a thin annealed glass, Corning 0317, was identified, which although slightly more expensive than FEK-244, can provide much better specular reflectance and durability. Finally, the BDM design team performed a trade-off on the collector size and determined that larger apertures were optimal.

The results of the sizing analyses are shown in Figure 3. Detailed designs were performed for larger LPT systems, and it was determined that the minimum LPT cost coincided with an aperture width of 21 feet. Larger parabolic troughs can be produced at lower costs because the number of components which have to be installed in the field is substantially decreased. The most substantial reduction is in the mounting and tracking pylons, tracking mechanisms, and receiver tube piping and interconnections. Through detailed costing it was determined that at production levels of 1 million square feet, the T-2100 (21-ft aperture LPT) could produce at a cost of slightly less than $9.00 per square feet. When a learning curve factor of 0.95 is applied, 80th plant costs of about $5.48 per square foot are realized. A schematic diagram of some of the specifications for the LFPP T-2100 is shown in Figure 4.

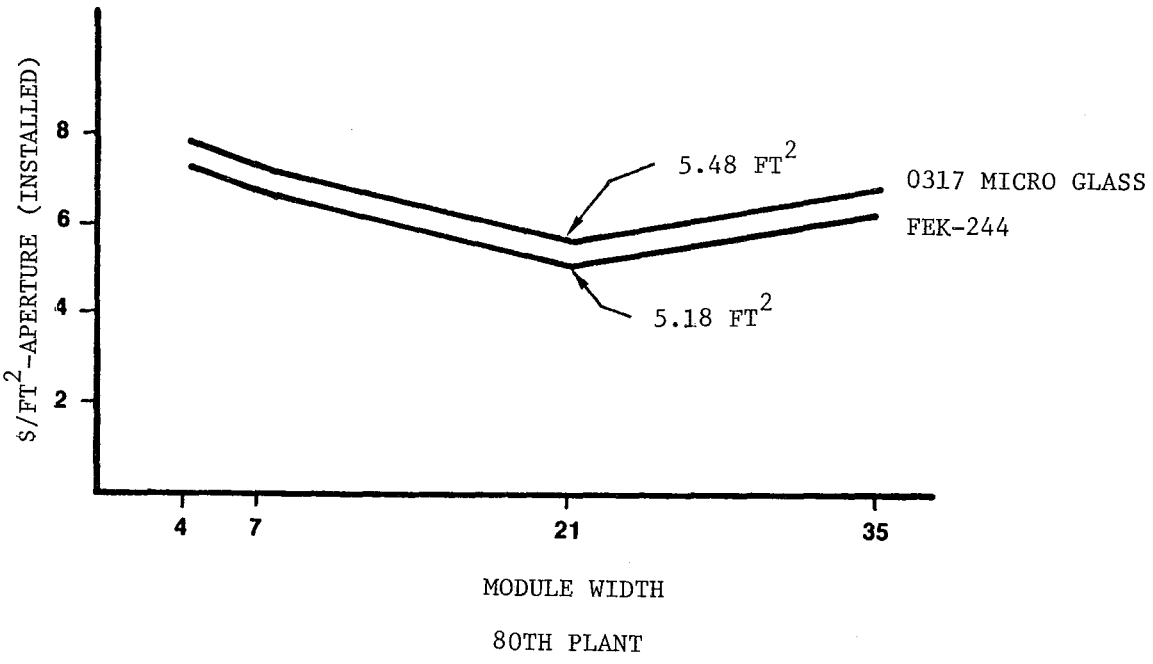

Figure 3. Collector Subsystem Sizing

T-2100 SOLAR COLLECTOR CONSTRUCTION

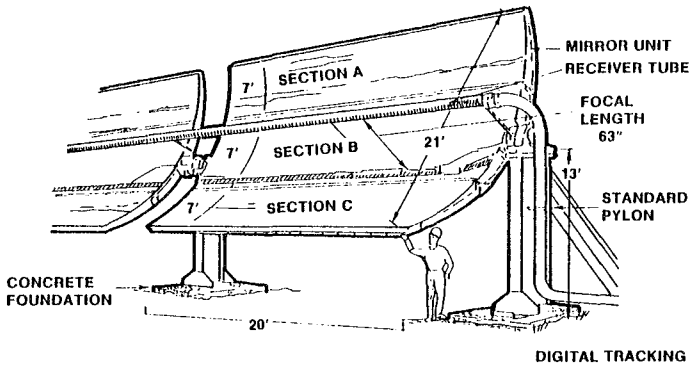

COLLECTOR SPECIFICATIONS

	STEEL T-2100
MODULE WIDTH	22'
MODULE LENGTH	20'
MIRROR WIDTH	21'
SOLAR AREA	420 ft^2
REFLECTANCE	.95
ROTATIONAL AXIS HEIGHT	13'
TRACKING ANGLE	270°
STOW ANGLE	INVERTED
SYSTEM WEIGHT	6.95#/ft^2
RECEIVER	4.5 X .095 STEEL
RECEIVER COVER	130 mm OD PYREX
SELECTIVE SURFACE	BLACK CHROME
ABSORBTIVITY	.96
EMISSIVITY @ 300° C	.15
COLLECTORS PER ROW	10
ROW LENGTH	210.5'
REFLECTIVE MATERIAL	GLASS 0317
RECEIVER UNIT LENGTH	20'
RECEIVER COVER LENGTH	10'
SOLAR AREA PER ROW	4,200 ft^2
INSTALLED COST	5.48 ft^2

Figure 4. Preliminary Design of 21-Foot Aperture Linear Parabolic Trough

BDM determined that the overall collector field efficiency could be improved if a larger portion of the field was operated at lower temperatures and only a small portion of the field was used for steam super heating at higher temperatures. Therefore, two receiver tube subsystems have been designed, one of which is optimal for collector operating temperatures up to 600°F (316°C) and one for temperatures up to 750°F (400°C).

During the analysis, it was also determined that substantial improvements in the overall collector performance could be achieved with an improved selective coating material for the receiver tube subassembly. The most applicable receiver tube coatings currently available are near commercial production, and use black chrome or black cobalt. The desired receiver tube coating for the line focus power plant must have very high absorbtivities (around 0.95) as well as low emissivities (around 0.05). Commercially available receiver tube coatings can provide absorbtivities of about 95 percent; however, emissivities range between 10 and 20 percent. The optical efficiency of the linear parabolic trough is most sensitive to the mirror reflectivity and the absortivity of the receiver tube coating and less sensitive to irradiation factors, as illustrated by the instantaneous efficiencies plotted in Figure 5. The bottom line represents currently available technologies. The top line represents that efficiency which could be achieved with the Corning 0317 reflective annealed glass mirror surface and improved absorbtivities and emissivities in the receiver tube coating. BDM has determined, through numerous discussions with manufacturers and researchers, that the top efficiencies can be achieved in the near future with the application of currently available or slightly improved materials.

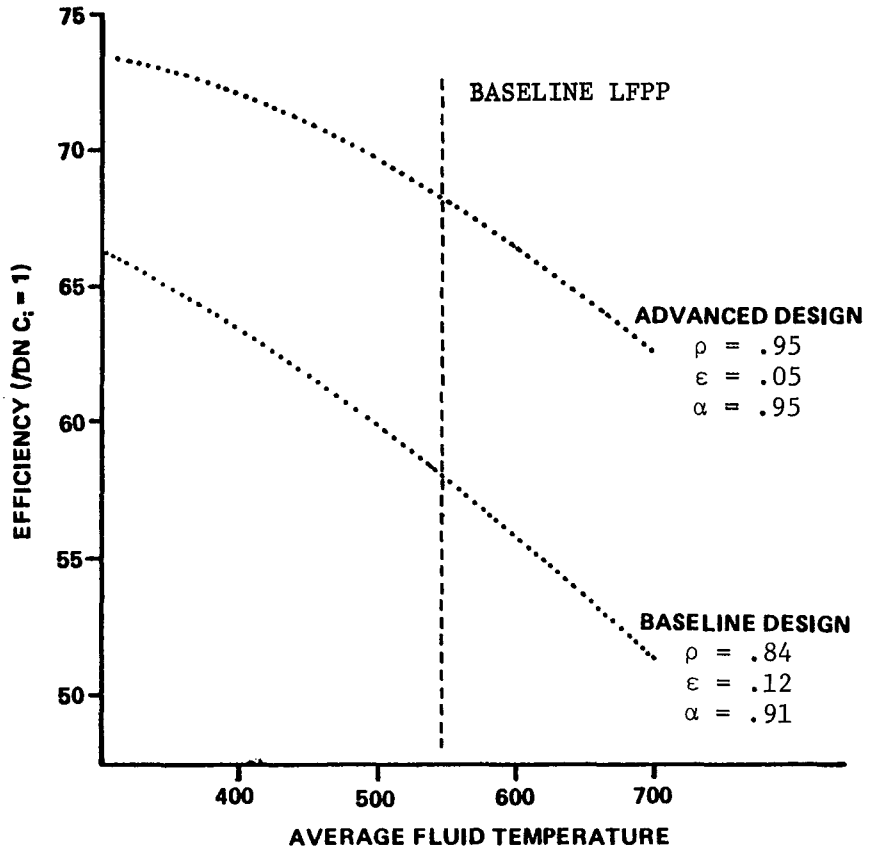

Figure 5. Collector Efficiency

The instantaneous efficiency must be reviewed with cognizance of the effects of the cosine factor, collector, and losses, and variations in receiver tube efficiencies as a function of insolation. With the use of annealed glass as a reflecting surface and improved receiver tube coatings, average daily efficiencies at summer solstice of 66.5% and 54.0% at winter solstice can be achieved, which will result in an annual efficiency of 64% for the north-south oriented collector system.

The thermal working fluid was a very important consideration in the overall plant design. Several organic base thermal fluids and salts were examined in detail during the conceptual design. Although high-temperature organic base fluids are relatively expensive, it was determined that the cost of the high quality piping required for salt working fluids had a far greater impact on the overall plant cost. Therefore, the organic base fluids were selected for the conceptual design. However, the requirement for developing low-cost organic base fluids or other non-corrosive high-temperature fluids was identified during the course of the analysis.

In the analysis of the electrical power generating subsystem (EPGS), several engineering trade-offs were made which encompassed reheat versus non-reheat cycles, mechanical steam separation at lower temperatures and pressures, feedwater heater requirements, and turbine back pressure. The resultant

design includes a reheat cycle operating at a throttle temperature of 700°F with four steam extractions/feedwater heaters.

The electrical power generating subsystem (EPGS) which is used for the baseline LFPP design is shown schematically in Figure 6. The turbine is a tandem compound four-flow reheat turbine which will operate with a throttle temperature of 700°F and a throttle pressure of about 600 psig. Discussions with General Electric and Brown Boveri indicate that this turbine is commercially available and could be delivered within 18 months of order. The EPGS will have four steam extractions and feedwater heaters, and with a reheat cycle, will operate with a cycle efficiency of about 34 percent.

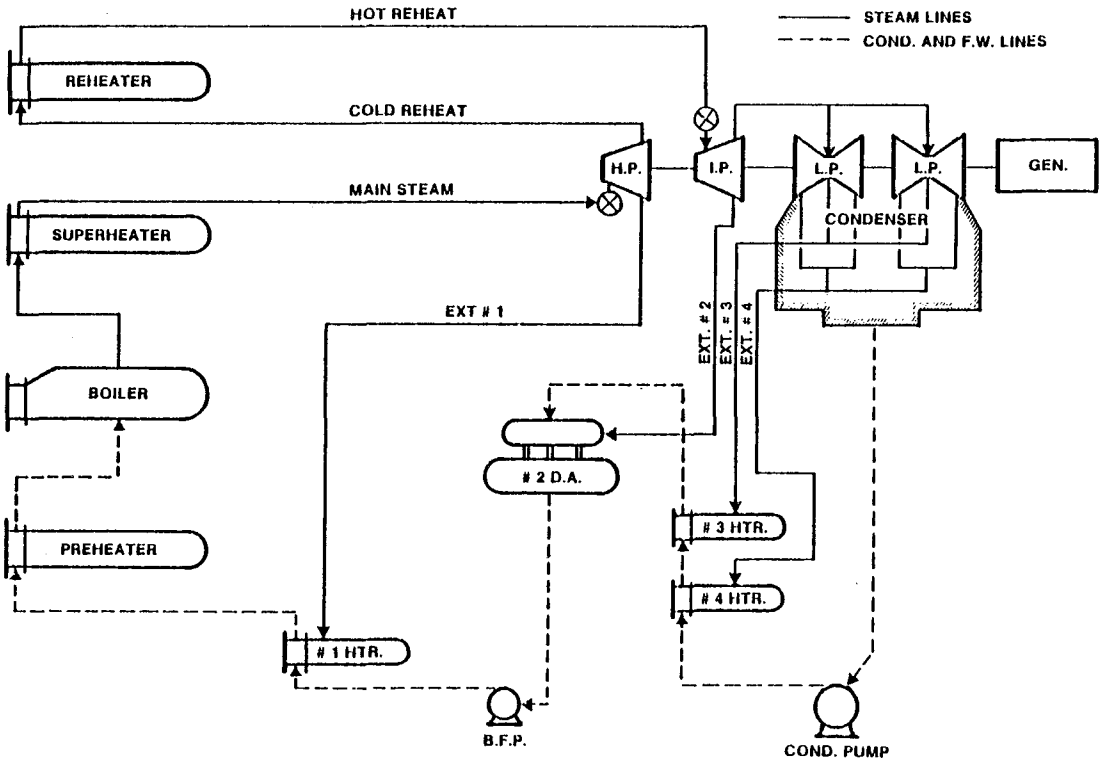

Figure 6. EPGS Steam and Feedwater Diagram

The heat transport subsystem includes all manifold piping required to transport the fluid between the collector field and the boiler super heater heat exchangers, which are in a centralized plant location. The key design factors in the heat transport subsystem involve minimizing the total amount of manifold piping in the field and performing the trade-off between the capital costs induced by large diameter pipes versus recurring costs of increased pumping, pressure for daily operation. It was determined that the heat transport subsystem represented only about 15 percent of the total capital costs of the plant, and the total parasitic pumping power was about 3-1/2 percent of the rated plant capacity.

The plant will use a centralized boiler, super heater, and turbine system with a collector field layed out in nearly a circular pattern, as illustrated in Figure 7. The thermal storage systems will also be centralized and adjacent to the boiler systems. The collector field will involve about 684 rows of collectors, each row being 1,000-feet long. The circular pattern proved to be optimal because it minimized the amount of manifold piping required to carry the fluid from a centralized location to the entire collector field. The heat transport subsystem will use tapered piping with heavier insulation on the hot temperature return loops. Approximately 11 million square feet of aperture will be required to provide the energy for a nominal 100-MW_e electrical power plant with storage-dependent capacity factors ranging between 0.4 and 0.6.

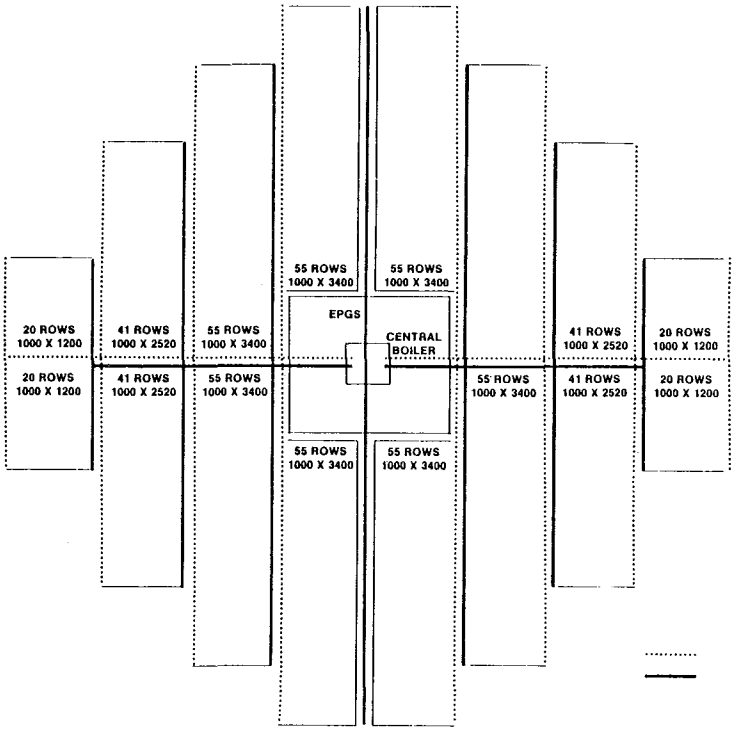

Figure 7. Optimized Field Layout

LFPP Configuration and Performance

The BDM design team examined different LFPP configurations with a variety of thermal working fluids and field configurations. The levelized bus bar energy costs for a selected sample of these configurations were calculated. On a levelized bus bar energy cost basis, the most attractive LFPP configuration was a two-stage field, a low- and high-temperature organic base thermal working fluid, and a turbine throttle temperature of about 700°F.

The preferred configuration described above was examined in more detail and the levelized bus bar energy costs were calculated for a nominal 100-MW_e plant with varied turbine sizes and storage capacities. Further, a baseline collector field which did not use improved reflective surface or receiver tube coating was compared to the same field with these improved materials. The bus bar energy cost versus capcity factors for these two configurations, referred to as baseline and advanced, are shown in Figure 8. The bus bar energy costs have been nominalized to show their relative cost effectiveness to the first-generation point focus central receiver strawman, i.e., the unity on the curve represents the bus bar energy costs for the point focus technology. As can be seen in the curves, even the low risk current state-of-the-art line focus power plant is substantially more cost effecgive than its counterpart. In addition, the improved materials in the area of reflective surface and selective receiver tube coatings further increase the cost effectiveness for the line focus technology.

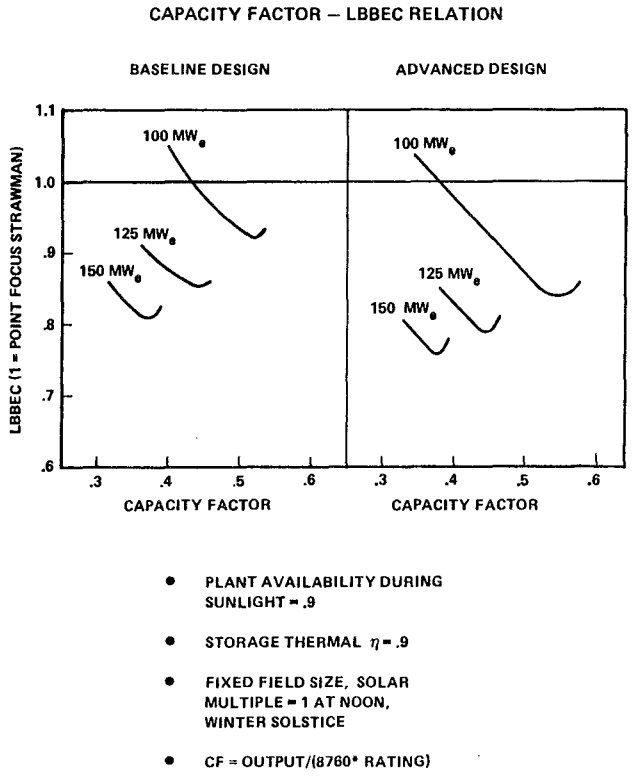

Figure 8. $\overline{\text{BBEC}}$ for Line Focus Power Plant Compared to Point Focus/Central Receiver Strawman

Future Research

Research continues in identifying and defining improved materials for the line focus technology. Systems analysis will continue to include the identification of the optimal line focus plant size. This will be concluded in the very near future, and the results of the analysis will be provided in the mid-program documentation. In the final half of the program, all design tools will be validated, the advanced receiver tube coatings will be tested at the BDM solar ·lar test facility, and the overall assessment and market penetration analysis for the line focus power plant system will be completed. The first phase of the line focus power plant contract will be concluded with the definition of the development plan and the Phase II proposal activities.

Summary

BDM feels that a very valuable resource has been identified for application to power production in central power plant configurations. Further, this technology provides an economically attractive alternative to solar central receiver technology for several reasons. First, a very significant capital cost differential can be achieved between the two power plant technologies. The line focus technology can be fabricated, implemented, and maintained in the field at a far less capital cost than the more complicated point focus central receiver technology. Second, the gross plant efficiency (collector efficiency x turbine cycle efficiency) is relatively insensitive to temperature in the specified temperature range. The reduced temperatures inherent to the line focus technology only result in a one to three point sacrifice in gross and net plant efficiency. Further, the line focus technology is very suitable for retrofit or repowering configurations where the majority of the energy would be supplied as part of the boiler duty and the super-heating would be provided by a fossil fuel.

Finally, the enhanced line focus collector technology identified in conjunction with this program is a significant advancement for the broad spectrum of solar technologies because of its inherent flexibility. The LPT concentrator can not only be applied to electrical power production but to industrial process heating and photovoltaic line focus applications. The improved optical performance and reduced costs is a very significant advancement in solar technology.

HELIOSTAT DEVELOPMENT PROGRAM

W. G. Wilson
Sandia Laboratories, Livermore

Two important milestones in the Heliostat Development Program have been achieved since the last semiannual meeting. First, twelve proposals submitted in response to the Production Heliostat RFP were reveiwed and contractors have been recommended for funding. The objective of this eighteen-month program is the detail design, fabrication, and testing of second-generation heliostats; the conceptual design of production facilities; and the formulation of cost estimates for DOE/utility evaluation. These heliostat efforts will be the major program activity for the next year or so and are intended to demonstrate a mass producible, low-cost, heliostat for early 1980 applications. At this time, no details are available; however, our intent is to award four or more contracts.

The second major milestone achieved was the "New Ideas" solicitation completed in December. The objective of this procurement was conceptual designs, materials development, and support equipment that will significantly reduce collector field costs when compared with second-generation technology. Fourty-two proposals were received for the categories of drive mechanisms, reflective surface modules, materials, and a catch-all category that included control systems, cleaning equipment, and alignment systems. Many clever ideas were submitted. We have ranked the proposals in descending order, and purchasing personnel are now in the process of working their way down the list as dollars permit. These efforts are intended to provide a data base for third-generation heliostat designs in mid-FY 80.

Figure 1 shows the major elements of the Heliostat Development Program. It also illustrates an attempt to reduce the confusion in the program caused by descriptors used in the past (low-cost, new ideas, etc.) by aggregating the major procurements into first, second, and third-generation activities. With this terminology, the first-generation designs involve the technology that is associated with the Barstow pilot plant. That program evolved from conceptual designs through prototype fabrication and test into the current efforts leading to the fabrication and testing of preproduction units. In early FY 80, the most cost effective design will be selected for the production of units to be installed during FY 81. As a footnote, the heliostats installed at the CRTF in Albuquerque are considered to be a one-time special design fabricated to meet the unique requirements of a test facility. Even though the experience gained and the operational data obtained from these heliostats are extremely valuable to the program, they do not logically belong in the development cycle for commercial power applications.

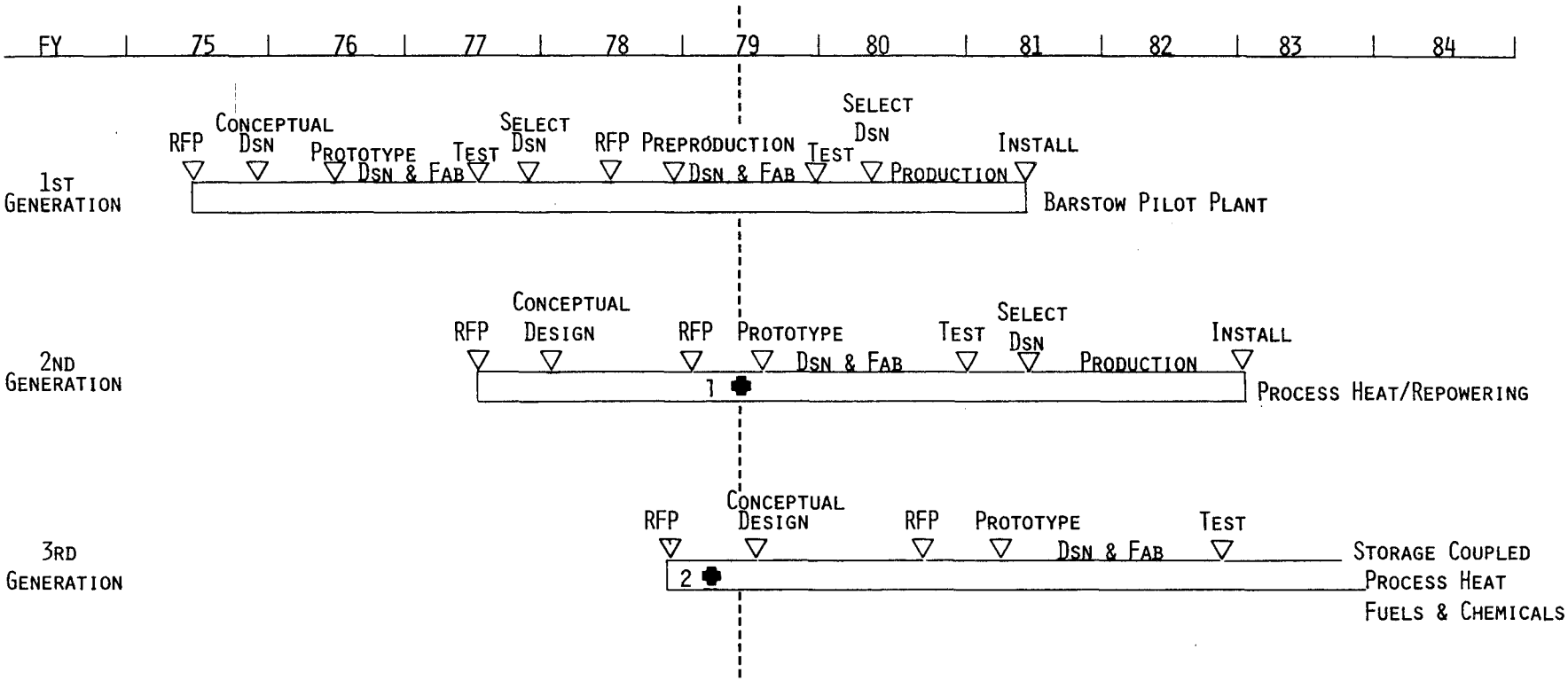

Figure 1. Heliostat Development Program

The second-generation activities were started in FY 77 with a procurement entitled "Prototype Heliostat RFP." From that solicitation, contracts were awarded to Boeing Engineering and Construction, General Electric, McDonnell Douglas, and Solaramics for conceptual designs of second-generation heliostats.

A composite schematic drawing of the four resulting designs is presented in Figure 2. In addition to the four designs entirely funded with federal dollars, an encouraging precedent in heliostat development is also illustrated in Figure 2. The design being pursued by Westinghouse is entirely funded with their internal funds. Under a no-cost agreement with Westinghouse, Sandia has been periodically reviewing their design progress and will test a resulting demonstration unit at a DOE facility. In exchange, Westinghouse has agreed to publicly disclose design features and cost figures.

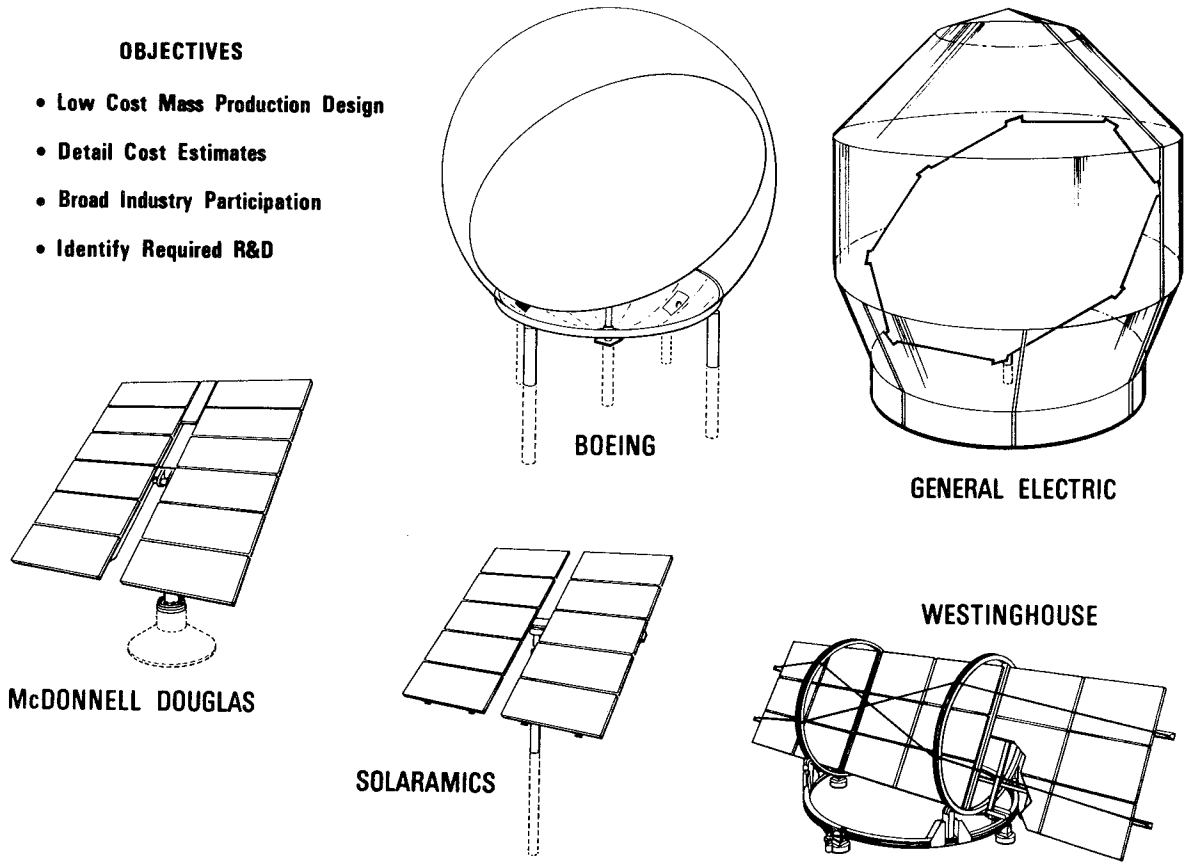

Figure 2. Large Power Systems Prototype Heliostats

An evaluation of the four federally funded designs was made by Sandia and the results published in Prototype/Second-Generation Heliostat Evaluation and Recommendations: Executive Summary, SAND78-8265, October 1978. The conclusions of that evaluation stated:

"The MDAC heliostat design is clearly superior to the other three designs for all three evaluation criteria and has no significant weaknesses. The MDAC design is the most mature, the best analyzed and tested, and carries the lowest risk of the four designs."

For a variety of reasons (including funding limitations, a desire to foster competition, and the emerging repowering/process heat applications) the originally planned follow-on efforts for the prototype/second-generation program were restricted to demonstration of the high leverage component and materials developments identified by the evaluation process. Subsequently, a new competitive solicitation was prepared and released as the "Preproduction Heliostat RFP" described earlier and shown by the cross labeled "1" on the second-generation development time line of Figure 1.

The cross labeled "2" on the third-generation development time line represents the "New Ideas RFP" milestone referred to earlier. The conceptual component design and materials data base generated under this procurement will serve as a precursor to future full heliostat designs for applications in the mid-1980s and beyond.

In summary, the total heliostat development program is attacking several fronts in an attempt to provide aggressive, forced development of this technology. By the end of FY 79, competitive first-generation heliostats for the Barstow pilot plant will be in side-by-side testing; four or more contractors will be doing detail design on second-generation heliostats for mass production in the early 1980s, and several component developers will be attmpting to reduce costs through conceptual innovation.

In addition to the major heliostat design efforts, a variety of special studies are under way to complement the development program. Table I lists those special studies activities which are reported elsewhere in these proceedings; hence no further discussion of them will be given here.

TABLE I

HELIOSTAT SPECIAL STUDIES

Inverted Stowage Study - McDonnell Douglas
Field Reflectometer Development - Beckman
One-Piece Plastic Dome Development - Boeing
Mirror Deterioration Studies - Sandia Laboratories
Drive System Development - Solaramics
Demonstration Heliostat Testing - Westinghouse
Full-Scale Wind Tunnel Test - Sandia Laboratories

Several other special studies are under way, however, which are just beginning and it is too early for their principle investigators to discuss them. Consequently, these studies are briefly described below.

Plastic Development - General Electric

Produce, characterize, and test plastic enclosure and reflector materials with the objective of establishing a firm data base for prediction of useful life. The mechanisms of degradation will be identified, and appropriate accelerated aging tests will be developed.

Mirror Specifications - Battelle Northwest

Survey existing mirror silvering capabilities of commercial suppliers. Analyze present methods of silver protection, quality controls, and costs, and establish a consistent mirroring specification.

Manufacturing Support - McDonnell Douglas

SERI is using the prototype heliostat designed by MDAC as an example for production costs in their Repowering Strategy Analysis. They have contracted General Motors and F. J. Lamb to independently assess the mass production costs and recommend production improvements. This contract is for MDAC to provide design details as necessary.

These and other studies funded by DOE are geared to reducing the life cycle costs of heliostats while maintaining acceptable performance capabilities. With the exception of the 222 special design heliostats for the CRTF, only a few handbuilt prototype heliostats have been built to date. As a result, we are forced to rely on paper studies, dollars per pound estimates, and analogies with similar mass produced items to project the future costs of heliostats. Even though many of the manufacturing estimates have gone into great detail and independent evaluations of the same designs have confirmed the costs projected, no firm cost figures exist. Consequently, questions persist.

Nevertheless, project sponsors must have some benchmark to determine if the development program is on schedule or if it is either too optimistic or pessimistic. Figure 3 presents another attempt at providing that insight. On the right side of the figure are plotted some data for the average list price of Model-T Fords versus cumulative units produced (expressed in 1958 dollars) for the years 1909 through 1923. The data runs from a few thousand units out to more than ten million cumulative units produced and takes into account product improvements, changes in manufacturing techniques, and materials substitutions. A line drawn through these data gives an 85 percent slope to the experience curve achieved.

If it is assumed that the experience curve in dollars per square meter for the installed costs of heliostats versus cumulative units produced will follow the same slope as the Model-T data, two curves can be plotted. The first curve originates at the recorded cost for the second buy (144 units) of the CRTF heliostats. This curve is labeled pessimistic because the CRTF units contain special features not needed by power production heliostats and hence the plot should be conservative. Similarly, if the estimate obtained for the tenth year of production at 25,000 units per year for second-generation/prototype heliostats is used to project back to lower numbers of units, the lower line, labeled optimistic, is generated.

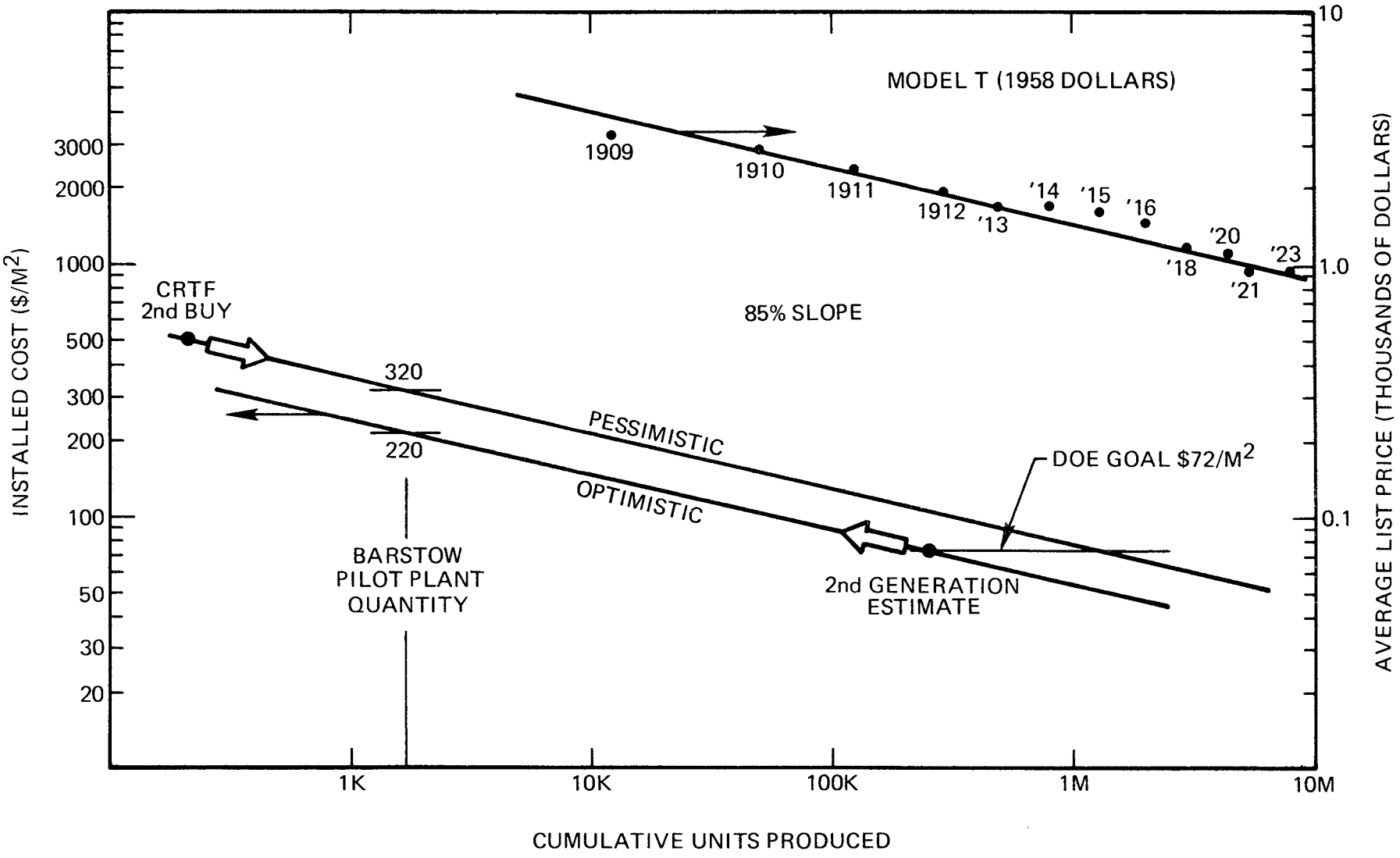

Figure 3. Experience Curve Comparison

Using the limited information of two data points and the assumption of the same experience curve slope as demonstrated by the early years of Model-T production, two interesting observations can be made. This chart suggests that for the Barstow pilot plant production quantity, an installed price of 270 dollars plus or minus 50 dollars per square meter might be expected. Additionally, the DOE cost goal of 72 dollars per square meter may require a differential of over 1 million cumulative units depending on whether the optimistic or pessimistic curve is actually attained. Obviously, hard data will significantly improve our cost projections. The cost figures for the Barstow pilot plant are due sometime this fall; it remains to be seen if they will confirm or refute the simplistic approach of Figure 3.

As a further indication of the development program progress, I have compiled the heliostat component breakdown illustrated in Figure 4. Here the cost contributors associated with the reflector, structure, drive system, controls, foundation, installation, and miscellaneous are broken out to illustrate their share in the overall cost for various designs. The miscellaneous category includes fee, contingency, and other incidentals that do not conveniently fit into the major categories. The data shown are for glass metal heliostats, all designs have been normalized to a reflectivity of 0.9, and the costs have been expressed in 1978 dollars. The six major reasons for the drop in installed prices as the quantity produced increases are shown in the development arrow. Table II provides some additional explanation of the terminology used. In essence, the dramatic drop in the future cost of heliostats is the result of the combination of efficient design and the unit savings associated with mass production.

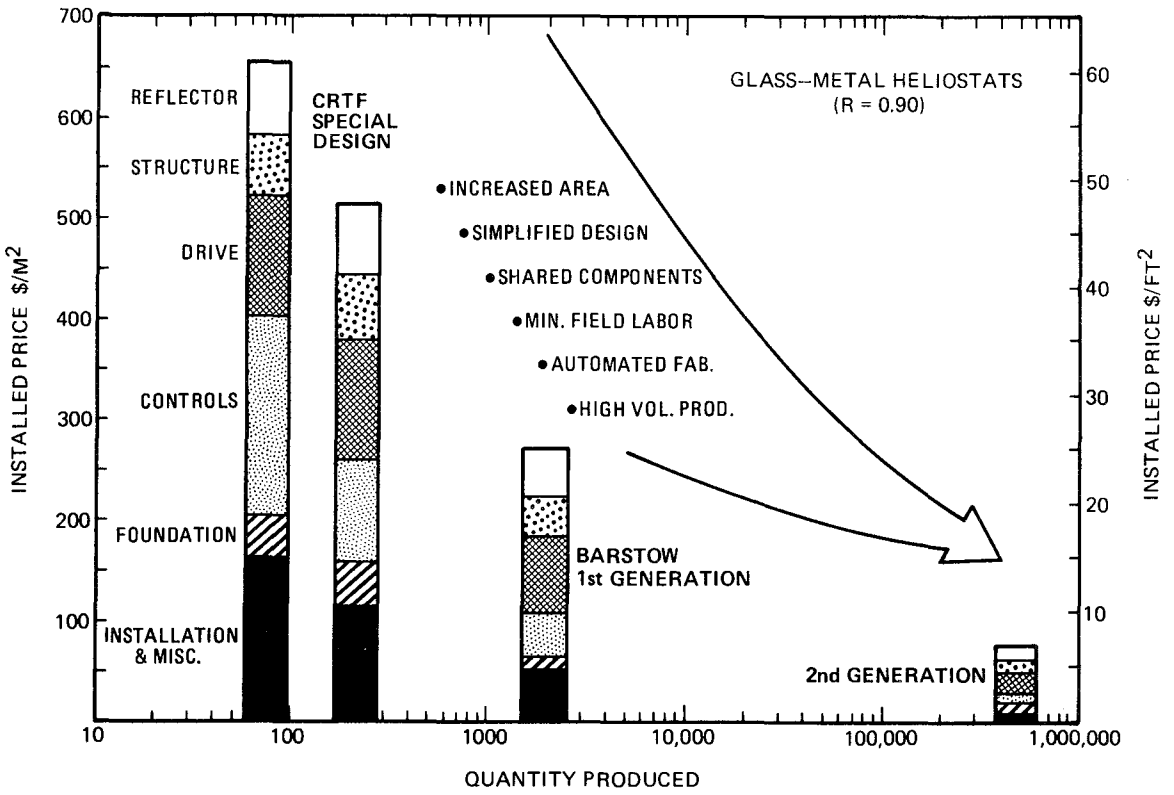

Figure 4. Heliostat Component Breakdown (1978 Dollars)

TABLE II

EXPLANATION OF COST REDUCTIONS

Increased Area	Incremental costs for larger components are generally less than purchasing two
Simplified Design	Off the shelf components, efficient assembly operations, standard tooling and relaxed tolerances have reduced initial costs
Shared Components	Field controllers spread over 10-100x more heliostats
Minimum Field Labor	Field assembly and alignment almost eliminated since field labor costs are double factory costs
Automated Fabrication	Production electronics, reduced manpower needs and interchangeable parts reduce fabrication costs
High-Volume Production	Unit costs spread over much larger population

Another way to look at the costs associated with heliostat components is presented as Figure 5. Here the component costs are illustrated as pit segments of the overall cost. Even though this approach is misleading in theat the circles are all the same size, it is a useful way to visualize how the component contributions are changing with design improvement. A case in point is the drive system. Its share of the whole has increased despite the dramatic reduction in overall costs. Conversely, because the designs have been concentrating on reducing expensive field labor costs, the installation and miscellaneous segments have been traded for foundation hardware costs. The point to be made from Figure 5 is that not all components costs may be reduced. Rather, design trade-offs may result in an increased percentage cost of individual components to achieve an overall reduced unit cost.

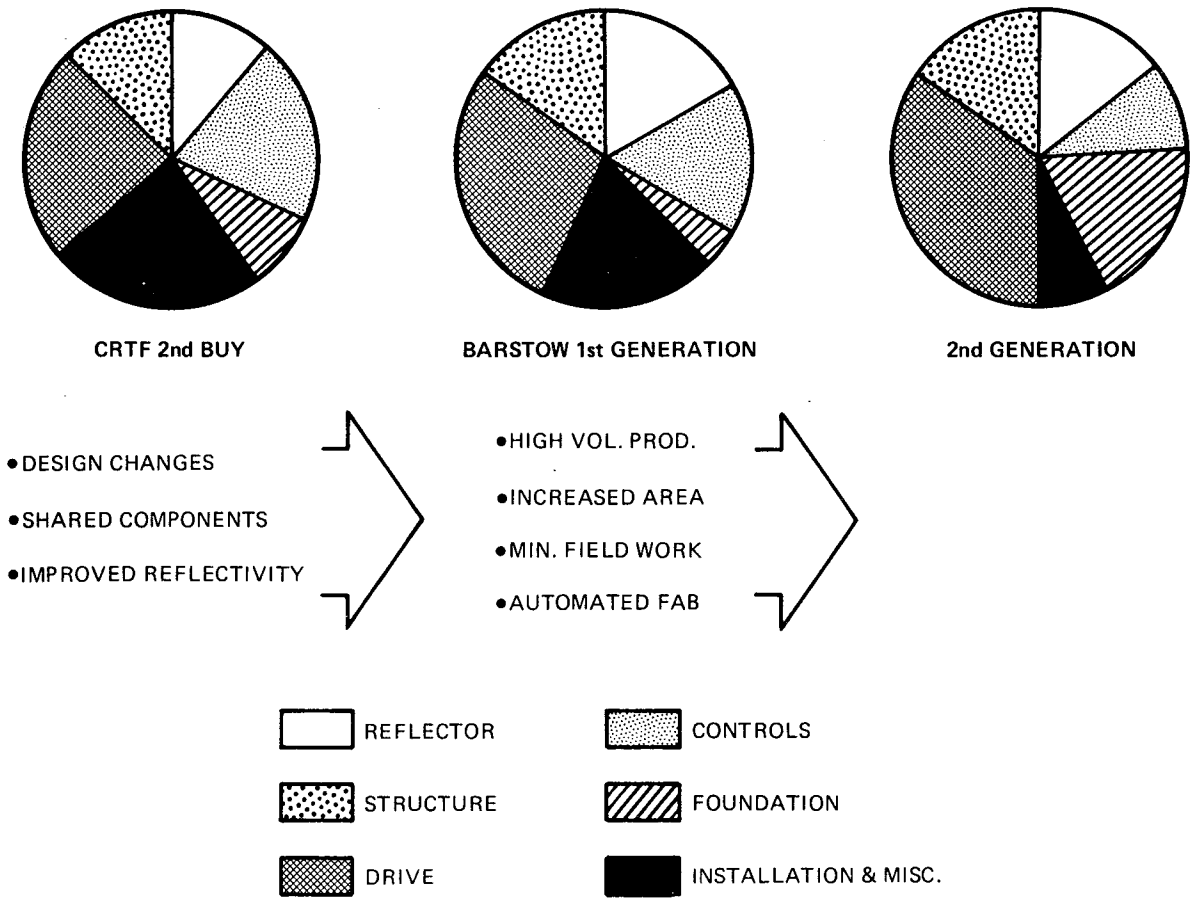

Figure 5. Heliostat Components

HELIOSTAT DRIVE SYSTEM DEVELOPMENT

W. Mitchell
Solaramics, Inc.

Introduction

The objective has been to design and test the modified azimuth-elevation heliostat drive mechanism designed by SOLARAMICS in the Low-Cost Heliostat Preliminary Design Program (contract #ET-78-C-03-1745). The preliminary design has been scaled up to accommodate a larger heliostat of 50 m^2 (524 sq ft) from the 40 m^2 design.

The design effort has stressed development of a low cost, low maintenance mechanism . The basic design concept using two linear actuators with bell crank linkages has been retained and refined. Significant progress has been made in actuator design trade-offs and in mechanism component producibility studies.

Drive Mechanism Design

The modified azimuth elevation drive mechanism (Figure 1) embodies an azimuth axis inclined 23 degrees from vertical. The tilted axis is in line with a vector to the tower, and is tilted away from the tower. This concept has the advantage of shifting the location of control singularities outside the operational zone of the tracking requirements. It also reduces the azimuth drive requirement to less than 180 degrees, compared to approximately 240 degrees for typical azimuth-elevation systems. The elevation requirement is increased from 180 to 203 degrees to achieve an inverted stowage position.

A unique double bell crank system achieves the required angular motions with linear actuators. By attaching the actuator shaft to the functional centerline and the actuator base to a fixed point by one link and to a rotating crank by another link, the rotational motion is amplified by two-to-one. Thus large angles are achieved with a bell crank system which is normally limited to angles only slightly greater than 90 degrees.

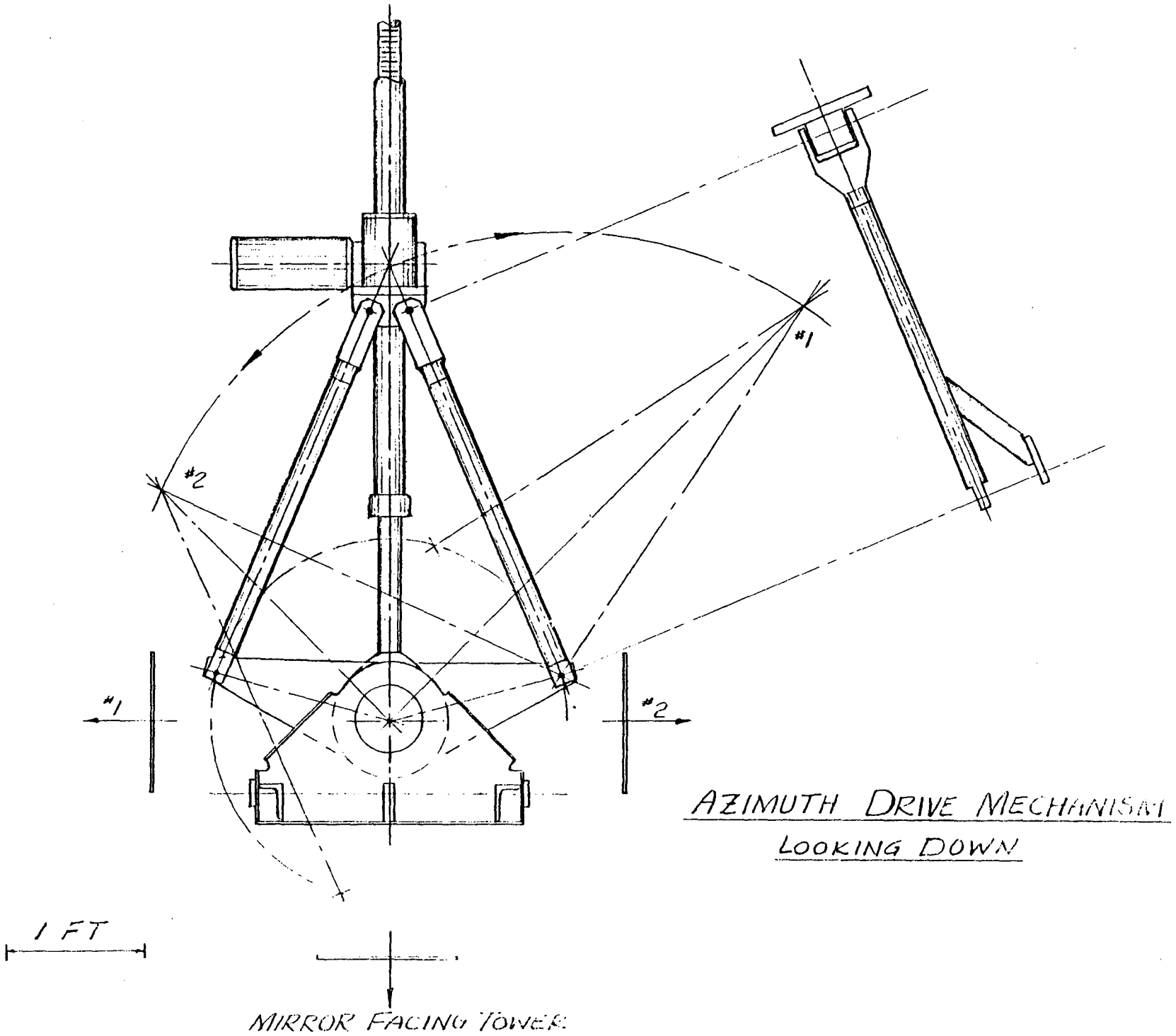

AZIMUTH DRIVE MECHANISM
LOOKING DOWN

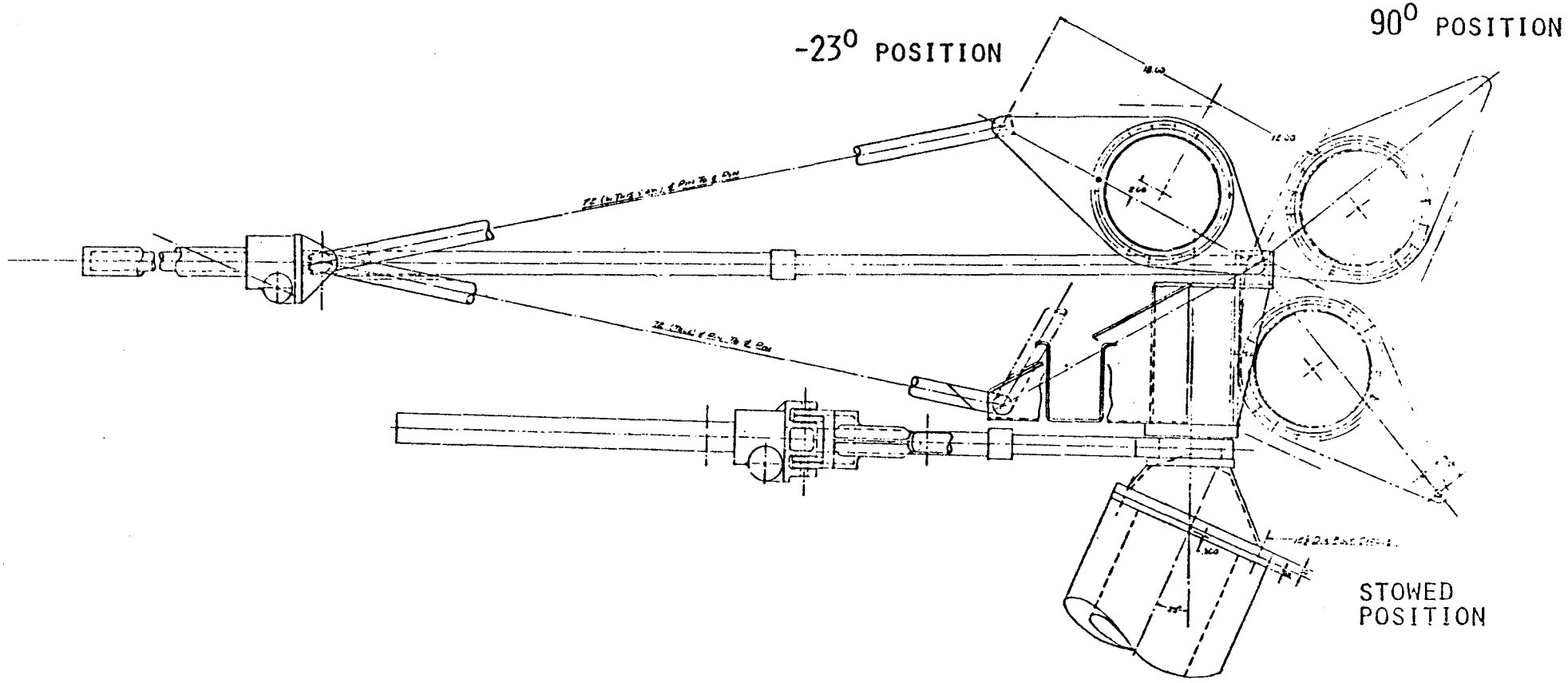

Figure 1. Azimuth Drive Mechanism

The drive mechanism stiffness is a prime consideration in determination of natural frequency of the heliostat array and in the performance throughout the operating environmental spectra. The design objective has been to achieve a heliostat natural frequency of approximately 3.0 Hz. The stiffness and backlash criteria have been tailored to meet the 1.7 mrad standard deviation deflection limit of para. 3.2.1c of the Heliostat Design Specification.

Actuators

The advantages of linear actuators chosen for this application include irreversible motion, i.e., self-locking, minimal backlash (0.003 to 0.005 in.) with adjustment capability for wear, and extensive experience with the design in industrial applications.

Special actuators are being designed specifically for this application. The actuators employ a 2 in. diameter, rolled, modified acme screw thread of 0.2 in. pitch. The screw thread will be roll formed from bar of the required stroke length, and then inertia welded to the unthreaded and zinc plated extension shaft.

A single gear reduction of 110:1 by a worm drive is currently planned. The actuator is to be powered by a "three-fourths" motor, i.e., a motor without the standard forward bell, which mounts directly on the actuator housing casting. The worm will be an integral part of the motor shaft, roll formed, and induction hardened.

The azimuth actuator rate requirement (1.5 in./min) is only half of the elevation actuator requirements (3 in./min.). This is accomplished with a 875-rpm motor for the azimuth drive and a standard 1750-rpm motor for the elevation drive. The clevis fittings for the drive link attachment are an integral part of the actuator housing casting.

Drive Linkage and Bearings

All links are fabricated from 2-in. diameter cold finished merchant bar, to which the forged end fittings are inertia welded. The forged ends are then milled and bearing holes bored.

A self-lubricating bearing fabricated by molding a composite teflon-phenolic material to a steel shell has been chosen for this design. It is produced by Kahr Bearing Company, Division of Sargent Industries. Close tolerance of the installed bearing is accomplished with a broach, which is an integral part of the installation tool.

Trunnion

The trunnion (Figure 2) is a welded steel fabrication made up of plate elements. The trunnion contains the elevation hinge pivot and the azimuth axis, which rotates on pre-loaded tapered roller bearings on the kingpin. The elevation fixed link pivot and the active azimuth crank pivot are also a part of the trunnion.

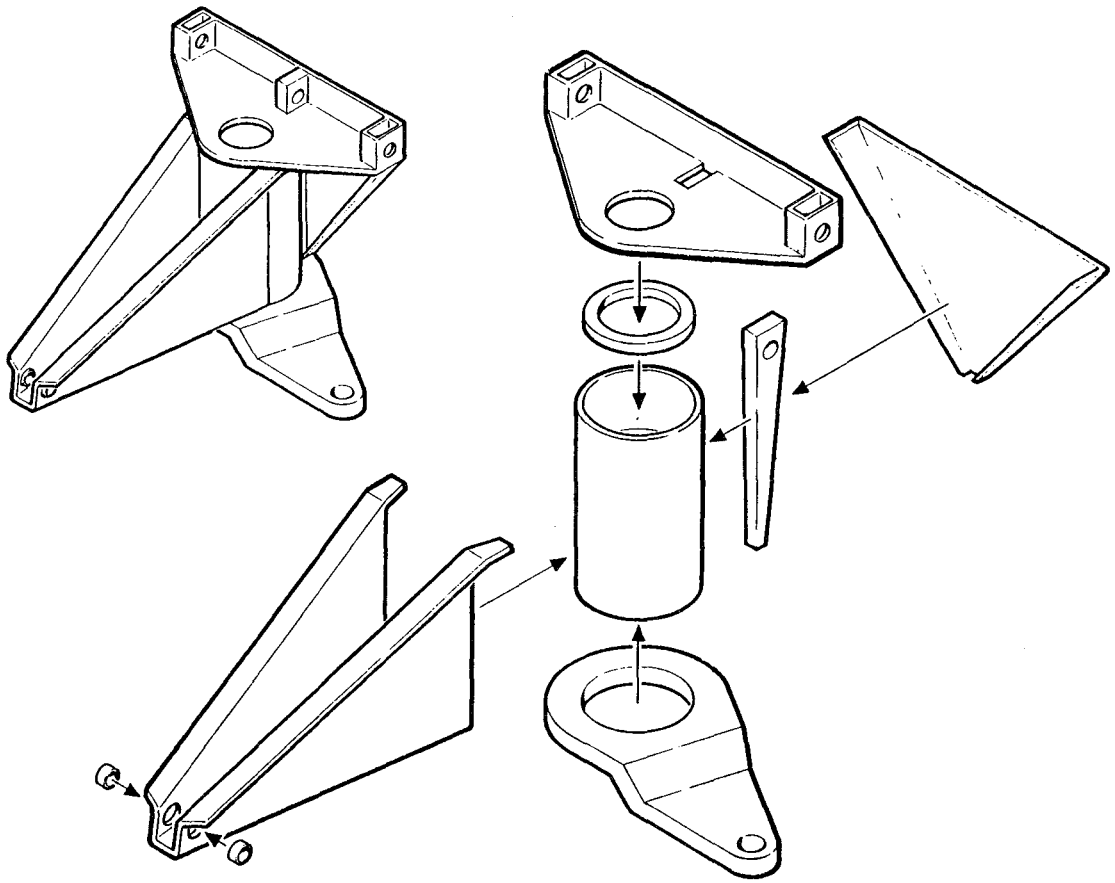

Figure 2. Trunnion Assembly

Kingpin

The kingpin (Figure 3) provides the tilted azimuth axis and the structural transition to the pedestal cap. This is accomplished by a 6-in. diameter shaft welded to a tilted, tapered cone and flange forging. The fixed crank for the azimuth linkage and the bearing surface for the azimuth actuator pivot are also provided by the assembly. The three elements are welded together in one set-up with an automated, double pass, MIG weld. To save material and machinery cost, a sleeve is pressed on the 6-in. diameter shaft for the azimuth collar bearing surface.

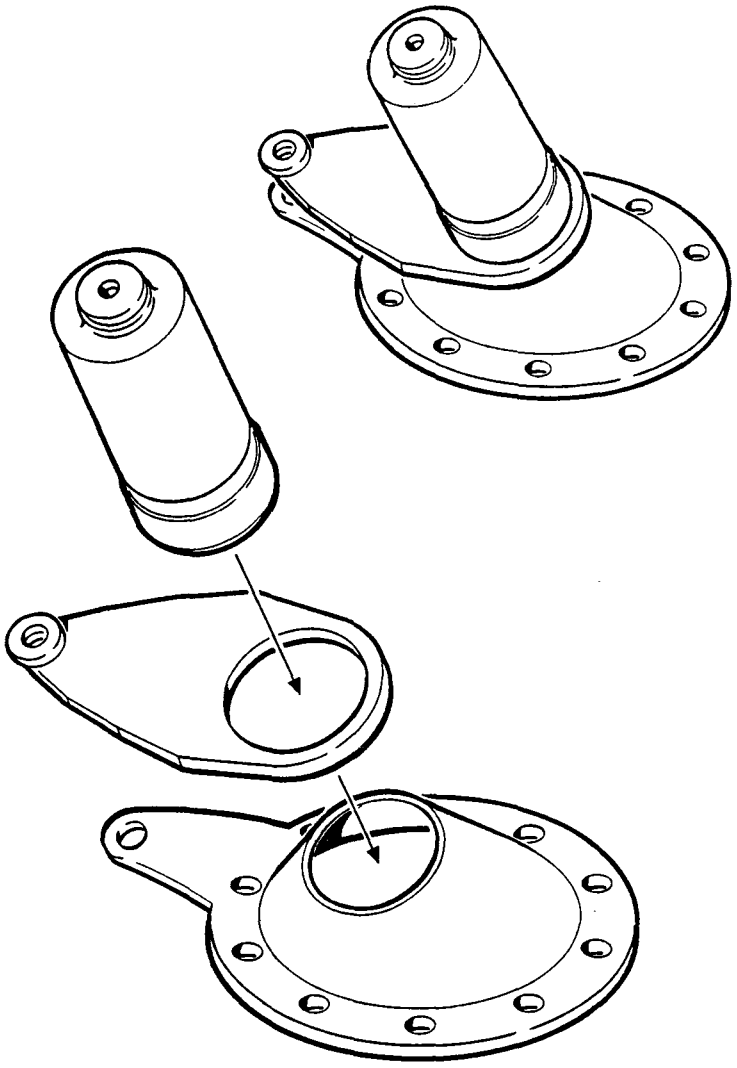

Figure 3. Kingpin Assembly

Design Criteria

The design criteria has been structured to meet the requirements of specification A10772, Collector Subsystem Requirements summarized as follows:

- Operational tracking with wind speed up to 16 m/s (35 mph)
- Structural integrity in a non-operational state in a 22 m/s (50 mph) wind in any orientation
- Stowage initiation @ 16 m/s (35 mph) with a maximum wind rise rate of 0.01 m/s^2 (0.02 mph/s)
- Stowed survival in a 40 m/s (90 mph) wind

The wind may deviate by up to ±10 degrees from the horizontal for all loading conditions.

- The drive systems must be capable of positioning the heliostat to stowage, cleaning, or maintenance orientation from any operational orientation within 15 minutes
- The collector subsystem must maintain structural integrity in any applicable combination of the environments described in Appendix 1 of the subject specification

The wind loads have been calculated from the coefficients reported in Wind Forces on Structures, ASCE Paper No. 3669.

ONE-PIECE PLASTIC DOME FABRICATION

R. Gillette
Boeing Engineering and Construction Company
Seattle, Washington

The primary objective is to develop a low-cost process for fabricating plastic heliostat domes. A thermoforming process is under development wherein spherical domes are blown from flat film blanks (preforms) at elevated temperature. Primary variables being optimized in the thermoforming process development include: temperature, time, pressure, and radiant heating geometry. Contract activities also include selection of preferred materials for thermoforming, investigation of techniques for forming large preforms from commercially available materials, weatherability testing, and a subcontract to Pennwalt Corporation to perform thermoforming experiments on polyvinylidene fluoride (KYNAR).

An existing facility has been modified to investigate: the capability of forming various materials into small domes less than 76 cm (30 inches) in diameter; materials and process variables; and the feasibility of various preform preparation techniques. Figures 1 and 2 show the major features of the facility. A blown dome is shown on the floor of the chamber in Figure 1. Overhead radiant lamps are used to heat the preform, and a circle of base radiant lamps apply heat while the dome is being blown. Heat flux is monitored with radiometers located adjacent to the preform.

An air supply provides pressurized air, and records flow rate and pressure during thermoforming. Plastic film temperature is monitored with an infrared pyrometer and a thermocouple.

A larger thermoforming facility is presently being constructed which will be capable of forming domes up to 2.4 m (8 ft) in diameter. The larger production simulation facility will be used to verify process parameter scale-up and to select the preferred approach for making large preforms.

The primary variables explored in experiments to date included heat distribution during forming, air pressure and flow-rate profiles, expansion ratios, pre-heat time and temperature, and blowing time. The heat distribution was varied during forming to determine its effect on shape and thickness uniformity. Both uneven heating and radiant cooling were found to effect geometry. Both pressure/flow variations and blowing times affected the shape and strength. Relatively high flow rates and pressure were required to obtain satisfactory properties. The straining rate required for good small domes is approximately

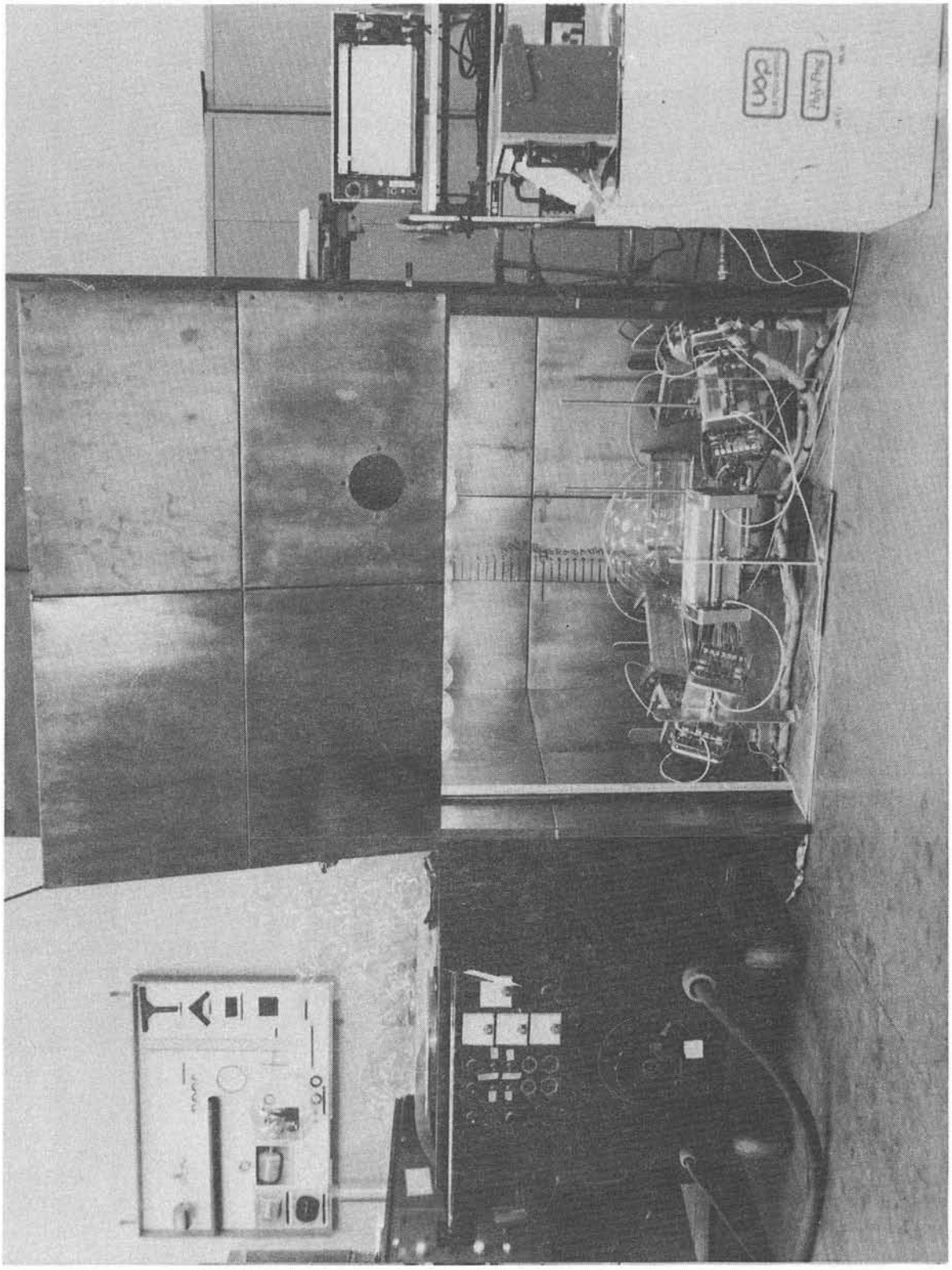

Figure 1. Experimental Dome Thermoforming Facility

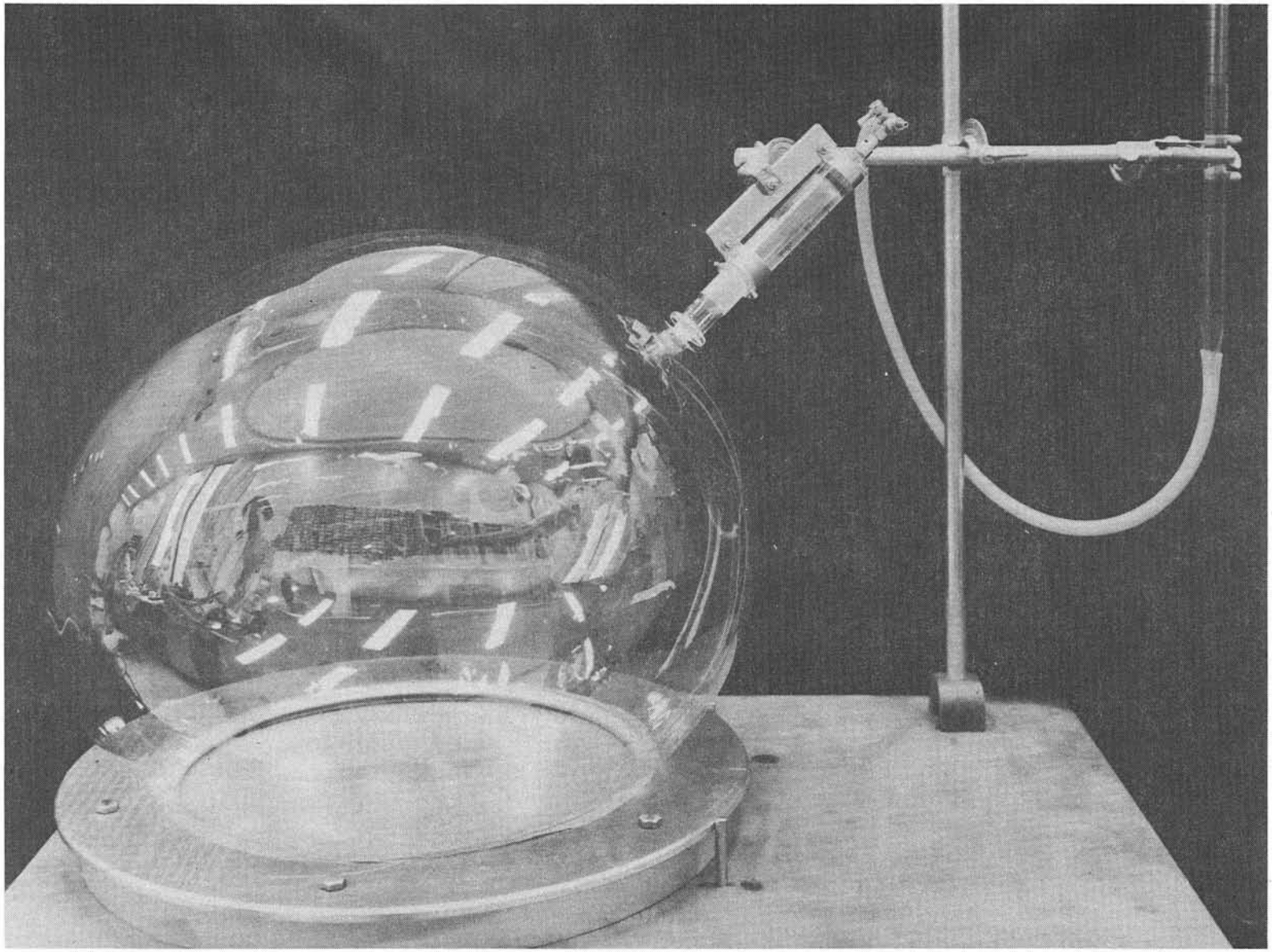

Figure 2. Thermoformed Polyester Dome Being Measured for Shericity

300 percent/minute. Expansion ratios up to 27:1 were investigated. Pre-heat time and temperature were found to be related to the required blowing pressure: the hotter the film, the lower the pressure required to form the dome.

The various types of plastic evaluated are shown in Table I. They included three types of fluorocarbons, three polyesters (PET), and cellulose acetate butyrate. Of the fluorocarbons, KYNAR was most successfully thermoformed. Petra A and AXB and PETG 7821 were successfully thermoformed polyesters. UVEX could only be thermoformed to an approximate hemispherical shape. Transmittance data for KYNAR and the three polyesters are shown in Figure 3. As indicated, KYNAR has a significantly higher transmittance (90.3 percent) than the thermoformed polyesters. Meliform had an unacceptably low transmittance (79 percent).

TABLE I

THERMOFORMING MATERIAL CANDIDATES

Fluorocarbons	
PVF_2 - KYNAR	Pennwalt
PVF - TEDLAR	DuPont
E-CTFE - HALAR	Chemplast
Polyester (PET)	
Petra A and AXB	Allied Chemical
Meliform & Melinex-O	ICI Americas
PETG 7821	Eastman Chemical
Cellulose Acetate Butyrate	
UVEX	Tennessee Eastman

Pennwalt, in their subcontract, performed a series of biaxial stretching experiments on flat-film KYNAR. A stretching machine, operated under a simultaneous two-direction stretching mode, simulated the biaxial stretching experienced by the pole of a thermoformed dome. This work was carried out as a fractional factorial experiment incorporating principles of statistical design. Seven variables were characterized quantitatively in terms of their influence on six final product properties, including the effect of thermal ageing on stability. Using the information thus obtained it was possible to specify preform preparation and thermoforming parameters that would optimize the dome's properties.

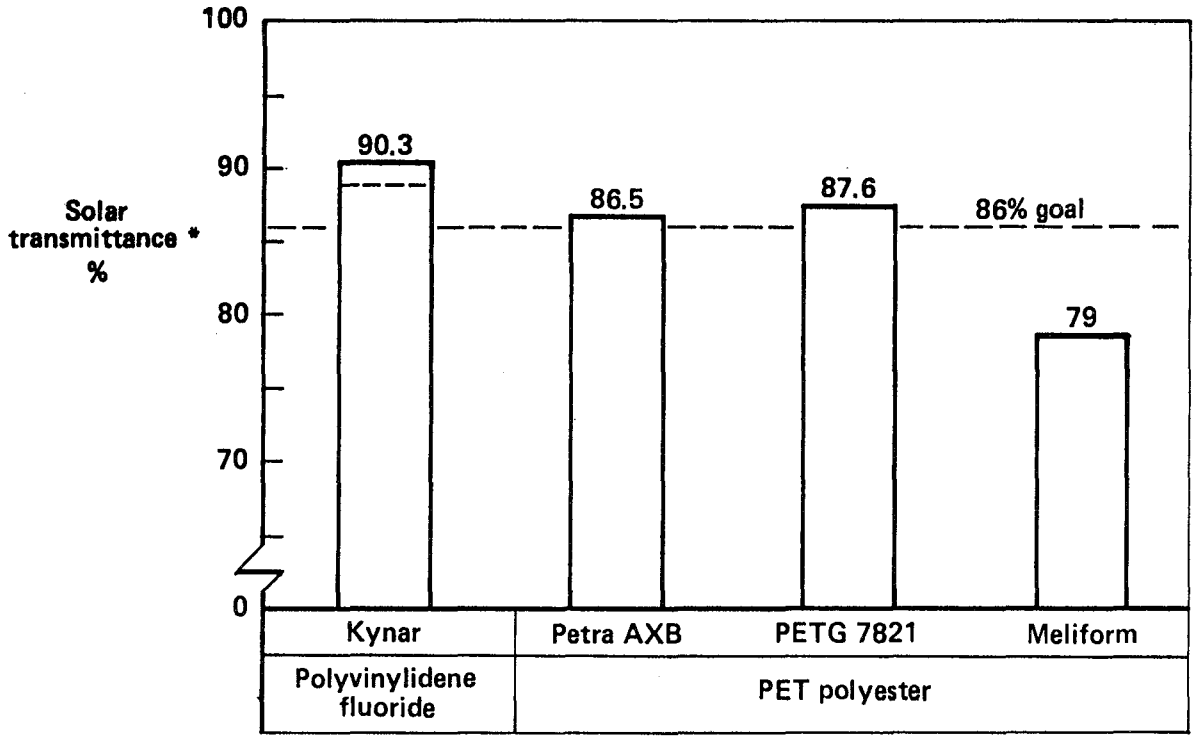

Figure 3. Transmittance of Thermoformed Domes

Domes fabricated to date are undergoing weathering tests at the Desert Sunshine Exposure Test Facility (DSET) near Phoenix. Figure 4 shows the rack of 25 domes.

The work performed thus far has indicated feasibility of using thermoforming techniques to fabricate one-piece domes. Experimental domes have been made with adequate transmittance, strength, and geometry. High strain rates, (short forming times) and minimum forming temperature were found to be important to obtain high strength and acceptable shape. Scale-up to domes of intermediate size (up to 8 ft) will be conducted during the remainder of the contract.

Figure 4. Domes on Test at Desert Sunshine Test Facility

SECOND-GENERATION HELIOSTAT DEVELOPMENT

D. A. Steinmeyer
McDonnell Douglas Company

Under contract to Sandia Laboratories, Livermore, California, MDAC is studying those processes and components identified in the Prototype Heliostat Program as potential areas for cost reduction. These areas include (see Figures 1 and 2): bonding techniques for mirror glass laminates, reflector panel-to-main beam joints requiring no field alignment, helicon input stages for azimuth and elevation drives, improved azimuth drive incorporating a welded housing and wire race turret bearing, and a tapered slipfit pedestal-foundation interface. This program was effectively initiated in January 1979, and will be completed in November 1979.

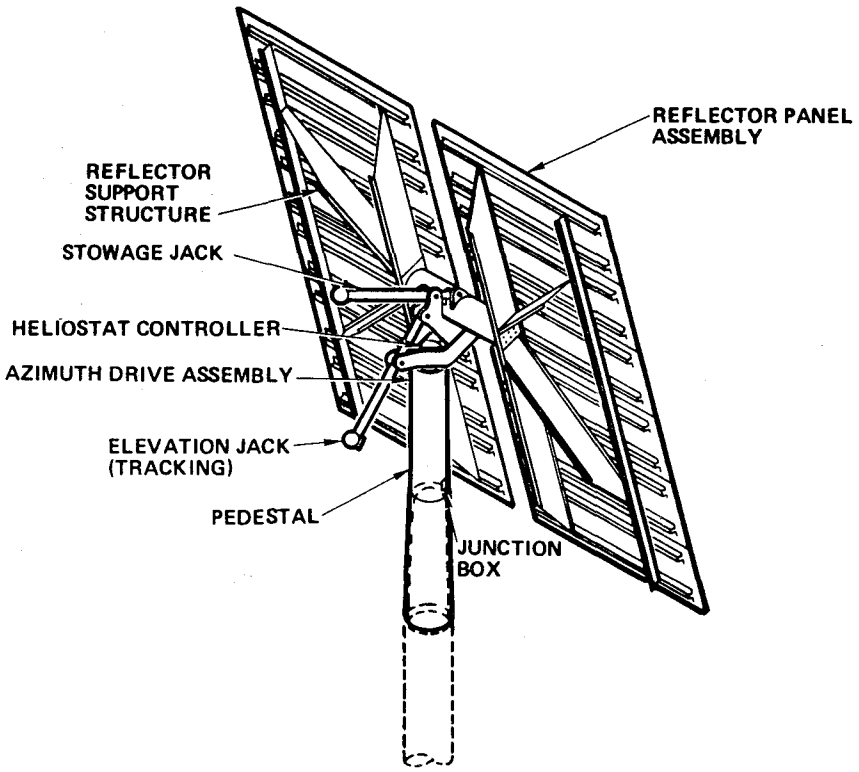

Figure 1. Prototype Heliostat Baseline

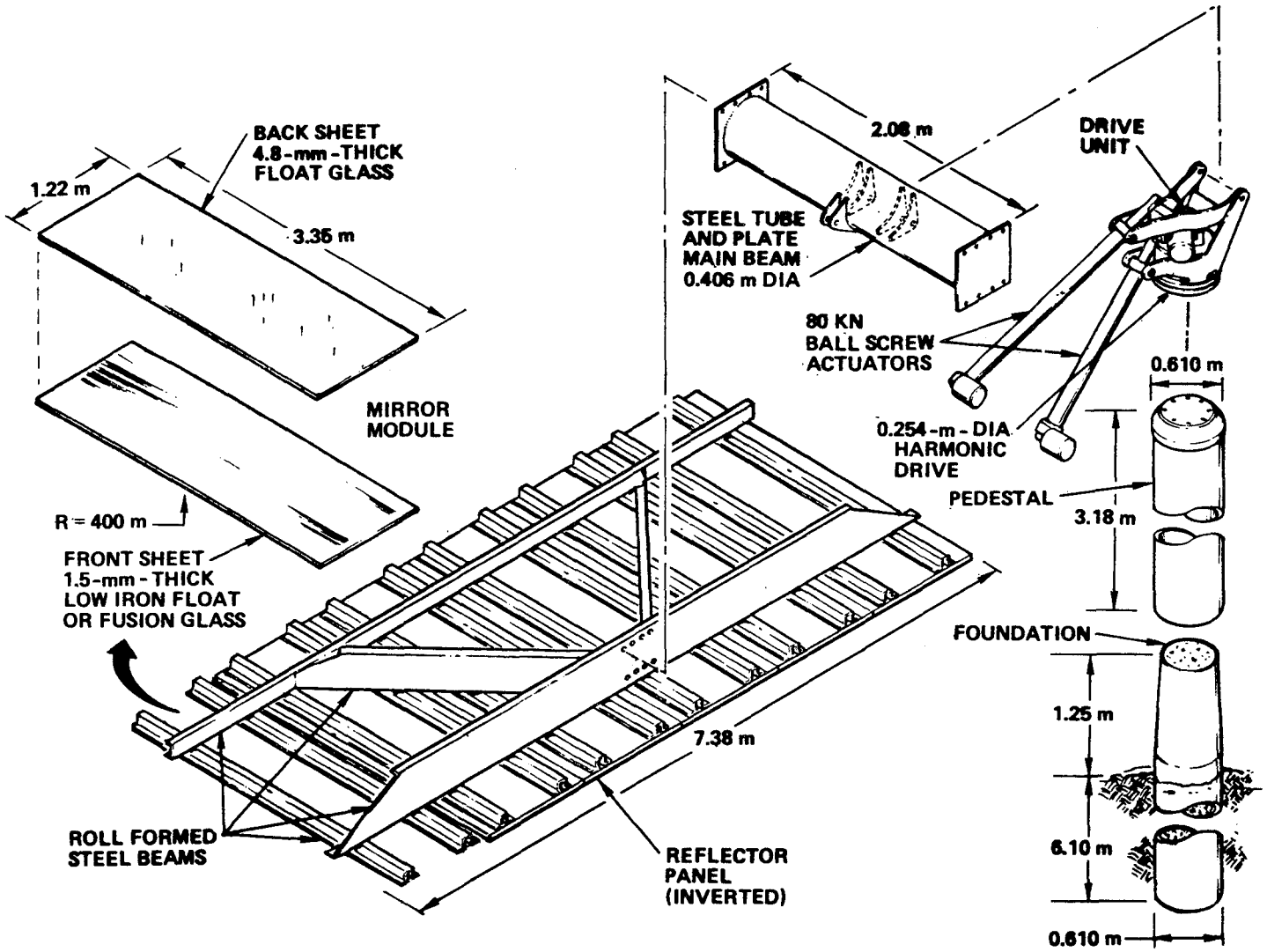

Figure 2. Second-Generation Heliostat Components

The bonded mirror development consists of selecting an adhesive compatible with the mirrored surface of the thin front lite, and providing sufficient bonding strength for laminating to a thicker back lite. Adhesive work life, application method, and cure method and time must be compatible with a continuous process application. It is also desirable that the adhesive material be less expensive than the polyvinyl butyral (PVB) currently used in glass laminating. However, unlike PVB, a transparent bond is not required since the bond is on the back side of the mirrored surface.

Several potential candidate adhesives were applied to glass which was silvered, silvered and coppered, and silvered and coppered with backing paint. In some cases, the adhesive was applied immediately after removal from the mirroring line at the respective process point; for other test specimens, it was applied after several days storage in ambient conditions and in an inert nitrogen atmosphere. These samples were then subjected to visual inspection for chemical reaction or attack on the mirrored surface. This was followed by adhesive strength tests, and exposure to salt spray and 140°F. Of the eight adhesives tested, the most satisfactory was a 3M polyurethane. PVB tare samples that were autoclaved or pinch rolled at 210°F were also acceptable after these tests.

Additional testing which will be performed prior to the next reporting period includes spray-on application techniques, and pinch roll pressure tests to determine the pressure necessary to obtain the desired optical flatness and structural bond on 4 x 11-ft panels.

The remainder of component development activity is in the initial design stage at this report period. Results from these activities will be presented at the next review.

DEMONSTRATION HELIOSTAT DEVELOPMENT

R. W. Devlin
Westinghouse Electric Corporation

The Westinghouse Electric Corporation has designed and fabricated a demonstration low-cost heliostat (Figure 1) for testing and evaluation by Sandia Laboratories at Albuquerque, New Mexico. Since the last meeting in September, the fabrication and assembly of the demonstration heliostat unit have been completed at the Westinghouse Advanced Energy Systems Division in Large, Pennsylvania. Functional and structural tests of the assembled unit indicated that its performance and structural behavior are within the limits expected from the design analyses. Following that test series, the unit was disassembled and shipped to Sandia, Albuquerque. Reassembly commenced on March 19, and is in progress at the present time.

As shown in Figure 1, the mirror support panels are supported upon the elevation rings, which are in turn supported by a horizontal azimuth ring which sits on three support columns on the floor. The computer for control of the heliostat is also shown in Figure 1. The mirror panels on this unit are each 4 x 6 ft and provide a total of 432 ft^2 of mirror surface. The individual panels are constructed from 3-mm thick Pittsburgh Plate Glass low iron float glass. The mirror sandwich construction consists of the glass backed by two inches of styrofoam backed in turn by a 1/16th inch steel plate with mounting cups. The glass was silvered by Carolina Mirror, and the sandwich was constructed by Hexel Corporation in Casa Grade, Arizona, according to a procedure supplied by Sandia.

The mirror support structure consists of a combination of horizontal and vertical beams. There are two horizontal beams spanning the full width of the heliostat which carry twelve vertical hat sections. The junction of the vertical and horizontal beams is joined by spot welding. The mirror panels are mounted to the vertical hat sections. A diagonal brace provides stiffness to the support assembly when the mirrors are in the vertical plane, and the guy rods from the elevation wheels to the ends of the support structure provide stiffness when the mirrors are in a horizontal plane. The main horizontal beams are attached to a spoke in each elevation wheel.

The elevation whells are thirteen feet in diameter and are constructed from a 4-9/16 in. square box. The guy rods between the two elevation wheels are crossed to lend rotational stiffness. The elevation wheels roll through a 270 degrees range for elevation aiming. They ride on four rollers, two each, on columns which ride on the azimuth ring. The 16-ft-diameter azimuth ring

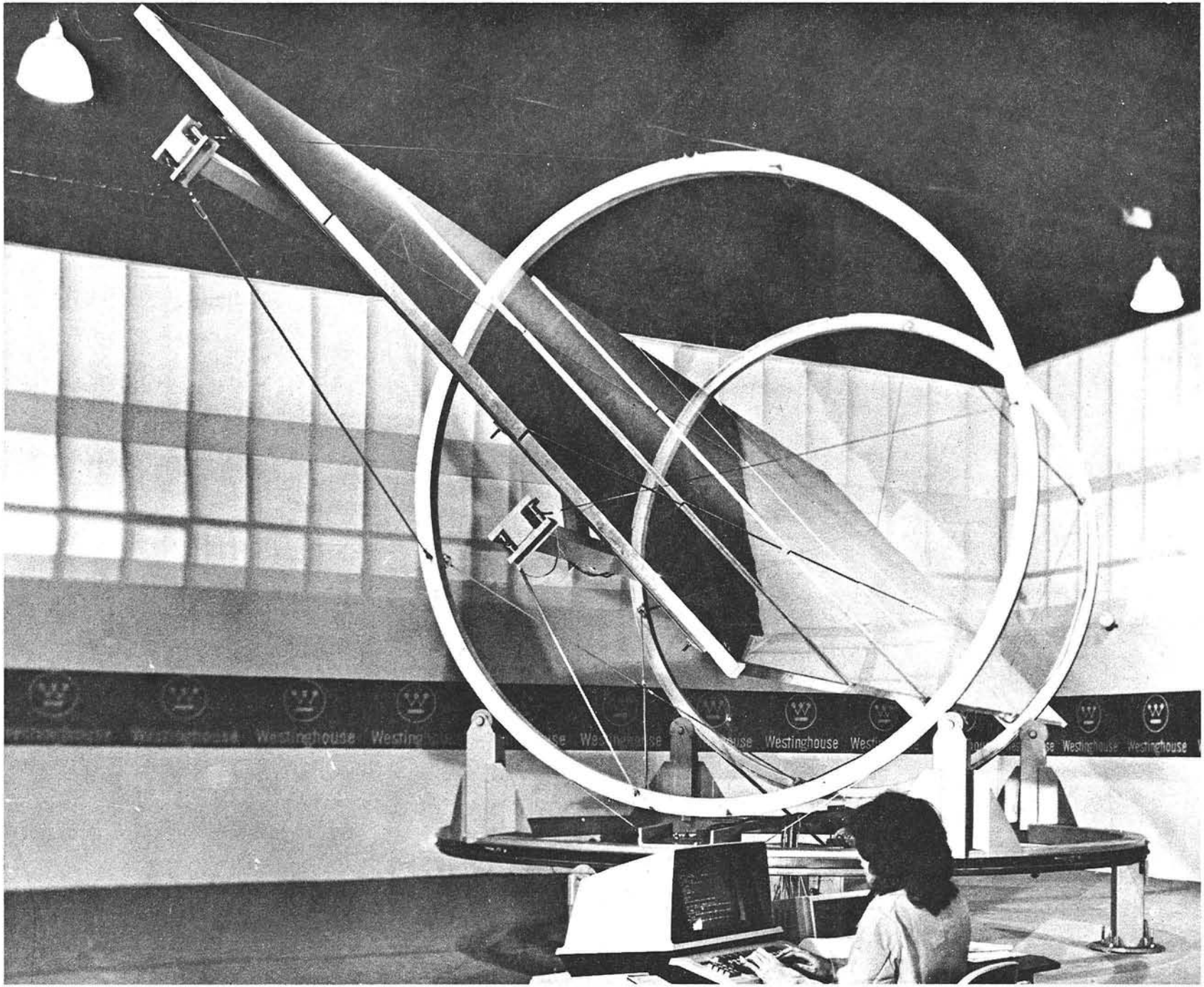

Figure 1. Mirror Support Panels and Heliostat Control Computer

is formed from a 6-in. square cross section member and rides on three pedestals that are bolted to a foundation. The azimuth ring also provides for 270 degrees range in aiming.

The unit is driven in both elevation and azimuth by a belt and gear box drive system. The elevation drive is taken off one elevation wheel. The opposite elevation wheel carries an idler cable for structural purposes only. Position indication signals are taken from both the elevation drive pulley and idler pulley. The azimuth position signal is taken off a spoke which is located diagonally across the azimuth ring. Therefore, the azimuth position signal is directly connected to the azimuth ring, whereas the elevation signals are separated from the actual mirror support frame by the drive belt and pulley. Comparisons of signals from these different encoder connections will indicate which method is the most cost effective manner of obtaining the pointing signal.

The heliostat is controlled by a Texas Instrument 990-10 mini computer which communicates with a micro-processor in the motor control box. The desired pointing angle is computed open loop, and the position indications from the instruments are compared with this computed signal to arrive at an error signal for driving the control motors.

This unit has been instrumented with twenty strain gages, one on each of the twelve guy rods and four on each of the two spokes in the elevation wheels. These strain gages are remaining on the unit for possible use at Sandia. The unit was functionally tested through all operating modes for smoothness of operation, power requirements, repeatability of positioning in response to control signals, and through a single day of tracking before shipment. In addition, structural tests were conducted in which static and dynamic measurements were made. We judged the results to promise satisfactory performance at Sandia.

ENERGY LABORATORY THROUGH ENERGY FOUNDATION OF TEXAS

L. L. Vant-Hull, Program Manager
University of Houston

- The optimization code RCELL has been provided data modules and restructured as a series of alternative subroutines.
- A draft copy of a user's guide for RCELL has been prepared.
- The Annual Performance Code has been adapted to read the same data modules as RCELL and restructured as an alternative series of subroutines.
- A new image generator has been created which can better deal with focusing, special sunshapes, and the Solar Aureole.
- RCELL can internally generate intercept factors for smaller flat receivers (rectangular or eliptic) and for shorter cylindrical receivers.
- The VRADII subroutine provides intercept factors for smaller diameter cylindrical receivers.
- The theory of collector field optimization has been extended to consider
  - Constraint to fixed annual energy
  - Constraint to fixed design point energy
  - Constraint to fixed field area
  - Constraint to fixed azimuthal spacing
  - Optimization of receiver geometry
  - Optimization subject to power dependent costs
  - Optimization including the effects of specific wiring models and land costs
- Methods of cost-effective reduction of receiver north side/south side ratios have been developed.
- Reasonable approximations to annual average interception fractions have been generated.
- Optimal cost effective deployment of heliostats has been defined for fields from 4 to 1000 MW thermal.

HELIOSTAT MIRROR DETERIORATION

V. P. Burolla
Sandia Laboratories, Livermore

The Problem

The deterioration of the reflective silver layer on second-surface mirrors in heliostats designed for large solar central power systems was first noticed on several polystyrene foam core mirror modules situated in the heliostat test facility at Sandia, Livermore. In order to assess the severity and extent of the deterioration, a detailed mapping was done on every module at Livermore. In addition, visual or photographic examination was made of several other mirror modules located in Baltimore, Maryland, St. Petersburg, Florida, and Sandia, Albuquerque. The mapping indicated that the deterioration was not limited to the edge of the mirror, that there was in many cases a definite pattern to the deterioration, that there were three types of deterioration, and that it was not restricted to one module design. The types of deterioration were classified as streaking, (gray parallel bands), spotting (black irregular spots), and delamination. Unfortunately, only the most approximate guess could be made on the loss of overall reflectivity due to the deterioration since there was at the time no instrument available to scan the entire surface of the module. In the worst case, it was estimated that the loss in reflectivity was not greater than 2 percent. The delamination of the silver surface was quite different from the steaking and spotting effect as there were no dark areas. Rather, the delamination appeared to be water droplets on the back surface of the mirror. On the larger spots the delamination appeared as a cone-like object (pointing away from the back side) with apparently no loss in total reflectivity of the silver.

The deterioration patterns on many modules were found to coincide with areas of high adhesive concentrations. In the two module designs most thoroughly studied (Martin Marietta, MMC, and McDonnell Douglas, MDAC), the MDAC design had a deterioration pattern that matched the adhesive joints used to bond the styrofoam together (see Figures 1 and 2), while the MMC design showed numerous rings of deterioration that apparently formed around the spots of adhesive used to hold the mirror to the substrate (see Figure 3). In many cases, the streaks observed could be related to the tooth pattern in the notched trowels used to spread the adhesive.

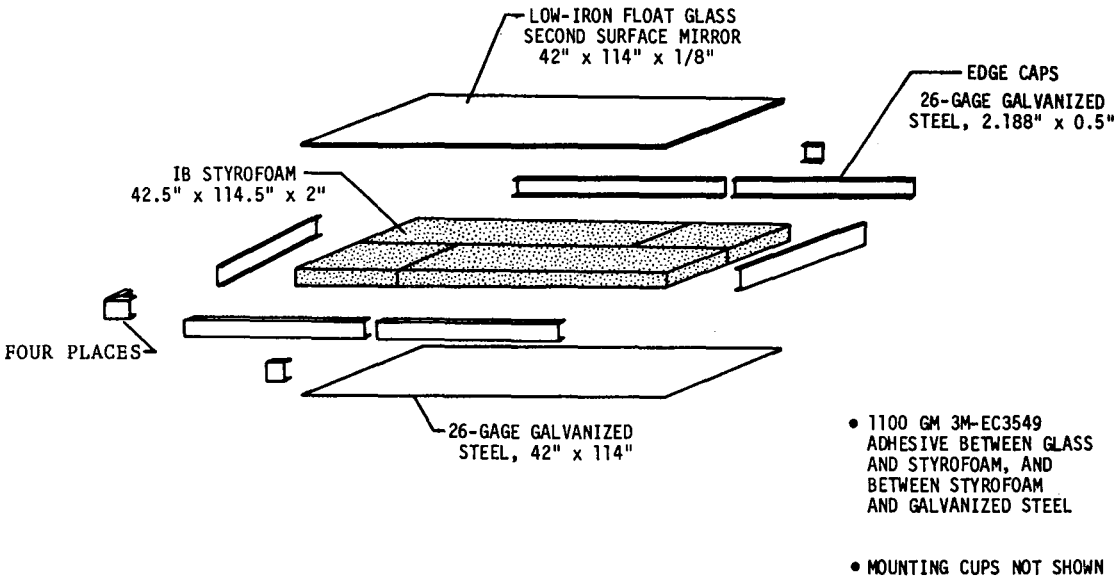

Figure 1. Typical Foam Core Mirror Module Assembly

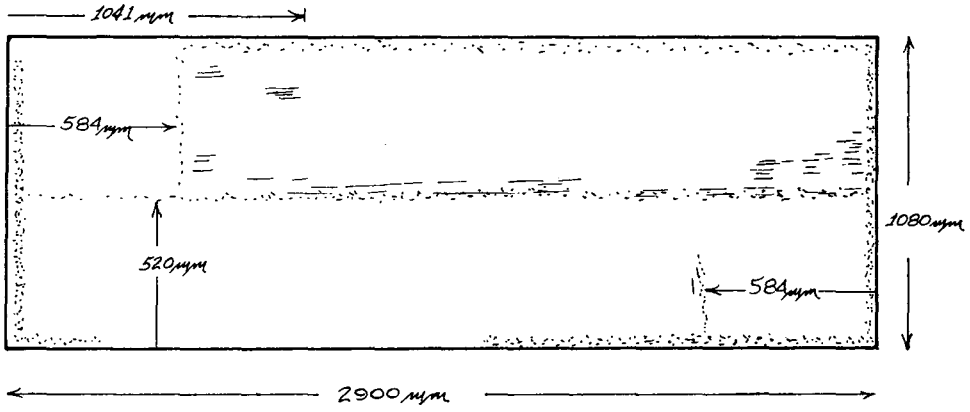

Figure 2. Deterioration Pattern on a Foam Core Mirror Module

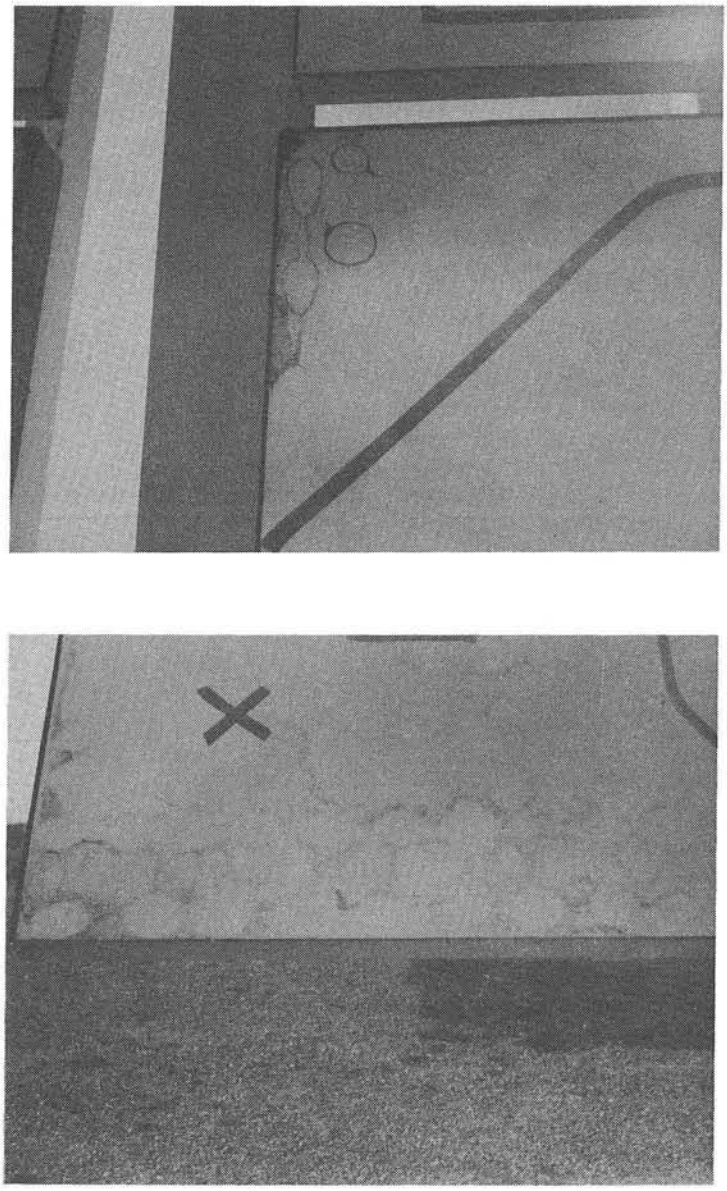

Figure 3. Photographs of Deterioration Patterns on Two Honeycomb Core Mirror Modules

The deterioration was not site specific. In fact, some geographic areas with relatively high humidity and pollution produced very littler deterioration. As mentioned earlier, the deterioration was not limited to a specific design, nor was it limited to a specific manufacturer. MDAC-designed modules that were built by Sandia suffered deterioration equivalent to identical MDAC-built modules.

The problem as defined after the survey indicated that if the rate of deterioration remained constant, the modules under question could suffer as much as a 10 percent reflectivity loss (10% of the area blackened by deterioration) over a five-year period in a relatively dry climate. This is assuming that the blackened areas could reflect no useful light.

Analytical Work

The first step in the search for the cause of the deterioration was to open and examine the effected modules. Specific analytical techniques included: (1) infrared scans of any moisture in the module, (2) visual examination of deteriorated areas, (3) auger analysis of the metallic layers, (4) atomic absorption analysis for copper and silver in the paint/adhesive layer, (5) SEM analysis of the silver layer, and (6) visual inspection for sealant integrity.

In addition to the analytical work on weathered modules, a great deal more was done to examine specific details of the module design; e.g., (1) infrared and gas chromatographic/mass spec (GC/MS) analysis of sealant extracts, (2) pH of water extracts from the adhesive, (3) analysis of the adhesive, (4) SEM and elemental analysis of the mirror backing paint for imperfections and impurities, (5) SEM analysis of the copper and paint layers, and (7) examination of a mirror silvering facility to detect potential quality control problems.

Observations

Many of the mirror modules examined did indeed have considerable quantities of water inside, even with the sealant apparently intact. Analysis of the water indicated in some instances the presence of an alcoholic compound in trace quantities which could be a breakdown product of an additive to the adhesive. On a microscale, the pattern of the deterioration followed the pattern of the adhesive laydown (see Figure 4) when a notched trowel was used to apply the adhesive. Where no trowel was used, there was no discernible pattern, just overall deterioration. Areas of mirrors that had no obvious exposure to liquid phase water showed very little, if any, deterioration. Auger analysis of deteriorated areas was not very conclusive; however, it can be inferred from that data that no one agent was responsible for the massive attack. Trace amounts of chlorine, sulphur, and oxygen were detected in the silver layer. Depth profiling of the copper/silver layers (accomplished at Battelle, Pacific Northwest Labs) revealed an ill-defined boundary between the copper and silver layers with trace quantities of carbon and some iron. Looking at the deterioration pattern in Figure 4, one cannot help but wonder where the copper is if, according to visual observation, it is not between the paint and silver. By carefully peeling

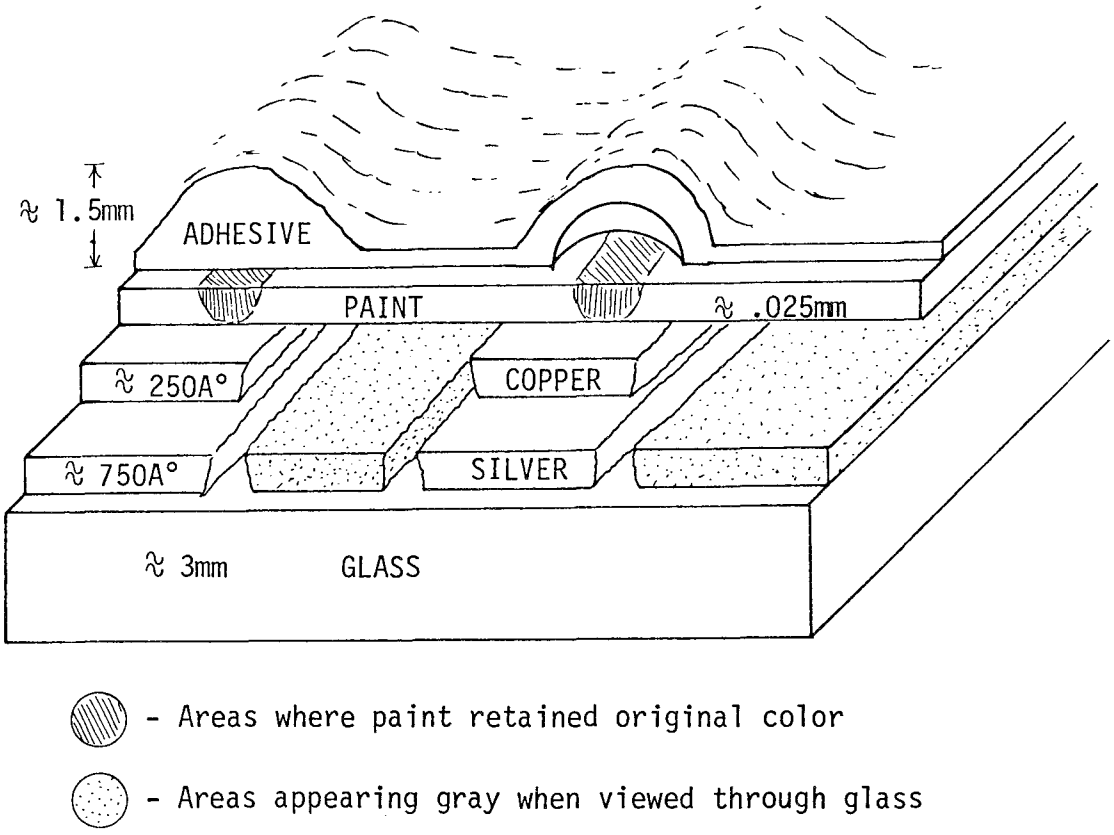

Figure 4. Exploded View of Deteriorated Mirror

off the paint adhesive layer immediately above the copper "free" regions and analyzing for copper and silver, it has been determined that the copper has either diffused into the paint/adhesive layer or formed a copper oxide with a dark gray color, thereby making it visually indistinguishable from the paint and destroying its bond to the silver. Analytical work accomplished at McDonnell Douglas Astronautics and Martin Marietta Corporation for the most part corroborate these data, with minor differences in the quantities of trace elements detected.

Early in the investigation, Dow Corning Corporation released information[1] indicating that one of their silicone-based compounds used as a sealant in some modules was not compatible with silver because of its outgassing products. Analysis of the liquid extract from this sealant indicated the presence of an amine. Consequently, a series of accelerated aging tests was begun to see if this could be pin-pointed as the causative agent. The test exposed the back side of a mirror to a liquid water environment containing isopropyl alcohol, sealant extract, or distilled water at 65°C. This method eliminated the possibility of intrusion from the edge. Some mirrors were coated with the same adhesive used in the module construction (see Figure 5). The tests indicated that although the sealant extract was responsible for corrosion, it was of a different nature than the deterioration found in the field. The test samples with adhesive, water, and isopropyl alcohol showed the best correlation with field observations. Some work being done at JPL[2] indicated the pH of the water extract from the adhesive must be neutral to ensure minimum deterioration; however, a water

extract of the same adhesive used in the degraded modules showed no significant change in pH. Analysis of the adhesive itself[3] revealed the presence of an amine but no other significant aggressive species. Since the deterioration pattern observed on many mirrors was predominantly darkened spots, it was thought that these spots may have been generated by pinholes or defects in the mirror backing paint. SEM analysis of numerous pinholes found in plain mirrors indicated that the pinholes were not process-induced, but rather created by rough handling after manufacture. Indeed, in several of the accelerated tests, pinholes were purposely introduced, and in every case the deterioration initiated elsewhere.

Some concern was expressed over the porosity of the silver layer[4] and its inability to prevent delamination. SEM analysis at 30,000 magnification reveals no porosity but this cannot be considered conclusive evidence, as higher magnification or better resolution may reveal more.

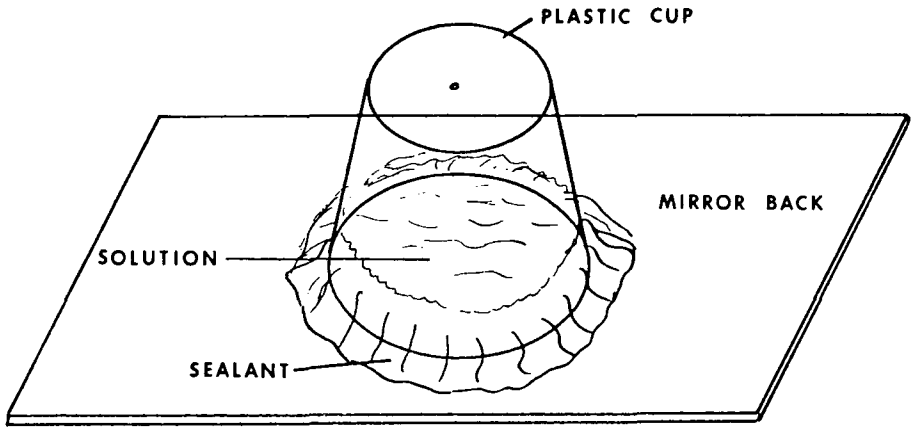

Figure 5. Accelerated Aging Test

In an effort to evaluate the quality control of silver and copper deposition, the coverage of five samples was measured. The values ranged from 35.3 to 48.3 mg/ft^2 for copper and 56.6 to 82.5 mg/ft^2 for silver, which was within specification for the silver but not for the copper. There is some disagreement in the mirror industry as to the optimum thickness of the silver and copper, but in general the desired values range from 15 to 25 mg/ft^2 for copper and 75 to 90 mg/ft^2 for silver.

Supplemental Testing

The results of the analytical testing seemed to indicate that no single chemical species (other than water) could be responsible for all the types of deterioration in the mirror modules. If this were true, some supplemental tests would be required to substantiate these findings.

Figure 6 represents a simple test apparatus designed to detect galvanic corrosion where one strip of mirror (with paint removed) is placed in a beaker of distilled water and one in water containing a large quantity of paint chips. The paint chips were introduced to determine if there was anything in the paint that could be accelerating the deterioration. The atmospheres in the bell jars were nitrogen, air enriched with sulfur dioxide, air enriched with carbon dioxide, and air. After 330 hours at 60°C, the mirror strips in the bell jar containing nitrogen had no copper visible where the mirror was in contact with the water. When the test was repeated in air with painted mirrors, there were areas of blistering on the paint that had no copper underneath. The results of these and other tests tend to indicate that just pure liquid phase water will cause significant deterioration of the copper layer over a relatively short period of time through galvanic sacrifice of the copper. Although the silver layer should be relatively immune to attack by distilled water, two points must be considered: (1) there is the possibility that the silver layer is indeed porous, which would allow the water to permeate to the glass where it could galvanically destroy the active tin sites on the glass and cause delamination of the silver; and (2) there is sufficient evidence to indicate that the presence of numerous organics in the module structure and of common constituents of polluted or clean air (CO_x, NO_xm, SO_x) can, with water, deteriorate the silver layer. There is no evidence as yet to indicate that moderate humidity conditions (vapor phase water) will cause similar deterioration.

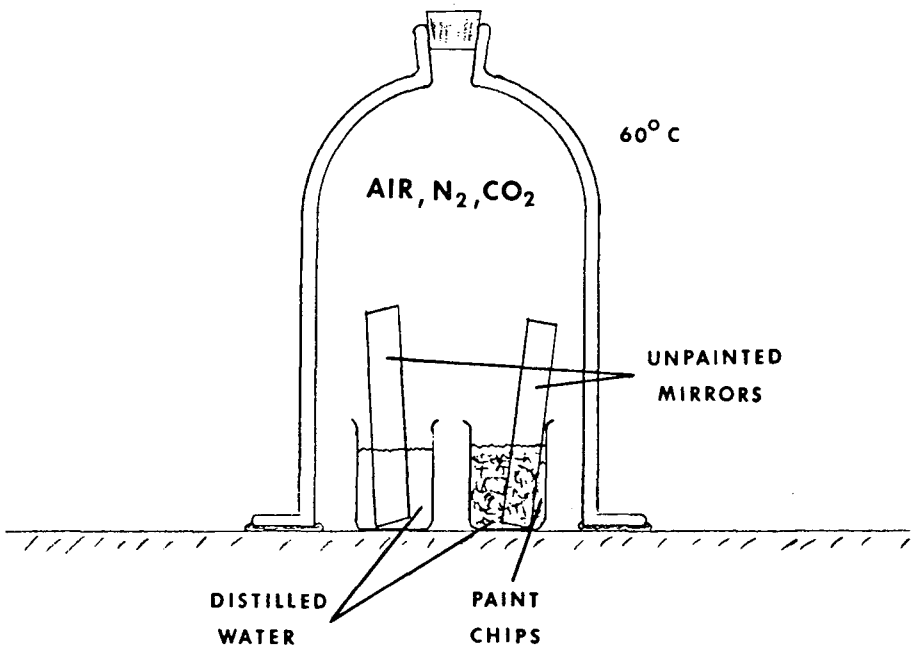

Figure 6. Test Apparatus to Observe Environmental and Galvanic Effects on Mirrors

Current Efforts

Based on the assumption that liquid phase water was the primary cause of the deterioration, the goal of the study became the identification of potential solutions to the problem. Exclusion of the water can be accomplished in several ways: (1) creation of an impermeable layer on the back of the mirror, (2) manufacture of a sealed module capable of maintaining a dew point less than -20°C for ten years or more, and (3) design of a breathing module that will allow water to evaporate as quickly as it condenses, thereby minimizing contact time.

Studies are currently under way to determine the feasibility of each of these concepts. For an impermeable layer, the first choice is a metal foil such as aluminum foil; however, planned measurements on the permeability of the present backing paints may indicate that an appropriately lower permeability organic coating may provide sufficient protection over a reasonable lifetime. For a module design that maintains a low dew point, much better sealants are being investigated, and for "breathing" module designs the rate at which the module allows the water to evaporate is important.

The solution to the problem may be complicated if the mechanism of deterioration is enhanced or induced by localized stresses[5] from either an adhesive or a substrate with a dissimilar coefficient of expansion. Tests are currently being planned in an attempt to measure the strength of the bond between the paint, the copper, the silver and the glass. In addition, we are planning to repeat some accelerated aging tests with higher and lower modulus adhesives with varying coefficients of expansion. By thermally cycling these samples 20 or 30 times and then subjecting them to accelerated testing as before (Figure 5), the effects of stress on deterioration should be more readily apparent.

REFERENCES

1. Memo from Nick DeLollis, 5813, Sandia Albuquerque, October 31, 1978.

2. Personal communication with Alec Garcia, Jet Propulsion Labs., November 7, 1978.

3. Work performed at Sandia, Albuquerque, Ron Allred, Nancy Hall et al., Division 5844.

4. Personal communication with Frank Worken, Falcomer Glass Industries, February 1979.

5. Memo from K. B. Wischmann, 5811, Sandia, Albuquerque, January 30, 1979.

DEVELOPMENT OF A PORTABLE REFLECTOMETER

R. A. Weagant
Beckman Instruments, Inc.

Background

Beckman Instruments, Inc., under contract 83-0385 with Sandia Laboratory, is developing a portable reflectometer that can be used to accurately assess reflectance degradation in heliostat mirrors. The instrument can be used with first- or second-surface mirrors 3-mm thick and is capable of accurately mapping absolute specular reflectance characteristics of mirrors larger than 8 x 13 inches. Variations in specular reflectance are difficult to assess by eye. Under given illumination conditions, the eye has only a dynamic range of about 50 to 1. A large mirror may look perfectly uniform to the eye when it actually has reflectance variations over its surface of ±2%. This is compounded by the fact that most of the solar energy is outside the wavelength range of the eye. This means that mirror reflectance characteristics can only be accurately assessed with a precision instrument.

Reflectometer Description

The reflectometer utilizes a geometry change as its principle of measurement in order to provide data on an absolute basis without need for reference standards or independent calibration techniques. The principle of operation is that of the VW reflectance technique. In this technique, a set of three mirrors is set up in a "V" arrangement, and the instrument is forced to reach 100%. The mirror at the bottom of the "V" is then placed in a different orientation so that the light can strike a sample mirror twice, forming a "W" light-path configuration. The new reading is then R^2--the square of the reflectance of the sample mirror--because of the two reflections. The light beams strike the sample mirror at a 20-degree angle of incidence with approximately 1 degree of collimation. The two spots being measured on the sample mirror are approximately 4-cm square. Because the measurement is reflectance squared, the sensitivity of the technique is greatly increased for surfaces having high specular reflectance.

The principle of operation is illustrated in Figure 1. In the "V" configuration, the light from the source strikes the mirrors M-2, M-3, and M-4 in succession. M-3 is then placed into an alternate position between M-2 and M-4, and the light strikes mirror M-2, the sample (M-0), M-3, M-0 again, M-4, and passes on to the detector. The mirror M-3 is physically removed from one position and inserted in the instrument in its alternate position. It cannot be rotated between the two positions, because the axis of rotation lies in the surface being measured.

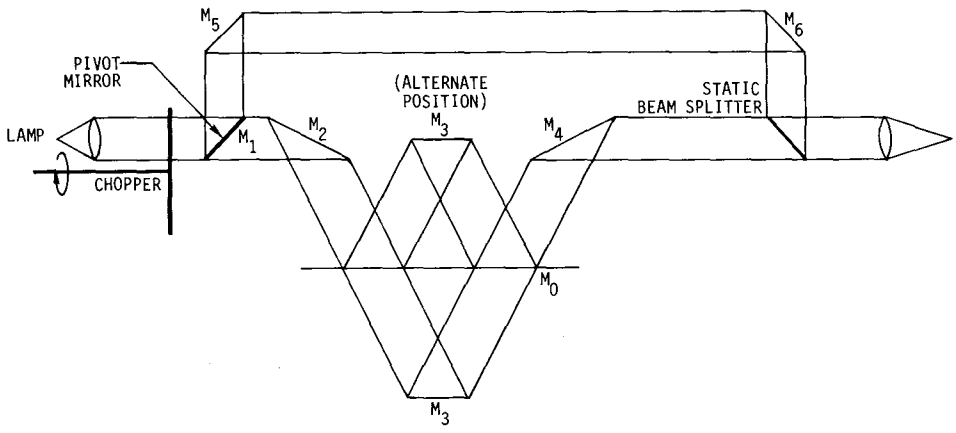

Figure 1. Diagram of Optical Paths

Note that there is a separate reference path using mirrors M-1, M-5, and M-6, together with the static beam splitter. When the light is following this reference path, the system is automatically adjusted to compensate for drift in lamp intensity and changes in detector sensitivity.

Figure 2 is the optical layout. The light from the source is brought to a focus and chopped, and a separate pivoting mirror is used to direct the light either through the sample or reference beam. Wavelength bandpass filters can be inserted to obtain spectral reflectance information.

Figure 3 is a simplified system block diagram. The lamp is a 3300°K, 6-watt, quartz-iodine incandescent lamp operated from a battery power supply. The current to the lamp is regulated. Although the lamp is current-controlled, changes in ambient temperature affect the intensity, so the reference channel is fundamentally necessary for high precision. The lamp driver is sized to handle lamps up to 20 watts. The light is chopped, and photodiodes on the chopper provide a synchronous reference signal for synchronous demodulation of the output signal from the pyroelectric detector. The signal is then amplified, the square root extracted, converted to digital, and displayed digitally on the instrument.

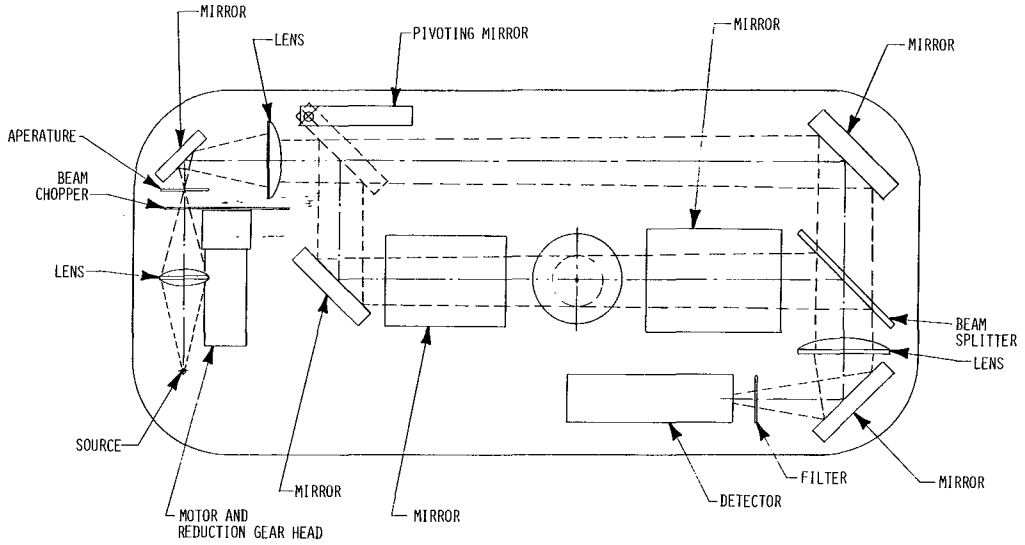

Figure 2. Optical Layout

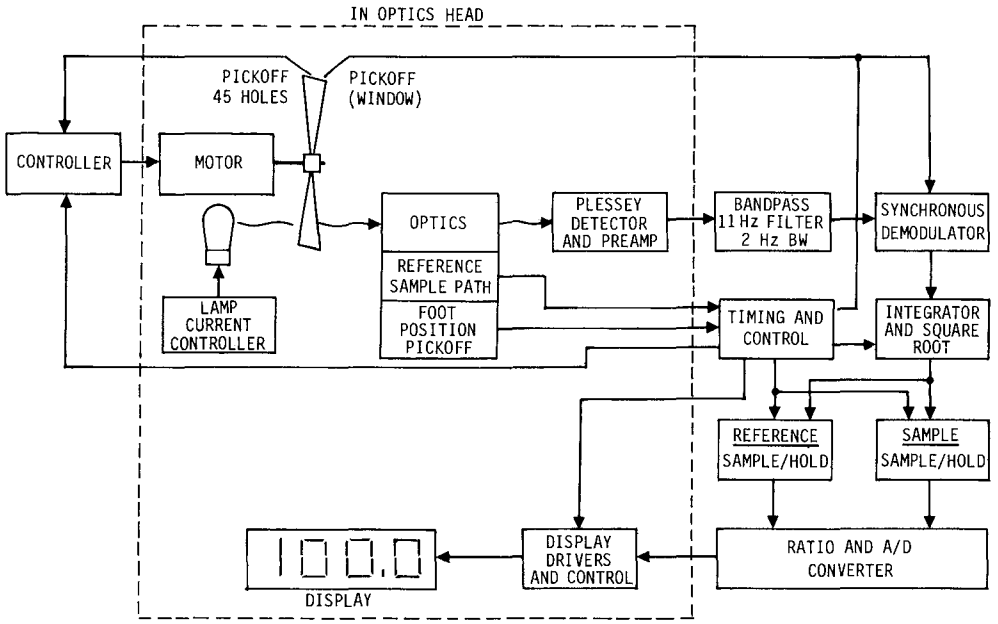

Figure 3. Reflectometer Block Diagram

The instrument has an available wavelength range from about 300 nm to 3 μm. As a consequence of measuring two spots on the sample mirror and then taking the square root, a small error is introduced. If the two spots being struck on the sample mirror differ in reflectance, the instrument does not measure their true average reflectance, but rather the square root of the product of their reflectances.

Table I indicates the non-uniformity that can be tolerated if the error is to be less than 0.1 percent. If the reflectance is approximately 90 percent, the difference in reflectance of the two spots can be as large as 10 percent reflectance before the error becomes greater than 0.1 percent absolute reflectance. This amount of non-uniformity would be obvious to the eye.

TABLE I

NON-UNIFORMITY ERROR SUMMARY

If the reflectances of the two spots differ, the measured 'mean' reflectance differs from the true mean reflectance. The error is 0.1% (0.001 absolute reflectivity) if:

Non-Uniformity R (%)	True Mean R (%)
10	90
9	80
5	50
2	20

Another important consideration is the multiple reflections that can occur in second-surface mirrors. Depending on refractive index and transmission, a minimum of 10 percent and a maximum of 20 percent of the incident energy lie in multiple reflections. The collection optics are all oversized to pick up three multiple reflections from 3-mm thick glass. If the mirror has a net true reflectance greater than approximately 50 percent, it is estimated that the resulting error from neglecting higher-order terms is less than 0.1 percent.

All of the mirrors in the system are made of glass except for the pivoting mirror, which is magnesium. The lenses used in this system are of single-element glass of plano-convex shape. This shape minimizes spherical aberration at the f/2 optical aperture, and the single element is actually superior to doublet lenses for color correction over the full wavelength range. Since the collimation angle of the system is approximately 1 degree, the total system error budget was set so that the sum total of alignment errors and figure errors would be no more than 0.2 degree. As a result, the surface figure error budgeted for each optical element is approximately 1 wave and the alignment accuracy is set at ±1 arc minute. Over the 2-inch diameter of the mirrors, this corresponds to a machining tolerance of approximately ±0.00025 inch.

The instrument is being designed to measure curved mirrors with some limitation. If the curvature of a test mirror is purely spherical, the instrument will rest on its mounting feet such that the slope error introduced at the first measurement spot will be compensated by an equal slope error in the opposite direction from the second spot. If the slope error occurs at one spot but not at the other, the magnitude of the slope error, which is equal to the system error budget, corresponds to approximately 0.001-inch displacement in 1-inch distance. If the figure error of the test mirror is worse than this, it means that the test mirror is unable to preserve the 1-degree collimation angle.

Figure 4 is a photograph of this instrument. The instrument is held against the mirror, and the measurement is commanded by a thumb switch on one of the handles. The digital display is a liquid crystal type so that it can be seen in bright daylight. In the top center of the assembly is the mounting bracket for the geometric change mirror.

The thumb screws at the bottom of the instrument control the adjustable mounting feet. These feet may be changed to one of three positions corresponding to the measurement of first-surface mirrors, 0.060-inch thick second-surface mirrors, and 0.120-inch thick second-surface mirrors.

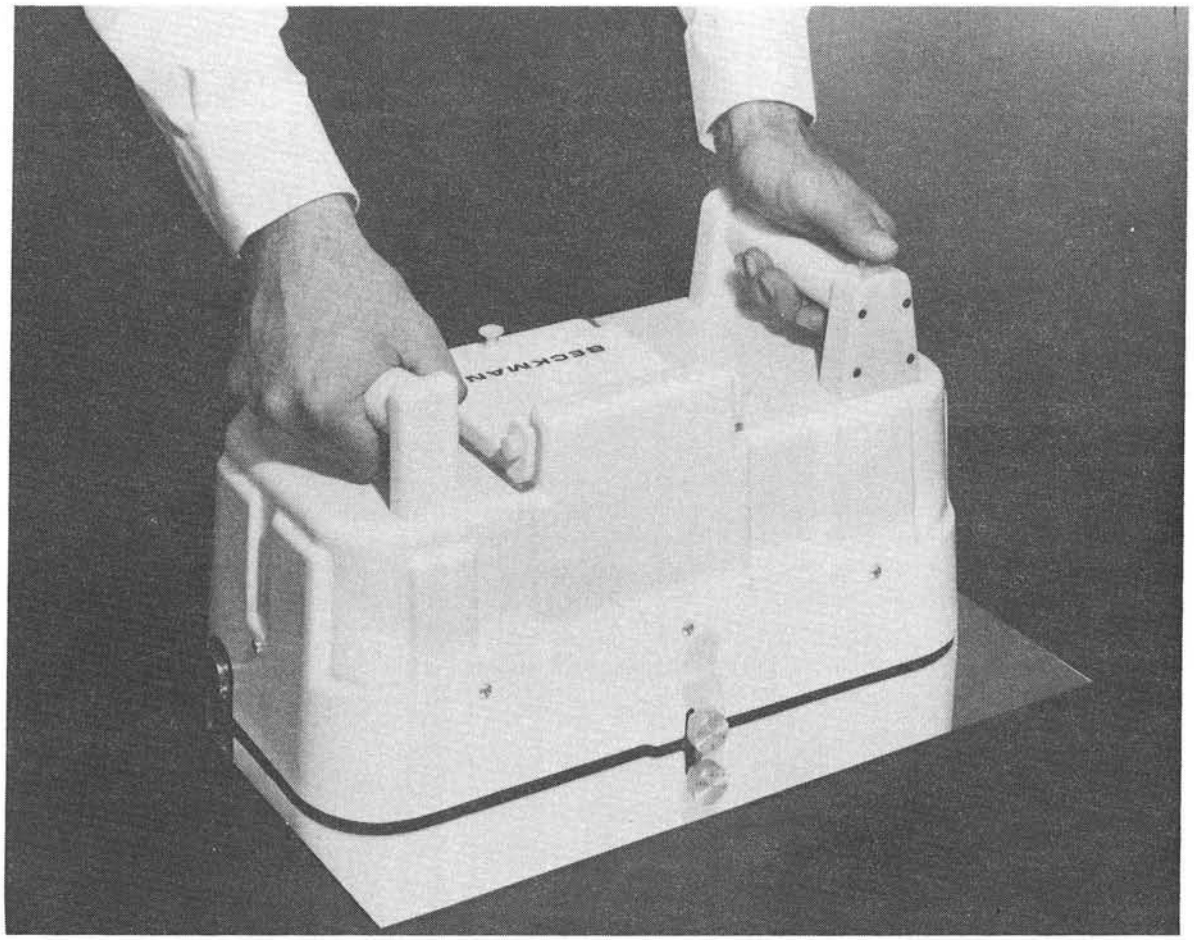

Figure 5 is a photograph of this assembly when resting on its calibration fixture. This is the "V" configuration, and this measurement is performed at the beginning of a set of sample measurements. The change mirror is moved, and the instrument is then set on the test mirror.

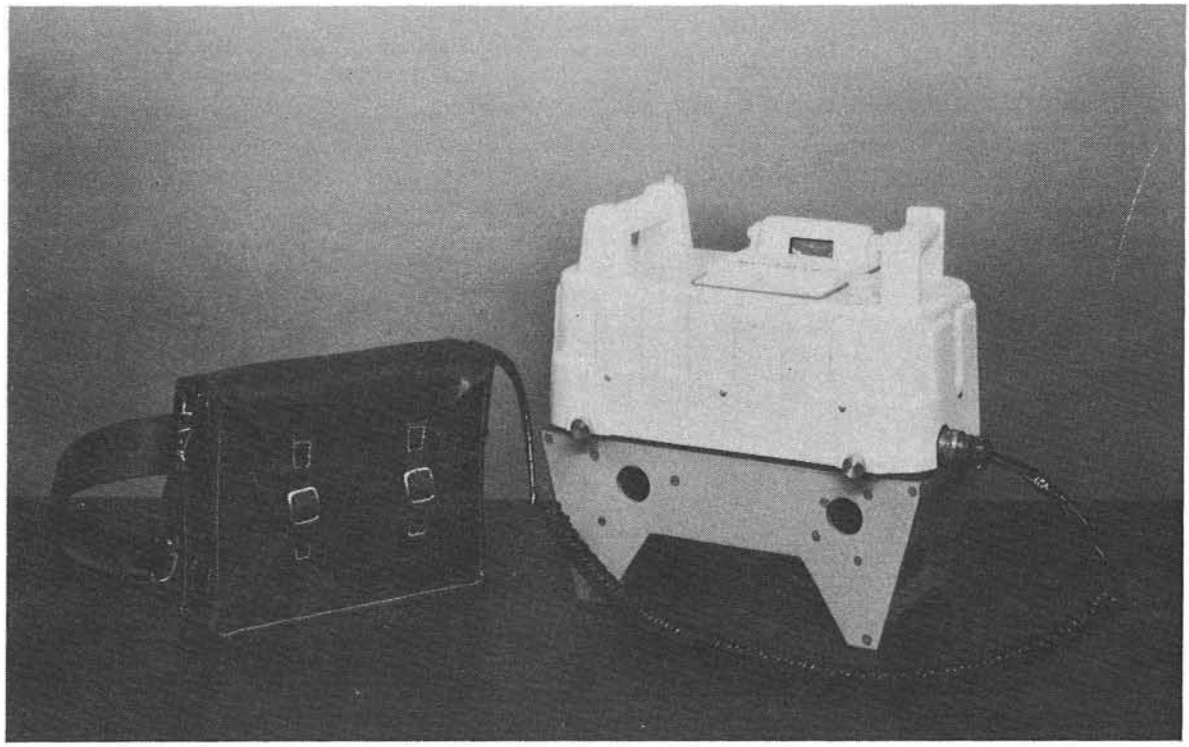

It is also possible to make a transmission measurement. The instrument is first calibrated in the "V" configuration, and then a thin glass or a plastic film is placed between the calibration fixture and the instrument. Two transmissions at a 20-degree angle of incidence occur so the light is attenuated by t^2, but the instrument automatically takes the square root and displays the correct value of t. Transmitting materials up to 3-mm thick can be measured; the adjustable instrument feet are set to compensate for the path length change.

The battery pack is attached to a strap which can either be worn around the waist or over the shoulder after the fashion of a photographer's bag. The battery pack contains rechargeable nickel cadmium batteries and some of the system electronic components.

When it is desired to check the optical quality of the test mirror, a separate eyepiece may be installed through a dust cover located on the top of the instrument. This eyepiece position is also used for the insertion of the band-pass filters.

The normal position of the pivoting mirror is such that the light beam is directed through the reference path. A foot position pickoff will cause the reference sample to be taken shortly after the instrument is set on the test mirror. The operator then presses a switch controlling a mechanical linkage to push the pivot mirror into the position that directs the light through the sample path. The measured value is then held on the display until another measurement is taken.

The calibration and operating sequence is as follows. The operator opens the carrying case and plugs the instrument into the battery pack. The instrument is still in the case and mounted on the calibration fixture in the "V" position. When the displayed signal stabilizes (generally less than five minutes), the instrument is ready to calibrate. Every four seconds a colon symbol on the display will light up and remain lit for approximately two seconds. When the colon is off, the instrument is taking a reference reading; when the colon is on, the instrument is holding the reference reading and is ready for a sample reading. When the colon is on, the operator simply depresses the sample button to cause the pivoting mirror to switch into the position that directs the light through the sample path. The calibration measurement is then made, after which the operator adjusts the gain potentiometer and repeats the measurement sequence until the display reads 100.0. The system is now calibrated and ready for measurement.

The geometric change mirror is moved to the "W" position and the instrument is placed on the mirror to be tested. As the instrument is placed on the mirror, a foot position pickoff automatically causes a one-second time delay to begin. The purpose of this time delay is to make certain that any mechanically induced microphonics have died out. After about two seconds, the colon on the display will light to indicate that the system is ready for a measurement. The sample switch on the instrument is depressed to make a measurement, and the colon is extinguished.

Preliminary Performance Test Results

The instrument has been tested on a few mirror samples and shows excellent repeatability. When mounted on the calibration fixture or placed at a position on a test mirror, the reflectance readings repeat to within $\pm 0.2\%$ reflectance even in test sequences lasting up to about 3 hours. It has not been necessary to reset the calibration control during these sequences. From one day to the next, the largest changes in the calibration control setting have been less than about 0.5% R, although the instrument has not yet been subjected to its design operating temperature extremes of +40° to +130°F.

Most testing has been done without spectral filters in place. Measurements, therefore, are made over the 0.3- to 3.0- m wavelength range with the mirror spectral reflectance distribution being convolved with the 3300°K source. For aluminum surfaces, the result is a slight overestimate of the integrated solar spectral reflectance.

A first-surface, aluminized no-overcoat laboratory mirror was tested and its reflectance mapped. The mean value of the reflectance was 92.4%. A variation of 1.0% reflectance was found from the best to the worst spots on this mirror. A glass second-surface test mirror, 0.060-inch thick, was measured and a larger reflectance variation was found over its area. The minimum reflectance area found was 91.3%, and the maximum 93.5%. A second-surface test mirror of 3-mm thick glass had the largest variation in reflectance noted. Areas of minimum and maximum reflectance were 82.4 and 88.6%, respectively. A first-surface mirror of highly polished pure aluminum sheet was measured and found to have

a mean reflectance of 81.3%. The variation in reflectance over its area was less than 1.0%, but there was a directionality effect. Measured in a direction parallel to the polishing sleeks, the reflectance was consistently about 1.8% higher than in the direction perpendicular to the sleeks.

These particular mirror samples were chosen primarily to exercise the instrument. Their exposure histories are unknown, so no definite conclusions can be drawn about the merits of the mirror types. The instrument, however, provided high precision data on their reflectance characteristics and should prove to be a useful instrument for mirror comparisons and reflectance degradation studies.

NON-INVERTING HELIOSTAT STUDY - EFFECTS OF DUST BUILDUP

J. B. Blackmon
McDonnell Douglas

Introduction

This study was conducted to assess the implications of employing a non-inverting heliostat design. With this design, vertical stow would normally be used at night or during occasional periods of nonoperation; mirror-up stow would be used to survive extreme winds. The three principal areas of concern are:

1. Dust buildup effects and cleaning frequency due to possible added dust buildup

2. Increased heliostat damage probabilities due to hail effects

3. Reflected beam safety issues

This study was concerned primarily with the added life cycle costs associated with heliostat cleaning. Possible additional heliostat damage due to hail and design and operational modifications to resolve hail damage issues were also considered. The McDonnell Douglas heliostat design and an equivalent non-inverting version were used as the heliostat models. The effects were considered for a commercial plant of approximately 18,000 heliostats located in the desert regions of the southwestern states.

Dust buildup data from specimens and heliostats exposed for various periods of the order of several weeks to over a year at the Naval Weapons Center, China Lake, California, and at Sandia Laboratories, Albuquerque, New Mexico, were in reasonable agreement and were used in establishing dust buildup rates and cleaning frequencies. Assumptions as to cleaning costs and the costs associated with inverting stow are based on data from previous MDAC tests and analyses, principally Reference 1.

Degradation Rates

Table I summarizes data on full-scale MDAC heliostats and 5 x 5-in. reflector specimens tested at the Naval Weapons Center. Table I gives the time-averaged reflectivity degradation and the degradation rate for full-scale heliostats as presented in Reference 2. The degradation rate is taken as the mean of the degradation rates occurring between measurements and is equal to the reflectivity difference divided by the number of days between measurements.

TABLE I

AVERAGE REFLECTANCE VARIATIONS

Heliostat No.	Exposure Time (Days)	Time Averaged Reflectivity (%)	Time Averaged Degradation (%)	Degradation Rate (% Per Day) Mean ± Standard Deviation	
H1 (Acrylic)	113	$\bar{\rho}$ = 75.46	7.76	0.4 ± 0.4	
H2 (Acrylic)	113	$\bar{\rho}$ = 68.37	8.13	0.45 ± 0.32	0.37 ± 0.09 for four heliostats stowed face-up
H3 (Acrylic)	97	$\bar{\rho}$ = 80.47	6.99	0.28 ± 0.18	
H4 (Laminate Glass)	121	$\bar{\rho}$ = 81.10	6.55	0.36 ± 0.32	
IH1 (Laminate Glass)	121	$\bar{\rho}$ = 83.30	3.19*	0.1 ± 0.13	

*IH-1 was stowed in the face-down position for most of the test period (≈2/3 of exposure time). Data above are for periods without rain or other significant natural cleaning conditions.

The following conclusions can be made:

- Near-vertical, vertical, and face-down stow positions decrease the buildup rate, compared to face-up stow, but daytime operation limits the improvement.
- Daytime degradation rate is a function of time at a given exposure angle; therefore, the south field degradation rate will be relatively higher than that of the north field.
- On the basis of available data, it appears that there is little difference in the degradation rate between face-down and vertical stow for benign conditions, and the preferred field average rate is 0.150%/per day.

Adding previously determined ranges of severe weather degradation rates to the above benign condition degradation rates gives the averaged total degradation rate.

Cost Analysis

Cost analyses were performed which consider labor, capital equipment, materials usage, and cleaning frequency cost implications from four standpoints. First, the costs of providing an inverted stow capability are determined. Second, the costs in constant 1978 dollars of cleaning a field of heliostats are determined for a range of reasonable values of manhours and quantity usage. Third, the effects of inflation and monetary discount rates are considered. Fourth, allowable degradation is determined based on a minimum total cost associated with both cleaning and adding heliostats to the field to make up for the lost energy due to additional allowed degradation. The cost optimized degradation values and associated cleaning frequencies are then compared on a total cost basis to determine the relative costs of the inverting and non-inverting designs.

The cost of providing an inverting stow capability to be used predominately during periods of high winds is $476 per heliostat, as shown in Table II.

TABLE II
COST OF INVERTING*

Azimuth Housing Weight			$ 0.90
Elevation Drive			
Drag Link	$ 22.56		
Bushing	.50		
Pin	1.50		
Invert Hinge Point	6.00		
Stowage Jack	224.58		
Motor	49.25		
Electronics	10.00		
			$314.39
Cost to Invert			315.29
Lost Mirror Surface			
Cost of Mirror (5.2 m^2)			(49.46)
Equivalent Cost			$210.17
		TOTAL -	$476.00
		$/$m^2$	$ 9.70
		$/$m^2$R(0.92)	$ 10.55

*From Reference 1: Solar Central Receiver Prototype Heliostat, final technical report, August, 1978, McDonnell Douglas Astronautics, Inc., Huntington Beach, CA, DOE Contract EG-77-C-1605.

This cost is associated with three aspects of the design: (1) added azimuth weight, (2) additional elevation drive parts, and (3) lost mirror area, less the cost of additional mirror surface area. These costs are from Reference 1 and

are based on the costs as factored for the production rate of 25,000 heliostats per year. An additional 5.2 square meter of mirror is lost due to the slot required to invert. The cost of the mirror includes both the added square footage of the mirror module and added stringer length, both of which are costed on a dollar per area basis. The overall cost per square meter is calculated as the difference in cost per square meter between the inverting heliostat at 49.05 m^2 and the non-inverting heliostat at 54.25 m^2, after adjusting the non-inverting heliostat total cost for net cost difference.

The cost of washing an entire field of heliostats is presented in Table III for assumed degradation rates and environmental condition. An optimization of the total cost of the field (washing cost and additional heliostat cost due to performance degradation) with respect to allowable reflectivity loss gives a total cost of $482 for the non-inverting heliostat and $295 for the inverting heliostat. The optimal reflectivity losses are 12.4 percent and 8.4 percent, respectively. Thus the cost of providing an inverted stow capability ($476) is significantly higher than the total cost difference found above; i.e., $482 less $295, or $187. Since these results are based on an analysis which has been somewhat biased in assumptions to give economic benefit to the inverting heliostat design, the actual cost savings associated with a non-inverting design is expected to be larger. For this example, the cost savings is $466 less the $187, or $289. The net potential cost savings associated with eliminating the inverted stow capability, assuming 50 m^2 at $72/$m^2$, is therefore approximately 8 percent.

Conclusions

1. A cost savings of approximately $280 per heliostat, or 8 percent of the heliostat cost, is achievable by eliminating the inverted stow capability, considering the reflectance degradation effects.

2. Monetary parameters have a significant effect on the cleaning costs.

3. For the optimum total cost condition of a non-inverting heliostat, with an 8 percent inflation rate and 10 percent discount rate, the number of cleaning operations ranges from 7 per year with natural clenaing to 10 percent per year without natural cleaning.

TABLE III

NUMBER OF WASHINGS PER YEAR AND COST PER HELIOSTAT FOR 30 YEARS

Stow Position Assumptions and Rate	Wash 8 Months/Year Allowed Loss and Associated Cost								Wash 12 Months/Year Allowed Loss and Associated Cost							
	3%	Cost	6%	Cost	9%	Cost	12%	Cost	3%	Cost	6%	Cost	9%	Cost	12%	Cost
Face-down Stow (R = 0.15%/Day)	12.2	483.1	6.1	241.6	4.1	162.4	3.0	118.8	18.3	724.7	9.1	360.4	6.1	241.6	4.6	182.2
Vertical Stow - with 0.05%/day additional degradation due to winds and light rain and forced face-up stow (R = 0.2%/Day)	16.2	641.5	8.1	320.8	5.4	213.8	4.1	162.4	24.3	962.3	12.2	483.1	8.1	320.8	6.1	241.6
Vertical Stow - with 0.19%/day additional degradation due to winds and light rain and forced face-up stow (R = 0.34%/Day)	27.6	109.3	13.8	546.5	9.2	364.3	6.7	265.3	41.4	1639.4	20.7	819.7	13.8	546.5	10.3	407.9

WIND TUNNEL TEST OF A FULL-SCALE HELIOSTAT IN THE NASA, AMES, 40- BY 80-FOOT FACILITY

S. G. Peglow
Sandia Laboratories, Livermore

Introduction

To build a heliostat that will operate in and survive the extremes of weather conditions at a typical desert site, the designer must be able to predict the forces expected to act on the structure. To underestimate the design loads is to invite failure and to overestimate will invariably lead to a more costly hleiostat.

The information needed to design or evaluate a heliostat for a wind environment consists of several elements. First, the environment must be characterized as well as meterological data will allow. This has been done, for example, at the 10-MW pilot plant site located near Barstow, California. This has led to the establishment of a wind specification that calls for a maximum operational velocity of 50 mph (including gusts) and a maximum survival velocity of 90 mph (including gusts). Both of these conditions are assumed to occur at a height of 30 ft., with a velocity profile of the form $V = V_{30}\ (Z/30)^{0.15}$ to be used for values of Z other than 30 ft. Secondly, the loads and moments, both static and dynamic, acting on the structure must be calculated to allow evaluation of the capabilities of the drive mechanism and structure to provide reliable operation of the heliostat for the specified wind environment. The performance of these calculations implies a knowledge of the aerodynamic coefficients associated with a heliostat structure. flow of air around bluff bodies and flat plates in two dimensions. Little data, however, is available for complex, three-dimensional flows at the large Reynolds numbers characteristic of a heliostat in a natural environment. It is to this end that a full-scale wind tunnel test of a DOE prototype heliostat was conducted.

Test Description

The NASA, Ames, wind tunnel used in these tests has a closed 40- by 80-ft test section with semi-circular sides of 20-ft radius and a closed circuit air return as shown in Figure 1. The model support system consists of three movable struts mounted on a turntable. The heliostat was mounted on a single strut support as shown in Figure 2. Each strut is separately connected to the balance frame system. Mechanical lever systems transmit the lift, drag, and side force link loads to seven separate scales for measurement of loads and moments.

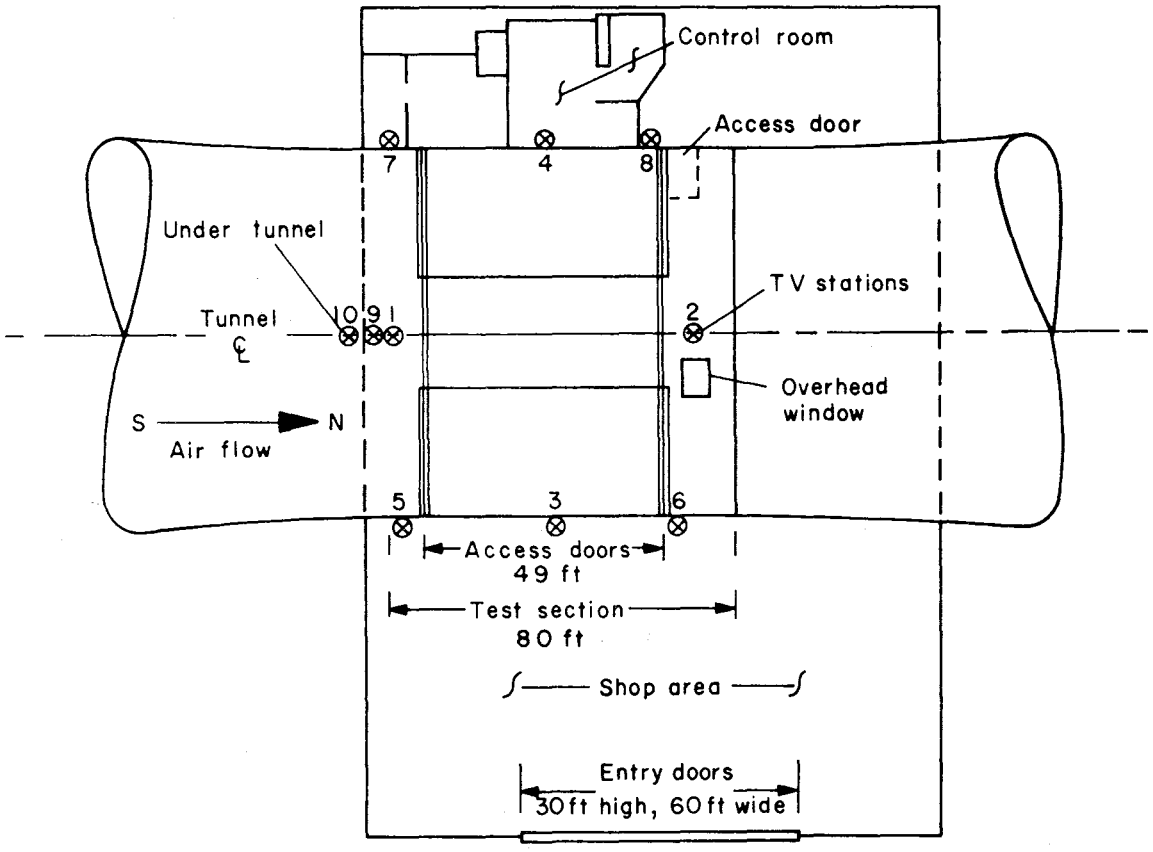

(a) Plan view.

Figure 1. General Arrangement of the Ames 40- by 80-Foot Wind Tunnel Test Section and Shop Area

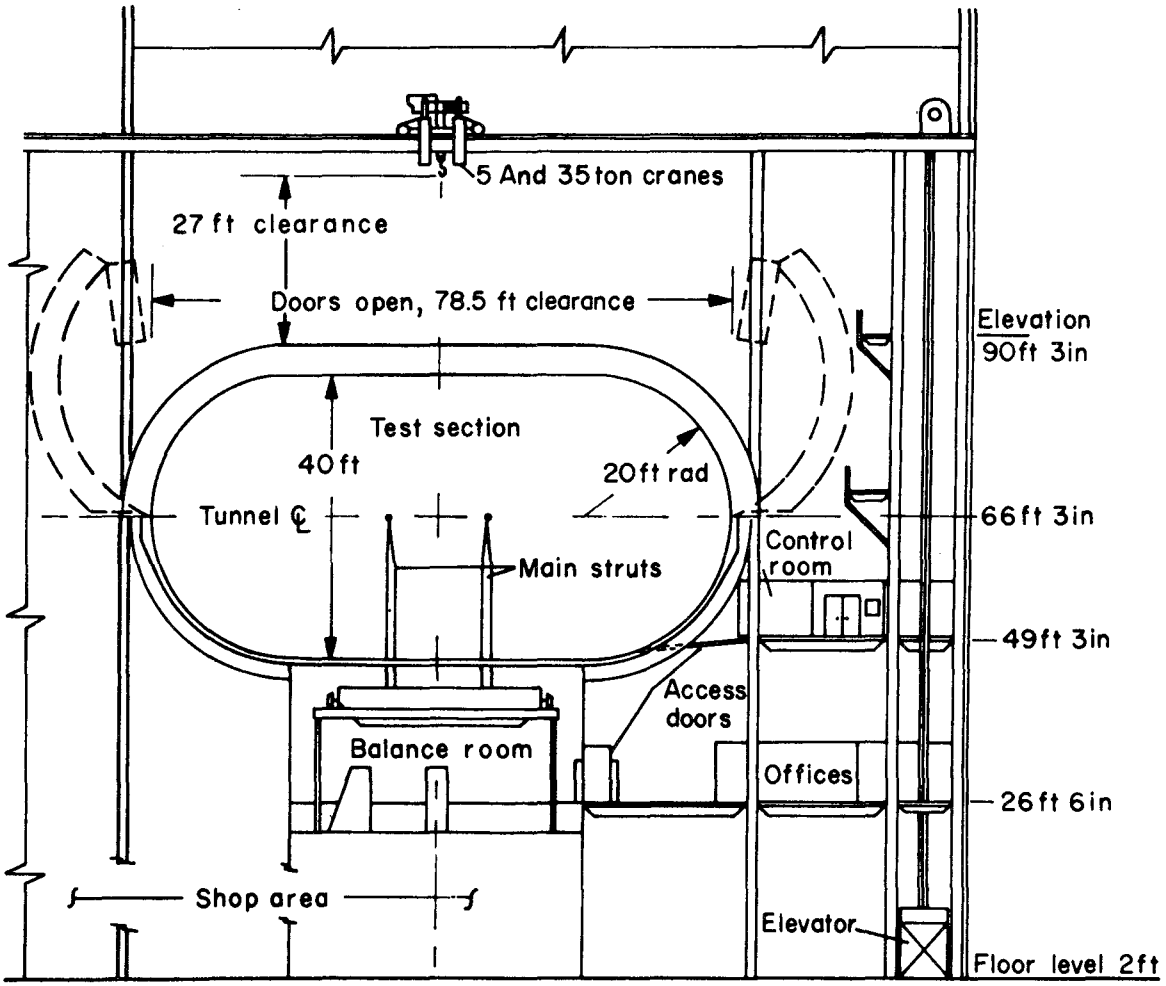

(b) Elevation view.

Figure 1. (Continued)

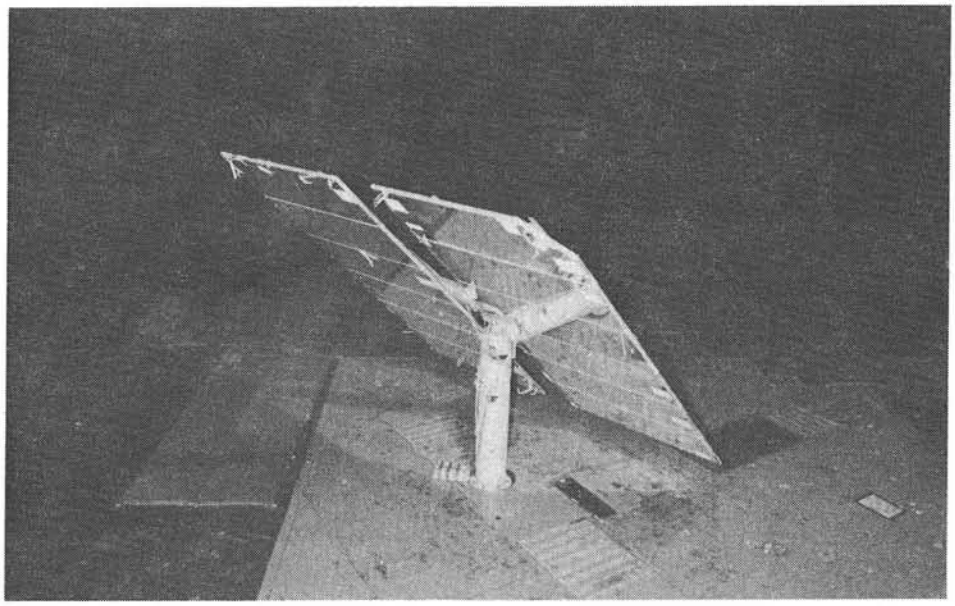

Figure 2. Strut Support in NASA Tunnel

The heliostat used in these tests was of the single pedestal, orbi-drive type built by McDonnell Douglas Astronautics for the DOE's prototype heliostat evaluation (Figure 3). The heliostat assembly consists of a galvanized steel pedestal supporting a torque tube to which are attached 8 frame arms and 12 mirror modules. Movement of the mirror assembly is provided by two DC motors, one for elevation and one for azimuth, acting through separate gear boxes. During the tests, azimuth and elevation angle were changed by using the on-board drive motors and set by comparing potentiometer outputs to a list of precorded settings, which were verified by an inclinometer.

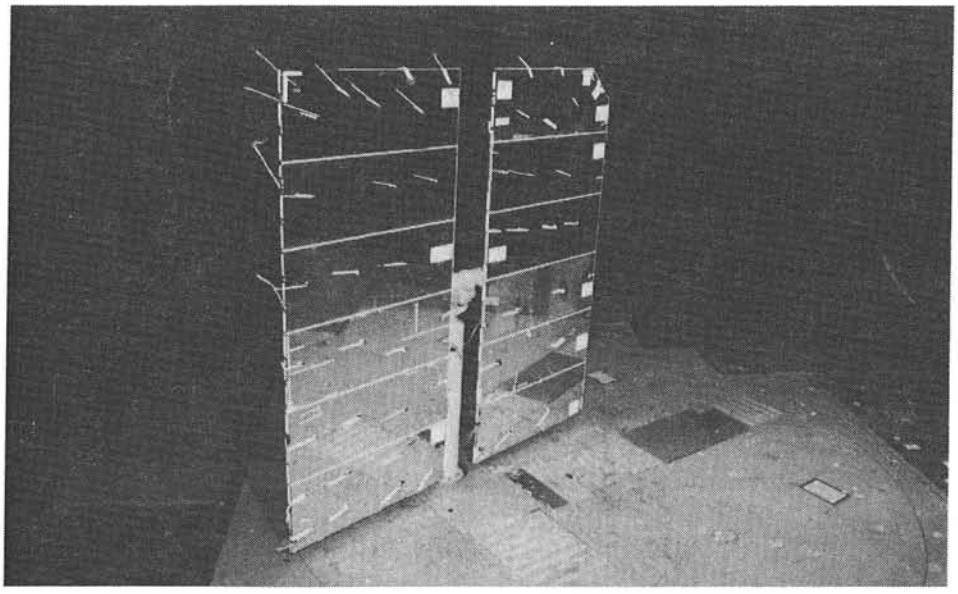

Figure 3. DOE Prototype Heliostat

Instrumentation

In addition to the force and moment data provided by the NASA balance system, twenty-six accelerometers were placed on the heliostat as defined in Reference 4. The type used were Sunstrand 3038 servo accelerometers with the gains in the amplifiers set to produce an output of ±3.2 g's or ±1.6 g's full scale depending on position. Several "scale" tests were run initially to establish the natural frequencies of the heliostat. As a more heuristic approach to the study of wind effects, strips of material were attached to the flow surfaces and the heliostat edges were Scotch-lifted as shown in Figure 4. Both stills (Nikon at 3 frames/s) and 16-mm movies were used to capture the flow patterns on the heliostat surfaces for a variety of velocities and configurations.

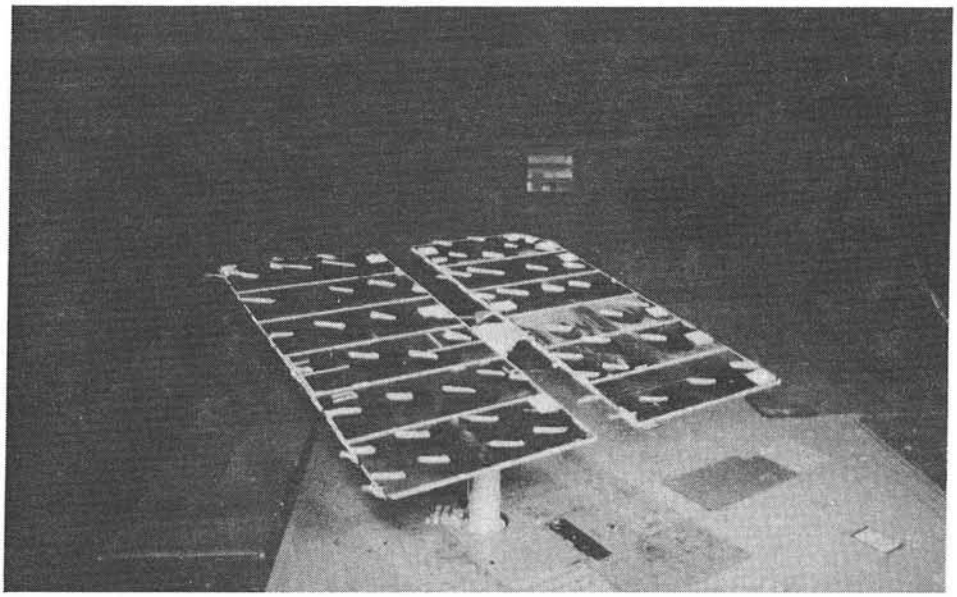

Figure 4. Flow Visualization

Proof Tests at the SLL Heliostat Development Laboratory

Prior to the NASA test, the prototype heliostat was subjected to a series of tests in which the 90-mph survival loads were applied to the heliostat mechanically as shown in Figure 5. The points of action were chosen so as to simulate the maximum torque about the elevation drive. Deflections of the frame arms were measured to evaluate the relative importance of dynamic deflections during the subsequent wind tunnel tests. The results are discussed in the next section and summarized in Table I. All accelerometers were first calibrated during static and shake tests and then checked at the NASA facility.

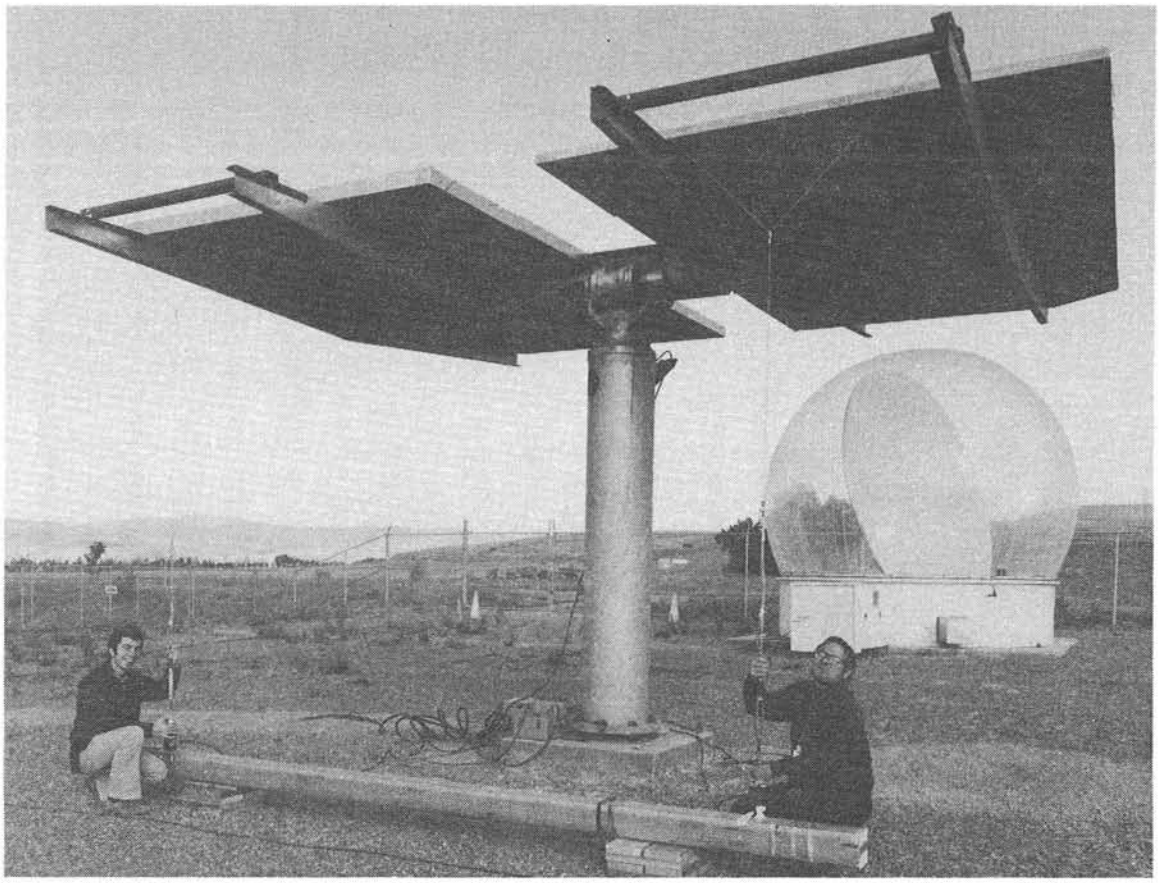

Figure 5. Elevation Drive Proof Test

Results

The force and moment data was taken at a point at the base of the heliostat as shown in Figure 6. The normal sense of lift and drag apply here, i.e., drag is positive down the tunnel and lift is positive upwards. In Figure 7, the lift force coefficient C_L is shown as a function of angle of attack (elevation), where positive α is opposite to the rotation shown for positive pitching moment and positive azimuth angle θ is in the same direction as shown for positive yaw moment. This somewhat unorthodox choice of positive angular displacement is a result of control singularities when trying to rotate through the full range of angles required in the normal counterclockwise direction. The other data presented on the plot is the result of using data from the American Society of Civil Engineers, ASCE Paper No. 3269 and applying it to the prototype heliostat. Figure 8 shows the drag coefficient versus angle of attack. It is interesting to note that as the heliostat begins to approach a bluff body configuration, the total drag is best represented by assuming that the contribution from the mirror modules is approximated by two flat plates of aspect ratio λ equal to 3. The effect of the center slot is thus more noticeable at higher angles of attack.

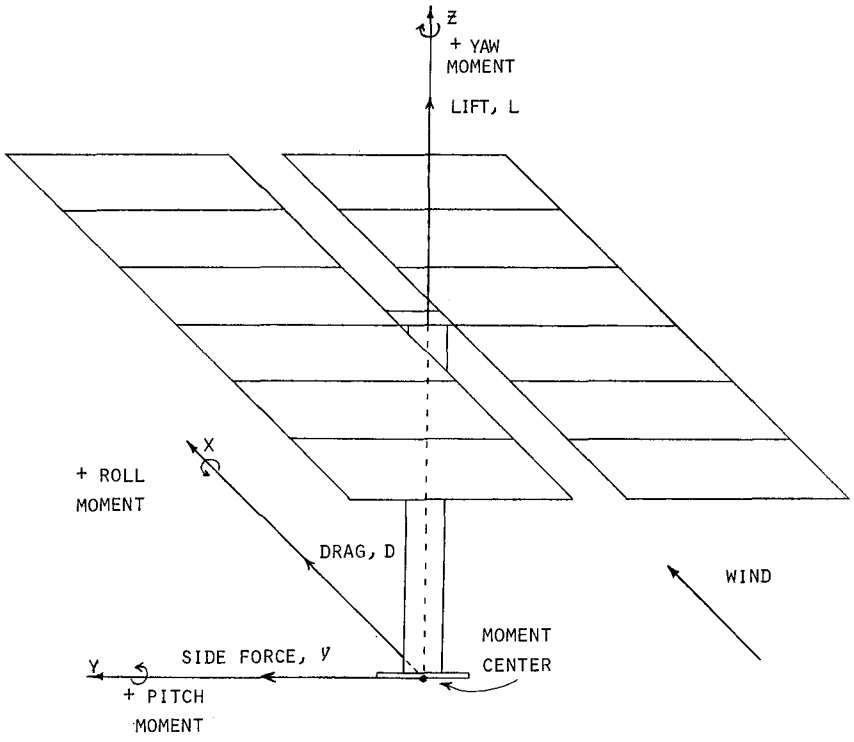

Figure 6. Coordinate System for Forces and Moments

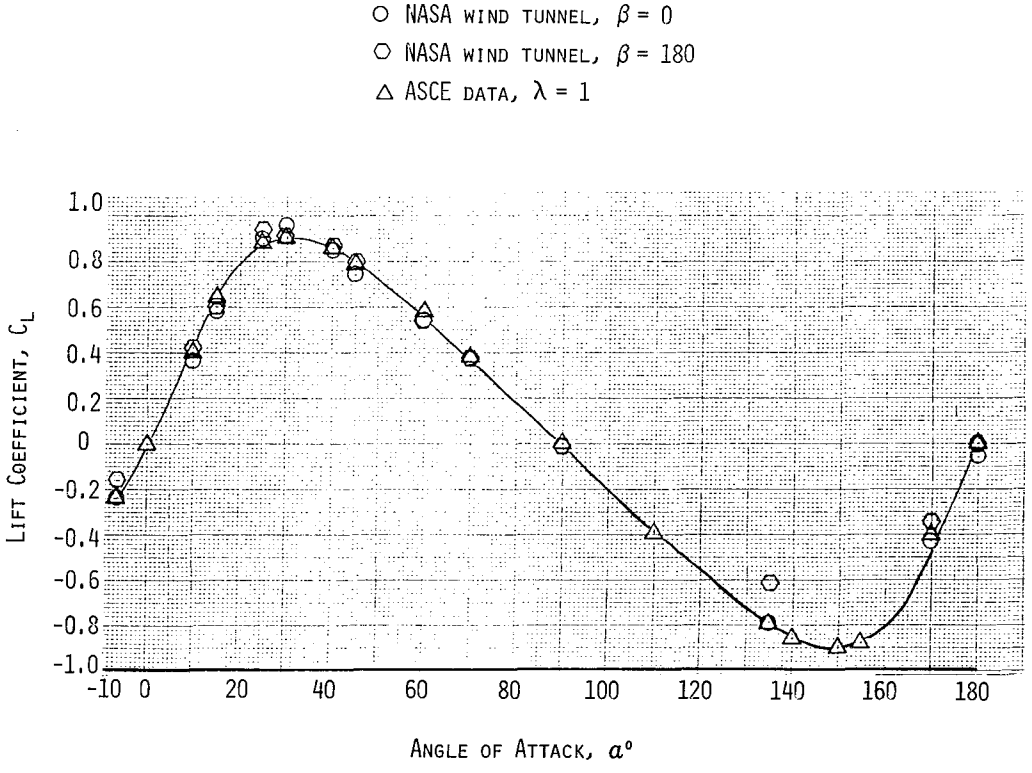

Figure 7. Lift Versus Angle of Attack

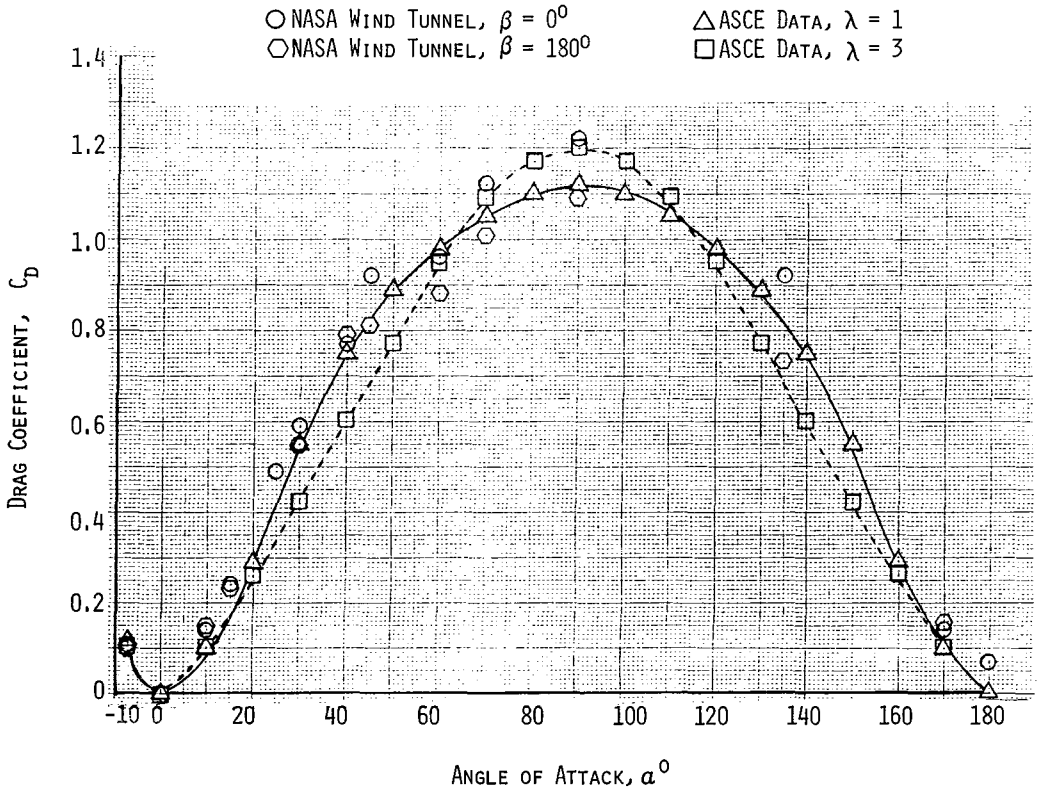

Figure 8. Drag Versus Angle of Attack

The variation of the base moment coefficient C_m with α is shown in Figures 9 and 10. With the glass side towards the flow, as shown in Figure 10, the pitch moment can be closely approximated by the flat plate data. With the structural side downwind, however, the effect of the additional turbulence generated by the frame arms can be seen in the range of α from 25 degrees to 45 degrees where the maximum lift is occurring.

The dynamic loads on the heliostat structure were analyzed by taking the recorded real-time outputs of the twenty-six accelerometers mounted on the torque tube, frame arms, and pedestal and integrating the signals to produce power spectral density (PSD) plots. The worst vibration case during the tests was for the survival condition when the elevation angle was 10 degrees, the wind speed was 83 mph, and the azimuth angle was 45 degrees. The outboard panels downstream appeared to receive the worst buffeting effect in this configuration, which is verified by the accelerometer data. The accelerometer showing the highest vibration level yielded a PSD curve which has a pronounced peak of 0.04 g/Hz^2 at a frequency of 12 Hz. This corresponded to a real-time acceleration of ±1.5 g's, which implies a dynamic displacement of less than 0.20 inches. As shown in Table I, the mechanically induced static displacements are greater than this dynamic value by more than an order of magnitude.

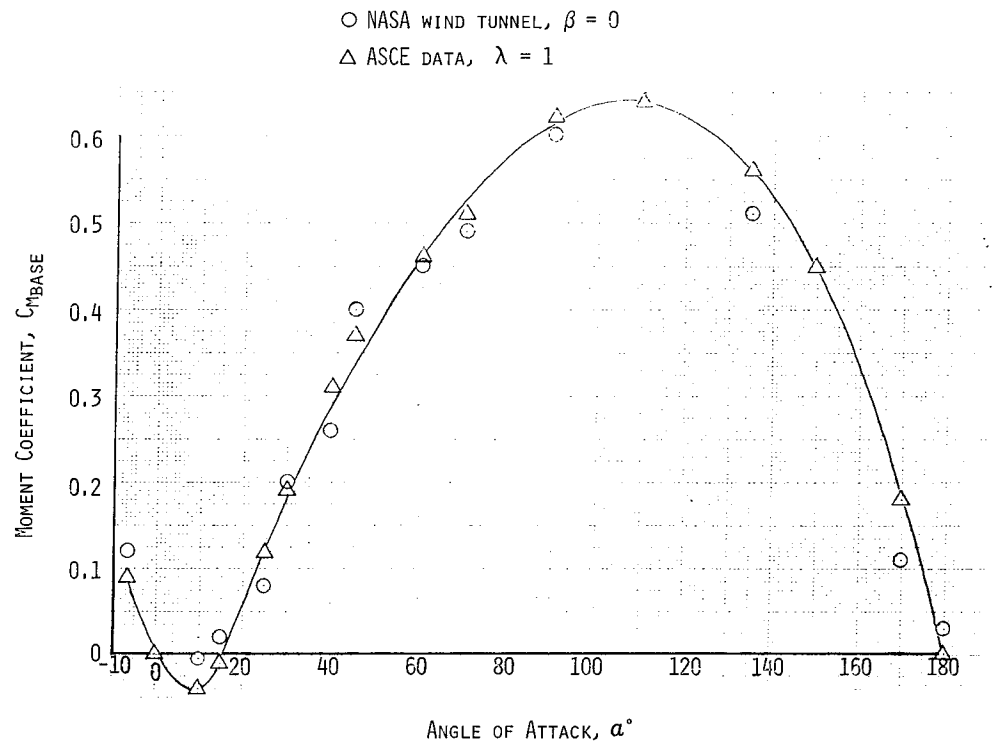

Fgiure 9. Base Moment Versus Angle of Attack, 0° Azimuth

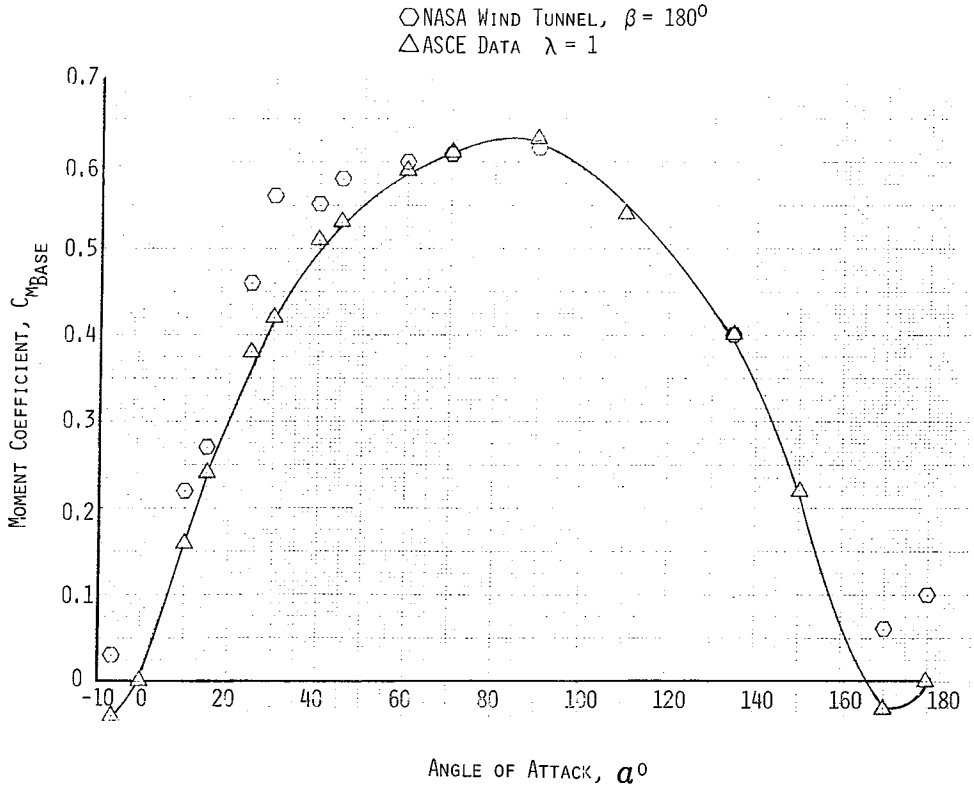

Figure 10. Base Moment Versus Angle of Attack, 180° Azimuth

TABLE I

STRUCTURAL DEFLECTION IN SIMULATED 90 mph WIND

Mechanically Applied Load
(195,000 in-lb about elevation drive)

Test No.	Deflection (in.)
1	3.15
2	3.24
3	3.26

Summary and Conclusions

The full-scale test of a DOE prototype heliostat in the NASA, Ames, 40- by 80-foot facility showed no severe airflow/structure dynamic interactions, such as low frequency vortex shedding. The heliostat survived the full range of configurations and wind speeds currently specified for heliostat design with no damage to any of the components. The results from this test indicate that the data and methodology defined in Reference 1 is appropriate for designing structures of this type. The proof tests outlined in this report would appear to be a valid way of mechanically simulating a survival moment about the critical elements (elevation or azimuth drive) to test future heliostats.

References

1. ASCE Paper No. 3269, "Wind Forces on Structures," Transactions, ASCE, Vol. 126, 1962.

2. "American Standard Building Code Requirements for Minimum Design Loads in Buildings and Other Structures," American National Standards Institute, 1971.

3. "Building to Resist the Effect of Wind, Vol. II," National Bureau of Standards, PB-266 333, May 1977.

4. Peglow, S. G., "Full Scale Heliostat Wind Tunnel Test Plan," Unpublished report, November 1978.

SERI/DOE QUALITY ASSURANCE AND STANDARDS PROGRAM

Dick DeBlasio
Solar Energy Research Institute

Quality assurance is an important element in the solar commercialization process. Users will want assurance that a solar energy system can provide safe operation. Moreover, system life-cycle costs are significantly influenced by the expenses of maintenance and of lost benefits in the case of failure. Solar energy systems must compete in the marketplace with conventional systems in which the user has an established degree of confidence. Broad scale commercialization of solar energy systems must create the same degree of confidence for solar systems through competent design and demonstration of long-term quality assurance.

The development of performance criteria and test methodologies is essential to the successful development of solar technology. These elements provide a basis for comparing different devices in terms of design, cost, production, and system integration. In addition, they provide the basis for standards development.

Obviously, standards affect product costs: they may reduce the number of unnecessary grades or product lines; they can enhance interchangeability of parts which can lead to reduced labor and reduced repair and maintenance costs; and they can affect the demand for a product to the extent that they lead to interchangeability with products from an existing technology. In addition, standards are the basis for building code provisions and for product certification programs--two important factors in ensuring user confidence and acceptance of a new technology. Carefully and deliberately established, standards can encourage the growth of an emerging industry. Carelessly established, they can inhibit innovation and retard commercial advancement.

The SERI/DOE Quality Assurance and Standards Development Program is designed to ensure that performance criteria and test methodologies for solar technologies are developed in a timely manner. The program will provide performance criteria test-method development, accreditation/certification guidelines, validation methodologies, and liaison with consensus standards and code organizations. Our approach is committed to development of standards through the voluntary consensus system for systems, subsystems, components, and materials. The QA program also will support this process in ways which will accelerate the development of standards as much as possible. However, project teams will not write standards but will operate through the traditional institutional framework for the development of consensus standards. Within this program, SERI

is managing a project to develop performance criteria and test methodologies together with laboratory accrediation and product certification program guidelines for photovoltaic systems.

The overall objective of the project is to stimulate the development and adoption of industry-established material, component, subsystem, and system performance criteria and standards for the design, application, and operation of reliable and safe photovoltaic power systems. In addition to the PV project, SERI, at the request of DOE, is initiating a planning activity looking at solar thermal in regards to a quality assurance and standards project.

SERI began management of the PV project in January, 1978, with the establishment of a Coordinating Council for the Development of Performance Criteria and Test Methodologies. The Council met three times in 1978. Its membership includes representatives from industry, voluntary consensus groups, public interest representatives, independent test laboratories, prime contractors in the DOE PV program, and SERI. The Council has made significant progress toward developing performance criteria by:

- Identifying the systems hierarchy of both flat-plate and concentrator systems
- Establishing definitions for elements of the PV subsystem
- Identifying
  - performance criteria to be measured
  - priorities in test methodology development
  - organizational resources and responsibilities for their development

During 1978 five subcommittees were convened to support the Council:

- PV performance criteria (now PV subsystems)
- Storage
- Power conditioning and control
- Safety
- Reliability and durability

The subcommittees provided additional expertise in their respective areas and identified needs, priorities, and resources.

A steering committee, made up of key program and project personnel, is charged with the specific function of overseeing the development of interim performance criteria and the test methods to support these criteria. The Steering Committee will work through three task groups:

- Task Group No. 1 on the photovoltaic subsystem

- Task Group No. 2 on other subsystems, (power conditioning, controls, cabling, and storage)

- Task Group No. 3 on total systems

Development of the Interim Performance Criteria (IPC) document, and its subsequent revisions, is one of the primary activities within this management hierarchy. This document will lead to other activities and tasks within the project. The task groups will develop the criteria and will prepare drafts of the IPC document. The task group steering committee will integrate these activities and products and will coordinate the review process through the subcommittees and the Coordinating Council.

In general, the project objectives are:

- Support and assist in the development of a comprehensive body of standards for performance, reliability, and safety for photovoltaic energy conversion systems

- Develop and assist implementation of criteria and procedures for the accreditation of laboratories to test photovoltaics

- Develop and assist implementation of certification criteria and procedures for photovoltaics

- Develop and implement validation methodologies and mechanisms for review and monitoring of criteria and test methods

- Coordinate DOE/SERI quality assurance activities, internally and externally, with national and regional consensus standards and codes organizations.

Planning Activity - Solar Thermal

For the remainder of FY 79, SERI's planning activity for Solar Thermal will include making contact with key people in both the large and small thermal programs in order to establish a core of resources needed to participate in this project. In addition, we will review progress to date and will establish liaison with the appropriate Standards and Industrial Associations. SERI will develop a Solar Thermal Quality Assurance and Standards Project Plan in the first half of FY 80. During the development of the plan, SERI may establish a special Ad Hoc committee of key program members to advise our project team on priorities in regard to near and long-term objectives. This determination will be made after the initial round of contacts. Once a draft project plan is developed, we plan on having an open workshop, possibly in conjunction with a program review meeting for input from all sectors within the solar thermal community. Implementation of the project plan's recommendations will start in the second half of FY 80.

TOWER COST STUDIES FOR CENTRAL RECEIVER STUDIES

W. R. Lang, R. J. Colasanti
Stearnes-Roger Engineering Company

Objective of Study

The objectives of this study were to generate cost data for twenty tower cases. The results of Cases 1 through 16 were used by Sandia Laboratories to arrive at a statistical model to predict tower costs. Cases 17 through 20 were used to evaluate the resulting model.

Tower Design Variables

The design variables used in determining costs for Cases 1 through 16 were as follows:

1. Material - concrete and steel
2. Tower height - 300 ft and 650 ft
3. Receiver weight - 200 kips and 8000 kips
4. Seismic ground acceleration - 0.05 Gs and 0.60 Gs
5. Wind velocity - 70 mph and 120 mph
6. Soil shear modulus - 10 ksi and infinity
7. Soil bearing capacity - 4 ksf and 12 ksf

Additional parameters specified were:

1. Receiver dimensions

   Height = tower height/10

   Diameter = tower height/15

2. Weight of piping, etc., within the tower = 2000 lbs/ft

3. Soil properties

Density = 130 lb/ft^3

Poisson's Ratio = 0.3

Analytical Procedure

Structural Model

Each tower was modeled as a multi-mass cantilever beam structure (Figure 1). The tower masses consisted of the tributary mass from the tower structure itself plus supported equipment.

Each concrete tower was divided into fifteen segments of equal length with the mass of each segment located at the segment centroid. The masses were connected by prismatic beam elements. Section properties were based on the gross uncracked concrete section, using the average radius and thickness along the length of the element.

For steel towers the masses were located at the level of each horizontal brace. The tower truss structure was represented by equivalent beam elements having a stiffness equal to that of the actual three-dimensional truss structure.

The receiver structure was modeled by beam elements having a stiffness of twenty percent of the topmost tower element for the concrete towers, and by elements having a stiffness equal to that of the adjacent tower element for steel towers. The receiver mass was distributed among the receiver nodes so that their centroid would lie at the receiver mid-height.

For those towers having a finite soil shear modulus, the soil was represented by discrete soil springs. The foundation translational and rotary inertias were lumped at the foundation centroid, with rigid elements joining the foundation mass to the soil springs and the tower.

Modal Analysis

All horizontal and vertical natural frequencies and corresponding mode shapes were computed for each tower by the Jacobi method.

Analysis for Earthquake

Tower response to both horizontal (one component) and vertical earthquake loading were computed using the response spectrum method. The ground response spectra were obtained from Regulatory Guide 1.60, "Design Response Spectra for Seismic Design of Nuclear Power Plants," issued by the U. S. Nuclear Regulatory Commission.

Modal damping ratios for the towers were obtained from Regulatory Guide 1.61, "Damping Values for Seismic Design of Nuclear Power Plants."

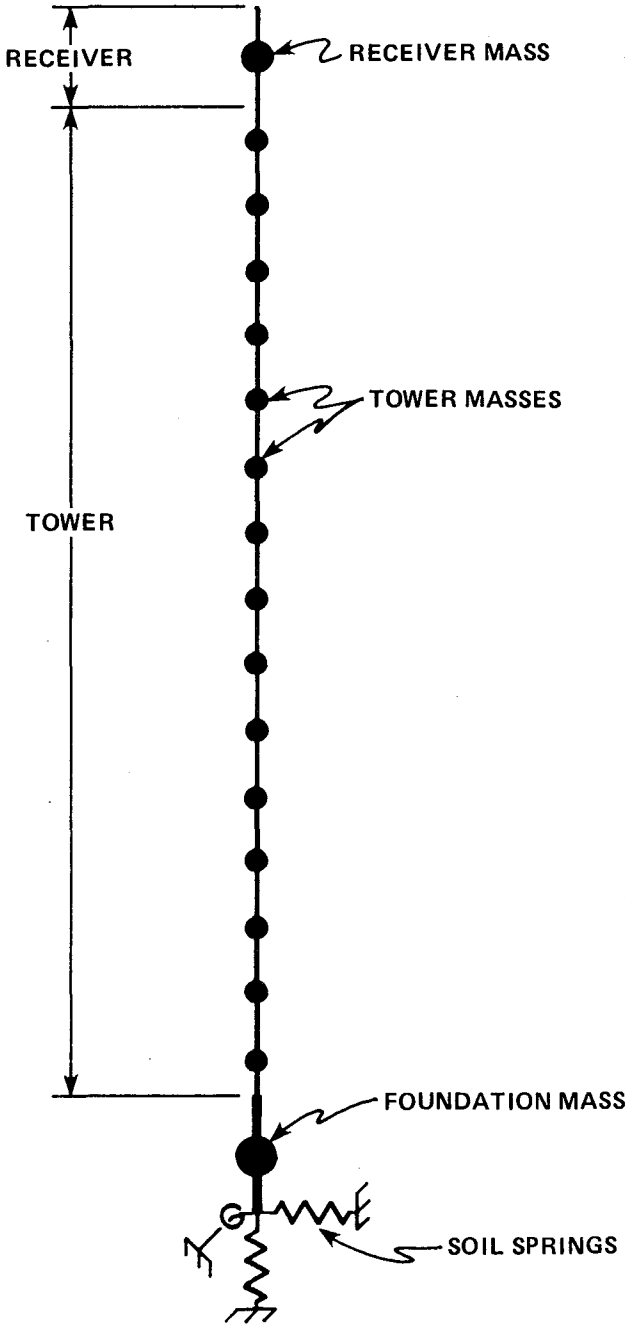

Figure 1. Structural Model

For tower models incorporating soil springs, the combined effects of material and radiation damping were considered. To combine soil damping with that of the tower, composite modal damping values were used, with the damping in each element weighted according to its strain energy.

The structural response to each earthquake component was computed from the appropriate modal responses using the square root of the sum of the squares (SRSS). To compute member forces for design purposes, these component responses were then combined to obtain the complete earthquake response. For steel towers the combined response of the components was computed by SRSS, while for concrete towers the absolute sum was employed.

Analysis for Drag Wind

Drag wind loads were computed per the provisions of the "American National Standard Building Code Requirements for Minimum Design Loads in Buildings and Other Structures (ANSI A58.1-1972)."

The towers were assumed to be located in flat, open country. Gust factors were applied in accordance with Appendix A6.3.4.

Analysis for Wind Induced Vortex Shedding

The concrete towers were assumed to be oscillating perpendicular to the wind in their fundamental mode.

Tower responses were calculated at the critical wind velocity, i.e., that velocity at which vortices are shed at a frequency equal to the fundamental natural frequency of the tower. The transverse forces resulting from the shedding of vortices were assumed to be harmonic in nature.

Since very few cases of severe vortex excitation have been observed for critical wind velocities above fifty to sixty miles per hour, it was conservatively assumed that vortex shedding would present no problems if the critical wind velocity exceeded seventy miles per hour.

Design Procedure

For the design of reinforced concrete towers, minimum shell wall thickness and minimum circumferential reinforcement were determined in accord with the "Specification for the Design and Construction of Reinforced Concrete Chimneys (ACI 307-69)." Vertical reinforcement was calculated using the strength design provisions of the "Building Code Requirements for Reinforced Concrete (ACI 318-71)." Load factors as specified in ACI 318-71 were used in investigating the combined effects of dead load and wind. Load factors of unity were used when considering the effects of dead load and seismic.

For the design of steel towers, members were sized in accordance with allowable stresses given in the AISC "Manual of Steel Construction," Seventh Edition. Load factors of unity were used in investigating the combined effects of dead load and wind. Allowable member stresses were increased by a factor of 1.6 when considering the effects of dead load and seismic.

Foundation mats were sized to meet the following two criteria:

1. Calculated soil bearing pressures should be less than or equal to the specified allowable soil bearing pressures. Load factors of unity were used in calculating soil bearing pressures. The foundation mats were assumed infinitely rigid and the calculated soil pressures were assumed to have a linear variation.

2. In the case of uplift, positive pressure must be maintained over at least eighty percent of the mat contact area.

Typical Steel Tower (Trial Tower Design No. 13)

Figure 2 shows a typical steel tower. This particular tower is 300 feet high and supports an 8000 kip receiver. It is subjected to high wind and seismic loads; hence it has a rather large base diameter and requires twelve columns of high strength structural steel.

Figure 3 shows a computer produced plot of the first five lateral mode shapes and plots of the deflection, shear, and moment diagrams for both the drag wind and seismic loading conditions.

Typical Concrete Tower (Trial Tower Design No. 8)

Figure 4 shows a typical concrete tower. This tower is 650 feet high and supports a 200 kip receiver. It is subjected to a 120 mile per hour drag wind and an earthquake of 0.05 G maximum ground acceleration. Wind loads controlled the design of this particular tower.

Figure 5 shows a plot of the first five lateral mode shapes and plots of the deflection, shear, and moment diagrams for vortex shedding, drag wind and seismic loads. The critical wind velocity to produce vortex shedding for this tower is 53 miles per hour.

Steel Tower Summary - Material Quantities and Costs

Figures 6 and 7 are tables summarizing the design parameters, material quantities, and costs of the steel towers. Shown for each trial tower design number are the tower height, receiver weight, design seismic ground acceleration, design wind velocity, soil shear modulus, allowable soil bearing pressure, total tower weight, tower cost, volume of concrete foundation mat, foundation cost, and total cost of tower plus foundation.

An inspection of the tables (Figure 8) indicates the following:

1. The least costly 300-foot-high tower is trial tower design number one ($270,000). It supports a receiver weighing 200 kips and is designed for wind and seismic loads of 70 miles per hour and 0.05 Gs, respectively.

2. The most costly 300-foot-high tower is trial tower design number thirteen ($2,978,000). It supports a receiver weighing 8000 kips and is designed for wind and seismic loads of 120 miles per hour and 0.60 Gs, respectively.

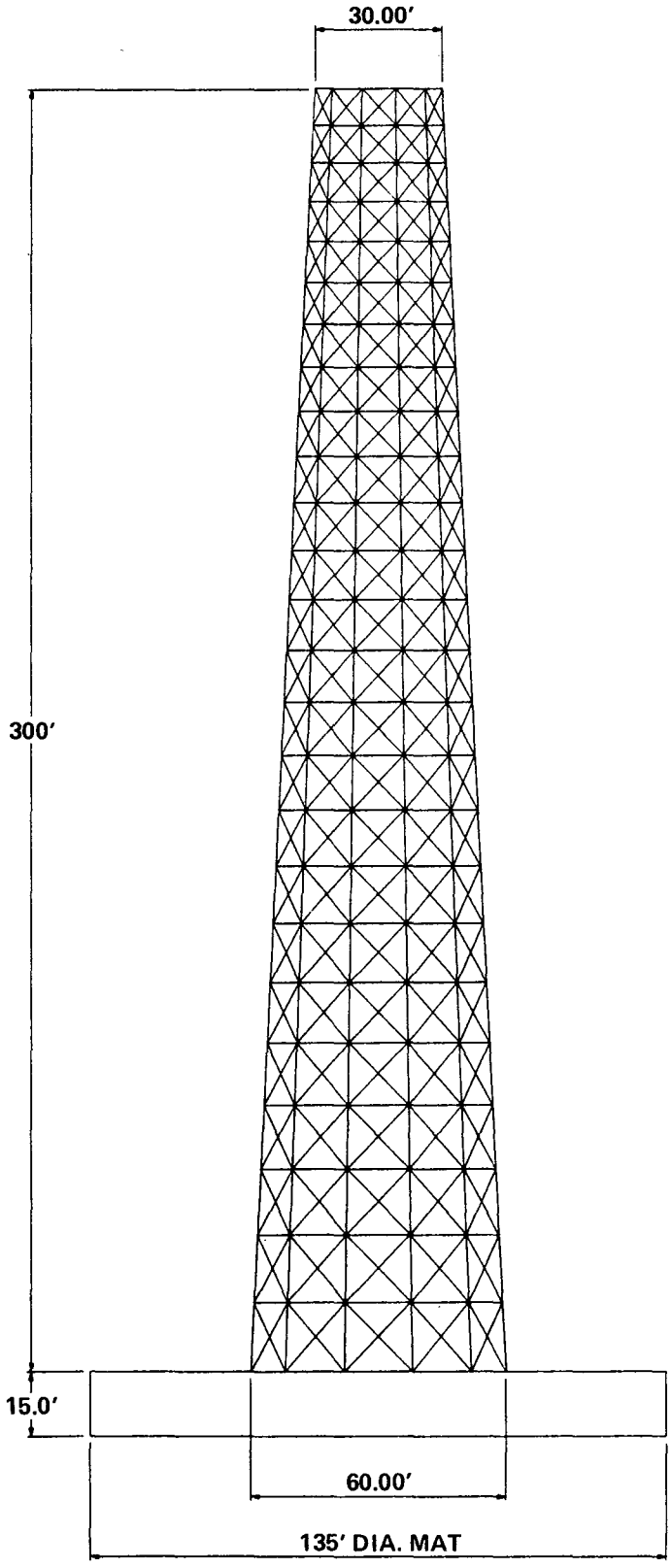

Figure 2. Trial Tower Design No. 13

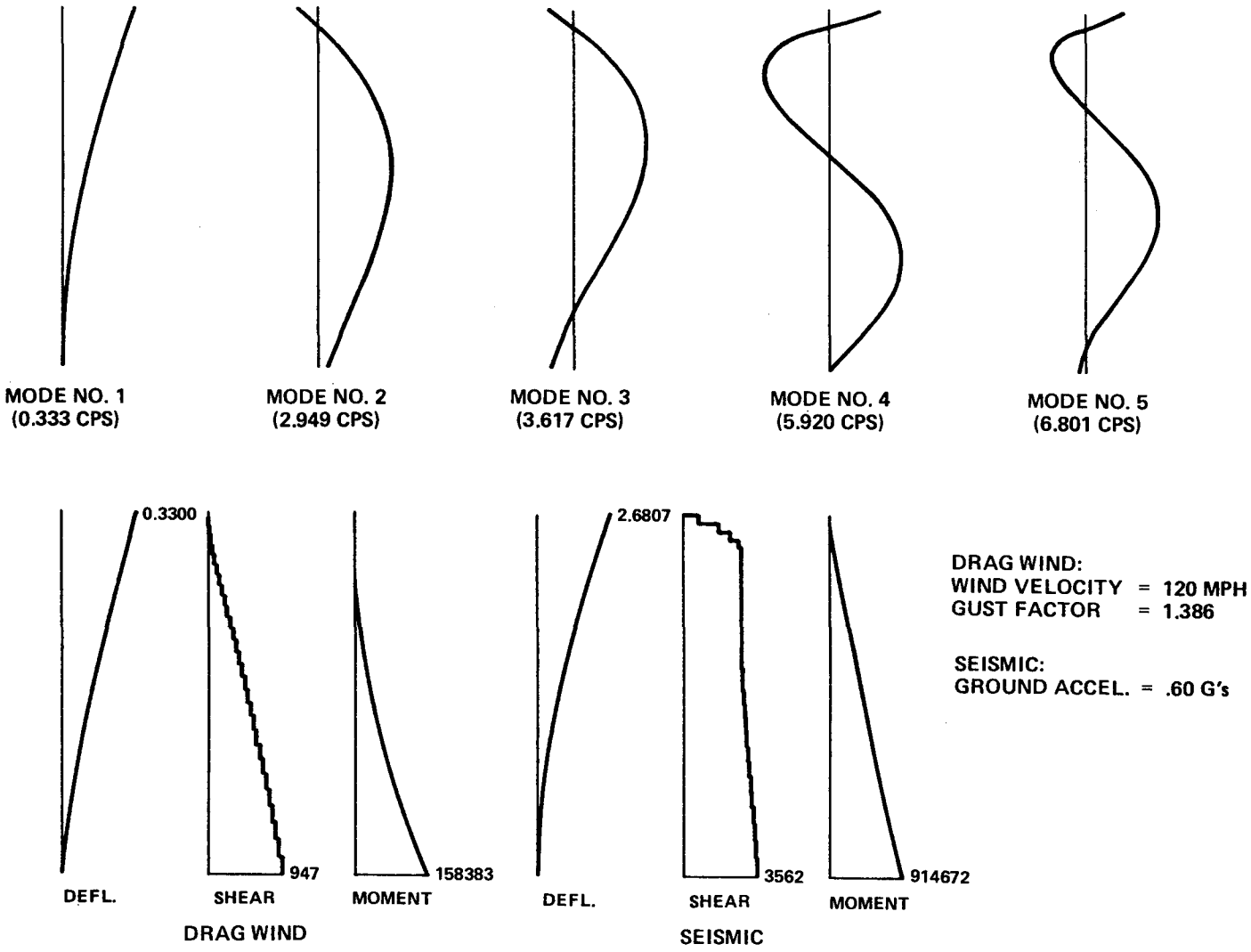

Figure 3. Trial Tower Design No. 13 (300-ft steel tower with 8000 kip receiver, Run No. 3B)

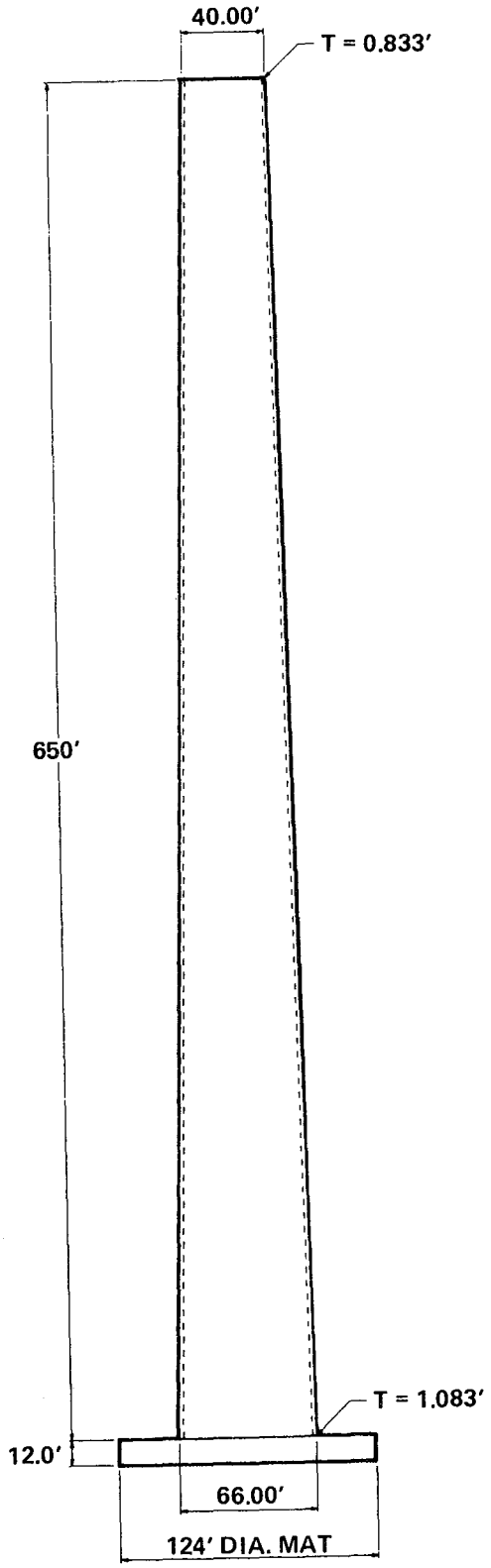

Figure 4. Trial Tower Design No. 8

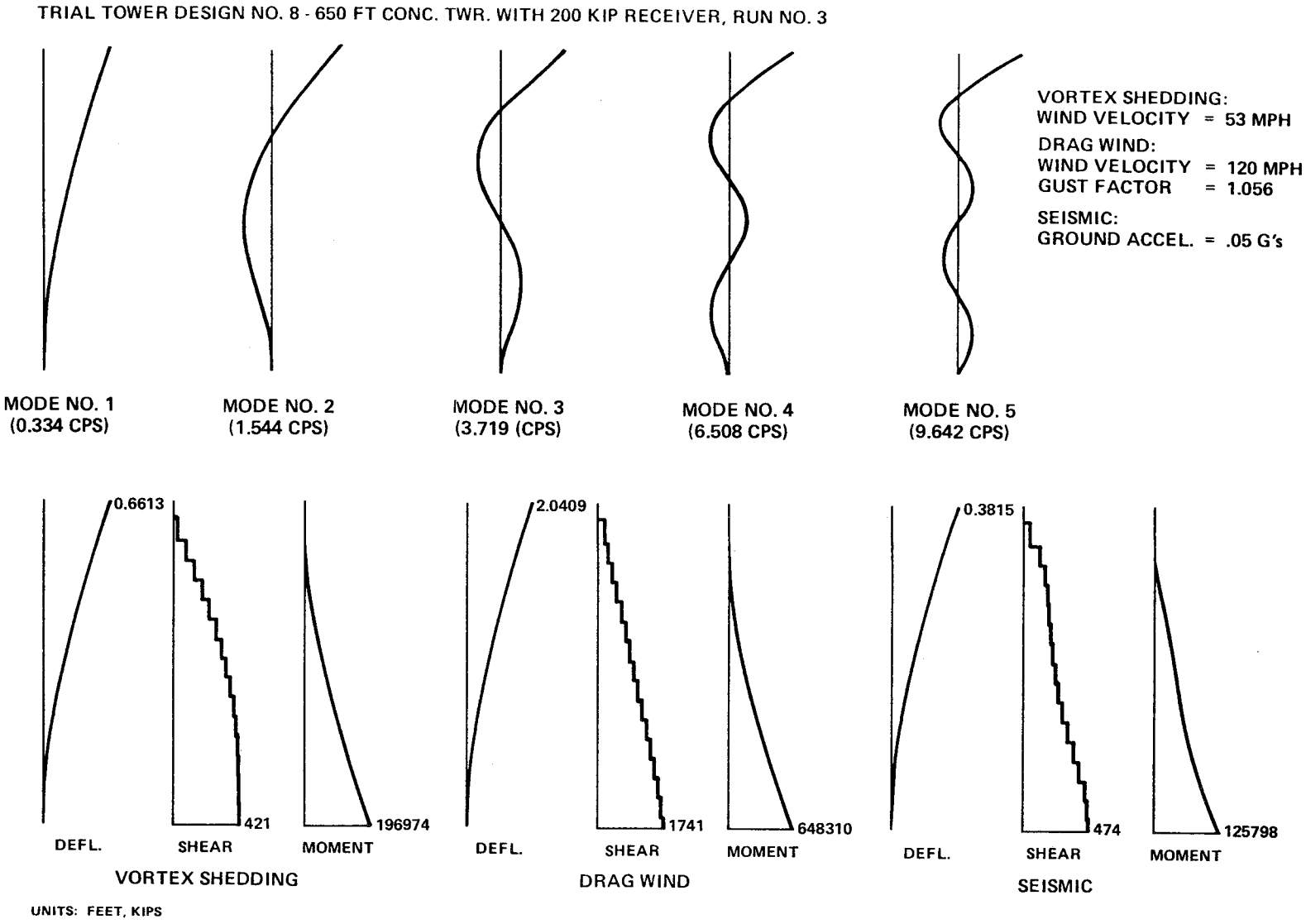

Figure 5. Trial Tower Design No. 8 (650-ft concrete tower with 200 kip receiver, Run No. 3)

DESCRIPTION	TRIAL TOWER DESIGN NUMBER				
	1	3	5	7	9
RECEIVER WT. (KIPS)	200	200	8000	8000	200
GROUND ACCEL (G'S)	0.05	0.05	0.05	0.05	0.05*
WIND VELOCITY (MPH)	70*	70*	120*	120*	70
SOIL SHEAR MODULUS (KSI)	10	∞	∞	10	∞
ALLOW. SOIL BEAR (KSF)	4	4	4	4	12
TOWER HEIGHT (FT)	300	650	300	650	300
TOTAL TOWER WEIGHT (TONS)	116	626	485	3378	204
TOWER COST (MILLIONS $)	.126	.728	.533	3.822	.223
FOUNDATION COST (MILLIONS $)	.144	.352	.367	3.187	.699
TOTAL COST (MILLIONS $)	.270	1.080	.900	7.009	.892

* CONTROLLING LOAD CONDITION

Figure 6. Summary - Steel Tower Quantities and Costs

DESCRIPTION	TRIAL TOWER DESIGN NUMBER			
	11	13	15	20
RECEIVER WT. (KIPS)	200	8000	8000	350
GROUND ACCEL (G's)	0.60*	0.60*	0.60*	0.30*
WIND VELOCITY (MPH)	70*	120	120*	90
SOIL SHEAR MODULUS (KSI)	10	10	∞	∞
ALLOW. SOIL BEAR (KSF)	12	12	12	10
TOWER HEIGHT (FT)	650	300	650	210
TOTAL TOWER WEIGHT (TONS)	1237	1089	3419	95
TOWER COST (MILLIONS $)	1.396	1.195	3.864	.105
CONCRETE VOLUME (CY)	4224	7952	16965	800
FOUNDATION COST (MILLIONS $)	.942	1.783	3.983	.178
TOTAL COST (MILLIONS $)	2.338	2.978	7.647	.283

* CONTROLLING LOAD CONDITION

Figure 7. Summary - Steel Tower Quantities and Costs

TRIAL TOWER DESIGN NO.	TOWER HT. (FT)	COST (MILLIONS $)	RECEIVER WT. (KIPS)	GROUND ACCEL. (G's)	WIND VELOCITY MPH
1	300	.270	200	.05	70*
13	300	2.978	8000	.60*	120
3	650	1.080	200	.05	70*
15	650	7.647	8000	.60*	120*

* CONTROLLING LOAD CONDITION

Figure 8. Extreme Costs - Steel Towers

3. The least costly 650-foot-high tower is trial tower design number three ($1,080,000). It supports a receiver weighing 200 kips and is designed for wind and seismic loads of 70 miles per hour and 0.05 Gs, respectively.

4. The most costly 650-ft-high tower is trial tower design number fifteen ($7,647,000). It supports a receiver weighing 8000 kips and is designed for wind and seismic loads of 120 miles per hour and 0.60 Gs, respectively.

Receiver weight has a significant effect on the cost of the steel towers. For a given tower height wind loads increase with heavier receivers due to an increase in the wind gust factor resulting from a lowering of the fundamental natural frequency of the tower. With regard to seismic loads, although the fundamental frequency is lowered, which reduces the first mode spectral acceleration, this effect is more than offset by the heavier receiver mass.

Concrete Tower Summary - Material Quantities and Costs

The next set of viewgraphs (Figures 9 and 10) shows tables summarizing the design parameters, material quantities, and costs of the concrete towers.

An inspection of the tables (Figure 11) indicates the following:

1. The least costly 300-foot-high tower is trial tower design number six ($334,000). It supports a receiver weighing 8000 kips and is designed for wind and seismic loads of 70 miles per hour and 0.05 Gs, respectively.

2. The most costly 300-foot-high tower is trial tower design number fourteen ($3,954,000). It supports a receiver weighing 8000 kips and is designed for wind and seismic loads of 70 miles per hour and 0.60 Gs, respectively.

DESCRIPTION	TRIAL TOWER DESIGN NUMBER				
	2	4	6	8	10
RECEIVER WT. (KIPS)	200	8000	8000	200	200
GROUND ACCEL (G's)	0.05	0.05	0.05*	0.05	0.60*
WIND VELOCITY (MPH)	120*	70*	70*	120*	120
SOIL SHEAR MODULUS (KSI)	10	10	∞	∞	∞
ALLOW. SOIL BEAR. (KSF)	12	12	12	12	4
TOWER HT. (FT)	300	650	300	650	300
CONCRETE VOL. (CY)	584	3066	584	3811	632
TOWER COST (MILLION $)	.299	1.140	.277	1.450	.383
CONCRETE VOL. (CY)	838	1490	269	5367	7156
FDN. COST (MILLION $)	.187	.366	.057	1.177	1.569
TOTAL COST (MILLIONS $)	.486	1.506	.334	2.627	1.952

* CONTROLLING LOAD CONDITION

Figure 9. Summary - Concrete Tower Quantities & Costs

DESCRIPTION	TRIAL TOWER DESIGN NUMBER					
	12	14	16	17	18	19
RECEIVER WT. (KIPS)	200	8000	8000	500	5200	1400
GROUND ACCEL (G's)	0.60*	0.60*	0.60*	0.30*	0.30*	0.30*
WIND VELOCITY (MPH)	120	70	70	90	90	90
SOIL SHEAR MODULUS (KSI)	10	10	∞	∞	∞	∞
ALLOW. SOIL BEAR. (KSF)	4	4	4	10	10	10
TOWER HT. (FT)	650	300	650	475	650	620
CONCRETE VOL. (CY)	6404	2272	3811	1716	3811	3563
TOWER COST (MILLION $)	2.300	.889	1.920	.784	1.470	1.410
CONCRETE VOL. (CY)	24621	13963	18974	5027	7854	7854
FDN. COST (MILLION $)	5.400	3.065	4.157	1.103	1.722	1.722
TOTAL COST (MILLIONS $)	7.700	3.954	6.077	1.887	3.192	3.132

*CONTROLLING LOAD CONDITION

Figure 10. Summary - Concrete Tower Quantities & Costs

TRIAL TOWER DESIGN NO.	TOWER HT. (FT)	COST (MILLIONS $)	RECEIVER WT. (KIPS)	GROUND ACCEL. (G's)	WIND VELOCITY MPH
6	300	.334	8000	.05*	70*
14	300	3.954	8000	.60*	70
4	650	1.506	8000	.05	70*
12	650	7.700	200	.60*	120

* CONTROLLING LOAD CONDITION

Figure 11. Extreme Costs - Concrete Towers

3. The least costly 650-foot-high tower is trial tower design number four ($1,506,000). It supports a receiver weighing 8000 kips and is designed for wind and seismic loads of 70 miles per hour and 0.05 Gs, respectively.

4. The most costly 650-foot-high tower is trial tower design number twelve ($7,700,000). It supports a receiver weighing 200 kips and is designed for wind and seismic loads of 120 miles per hour and 0.60 Gs, respectively.

An interesting observation can be made with regard to the influence of the receiver mass on seismic loads for the 650-foot-high towers. Since the mass of these towers is quite large when compared to that of the receiver, a reduction in the first mode spectral acceleration produces a smaller response to seismic loads (Figure 12). A comparison of trial tower design number twelve (200 kip receiver) and trial tower design number sixteen (8000 kip receiver) indicates that because tower number sixteen supports a heavier receiver, its fundamental natural frequency and corresponding first mode spectral acceleration will be less than that of tower number twelve. Hence the situation exists where the tower supporting the lighter receiver is more costly than the tower supporting the heavier receiver.

Phase II of this study will consist of thirteen additional towers--six concrete and seven structural steel. They will have various different parameters designed to fill out Sandia's statistical model.

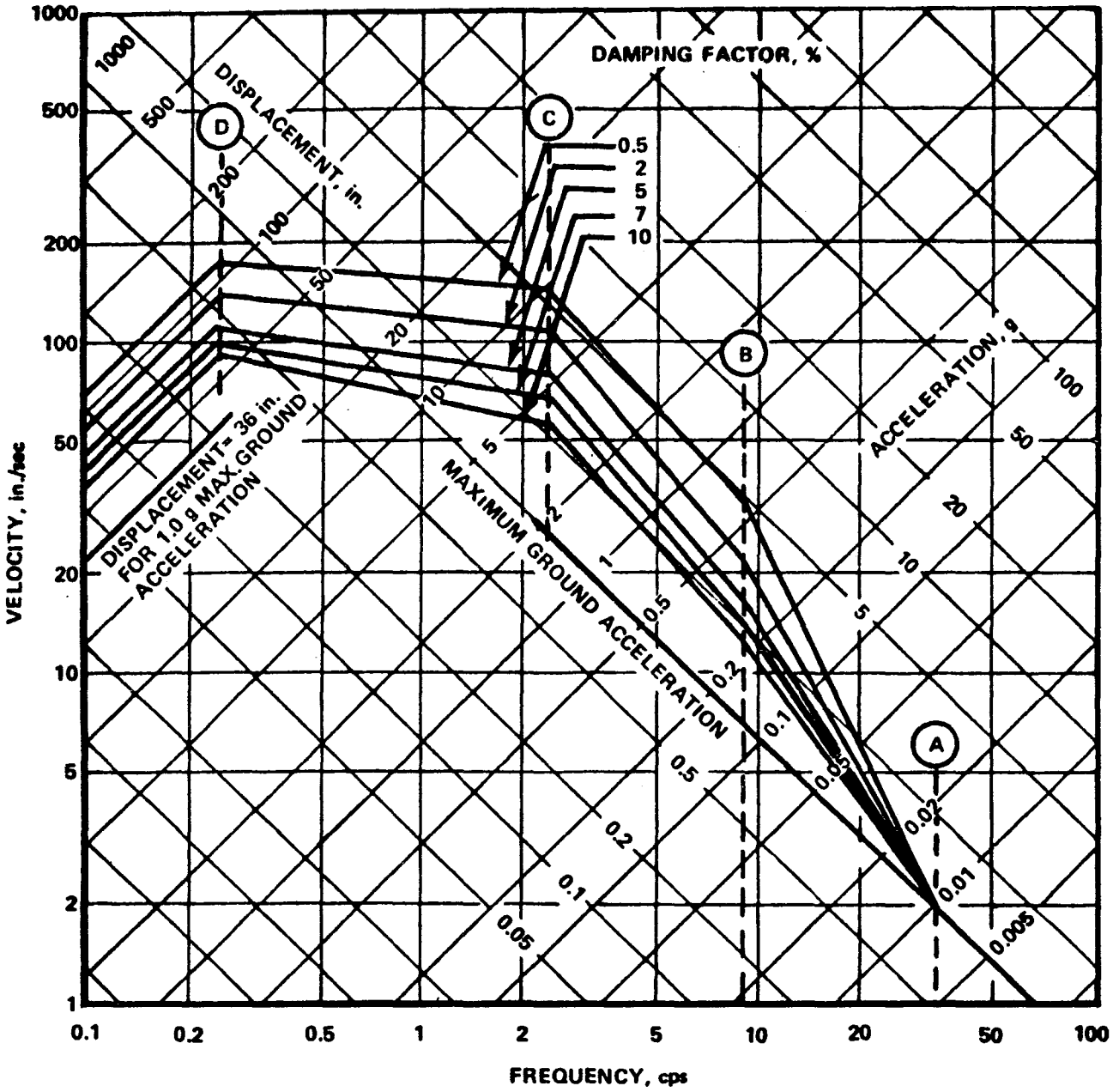

Figure 12. Horizontal Design Response Spectra
(Scaled to 1G Horizontal Ground Acceleration)

AN EXPERIMENTAL INVESTIGATION OF CONVECTIVE LOSSES FROM SOLAR RECEIVERS

A. M. Clausing, G. L. Clark, Jr.,
M. H. Mueller, J. G. Weiner
University of Illinois

Introduction

The UIUC Cryogenic Heat Transfer Tunnel, shown schematically in Figure 1 and 2, has been completed. It was designed to simultaneously obtain high Reynolds and Grashof numbers in order to study the convective loss from solar receivers. Figure 3 shows the approximate operating envelope of the new facility, the regions previously explored by other investigators, and the extreme operating conditions of typical receivers. When the heat transfer and flow validations have been completed, the UIUC facility will provide a means to: (i) drastically extend the range of available combined convection data, (ii) improve our understanding of combined convection mechanisms, and (iii) improve the predictions of convective losses from solar receivers.

Tunnel Validation

Velocity Distribution

Earlier velocity testing indicated some flow separation downstream of the sharp 180 degree turn before the test section (see Figure 4). To investigate the effects of reorienting some nearby cornering vanes, water table experiments were conducted. The original vane configuration proved to be superior to the high-lift arrangement, proposed by Frey and Vasuki[1] (Figure 5), and was retained.

[1]Frey, K. P. H. and Vasuki, N. C., "Detached Flow and Control," University of Delaware, Newark, 1966.

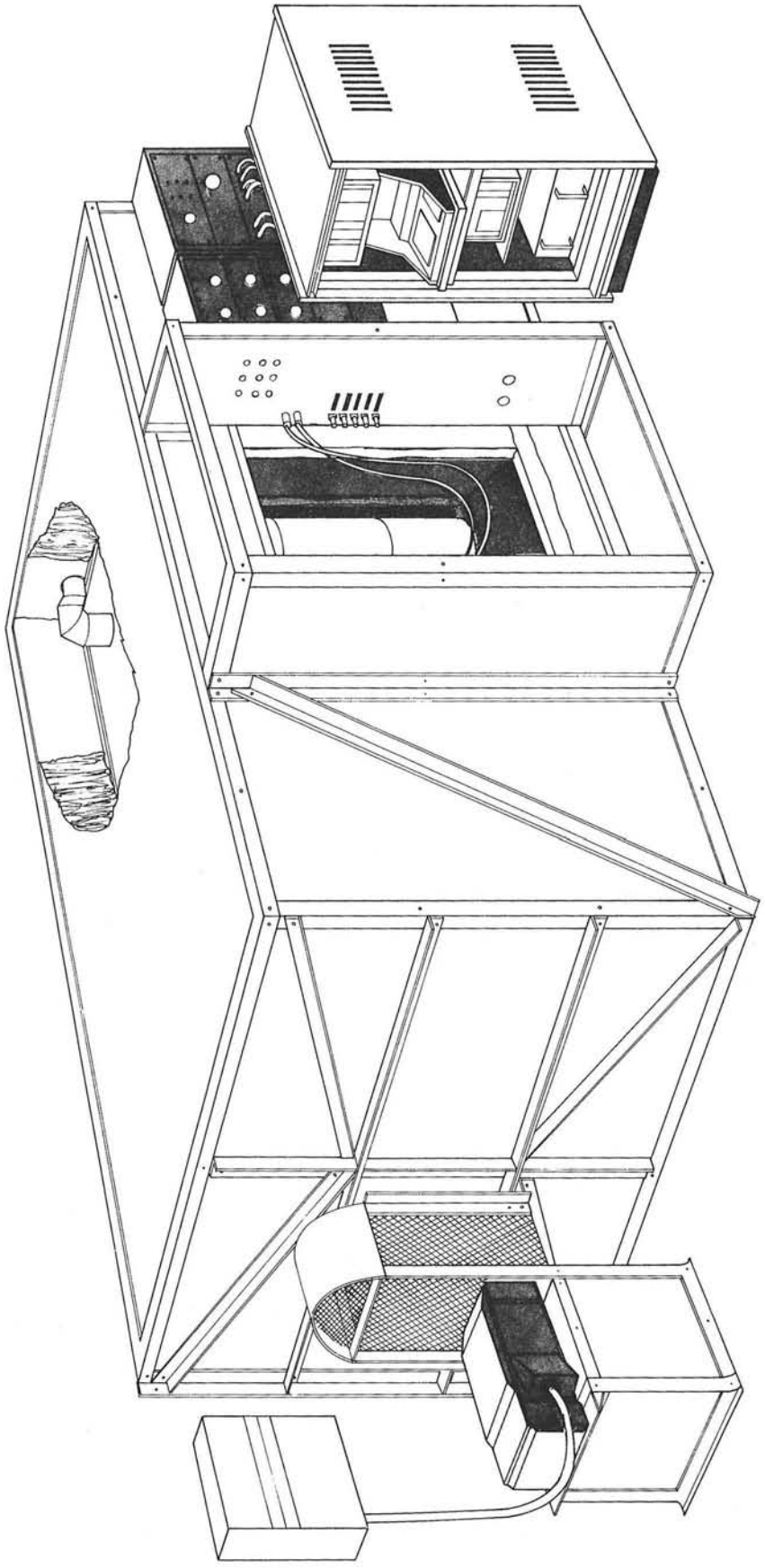

Figure 1. External View of the Cryogenic Heat Transfer Tunnel

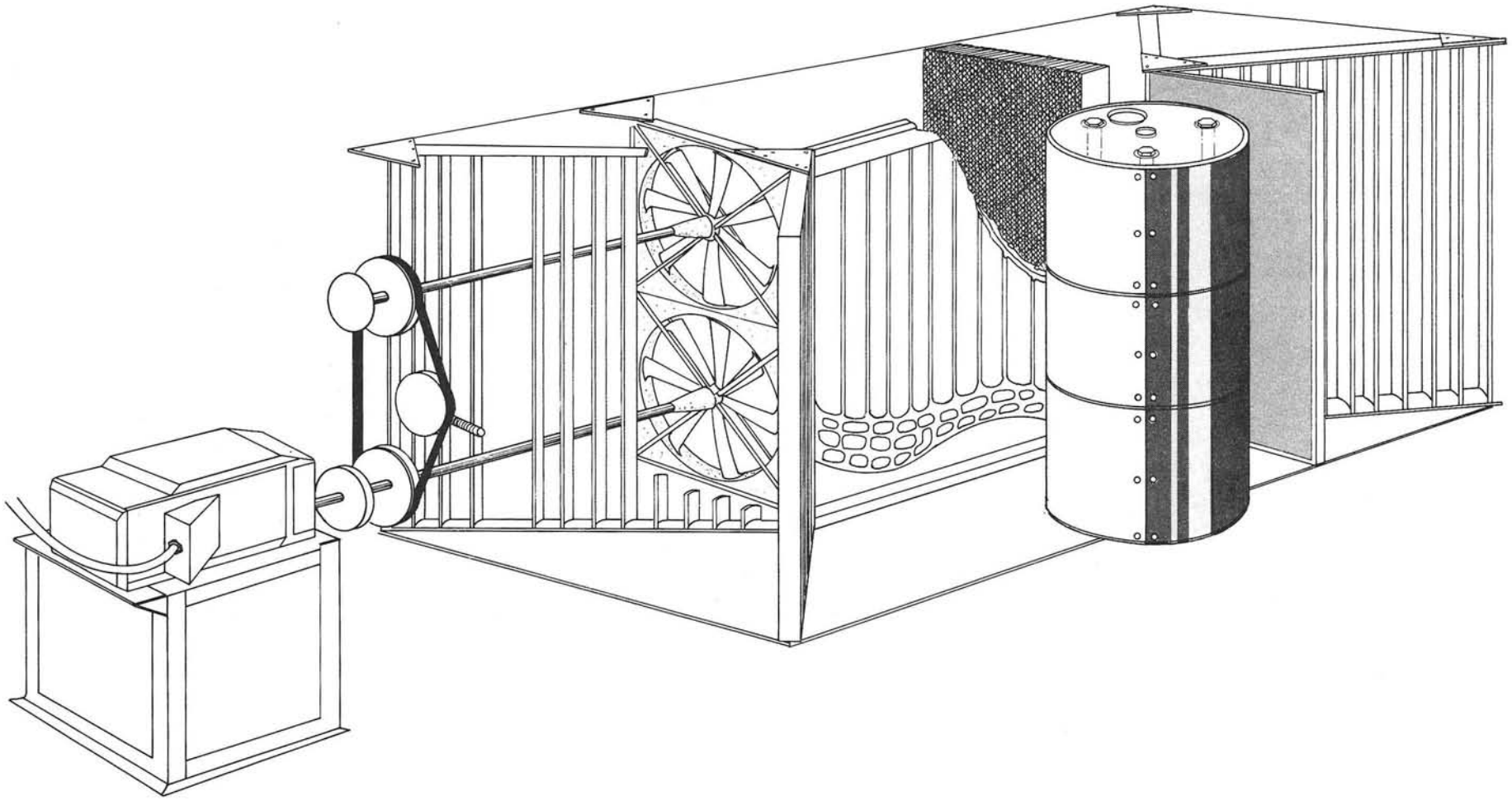

Figure 2. Sectioned View of the Tunnel Interior

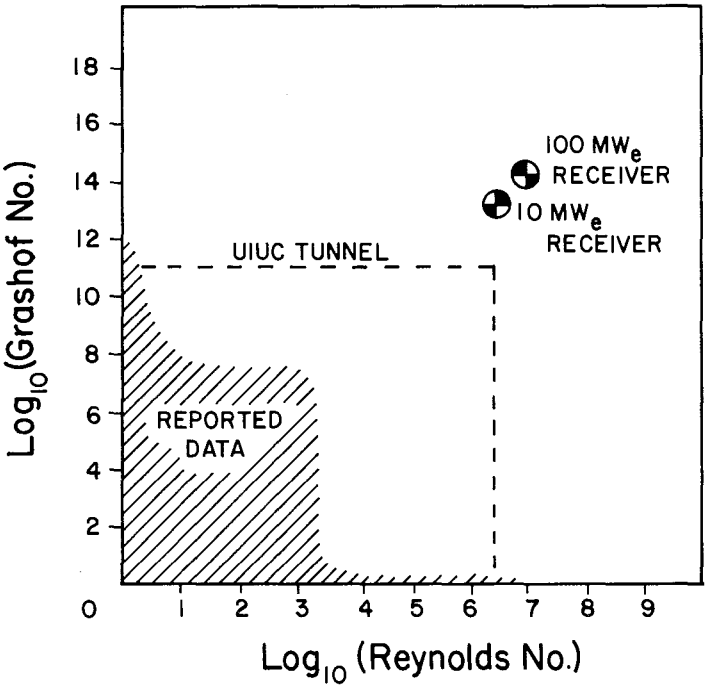

Figure 3. Operating Range of the UIUC Tunnel

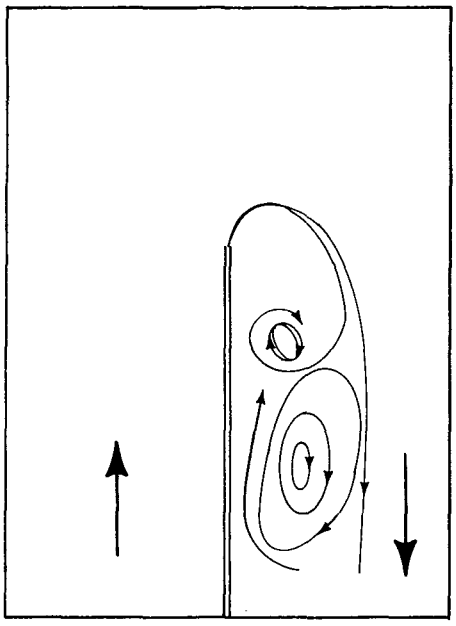

Figure 4. Flow Separation Downstream From a Sharp Corner

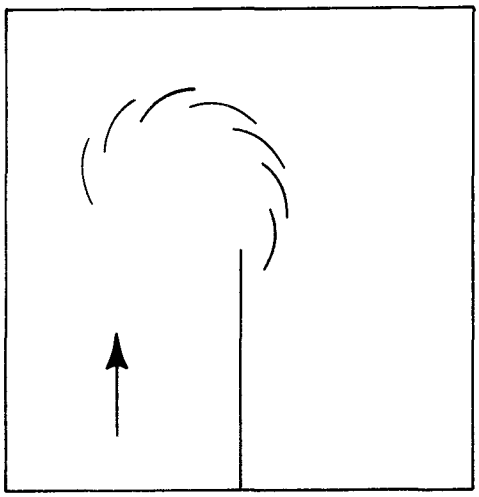

Figure 5. High Lift Vane Configuration
(after Frey and Vasuki)

Addition of a settling screen, upstream from the test section, reduced non-uniformity for both velocity by 45 percent and pitch angles by 37 percent. The mean velocity was reduced from 9.4 to 8.6 m/s due to increased drag.

Significant non-uniformities were still apparent in the flow. Modifications were made to the vaporizer shields and cornering vanes in order to move unavoidable flow restrictions as far upstream as possible. A flow straightener was inserted between the fans and the following downstream corner, as shown in Figure 6. The unit was constructed of round (30.5 mm diameter) tubes with a slenderness ratio of 7:1. As a result of these modifications, velocity non-uniformity was reduced an additional 44 percent (-69 percent total) and pitch angle non-uniformity was reduced an additional 75 percent (-84 percent total). The cost of the improvement was an additional velocity reduction of 3.5 percent to 8.3 m/s.

Next, the round-tube straightener was replaced by a commercial aluminum honeycomb with 9.5 mm cell size and a slenderness ratio of 16:1. Velocity non-uniformity was reduced an additional 71 percent to ±1.8 percent of the mean flow velocity and pitch angle non-uniformity was unchanged.

Free Stream Turbulence

The turbulence of the incoming fluid exerts an important influence on the heat transfer from cylinders in cross-flow. In order to compare the results of experimental studies in different facilities, it is desirable to know the intensity and the scale of the free stream turbulence. The intensity of turbulence, a measure of the temporal velocity fluctuation, has a much larger effect on the Nusselt number than does the scale[2] which characterizes the eddy size.

[2]Lowery, G. W. and R. I. Vachon, "The Effect of Turbulence on Heat Transfer from Heated Cylinders," Int Journal of Heat and Mass Transfer, Vol. 18, pp. 1229-1242, 1975.

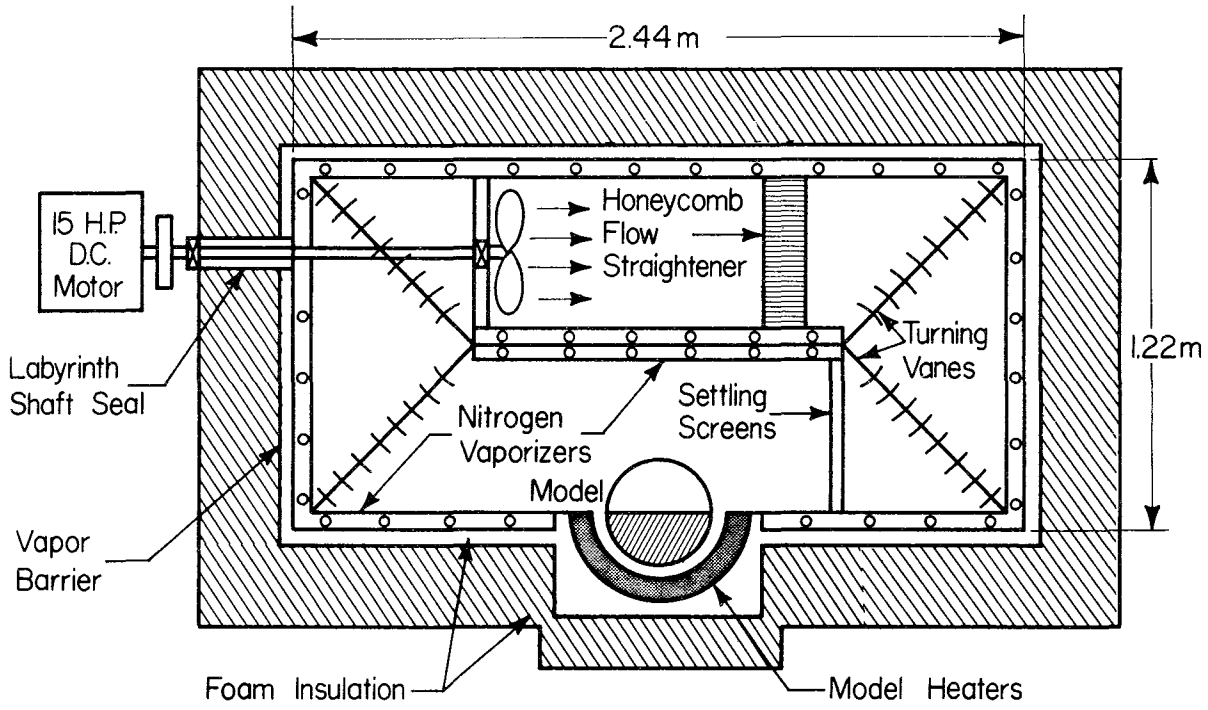

Figure 6. Schematic Diagram of the Cryogenic Wind Tunnel

Measurements of both quantities are being conducted using the hot film anemometry equipment shown schematically in Figure 7. Early indications are that the magnitudes of both intensity and scale are within the range for which corrections are available in the literature.[3]

Forced Convection

When combined convection results have been obtained, it will be desirable to report the specific effects of the additional buoyancy-induced flow on the forced convection heat transfer. The local Nusselt number for combined convection could be directly compared to forced convection data from the literature. Unfortunately this procedure would allow differences due to tunnel variables (blockage ratio, turbulence, etc.) to masquerade as buoyancy effects--an unacceptable situation. To avoid this source of error and to allow a direct comparison of cases, it is considered essential that forced convection measurements be made in the UIUC tunnel. A special low aspect ratio model is under construction, and testing is scheduled for late March.

[3]Morgan, V. T., "The Overall Convective Heat Transfer from Smooth Circular Cylinders," Advances in Heat Transfer, Vol. II, pp. 199-264, 1975.

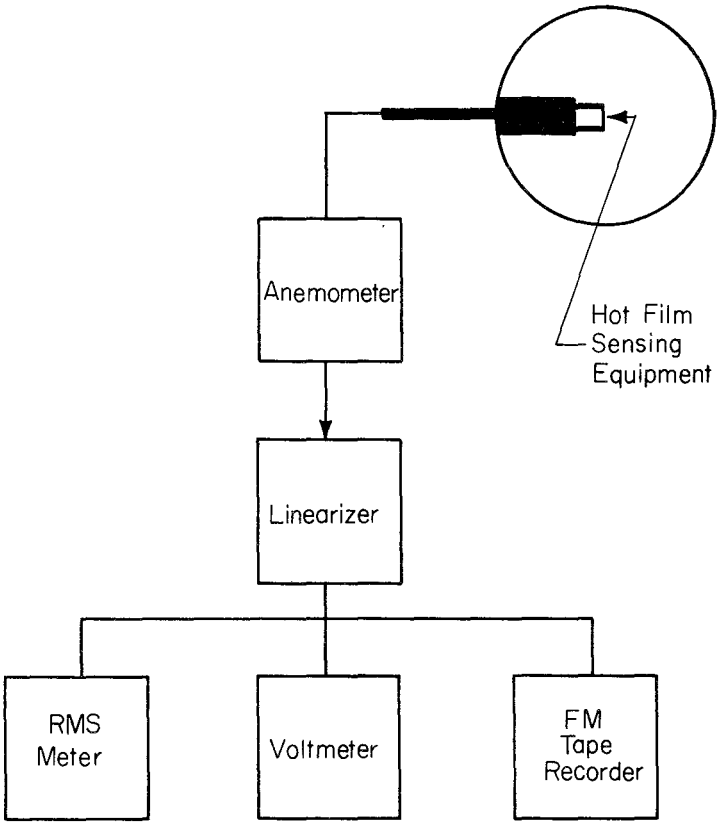

Figure 7. Turbulence Measuring Equipment

Cryogenic Tests

The third cold test was conducted on January 11, 1979. The purpose was to determine the effects of the soldered-copper vapor barrier on the low-temperature performance of the tunnel. The vapor barrier was installed when alternate methods of sealing the cryogenic chamber against infiltration proved unsuccessful. The modified tunnel operated without problems; a summary of measured performance parameters follows.

Cooling time (ambient to 90K)	2.25 hr
Initial LN_2 flow rate	1.6 /min
Cooling rate (from ambient temperature)	1-1.5 K/min
Minimum temperature achieved	84.4K
Temperature variation (fans idle, 90K)	9.5K
Temperature variation (fans operating, 90K)	1.2K
Maximum velocity (90K)	10.5 m/s
Heating rate (maximum power input)	4 K/min

ANALYSIS OF MESOSCALE WEATHER AND CLIMATE CHANGES CAUSED BY LARGE SOLAR ELECTRIC POWER PLANTS AND THEIR EFFECT ON PLANT PERFORMANCE

Chandrakant M. Bhumralkar
Arthur J. Slemmons
SRI International

Objectives

The objectives of this research are to:

- Analyze the effects of large solar thermal electric plants on local and regional weather
- Determine the effects of changes in weather (if any) on the performance of the solar thermal electric plant

In order to achieve the first objective we propose to use a mesoscale atmospheric model that has been specifically designed to study advertent or inadvertent modifications of local/regional atmospheric conditions caused by localized sources of heat and moisture as well as by localized changes in the surface energy balance.

Progress

During the past six months we have been conducting preliminary research to determine the site location, design, and capacity of a solar thermal power plant for use with our mesoscale model. We have also identified various characteristics of the solar thermal plant for incorporating in our atmospheric model.

While we performed these tasks for the DOE project, we were working on a related project for the Institute for Applied Systems Analysis (IIASA), Laxemburg, Austria, which also involved analyzing the impact of large solar thermal power parks on local and regional weather. The results of this research are described below. We believe that the experience gained during this related project will be of value to the current DOE project.

Description of Related Research

In this related study we considered the "power tower" central receiver configuration type of solar thermal electric conversion (STEC) system in which solar energy is focused by an array of two-axis aiming reflectors (heliostats) onto a central tower receiver. The receiver produces either superheated steam for operating a steam turbine of conventional design or very hot air or other gases for operating a high-temperature, Brayton-cycle gas turbine. The steam-generating systems also require cooling in the form of wet or dry cooling towers.

The major changes caused by the installation of a STEC facility that have implications for regional meteorological conditions are:

- Changes in the surface-energy balance due to changes in the reflectivity (albedo) of the surface or its thermal characteristics.
- Changes in surface roughness caused by power plant ancillaries and heliostats.
- Changes in surface hydrological characteristics--e.g., wetness, if the area is paved.
- Dissipation of waste heat into the atmosphere from cooling towers.

Numerical Mesoscale Atmospheric Model

The important characteristics of the mesoscale model used in this study are shown in Table I.

The equations are formulated for a vertical plane normal to the power plant by using a rectangular coordinate system $xy\sigma$, where x is normal to the power plant, y is parallel to it, and σ is along the vertical. The dependent variables are predicted by the equations

Horizontal equations of motion:

$$\frac{\partial u}{\partial t} = -u\frac{\partial u}{\partial x} - \dot{\sigma}\frac{\partial u}{\partial \sigma} + fv - c_p\,\theta\frac{\partial}{\partial x}\left(\frac{p}{p_o}\right)^k - g(1-\sigma)\frac{\partial h}{\partial x} + \frac{1}{(H-h)^2}\frac{\partial}{\partial \sigma}\left(K_z\frac{\partial u}{\partial \sigma}\right) + K_x\left[\frac{\partial^2 u}{\partial x^2} - \frac{1-\sigma}{H-h}\left(\frac{\partial^2 u}{\partial \sigma \partial x}\right)\frac{\partial h}{\partial x}\right] \tag{1}$$

$$\frac{\partial v}{\partial t} = -u\frac{\partial v}{\partial x} - \dot{\sigma}\frac{\partial v}{\partial \sigma} + f(u_g - u) + \frac{1}{(H-h)^2}\frac{\partial}{\partial \sigma}\left(K_z\frac{\partial v}{\partial \sigma}\right) + K_x\left[\frac{\partial^2 v}{\partial x^2} - \frac{1-\sigma}{H-h}\left(\frac{\partial^2 v}{\partial \sigma \partial x}\right)\frac{\partial h}{\partial x}\right] \tag{2}$$

TABLE I

SOME IMPORTANT CHARACTERISTICS OF THE MESOSCALE MODEL

Characteristics	Treatment in Model
Geometry	Rectilinear, two-dimensional vertical cross section
Domain	Variable grid mesh size
Model equations	Hydrodynamic, thermodynamic, continuity of water substance, hydrostatic
Surface conditions	Prediction equation for surface temperature involving components of surface energy balance
	Includes effects of complex terrain and aerodynamic roughness
Atmospheric boundary layer	Heat and moisture flux through the boundary layer
Treatment of clouds	Large scale clouds, implicit mesoscale clouds, parameterized
Cloud microphysics	Liquid phase only
	Kinematic treatment of water-vapor cycle: vapor → liquid → vapor
	Feedback diabatic effects of condensation and evaporation included
Rainfall	Convective rain parameterized
	Large-scale rain is natural extension of in-cloud micro-physical processes
Environmental interaction	Includes interaction of clouds and environment

Thermodynamic energy equation:

$$\frac{\partial\theta}{\partial t} = -u\frac{\partial\theta}{\partial x} - \dot{\sigma}\frac{\partial\theta}{\partial\sigma} + \frac{1}{(H-h)^2}\left(K_z\frac{\partial\theta}{\partial\sigma}\right) + K_z\left[\frac{\partial^2\theta}{\partial x^2} - \frac{1-\sigma}{H-h}\left(\frac{\partial^2\theta}{\partial\sigma\partial x}\right)\frac{\partial h}{\partial x}\right]$$

$$+ \mathrm{CON}\theta + \frac{\theta}{C_pT}(S_1 + S_2) + \frac{\theta}{C_pT}S_3 \qquad (3)$$

Equations for water vapor plus cloud water, and rainwater:

$$\frac{\partial Q}{\partial t} = -u\frac{\partial Q}{\partial x} - \dot{\sigma}\frac{\partial Q}{\partial\sigma} + \frac{1}{(H-h)^2}\frac{\partial}{\partial\sigma}\left(K_z\frac{\partial Q}{\partial\sigma}\right) + K_x\left[\frac{\partial^2 Q}{\partial x^2} - \frac{1-\sigma}{H-h}\left(\frac{\partial^2 Q}{\partial\sigma\partial x}\right)\frac{\partial h}{\partial x}\right]$$

$$+ \mathrm{CONQ} - \mathrm{AUCON}(Q\rightarrow Q_R) - \mathrm{ACR}(Q\rightarrow Q_R) + \mathrm{EVAP}(Q_R\rightarrow Q) \qquad (4)$$

$$\frac{\partial Q_R}{\partial t} = -u\frac{\partial Q_R}{\partial x} - \dot{\sigma}\frac{\partial Q_R}{\partial\sigma} + \frac{1}{(H-h)^2}\frac{\partial}{\partial\sigma}\left(K_z\frac{\partial Q_R}{\partial\sigma}\right) - \frac{1}{(H-h)^2}\frac{\partial}{\partial\sigma}(\rho_S V_R Q_R)$$

$$+ \mathrm{AUCON}(Q\rightarrow Q_R) + \mathrm{ACR}(Q\rightarrow Q_R) - \mathrm{EVAP}(Q_R\rightarrow Q) \qquad (5)$$

The terms CONθ and CONQ in Equations (3) and (4) represent the effects of subgrid cloud convection. The values $(S_1 + S_2)$ and S_3 in Equation (3) are the contributions to changes in potential temperature θ due to phase change of water substance. The arrows in the different cloud microphysical and precipitation terms in Equations (4) and (5) indicate the direction of conversion of one form to another. For example

(1) Condensation of water vapor into cloud in rising saturated air, and evaporation of cloud in descending air.

(2) Autoconversion (AUCON) of cloud drops into raindrops.

(3) Accretion (ACR) of cloud/raindrops by the larger raindrops.

(4) Evaporation of rain in unsaturated air.

The ground surface temperature T_g is predicted by the equation

$$\left[c + \left(\frac{\lambda c}{2\omega}\right)^{1/2}\right] \frac{\partial T_g}{\partial t} = SW - LW - LH - SH - \left(\frac{\lambda c \omega}{2}\right)^{1/2} (T_g - \overline{T}) \qquad (6)$$

where c is volumetric heat capacity, λ is thermal conductivity, ω is frequency, SW is incoming short-wave radiation, LW is long-wave radiation, LH and SH are, respectively, latent and sensible heat components of surface energy balance, and T is average daily surface temperature.

Description of Numerical Experiments

The atmospheric effects of a conceptual STEC facility located in southern Spain have been investigated. To examine the effects of large-scale installations, we have assumed an area of about 1,000 km^2 for the STEC plant. Such a plant could generate roughly 30 GW(e) and might be considered more as a "solar power park." Figure 1 shows the location of the STEC plant. We have used a cartesian grid consisting of 25 points along the x direction and 12 points along z. A variable grid spacing both in the horizontal and vertical is designed in such a way that we obtain a higher resolution at lower levels and in the vicinity of the power plant complex. The horizontal dimension of the plant itself is 32 km, with heliostats covering a distance of 8 km. We have considered a total horizontal dimension of 400 km so that meteorological conditions upstream and downstream of the STEC plant could be included in the model's domain. The power plant complex, including heliostats, is specified in the model by prescribing albedo values that are characteristic of heliostats and land areas that have been cleared for installation of power plant ancillaries.

Figure 2 shows the division of the land surface in the model that represents the effects of the STEC installation on the surface. It also shows the distribution of the components of the surface energy balance for the areas affected by STEC and also those not so affected. The arrows in Figure 2 indicate the disposition of the incoming direct solar radiation over areas I, II, and VI, which are not affected by the STEC plant. The inset shows, on a more expanded scale, the components of the surface energy balance in the area of the STEC plant, given that there are two types of surface. For the grid points in the land area containing STEC structures, the only difference in the energy balance components arises because of the different reflectivity of the surface. In this study, we consider that the STEC system uses natural draft wet cooling towers for dissipating waste heat into the atmosphere at heights of 100 m or more, in the form of water vapor and sensible heat. This causes the temperature and moisture in the power plant area to be perturbed in relation to the atmosphere surrounding it. We have estimated the perturbation in temperature and water vapor at 200 m above the power plant complex and incremented, at each time step, the predicted temperature and humidity by these perturbations at the grid points located at the power plant complex at a height of 200 m.

Results

Two numerical experiments were performed with the model using initial and boundary conditions typical of the summer and the winter conditions in southern Spain. In each experiment, the integrations consist of two simulations. The first is the "without STEC" case, in which:

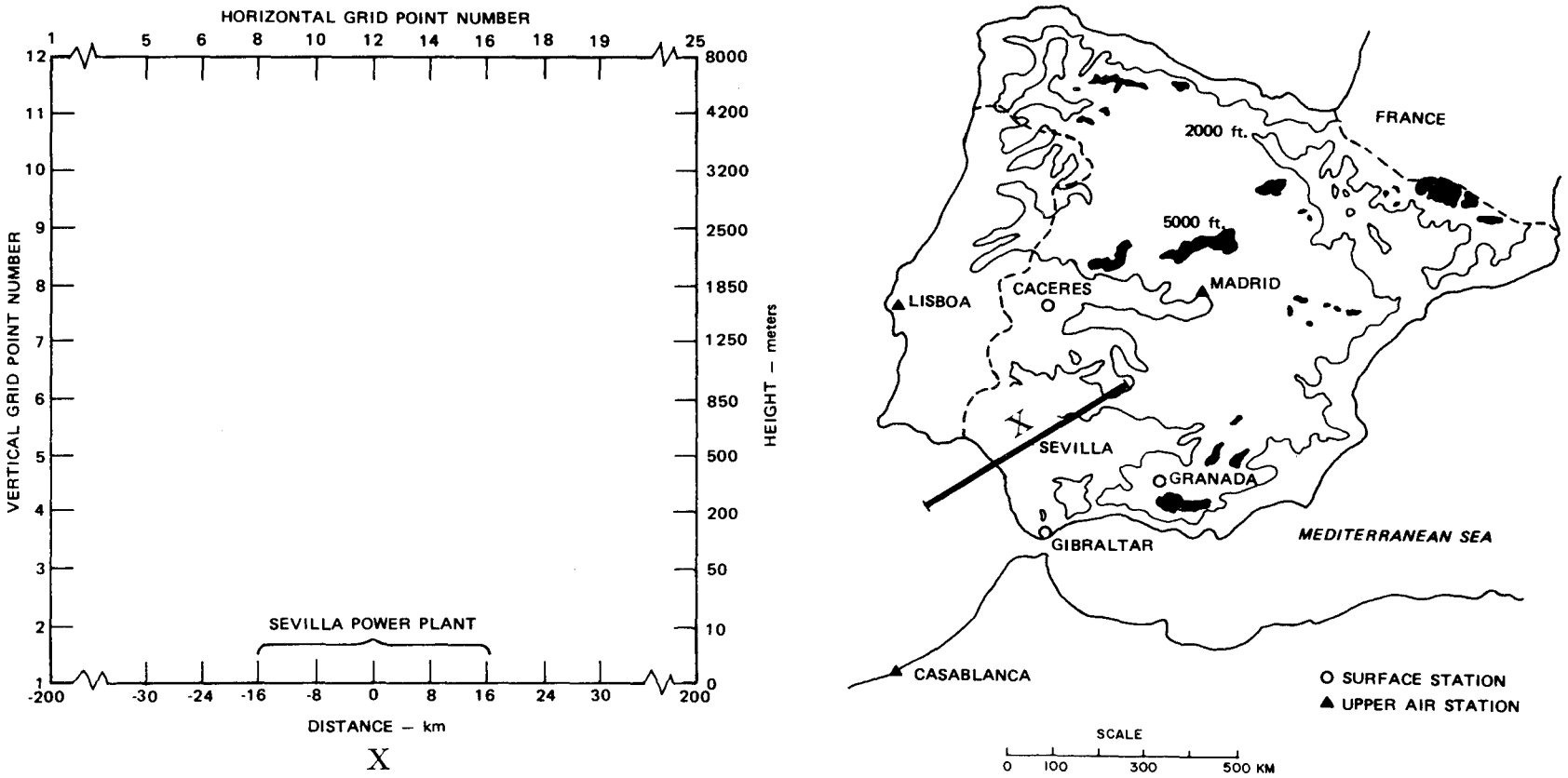

Figure 1. Map Showing Location of Solar Thermal Electric Conversion Plant at Sevilla, Spain

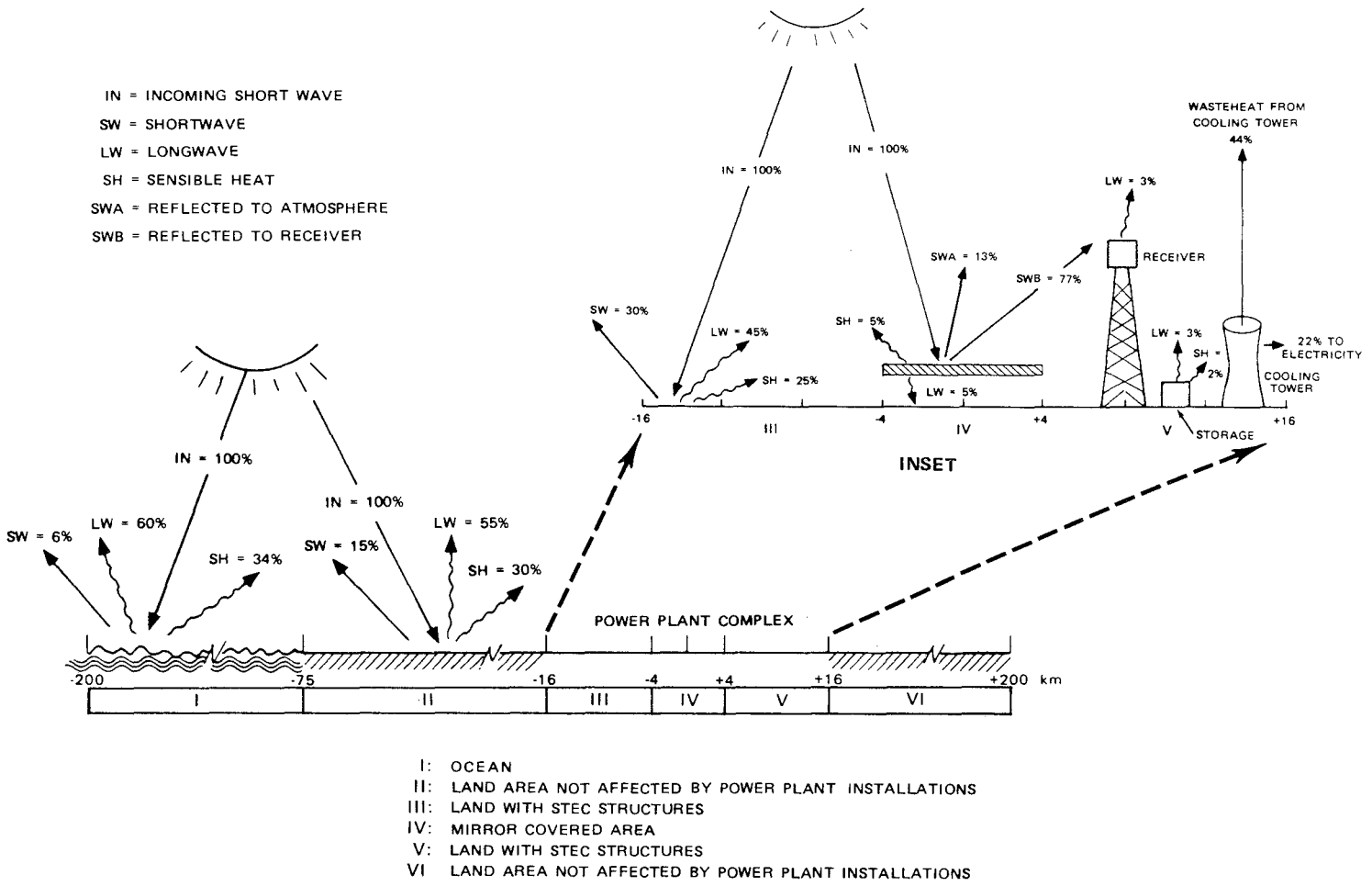

I: OCEAN
II: LAND AREA NOT AFFECTED BY POWER PLANT INSTALLATIONS
III: LAND WITH STEC STRUCTURES
IV: MIRROR COVERED AREA
V: LAND WITH STEC STRUCTURES
VI LAND AREA NOT AFFECTED BY POWER PLANT INSTALLATIONS

Figure 2. Distribution of Solar Energy at the Surface (Inset shows the distribution over surface of power plant complex)

- Surface energy balance is not perturbed
- No waste heat is dissipated into the atmosphere

The second case is the "with STEC" case, in which we introduce into the model domain, at grid points representing the STEC area, the perturbations in the surface energy balance caused by power plant installations and the waste heat dissipated into the atmosphere from cooling towers. In this study we have assumed that the heliostats are all grouped together centrally, covering 25% of (8 km on a side) of the STEC area. We believe this to be a "worst case" assumption, since in reality the heliostats and cooling towers would be distributed rather generally over the entire power plant area.

Initially, there are not deviations of wind, temperature, or humidity from the upwind boundary values over the entire model grid except at the surface, where we allow variations that represent the meteorological and physical characteristics of the underlying terrain. The perturbations due to the STEC are introduced as differential reflectivity (albedo) at the surface and differential potential temperature and relative humidity at a height of 200 m over a length of 32 km. Subsequently, while the surface reflectivity parameters are not changed, the heat and moisture conditions are input at 2-minute integration intervals. This technique enables us to simulate perturbations in surface energy balance and the waste heat dissipated into the atmosphere from cooling towers. The model was integrated for a 9-hour, real-time duration for each case, starting from 0800 hours local time; this implies that the simulation covers the period from 0800 to 1700 hours local time. Figure 3 shows the evolution of relative humidity and cloudiness fields during the 9-hour simulation of the mesoscale model. Figure 3(a) shows the relative humidity field in the model domain at the initial time, and as discussed earlier, at first there are no perturbations in relative humidity. A comparison of the moisture (relative humidity) distribution after 5-1/2 hours of simulation in both the control [Figure 3(b)] and "with STEC" [Figure 3(c)] cases shows that the power plant has caused the model atmosphere to be relatively more moist than that in the control case--there are even clouds. (We define cloud as an area characterized by supersaturation--i.e., relative humidity greater than 100 percent.) A comparison of relative humidity at subsequent times shows very clearly that in the control case the clouds (forming the first time at t = 7 hours) are sporadic and cover relatively small areas of the domain, whereas they are quite pronounced and persistent in the "with STEC" case. Figure 4 shows variation in rainfall at the surface in both the control and "with STEC" cases. Rainfall occurs much earlier in the "with STEC" case and the amount is much greater. These differences can be attributed to changes in the surface energy balance caused by the STEC installations, together with waste heat dissipated into the atmosphere from the cooling tower.

Results of Winter Simulation

We integrated the mesoscale model for 9 hours for the initial conditions corresponding to winter meteorological conditions prevailing in southern Spain and the zenith angle of the sun. The latter affects the amount of short-wave radiation (at the surface) used in calculating the ground surface temperature. The most important result of the winter simulation is that no clouds formed anywhere in the model domain during the simulation of both the control (without STEC) and "with STEC" cases. Figure 5 shows the relative humidity field after

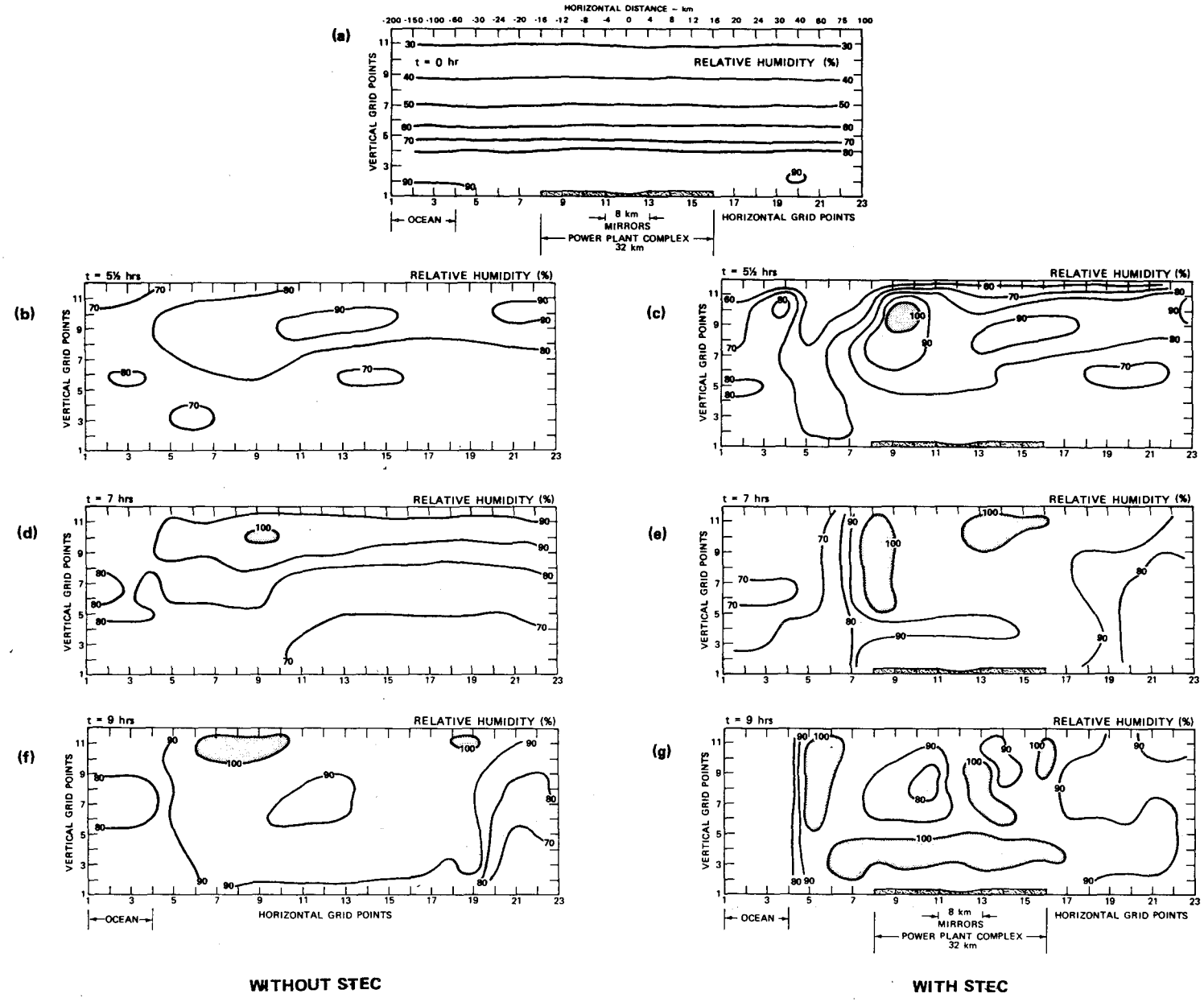

Figure 3. Simulated Relative Humidity (Percent) for Summer at T = 0, 5-1/2, 7, and 9 Hours of Real Time (Without STEC (b, d, f) and with STEC (c, e, g); shaded portions represent cloudy supersaturated) areas.)

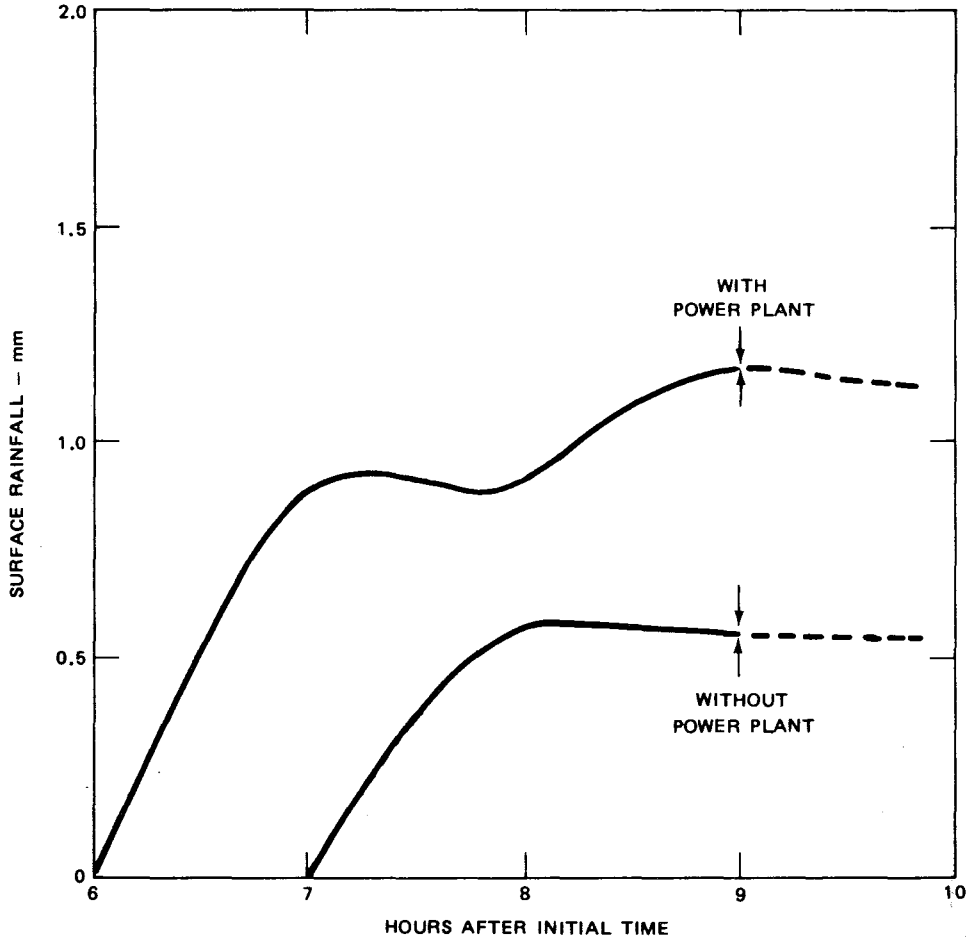

Figure 4. Simulated Surface Rainfall for Summer

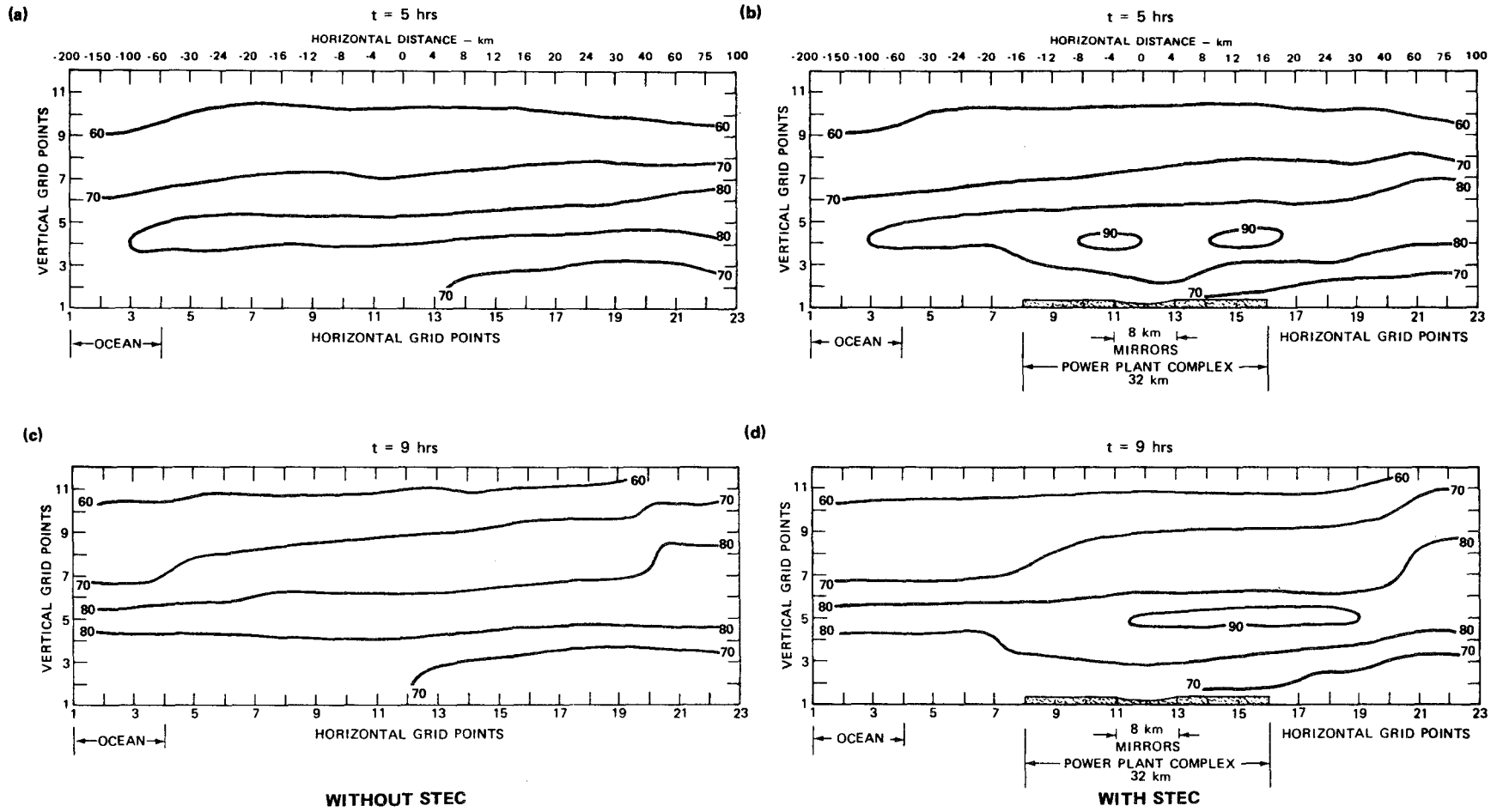

Figure 5. Simulated Relative Humidity (Percent) for Winter at T = 5 and 9 Hours of Real Time for "Without STEC" (a,c) and "With STEC" (b,d)

9 hours of simulation. We believe this to be due to very strong prevailing winds during the winter simulations, which result in advective influences becoming stronger than buoyance and frictional effects, and the air does not stay over the power park long enough to rise to higher levels and form clouds.

Conclusions

The results of model integrations, which should be considered as very preliminary, indicate that for summer meteorological conditions, a STEC installation covering 1,000 km^2 and using wet cooling towers would have a considerable potential for changing atmospheric conditions. These effects extend to a distance of a few hundred kilometers from the power plant. Such effects could, in turn, alter the performance of the STEC plant because of the depletion of solar energy reaching the surface. For the winter case, however, the prevailing wind used in the model simulations was so strong that the area around the STEC plant was ventilated and no regional meteorological effects could be found.

Further simulations are required before definitive conclusions can be drawn about the impacts of STEC plants on regional weather. In particular, there is a need to investigate these impacts over a wide range of meteorological conditions and with variations in the design, areal extent, capacity, and location of the STEC systems. For example, it should be possible to determine the effect of variations in the direction of the prevailing wind, when orienting the STEC system. It would also be valuable to investigate the impact of dry cooling towers instead of wet. The effects of a STEC plant covering a much smaller area, with a much smaller capacity than that considered in this study, should also be investigated.

MATERIALS TESTING FOR CENTRAL RECEIVER SOLAR-THERMAL POWER SYSTEMS

S. Majumdar
Argonne National Laboratory

Background

The present program is concerned with the determination of specific elevated-temperature mechanical properties of materials used for critical components in solar central receiver power systems. Several general features of solar central receiver operating conditions are likely to create difficult structural design problems. The first of these is the highly cyclic nature of the thermal loading of critical components. Solar plants will undergo at least one major start-up and shutdown cycle per day, with the likelihood of additional thermal cycles being imposed by intermittent cloud cover and unscheduled maintenance and repair. Thus critical elevated-temperature components may be expected to accumulate of the order of tens of thousands of thermal and associated strain cycles over a 30-year design life. In addition, repeated thermal cycling of superheater or boiler tubing while under internal pressure can lead to incremental growth or ratchetting. The analyst must therefore design against structural failure caused by thermal fatigue and creep-fatigue interaction and must also avoid excessive deformation caused by incremental growth.

A related feature of solar central receiver operation is the phenomenon of departure from nucleate boiling (DNB), which occurs in the boiler tubing. During daytime operation, coolant water from the condenser first experiences local, or nucleate, boiling as it travels through the boiler tubing. With further heating, general, or film, boiling occurs somewhat farther along the tubing. Since the efficiency of heat transfer from the inner wall of the boiler tubing to the coolant is greatly decreased with the onset of film boiling (i.e., the DNB), a rather abrupt increase in inner-wall temperature is present at the location where DNB occurs. The position of this boundary between film and nucleate boiling in the boiler tubing generally fluctuates in a cyclic manner with time, and the inner wall in this fluctuating region experiences rapid alternate heating and cooling. The frequency of the temperature and associated strain cycles is typically of the order of one cycle per second, and so 10^8 or more cycles may be accumulated over the life of the tubing. Elevated-temperature high-cycle fatigue data on boiler tubing materials are therefore needed to design against possible failure associated with DNB.

The third aspect of solar-plant operating conditions likely to cause design difficulties is that during steady-state operqtion the boiler and superheater tubing will be loaded nonaxisymmetrically at elevated temperatures. In particular, critical passes of the superheater tubing will be loaded during daytime operation such that the outer tubing wall on the high-temperature side will experience a large compressive axial stress and a moderate compressive hoop stress. On the other hand, the inner wall on the high-temperature side will be subjected to a moderate compressive axial stress and a small tensile hoop stress. Considerable information on constitutive relations under compressive and mixed tensile-plus-compressive creep conditions will be required to permit structural analyses of the components. In addition, failure criteria for nonaxisymmetric multiaxial tensile-plus-compressive creep-fatigue conditions must be developed. Finally, the nonaxisymmetric loading further complicates the ratchetting analysis.

Elevated-temperature design rules applicable to solar-power-plant boilers and piping are set forth in Section I of the ASME Boiler and Pressure Vessel Code. However, Section I was not developed with the highly cyclic and often complex loading conditions of solar power plant components in mind, and no specific design rules for treating fatigue, creep fatigue, or ratchetting are provided. Applicable design rules from the nuclear portions of the Code (Section III and Code Case N47) are likely to result in excessively conservative designs. For example, N47 would consider the compressive loading on the hot side of the superheater tubing to be as damaging as an equal tensile loading, although available data indicate that this is not the case for many materials, at least for uniaxial loadings. The ratchetting analysis rules of N47 are also likely to be overly conservative when applied to the nonaxisymmetric multiaxial loading of superheater tubing. Thus a modified set of Code rules is needed that is more appropriate to the design of solar components. The development of these rules, in turn, requires the creation of a supportive base of mechanical-properties data.

In some of the more advanced designs for future solar central receiver systems, liquid sodium is one of the proposed coolants in the central receiver. The heated sodium would flow from the tower to a steam generator at ground level, where the steam to drive the turbines would be produced. Such an arrangement offers several advantages over the direct generation of steam in the receiver tower, including (1) the benefits of the superior heat-transfer characteristics of the sodium coolant, (2) the elimination of high internal pressure in the receiver tubing, and (3) the elimination of problems associated with stress-corrosion cracking and DNB in the receiver tubing. Considerable information has been obtained on sodium effects on structura materials in the Liquid-Metal Fast Breeder Reactor (LMFBR) program. However, this information, particularly with respect to material-sodium compatibility and sodium effects on elevated-temperature mechanical properties, needs to be reviewed and extended to the materials and anticipated operating conditions associated with solar central receiver systems.

Program Objectives

The present program has been developed in response to the needs outlined above and is divided into three subtasks. The first subtask, being performed

in support of solar central receiver designs developed by Martin Marietta Corporation and Honeywell, Inc., is concerned with the beaxial creep-fatigue testing of Type 316-H stainless steel superheater tubing. Current design procedure for the superheater tubing is to perform a creep-fatigue analysis using elevated-temperature nuclear rules (N47) but to ignore creep damage caused by compressive stresses. Thus hold times under compressive stresses are assumed to be nondamaging. As stated above, this assumption appears to be reasonable for austenitic stainless steels under uniaxial loading conditions, but it has never been verified for biaxial loading situations, particularly where the stress is tensile in one direction and compressive in the other. Furthermore, virtually no creep-fatigue data exist for Type 316-H even under uniaxial loading conditions. Under this subtask, biaxial creep-fatigue tests (constant tensile hoop stress and cyclic axial strain with hold times in compression) have been performed on Type 316-H superheater tubing material. Times-to-failure have been shortened by increasing the magnitude of the axial strain range over that expected in service and by using a considerably shorter compressive hold time.

Under the second subtask, a comprehensive survey of available information on sodium effects on candidate materials for solar-thermal electric piping and steam generators has been conducted. The survey includes information on sodium effects on mechanical properties, sodium compatibility, mass-transfer effects, and friction, adhesion, and self-welding behaviors in a sodium environment. A report summarizing the survey and including recommendations for future testing has been completed.

The third subtask is concerned with mechanical-properties data generation in support of the ASME Code development. This work interfaces directly with a program being conducted by Foster Wheeler Energy Corporation entitled "An Interim Structural Design Standard for Solar Energy Applications." In the Foster Wheeler program, design standards and criteria are to be established for solar central receiver systems that will eventually lead to the development of a set of ASME Code rules for Solar Applications. A critical phase in this development is the formulation and execution of an extensive mechanical-testing program to generate the required design-limits data. This mechanical-testing program is to be conducted by Argonne National Laboratory. As an initial effort under this subtask, a test matrix has been developed for the high-cycle fatigue testing of Incoloy 800 boiler tubing under biaxial (constant internal pressure plus cyclic axial loading) conditions. In parallel with the high-cycle fatigue testing, biaxial low-cycle fatigue testing of Incoloy 800 is being carried out with a test matrix which is similar to the test matrix for Type 316-H stainless steel under Subtask 1. Available fatigue data for Incoloy 800 and 800H, totaling some 480 data points, have already been collected and published.

Projected schedules and levels of effort for the three subtasks are as follows:

Subtask	Begin	End	Total Man-Years
1	7/77	11/78	2
2	10/77	12/78	0.5
3	10/78	10/80	5

Accomplishments During Previous Six Months

Subtask 1

All testing (16 tests) under Subtask 1 has been completed. The results are summarized in Table I. A significant development in the last six months was the decision to change the specimen geometry from straight-gauge (parallel-sided) to hourglass (10-in. radius). The slight hourglassing helped to restrict the failure location to the neck area without causing unacceptable stress concentration effects ($K_t \approx 1.01$). Figure 1 shows a comparison of the axial stress responses for identically loaded straight-gauge and hourglass specimens. The difference in the stress response is within the scatter of the data, and the slightly reduced stress for the hourglass specimen may be the result of a 30°C higher temperature at its gauge section compared to the straight-gauge specimens. Figure 2 shows a comparison of the ratchetting strains for the two types of specimen under identical loading. Again, the difference does not appear to be significant. An interesting observation in Figure 2 is the different ratchetting response of the hourglass specimen to tension-hold versus compression-hold loading. From the limited series of tests performed on 1-in. diameter tubular specimens, one can conclude the following for Type 316-H stainless steel:

(1) The addition of up to 2000 psi internal pressure does not adversely affect the continuous-cycling fatigue life at 593°C at a strain range of 0.5 percent.

(2) The imposition of a one-minute tensile hold period every cycle under a biaxial state of stress reduces the fatigue life by almost a factor of five.

(3) The imposition of a one-minute compressive hold period every cycle under a biaxial state of stress does not significantly reduce the fatigue life.

A detailed report including all the data and conclusions will be published in the near future.

Subtask 2

A report entitled "Sodium Effedts on Candidate Materials for Solar-Thermal Electric Superheaters and Steam Generators" has been written and will be published as an ANL report. It summarizes all available mechanical properties of candidate materials in sodium and identifies the most promising material for solar application and key areas that require further technological development.

Subtask 3

Biaxial creep-fatigue testing of 1-in. diameter Incoloy 800 tubing has already been started. Four tests have been completed to date. The test data will be reduced and reported in the next semiannual review.

TABLE I

SUMMARY OF BIAXIAL FATIGUE DATA FOR 316-H STAINLESS STEEL

(T and C Denote Tensile and Compressive Hold, Respectively)

Test No.	Hold Time (min)	Temp. (°C)	Int. Press. (MPa)	Axial Strain Range Total (%)	Axial Strain Range Plastic (%)	Diametral Strain Range (%)	Axial Stress Range (MPa)	Axial Stress Mean (MPa)	Average Hoop Stress (MPa)	N_f (cycles)	Mean Diametral Strain @ N_f (%)	Specimen Type
997	0	574	0	0.51	0.19	0.20	493	1	0	14156	-0.02	Straight Gauge
999	0	576	0	0.50	0.19	0.19	482	0	0	8110	-0.02	
1001	0	568	7.58	0.50	0.17	0.19	510	19	42	16661	+1.05	
1012	0	577	7.58	0.50	0.17	0.20	500	20	42	9229	+0.96	
1031[a]	0	609	13.79	0.50	0.15	0.17	535	1	76	6739	+2.50	
1027[b]	IC	618	0	0.50	0.17	0.21	514	7	0	4047	-0.13	
1024[c]	IC	611	7.58	0.50	0.18	0.18	498	-5	42	5369	+1.19	
1033[a]	IC	606	7.58	0.50	0.17	0.18	507	12	42	4538	+0.83	
1035[a]	IC	593	0	0.49	0.16	0.21	519	1	0	9750	0	Straight Gauge[d]
1038	IT	593	7.58	0.50	0.16	0.17	530	0	42	3821	1.21	Straight Gauge[e]
1041	IT	607	7.58	0.50	0.16	0.18	516	0	42	2746	0.98	Hourglass
1044	0	599	7.58	0.50	0.18	0.20	491	3	42	13474	1.57	
1049	IC	594	7.58	0.50	0.16	0.20	518	10	42	8283	1.98	
1050[a]	IC	594	13.79	0.50	0.12	0.20	582	11	76	6703	4.67	
1052	IC	593	0	0.50	0.17	0.19	509	12	0	13518	-0.10	
1059[c]	0	593	13.79	0.50	0.15	0.19	534	-8	76	14583	3.15	

[a]Specimen failed outside gauge section.

[b]Specimen overstrained due to power interruption.

[c]Specimen failed at thermocouple.

[d]Wall thickness reduced by 0.005 in. at the center by polishing.

[e]Wall thickness reduced by 0.010 in. at the center by polishing.

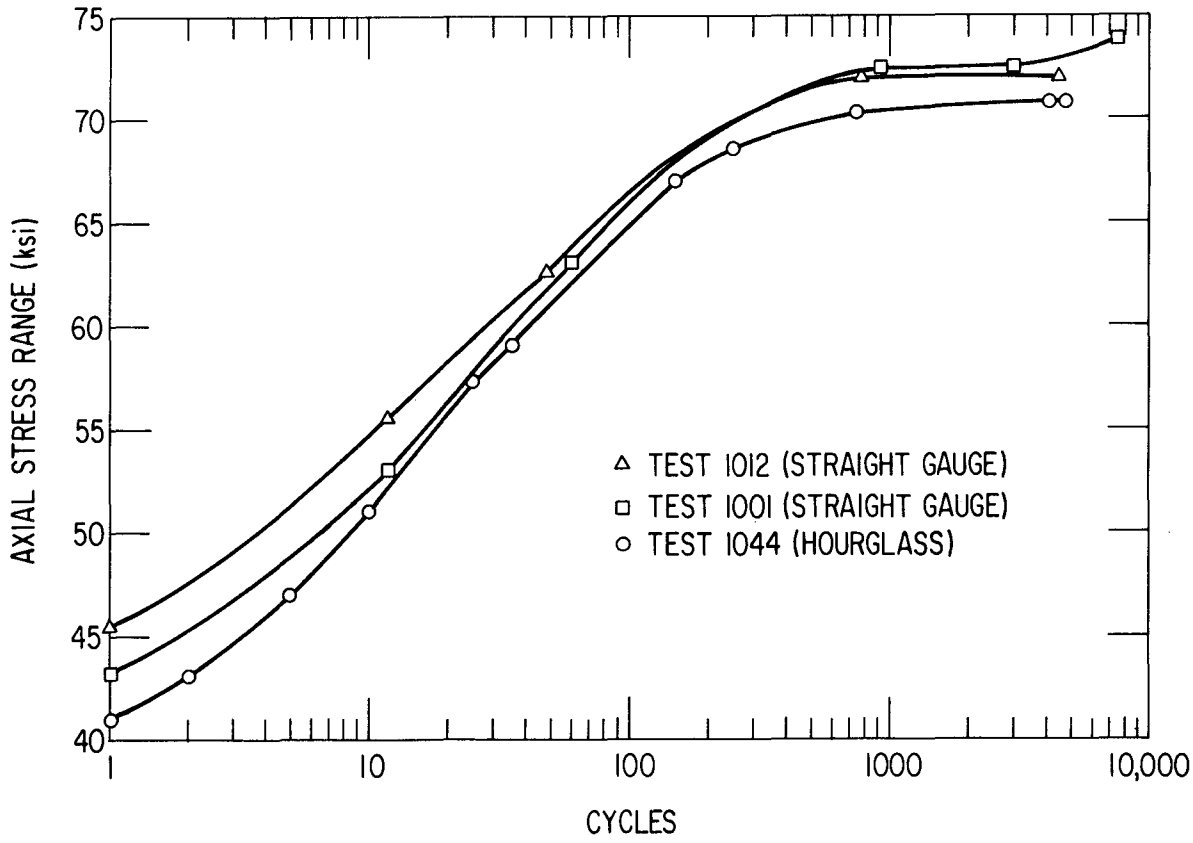

Figure 1. Effect of Specimen Geometry on the Axial Stress Response of Type 316-H Stainless Steel Tube

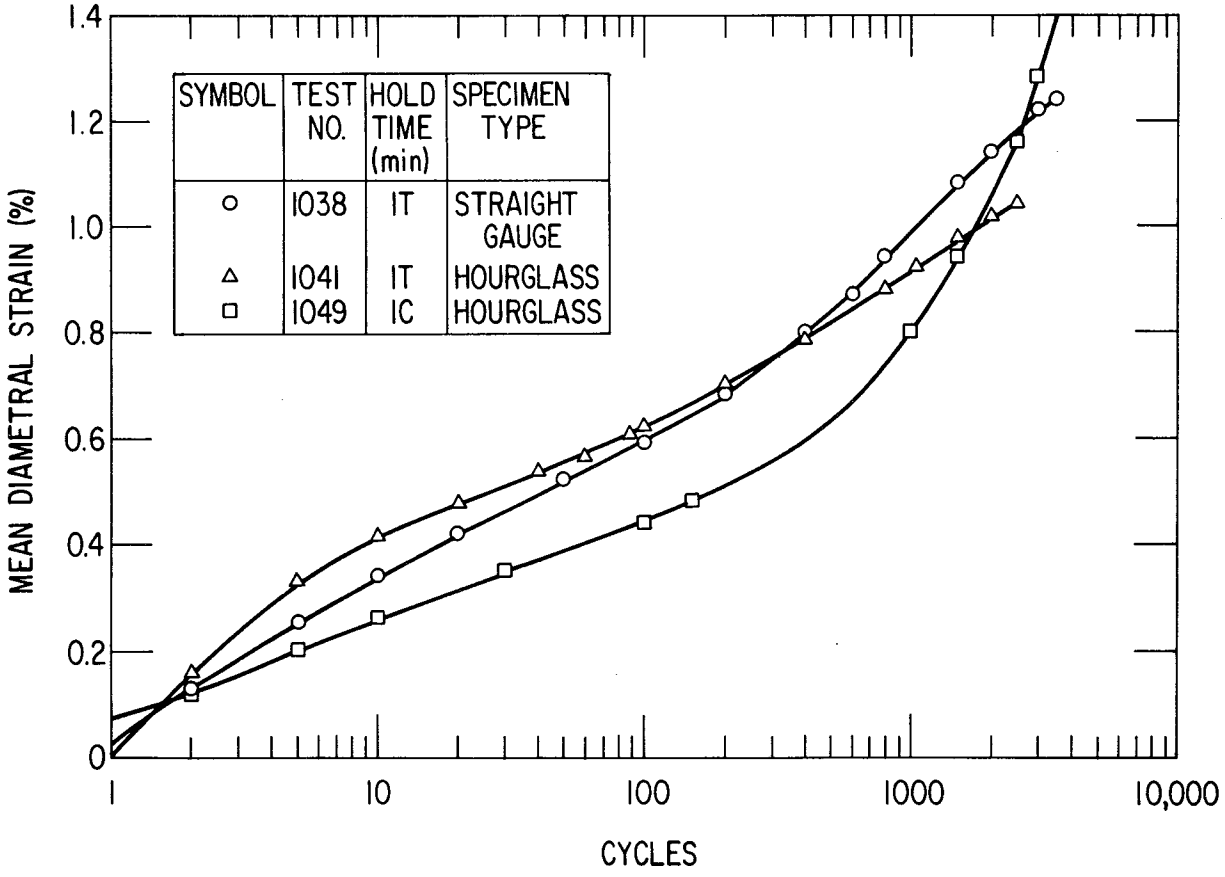

Figure 2. Effect of Specimen Geometry on the Ratchetting of Type 316-H Stainless Steel Tube

Plans for Next Six Months

Testing will continue on the 1-in. diameter Incoloy 800 tubing according to the test matrix shown in Table II.

The high-cycle fatigue testing of 1/2-in. diameter Incoloy 800 tubing is also expected to begin within the next six months. A preliminary test matrix is shown in Table III.

TABLE II

PROPOSED LOW-CYCLE FATIGUE TEST MATRIX FOR INCOLOY 800

Axial Strain Rate = $4 \times 10^{-3} s^{-1}$
Temperature = 1100°F

Axial $\Delta\epsilon_t$ (%)	P_i (psi)	Hold Time (min)	Expected Life N_f (cycles)	Expected Life t_f (h)
0.5	0	0	16,000	11
	1100	0	16,000	11
	1000	0	16,000	11
0.5	0	IT	3,000	52
	1100	IT	3,000	52
	2000	IT	3,000	52
0.5	0	IC	16,000	278
	1100	IC	16,000	278
	2000	IC	16,000	278
0.5	0	5C	16,000	1344
		Total time =	=	2367 h
		Time for 100% duplication =		2367 h
		Total testing time =		4800 h

TABLE III

PROPOSED HIGH-CYCLE FATIGUE TEST MATRIX[a] FOR INCOLOY 800 AT 1100°F

Int. Pressure (psi)	Axial Strain Range (%)	Frequency (cps)	Strain Rate Tensile (s^{-1})	Strain Rate Compressive (s^{-1})	Estimated N_f	Estimated t_f (h)	Maximum N_f	Maximum t_f (h)
0	0.5	10	0.1	0.1	40,000	1.1	10^6	27.8
	0.4	12.5	0.1	0.1	10^5	2.2	3×10^6	66.7
	0.3	16.7	0.1	0.1	10^6	16.6	5×10^7	832
1000	0.5	10	0.1	0.1	40,000	1.1	10^6	27.8
	0.4	12.5	0.1	0.1	10^5	2.2	3×10^6	66.7
	0.3	16.7	0.1	0.1	10^6	16.6	5×10^7	832
	0.25	20	0.1	0.1	10^8	1389	10^{10}	138,900
0	0.5	1	0.01	0.01	40,000	11	10^6	278
	0.4	1.25	0.01	0.01	10^5	22	3×10^6	667
1000	0.5	1	0.01	0.01	40,000	11	10^6	278
	0.4	1.25	0.01	0.01	10^5	22	3×10^6	667
0	0.4	2.27	0.1	0.1	30,000	3.7	8×10^5	98
1000	0.4	2.27	0.1	0.1	30,000	3.7	8×10^5	98

[a]Allowing for duplicate tests, estimated total test time ~ 3000 h and maximum total test time = 11,000 h (using a runout of 1400 h).

INTERIM STRUCTURAL DESIGN STANDARD FOR SOLAR ENERGY APPLICATIONS

A. C. Gangadharen
Foster Wheeler Development Corporation

Introduction

A program to develop an "Interim Structural Design Standard for Solar Energy Applications" was authorized by Sandia Laboratories under Contract No. 87-9151, with a period of performance from June, 1977, to December, 1978.

This program is aimed at the development of a set of interim design rules and standards applicable to the Central Receiver Solar Thermal Power System (CRSTPS) components that generally fall under the scope of the ASME Boiler and Pressure Vessel Code.* Test programs and additional development work required in order to upgrade the interim standard are also to be identified. This program has now been extended to perform creep-fatigue analysis of ANL tests and to evaluate these tests so that they may be used to update the Interim Design Standard.

The first part of the work, that is, the preparation of the Interim Design Standard and the identification of test and development needs, has been completed. The second part, analysis and evaluation of ANL tests, is continuing. Four tests have already been analyzed.

The work completed up to March, 1979, is summarized below.

Review of Solar Systems and Applicable Codes

During Phase 1 of this program, CRSTPS system components were reviewed. This review consisted of a study of the range of loading conditions, the environment, and possible failure modes in CRSTPS components that fall under the scope of the ASME Boiler and Pressure Vessel Code. In this study, primary attention was given to the receiver subsystem and the thermal storage subsystem, including the heat exchangers and piping. The electrical power generation subsystem,

*Subsequently called the Code

pumps, and valves were excluded. A detailed review of the varous pertinent sections of the Code was also conducted in order to determine their applicability to solar power system components. A reliability study involving a review of the available failure-rate data and other reliability information related to pressure components designed according to the Code was also undertaken as a part of this program. The purpose was to determine the appropriate level of reliability for solar components in order to aid in choosing the Code rules for solar applications.

CRSTPS System Review

First-generation CRSTPS components are subjected to loads similar to those of power boilers which are generally designed to Section I and Section VIII-Divison1 specifications except for the following:

- Control of thermal gradients in made necessary by the possibility of very high flux due to the concentration of solar energy.
- Number of important cycles of load is higher by about an order of magnitude than for power boilers. This cycling is more critical because of the possibility of high thermal stresses.
- Seismic loads may be greater than for power boilers because of great tower height. Special consideration is required. The sloshing effect due to seismic loads on storage may also be important.
- Wind loads may be large and need special evaluation.

Review of Codes and Standards

Section I of the Code is based on power boiler experience and Design by Rule. A power boiler which is designed, built, inspected, and stamped in accordance with the rules of Section I must meet all applicable rules of Section I. The use of other design rules and guides, whether part of the Code or not, may be used to aid the designer, but will have no bearing on the boiler's acceptability under rules of Section I. Thus Section I does not guard against the loads by which solar components differ from the power boiler components on which Section I experience is based.

Other sections of the Code wer reviewed in the same manner with the following results:

- Section VIII-Division 1, is based on general pressure vessel experience and Design by Rule. Section VIII-Division 1 does indicate specific loads that should be considered in design, and includes earthquake load. However, the large number of cycles is not covered, and there is no explicit method of consideration of the thermal, seismic, or wind loads.
- Section VIII-Division 2 is based on Design by Analysis. It considers the nature and magnitude of the stresses for all loads. It also explicitly evaluates fatigue stresses. This the cycles of

It also explicitly evaluates fatigue stresses. Thus the cycles of load, thermal loads, seismic loads, and wind loads may all be evaluated. This section is limited in its use to metal temperatures at which creep is negligible. The cost of the analysis is substantially greater than that for Design by Rule codes.

- Section III-Division 1 is divided into three design subsections. Subsection NB is Design by Analysis, which is more inclusive in its load analysis than Section VIII-Division 2. Subsection ND is similar to the Design by Rule of Section VIII-Division 1 and Subsection NC allows the use of Subsections NB or ND. For all cases, the design is limited to temperatures below those at which creep would take place.

- Code Case 1592 is similar in concept to Section III-Division 1, Subsection NB. It allows all loads to be considered and is applicable to temperatures in the creep range.

- Code Case 1481 is similar in concept to Section III-Division 1, Subsections NC and ND and is applicable to temperature in the creep range.

Reliability Considerations

The study of reliability considerations indicated that there is a "quality" difference between vessels built according to Section III (Nuclear Components" and Section I and VIII-Division 1. This should lead to a failure rate of at least two orders of magnitude smaller for nuclear components than for fossil-fuel components. The requirements of a solar standard in terms of reliability lean more toward that of fossil fuel codes than nuclear codes because the parts are accessible and the usual tube failure would be disruptive but not critical. It may be of value to upgrade the fossil fuel Code rules with applicable elements of the Code developed for nuclear components.

Interim Structural Design Standard

The Interim Design Standard is specifically directed toward the first generation solar power systems of the water/steam type. The Interim Standard was prepared by selecting rules from the Code and modifying these rules whereever necessary. In selecting the rules, the following criteria were considered to be important:

- Simplicity - The Interim Design Standard must be simple to use. An approach similar to that of Section I or Section VIII-Division 1 would be most appropriate from this point of view. This approach essentially involves Design-by-Rule. The thickness of the pressure boundary is set by limiting the primary stresses to conservative allowable stress values, thus preventing burst and gross distortion. The remaining failure modes are prevented by liberal safety factors and accepted design practices. This approach, however, may result in greater component weight.

- Design-by-Analysis Alternative - It is considered useful to give an option of Design-by-Analysis. Thus the user may decide whether or not to perform additional analyses that might justify a reduction in wall thickness. This is especially important in view of the fact that modern computer methods of analysis are within reach of most engineers.

- Avoidance of Excessive Conservatism - One of the challenges in the development and commercialization of a viable solar power technology is the reduction in capital costs. A design standard which is unduly conservative will drive up the costs and price the technology out of the market.

- Appropriate Levels of Reliability - Although the prime consideration in the development of the Interim Design Standard is safety, effectiveness and reliability are also important.

Selection and Modification of Code Rules for the Interim Standard

There are four basic failure modes in solar power systems that should be prevented by explicit criteria. These are:

- Bursting and gross distortion from pressure
- Excessive plastic incremental distortion from cyclic loading
- Fatigue or creep fatigue from cyclic loading
- Buckling due to short- or long-term loading

In addition to the above, consideration must also be given to brittle fracture, stress corrosion, and corrosion fatigue. In the Interim Design Standard, protection against these latter failure modes is left to the responsibility of the designer.

Because solar thermal power systems are in an early stage of development without a reserve of explicit experience, the experiences of similar applications must be adapted for an interim solar standard. The following three approaches based on adaptations of the various Sections of the Code could give adequate protection against the four basic failure modes mentioned above.

- A combination of Sections I and VIII plus some additional rules based on the elevated temperature nuclear Code
- Section VIII plus some additional rules based on the elevated temperature nuclear Code
- Section III-Division 1 plus Code Case 1592 or Code Case 1481.

The third approach would involve very sophisticated and complex analyses and should result in unduly conservative designs. Hence it was not given any further consideration. The other two approaches were evaluated in greater detail. In the first approach, Section I is the base Code for the receiver components; Section VIII for other components such as thermal storage and heat exchangers; and ANSI B31 for piping. In addition, new rules are provided

for components that operate at elevated temperatures. In the second approach, Section I is replaced by Section VIII for the receiver components. After considering these two options, the second option was chosen for the Interim Design Standard for the following reasons:

- It is more consistent: In the first approach, the receiver alone is to be designed according to Section I and the rest of the components according to Section VIII; in the second approach, Section VIII may be used for all components including the receiver.

- Section VIII-Division 1 may result in a lighter and less conservative design than Section I. By using the Design-by-Analysis alternative of Division 2, components can be made even lighter. This is important because the receiver is placed atop a tower which could be several hundred feet high.

- Section VIII has a wider material choice.

- The rules of Section I are based on specific experience which may not be applicable to solar requirements. Section VIII is written for a broader scope of vessel.

In summary, the Interim Structural Design Standard is based on Section VIII-Division 1 of the Code. For subcreep temperatures, a design-by-analysis alternative of Section VIII-Division 2 is provided. The Interim Standard includes modified portions of other sections of the Code in order to prevent failure modes that directly concern solar applications but not most Section VIII applications. In most cases, the modifications were taken from sections of the Code governing nuclear components. Thus the levels of reliability are much more stringent than needed for solar applications. An attempt was made in developing the Interim Design Standard to reach a reasonable compromise between the lack of adequate requirements of Section VIII and the overly conservative rules governing nuclear applications to obtain a uniform level of reliability that is appropriate to solar needs. The major changes relate to component applications at temperatures where creep is a factor. Some of the important changes are:

- Creep Damage - At temperatures for which creep is a factor, there is a requirement that creep damage be considered. In the "nuclear codes" this damage is based on the effective stress or stress intensity during hold time. In the Interim Design Standard, the creep damage is based on the maximum principal tensile stress. The justification for this is shown in uniaxial data for 304 and 316 stainless steel. This criterion is much less conservative and simpler to apply than the nuclear Code criterion and is of great importance to the practicality of solar component design.

- Fatigue Damage - The nuclear Code requirement has been eased somewhat by permitting the general use of the curves for inelastic analysis at "elevated temperatures."

- Creep Fatigue Evaluation - Various exemptions have been specified and the exemption rules in Code Case 1481 have been modified for solar applications.

- Ratchetting and Creep Ratchetting - No additional requirements for ratchetting or creep ratchetting evaluation have been placed in the Interim Design Standard. Thus the evaluations that are made in the nuclear codes are deemed unnecessary. One related area is weld material. The nuclear codes deal with this by allowing only one-half the allowable strain limits for weld material as for base material when calculations use data for base material.

- Buckling Instability - Since the rules for buckling in Section VIII apply only to specific configurations and loading, additional limits are provided which are applicable to general configurations and loading conditions. The additional requirements for the evaluation of creep buckling and strain-controlled buckling that appear in the elevated temperature nuclear Code are not mandatory.

Test and Development Needs

The main objectives of the test and development program are:

- Substantiation of the basis of the Interim Design Standard and/or the reduction of unnecessary conservatism in the Interim Design Standard.

- Simplification of the application of the Interim Design Standard.

- Expansion of the coverage of the standard to include additional materials and applications.

In order to meet these objectives, the following test and development needs were identified.

Tests Related to Creep-Fatigue Criteria

Since creep fatigue is an important failure mode in solar components, tests are needed to verify or modify the creep-fatigue criteria and to generate design data. The following tests are recommended.

- Elevated Temperature Fatigue Data - For temperatures in the sub-creep regime, fatigue curves are available in ASME Code Section VIII-Division 2. However, acceptable fatigue curves at elevated temperatures are available only for three materials--Type 304 and 316 stainless steels and Incoloy 800H (Code Case 1592). For other candidate materials such as Incoloy 800, Inconels, and Haynes 188, fatigue data and design curves at elevated temperatures are needed.

- Creep-Rupture Data - Code Case 1592 gives creep rupture times for four materials: Type 304 and 316 stainless steels, Incoloy 800H, and 2-1/4% Cr-1% Mo. For other candidate materials such

as Incoloy 800, Inconels, and Haynes 188, tensile creep-rupture data are needed.

- Cyclic Compressive Hold-Time Tests - The Interim Design Standard chooses the maximum principal tensile stress as the criterion for creep damage. The use of the maximum principal tensile stress criteria is generally less conservative than the choice of the stress intensity or the effective stress that is used in Code Case 1592. The applications in nuclear systems have not suffered unduly under this rule because most of their applications exhibit high tensile stresses. However, solar applications generally exhibit high compressive stresses in critical areas. There is some justification for the use of this criterion. This justification is material dependent and has been obtained with uniaxial specimens. There is a limited amount of data mainly for Type 316 and 304 stainless steels. Cyclic compressive as well as tensile hold-time tests are recommended for other candidate materials.

- Multiaxial Creep-Fatigue Tests - Multiaxiality effects on creep-fatigue damage are an important consideration in solar applications. Multiaxial tests are generally complex and expensive. As a minimum, beaxial creep-fatigue tests are recommended. Argonne National Laboratory (ANL) is currently conducting such tests on Type 316 stainless steel tubes. Multiaxial tests using other candidate materials are necessary.

- Structural Tests on Solar Receiver Tubes or Panels - Tests on solar receiver tubes under nonaxisymmetric flux conditions would be useful for evaluating the validity of the criteria proposed in the Interim Design Standard. These tests may be performed in a solar test facility or under simulated conditions with infrared heating. It may be noted that these tests would take into account the effects of bending, which are excluded from the ANL tests.

Ratchetting Tests

The Interim Design Standard does not give any specific requirements to prevent excessive thermal or creep ratchetting. This is different from the nuclear Code, which contains requirements for ratchetting analysis and limiting the ratchetting strain. The assumption for the Interim Design Standard is that the requirements to prevent ductile and creep rupture, the $3S_m$ limit (if Section VIII-Division 2 is used) and the creep fatigue limit will preclude excessive ratchetting. This assumption, however, needs to be verified by ratchetting tests that simulate solar conditions.

In addition to the above, more test and development needs have been identified. They include:

- Development of exemptions from creep-fatigue analysis to meet the requirements of the Interim Design Standard

- Review of thermal and creep ratchetting requirements in the Interim Design Standard

- Development of design and analysis curves for specific components such as receiver tubes
- Study of the effect of material property variations on multiaxial analysis
- Study of the effects of weld material on elevated temperature long-time behavior
- Experimental and analytical evaluation of attachments and joining methods.

More details regarding the above may be found in Reference 1.

Analysis and Evaluation of ANL Tests

FWDC has completed evaluation of four tests. These tests were performed on Type 316 stainless steel cylindrical tubes at 1100°F (593°C) with a cyclic axial-strain range of approximately 0.5 percent. Two tests were performed without any internal pressure; the reamaining two included application of a constant internal pressure of 1100 lb/in.^{2} (7.58 MPa) throughout the test. A comparison of the test observations and the analytical results showed excellent agreement except in the following two areas:

- The stress range in the ANL tests was approximately 70 x 10^3 lb/in.^{2} (483 MPa), and the corresponding value obtained from the analysis was 35.5 x 10^3 lb/in.(245 MPa).
- Mean diametral strain in the two tests with internal pressure increased steadily throughout the test (i.e., no shakedown) to a final value of approximately 1 percent at failure. This observation was in disagreement with the analysis, which had shown that shakedown should occur at about 20 cycles and a final diametral strain should be about 0.8 percent.

Further analytical studies were performed to explain these two anomalies. First, an analysis was done for the case with internal pressure, using the experimentally observed material properties. These results, presented in Table I, show that shakedown is indicated even if experimentally measured properties are used in the analysis. As shown in Table I, the stress range obtained in an analysis that uses the 100th-cycle properties is very close to that observed in the ANL tests. Thus from the stress-range point of view, 100th-cycle properties give much more realistic results. However, the diametral strain at shakedown is 0.16 percent, as opposed to the experimentally observed value of 1 percent.

The steady increase in the diametral strain was suspected to be a creep-ratchetting phenomenon. Since these tests do not have explicit hold times, creep behavior was omitted from the analysis. Upon seeing the experimental results, the possibility of creep-ratchetting during loading and unloading was

considered. This effect was simulated in the analytical model by subjecting the specimen to a 6-minute hold at each of the tension and compression sides of the cycles. This analysis used 100th-cycle properties. The result of the analysis is also shown in Table I. Instead of obtaining a shakedown and a corresponding accumulated diametral strain of 0.16 percent, a continual increase in the diametral strain occurred; in 27 cycles the accumulated diametral strain became 0.5 percent.

More details regarding these analyses and evaluation may be found in References 2 and 3. The evaluation of additional tests is continuing.

TABLE I

SUMMARY OF THE ANALYTICAL RESULTS

(Material: Type 316 SS,
Temperature: 593°C,
= 0.5%)

Internal Pressure (MPa)	Case	Stress Range	Diametral Strain* (%)	Does Shakedown Occur?
7.58	Book Values	254	0.80	Yes
	Cycles without creep:			
	1st	296	0.40	Yes
	5th	338	0.34	Yes
	100th	503	0.16	Yes
	Cycles with creep:			
	100th	503	0.50**	No
14.4	Cycles without creep:			
	1st	296	0.70	Yes
	100th	338	0.22	Yes
	Cycles with creep:			
	100th	503	0.85	No

*Diametral strain at shakedown or after the given number of cycles.

**Strain after 27 cycles.

References

1. Foster Wheeler Development Corporation, "Final Report: An Interim Structural Design Standard for Solar Energy Applications," prepared for Sandia Laboratories, Livermore, California, January, 1979.

2. Foster Wheeler Development Corporation, "Semiannual Report: An Interim Structural Design Standard for Solar Energy Applications," prepared for Sandia Laboratories, Livermore, California, December, 1977.

3. Foster Wheeler Development Corporation, "Semiannual Report: An Interim Structural Design Standard for Solar Energy Applications," prepared for Sandia Laboratories, Livermore, California, June, 1978.